Mitochondrial Biology & Radiation Research Centre

IT Sligo Research

An *in vitro* investigation of the antitumour efficacy of novel hybrids containing artemisinin, porphyrin, or naphthalimide derivatives

By

James P. Murray

A thesis submitted to the Institute of Technology Sligo

for the degree of Doctor of Philosophy

Supervised by

Dr. James E.J. Murphy

Dept. Life Sciences, IT Sligo

IRISH RESEARCH COUNCIL
An Chomhairle um Thaighde in Éirinn

March 2017

Declaration

I declare that this thesis which I now submit for examination for the award of Doctor of Philosophy, is entirely my own work and has not been taken from the work of others, and to the extent that such work has been cited and acknowledged within the text of my work.

This thesis was prepared according to the code of practice for the quality assurance of postgraduate research at Institute of Technology Sligo and has not been submitted in whole or in part for another award in any other third level institution.

IT Sligo has permission to keep, lend or copy this thesis in whole or in part, on condition that any such use of thesis material is duly acknowledged.

Signature James Murray Date 06/07/17

Abbreviations

2-ME	2-methoxyestradiol
2-VP	2-Vinylpyridine
8-OHdG	8-hydroxydeoxyguanosine
ABC	ATP-binding cassette
ACTB	Beta actin
ADP	Adenosine diphosphate
ALA	Aminolevulinic acid
ANOVA	Analysis of variance
AP-1	Activator protein-1
APAF-1	Apoptosis protease activating factor 1
ART	Artemisinin
ASK	Apoptosis signal-regulating kinase
ATP	Adenosine triphosphate
Bax	Bcl2-associated X protein
Bcl-2	B-cell lymphoma 2
BCRP	breast cancer resistance protein
BER	Base excision repair
BPD	Benzoporphyrin derivative
BSO	Buthionine sulphoximine
CI	Cell index
CPM	Cyclophosphamide
DCFH-DA	Dichloro-dihydro-fluorescein diacetate
DDR	DNA damage response
DHA	Dihydroartemisinin
DISC	Death inducing signaling complex
DIT	Dublin Institute of Technology
DMBA	7,12-dimethylbenz[a]anthracene
DMEM	Dulbecco's Modified Eagle's Medium
DMSO	Dimethyl sulfoxide

DNA	Deoxyribonucleic acid
DR	Death Receptor
DSB	DNA double strand break
ECACC	European Collection of Authenticated Cell Cultures
EPO	Erythropoietin
ETC	Electron transport chain
FADD	Fas associated protein with death domain
FBS	Fetal bovine serum
FITC	Fluorescein
FLIP	FLICE-like inhibitory protein
GAPDH	Glyceraldehyde 3-phosphate dehydrogenase
GCL	Glutamate-cysteine ligase
GGT	□-glutamyl transferase
GPx	Glutathione peroxidase
GSH	Glutathione
GSR	Glutathione reductase
GSS	Glutathione synthetase
GSSG	oxidised glutathione
GTP	Guanosine triphosphate
HIF	Hypoxia inducible factor
HIV	Human immunodeficiency virus
Hp	Haematoporphyrin
HpD	Haematoporphyrin derivative
HRE	Hypoxia responsive element
HUVEC	Human umbilical vein endothelial cells
IC_{50}	Inhibitory concentration 50
IL	Interleukin
ISC	Intersystem crossing
JNK	c-Jun N-terminal kinases
KTP	Potassium-titanyl-phosphate
LC-MS	Liquid chromatography–mass spectrometry

LED	Light emitting diode
LIGIV	DNA ligase IV
MAPK	Map kinase
MDR	Multidrug resistance
MnSOD	Manganese superoxide dismutase
MOMP	Mitochondrial outer membrane permeabilisation
MRP	Multidrug resistant protein
MtDNA	Mitochondrial DNA
mTHPC	m-tetrahydroxyphenylchlorin
MTT	3-(4, 5-dimethylthiazolyl-2)-2, 5-diphenyltetrazolium bromide
NADPH	Nicotinamide adenine dinucleotide phosphate
NAP	Naphthalimide
NCRI	National Cancer Registry Ireland
NER	Nucleotide excision repair
NF-κB	Nuclear factor kappa-light-chain-enhancer of activated B cells
NHEJ1	Non-homologous end joining factor 1
NLCQ-1	4-[3-(2-nitro-1-imidazolyl)-propylamino]-7-chloroquinoline hydrochloride
NMR	Nuclear magnetic resonance
PARP	Poly (ADP-ribose) polymerase
PBD	Pyrrolobenzodiazepine
PBS	Phosphate buffered saline
PDT	Photodynamic therapy
PEP	Phosphoenolpyruvate
PDK1	Phosphoinositide-dependent kinase-1
PI	Propidium iodide
PKM2	Pyruvate kinase muscle isozyme M2
PO_2	Oxygen pressure
PpIX	Protoporphyrin IX
PS	Photosensitiser
PTM	Post translational modification
RNA	Ribonucleic acid

RORγt	RAR-related orphan receptor gamma t
ROS	Reactive oxygen species
RPMI	Roswell Park Memorial Institute Medium
RTCA	Real-time cell analysis
RT-PCR	Reverse transcription polymerase chain reaction
SCLC	Small cell lung cancer
SD	Standard deviation
SiRNA	Short interfering RNA
SIRT	Sirtuin
SMT	Somatic mutation theory
SOD	Superoxide dismutase
SSB	DNA single strand break
TNF	Tumour necrosis factor
TNF	Tumour necrosis factor
TOFT	Tissue of field theory
TPE	Two photon excitation
TPP	Tetraphenylporphyrin
TRADD	TNF-1 associated death receptor domain
TRAIL	TNF-related apoptosis inducing ligand
UV	Ultraviolet
VEGF	Vascular endothelial growth factor
VHL	Von Hippel-Lindau
vWA	von Willebrand factor
WHO	World Health Organization
XRCC4	X-ray repair cross-complementing protein 4

Acknowledgements

Firstly, I would like to express my gratitude to my supervisor Dr. James Murphy for his support and guidance throughout my PhD, and for introducing me to the world of research back in 2011 as a summer student. I also thank my secondary supervisor Dr. Sarah Rawe, Dublin Institute of Technology, for her guidance and intellectual input throughout the project. The Rawe group in DIT were responsible for synthesising and preliminary analysis of hybrid drugs discussed in this work. I would like to extend special thanks to Dr. Sandra Gannon, Dr. Miriam Kennedy and Dr. Anna Przybył for their hard work. I would like to thank the Irish Research Council who funded my research project.

I would like to acknowledge both past and present members of the MBRR research centre; Dr Naimj Gambi, Marcus Colon, Julia Powers, Janis Kelly, Rebecca Ward, and Dr Gianfranco Bartolini. Thank you all for the chats, coffees, jokes and discussions which kept me going throughout my PhD. A special thanks to Dr Alice Grassick who ensured our lab ran seamlessly and was “the mammy” of the group, always on hand to offer advice and encouragement. I thank also my postgraduate peers in IT Sligo who provided an excellent support network throughout my studies. I would like to thank my fiancée Avril for her continuous and loving support throughout this hectic and challenging journey. Finally, I would like to thank my mother and father, for giving me the opportunity to fulfil my potential by allowing me to stay in “school” just a little longer. I will always be extremely grateful.

Abstract

Novel hybrid drugs have emerged as a promising new anticancer strategy. A hybrid drug is a compound in which two active 'parent' drugs are linked to create a single molecular entity with a multimodal action. The main objective of this study was to evaluate the anticancer potential of several novel hybrid drugs which contained a combination of artemisinin (ART) and either a porphyrin or naphthalimide (NAP) derivative. ARTs, NAPs and porphyrins have already shown promising anticancer activity both *in vitro* and *in vivo*. Real time cell analysis (RTCA) and cell count analysis were the chosen methods to evaluate cell growth and cell number following hybrid treatment. Another key objective of the current study was to determine if oxygen concentration could affect anticancer drug efficacy *in vitro*. This hypothesis was investigated in Chapter 2. Hypoxia, which often develops in tumour tissue, has been reported to adversely affect chemotherapy and radiotherapy during cancer treatment. Despite this evidence, standard atmospheric oxygen levels are employed during *in vitro* analyses of novel anticancer agents. The generated results clearly demonstrate that artesunate anticancer efficacy against HeLa cells was increased when oxygen levels were lowered to 4% (v/v) or 1% (v/v). This highlights the importance of oxygen concentration when evaluating novel anticancer agents.

Photodynamic therapy (PDT) was applied to PC-3 cells in Chapter 3. PDT involves the combination of a photosensitiser (drug), light and oxygen to induce cell death. Hypoxia development in tissues during PDT has been shown to induce resistance highlighting the importance of oxygen in PDT outcome. Oxygen concentration was maintained at 4% (v/v) throughout analysis based on the results from Chapter 2. Protoporphyrin IX (PpIX) and hybrid **AP433** were investigated in PC-3 cells. A novel light activation procedure was performed using a Q-Sun solar simulator. Light activation of both PpIX and hybrid **AP433** could be observed. However, light irradiation procedure alone accounted for a loss in cell numbers. Therefore, PDT treatment will need to be further optimised before this family of hybrids can be effectively evaluated.

ART-NAP hybrids were then investigated across four cell lines in 4% (v/v) oxygen environment. **SG76**, **SG77** and **SG81** were particularly effective against HL60 and PC-3 tumour cell lines. PNT1A prostate non-tumour cells were more tolerant to hybrid drugs than both parent compounds. Furthermore, **SG77** was found to be the most selective hybrid with 11 times more activity in PC-3 when compared to PNT1A. The next objective was to investigate the potential mechanisms responsible for **SG77** drug action. Gene expression analysis was performed to determine the potential for **SG77** to induce oxidative stress, DNA damage and apoptosis. In addition, ROS generation, glutathione levels and apoptosis induction were quantified following **SG77** treatment. Based on the data generated, intrinsic apoptosis, DNA damage and glutathione antioxidant response may be important in **SG77** drug action. Furthermore, PC-3 were more sensitive to **SG77** than non-tumour PNT1A with increased cytotoxicity, ROS generation, glutathione depletion and apoptosis. **SG77** should be considered as a promising candidate for animal trials with the potential for a potent and selective cancer therapy which will improve patient outcome.

Dissemination List

Publications

Murray, J.P., Gannon, S., Rawe, S. & Murphy, J. E. J. In Vitro Oxygen Availability Modulates the Effect of Artesunate on HeLa cells. *Anticancer Res.* **34,** 7055–60 (2014).

Murray, J.P., Jones, M., Gannon, S., Kennedy, M. E., Rawe, S. L., O'Neill, P.M. & Murphy, J. E. J. Selective Anticancer Activity of Novel Artemisinin-Naphthalimide Hybrids In Vitro. (Submitted to *Journal of Cancer*)

Murray, J.P., Jones, M., Gannon, S., Kennedy, M. E., Rawe, S. L., O'Neill, P.M. & Murphy, J. E. J. "Role of Oxidative Stress in Artemisinin-Naphthalimide hybrid drug action. (prepared for submission)

Conferences

Oral presentation at the xCELLigence User Group Meeting (2013) held in Birmingham, UK. "Real time *In Vitro* Evaluation of Cancer Strategies: From Novel Hybrid Drugs to Non-ionising Radiation". Murray, J.P.*, Gambi, N., Gannon, S., Kennedy, M.E., Loftus, N., Rawe, S.L. & Murphy, J. E. J

Poster presentation at the 14th Annual Multidisciplinary Research Conference November 29th (2013) held in Sligo, Ireland. "Oxygen Availability Modulates the Efficacy of Artesunate In Vitro". Murray, J.P.*, Gannon, S., Rawe, S.L. & Murphy, J. E. J

Poster presentation at Cancer Pharmacogenomics and Targeted Therapies Meeting (2014) held in Cambridge, UK. "Anticancer Activity of Novel Hybrid Compounds". Murray, J.P.*, Gannon, S., Rawe, S.L. & Murphy, J. E. J

Poster presentation at IACR Annual Meeting (2016) held in Cork, Ireland. "Selective anticancer activity of a novel endoperoxide-naphthalimide hybrid in vitro". Murray, J.P.*, Gannon, S., Rawe, S.L. & Murphy, J. E. J

Awards

Irish Research Council Postgraduate Scholarship (2012)

Cancer Pharmacogenomics and Targeted Therapies Student Bursary (2014)

ACEA Travel Award (2016)

Contents

List of figures

Chapter 1. General Introduction

1.1 Overview

Chemotherapy, radiation, and surgery are the standard methods of cancer treatment today. However, multidrug resistance is a reoccurring drawback with chemotherapy in many patients. In addition, most chemotherapeutics have side effects associated with high toxicity levels. Most chemotherapeutics administered in the clinic today interfere with DNA replication and cause cell cycle arrest [1]. As cancer cells undergo rapid cell divisions they are generally more susceptible to chemotherapy than non-tumour cells. Furthermore, cancer cells often have impaired DNA repair mechanisms leading to more DNA damage and cell death [2]. Unfortunately, these anticancer drugs are will also interfere with non-tumour cells. Rapidly dividing non-tumour cells such as and hair follicles, stomach epithelia and haemopoietic cells are particularly susceptible to chemotherapy resulting in hair loss, ulcers and anaemia [3]. Therefore, the search is ongoing for novel anticancer compounds with potential for more selective chemotherapy.

Exploiting the differences between non-tumour cells and tumour cells has led to strategies targeting cancer related mutations or the deficiency of tumour suppressor pathways in cancers [4]. Another strategy that is being employed is the development of hybrid drugs. A hybrid, in the context of drug design, refers to a compound in which two active 'parent' drugs are linked to create a single compound with dual activity [5]. The two parent drugs, from which the hybrid is prepared, each have their own unique mode of action. By combining two compounds in this way, several advantages are possible including simultaneous delivery of the parent drugs, enhanced potency, improved cellular uptake, reduced drug resistance and reduced non-tumour toxicity. Indeed, improved efficacy and selectivity have been successfully demonstrated in hybrids when compared to their parent drugs *in vitro* [6,7].The hybrid approach has been employed successfully in the treatment of several diseases and disorders including cancer [8–11], neurodegenerative disorders [12] and malaria [13,14]. Unlike drug combination therapies for cancer treatment, the biological activity of hybrid compounds results from a single molecule in which two or more active compounds, with specific mechanisms of action and/or biological targets.

The overall aim of the current study is to evaluate the antitumour efficacy of several novel hybrids containing artemisinin, porphyrin, or naphthalimide derivatives. Artemisinin (ART), and it's derivatives are endoperoxide containing compounds which has been used in malaria treatment for more than 30 years [15–17]. ART and its derivatives have been shown to have excellent anticancer properties in vitro in many cancer types including leukaemia, prostate and breast cancer [18–21]. This activity has been further supported with *in vivo* studies involving xenografted animal models [22–24]. Naphthalimides (NAPs) are a family of compounds containing an aromatic naphthalene system fused to an imide group and were first synthesised as antitumour agents in 1977 [25]. These potent compounds are proposed to exert their antitumour effects by DNA intercalation [26]. Some NAPs have reached clinical trials, severe toxicity in non-tumour tissues has prevented them being further developed [27,28].

Porphyrins are naturally occurring compounds with unique photo-activation properties. These properties have been exploited to treat several medical conditions including psoriasis, acne and cancer in a procedure coined photodynamic therapy (PDT) [29]. PDT involves either systemic or topical administration of a photosensitiser (PS), followed by irradiation of the diseased area with light of a specific wavelength. The irradiation process elevates the PS to an excited state where it can elicit its toxic action [30–32]. Porphyrins are thought to preferentially locate in tumour tissue due to the poorly formed, leaky vasculature. This theory, coupled with the fact that light activation is only performed on target tissue means that a "dual selectivity" is possible [5]. Furthermore, the porphyrin compound may be even more beneficial in a hybrid by directing the second anticancer agent to the tumour site where both parents can take effect upon light activation [33].It is anticipated that by combining ARTs with porphyrins that there will have increased potency and efficacy. ARTs ROS producing properties could potentially work in synergy with the unique light activation properties of porphyrins which result in the generation of toxic singlet oxygen. On the other hand, by combining ARTs with NAPs it is anticipated that there will be a synergistic effect with DNA intercalation/damage of potent NAP combined with tumour selective ROS production of ART. To our knowledge, this

is the first time such novel ART-NAP and ART-porphyrin hybrids have been investigated *in vitro*.

Another novel aspect of the present research project involves maintenance of oxygen environment to better reflect *in vivo* conditions of normoxia (4% (v/v) oxygen) and hypoxia (1% (v/v) oxygen). Tissue hypoxia is defined as a decrease in oxygen availability below critical levels which compromises the function of cells tissues or organs [34]. Hypoxia often develops in tumours due to poor blood supply and inadequate oxygen diffusion. More than 50% of solid tumours exhibit areas of hypoxia throughout the tumour mass, with areas of anoxia often occurring [35]. Hypoxia has also been shown to adversely affect chemotherapy and radiotherapy [36–38]. Despite the large body of evidence suggesting that hypoxia is crucial to chemotherapy outcome, almost all *in vitro* evaluations of novel compounds have been performed in the standard oxygen rich environment (20-21% O_2) [39–41]. This is markedly different from the normoxic oxygen levels typical of normal cells *in vivo* or indeed from the hypoxic or anoxic regions of a typical tumour mass [42,43]. There is a need to factor oxygen concentration as standard procedure for *in vitro* analyses of novel drug compounds.

1.2 Cancer

Cancer is characterised by the uncontrolled growth of cells and can often metastasise from the origin to distant sites of the body [44]. After diseases of the circulatory system, cancer remains the second most common cause of death in Ireland with an annual average of 8,827 deaths from 2011 to 2012 [45]. Furthermore, 1 in 3 men and 1 in 4 women in Ireland will develop some form of invasive cancer in their lifetime with lung, breast and prostate cancer the most common cancer types reported [45]. Due to an increasing aging population in Ireland, it is predicted that the total number of new invasive cancer cases will increase by 84% for females and 107% for males between 2010 and 2040 [46]. Cancer in Europe is also on the rise with more than one and a quarter million cancer deaths recorded in 2013 [47]. Furthermore, cancer is a major cause of mortality worldwide with approximately 8.2 million cancer deaths reported in 2012, affecting populations in all countries and all regions [48].

1.3 Characteristics of cancer

Cancer can be defined simply as the uncontrolled growth of cells. This aggressive, unregulated growth and unsuppressed cell division is caused by gene mutation and can occur at nearly any location in the body. The resulting cancer is often metastatic in nature [49]. Risk factors which are known to cause cancer include tobacco smoke and ultraviolet (UV) radiation [50–52]. As non-tumour cells progress to a neoplastic state, they adopt several distinct properties which allow evasion of regulatory processes and favour uncontrolled growth and metastases. Figure 1 illustrates the most common characteristics of cancer cells including evading cell death, sustained growth, angiogenesis induction, evading immune destruction and metastasis [4,44]. These physiological changes in cells represent a failure of the anticancer defence mechanisms which typically combat the formation of tumours. Many cancer therapies have been aimed to target one or more of these cancer characteristics (Figure 1).

Possibly the most fundamental property of cancer cells is their ability to maintain cell growth [4,44]. In contrast, non-tumour cells regulate the release of crucial growth factors involved in the initiation of cell growth, thus maintaining an optimal balance of cell numbers. Cancer cells sustain growth by directly producing growth factors or stimulating cells surrounding them to produce growth factors. Moreover, cancer cells are known to have more growth factor receptors on their cell surface [53]. Negative feedback loops in the body are key in regulating homeostasis in the body. For example, the Ras pathway is a frequently deregulated negative feedback pathway in human cancer [54]. Ras protein is a monomeric G protein which is activated by bonding with guanosine triphosphate (GTP) to activate several kinase proteins in a cascade of events which trigger cell growth. Importantly, this process is self-limiting and when Ras binds to GTP it is quickly hydrolysed to form guanosine diphosphate (GDP) [55,56]. When bound to GDP, Ras is deactivated. Therefore, RAS activity depends on the amount of the corresponding GTP in the cell. Ras mutations affect downstream growth signalling pathways involved in numerous functions including cell cycle progression, growth, apoptosis, senescence and migration [54,56].

An unlimited replicative potential is another trait acquired by cancer cells (Figure 1). In non-tumour cells, growth and replication are limited by cell death in response to stress and cell ageing. Telomeres have been demonstrated to have a crucial role in cell ageing [57]. Telomeres protect the ends of chromosomes ensuring chromosome stability and have a role in cellular response to DNA damage and stress. In non-immortalised cells, telomeres shorten progressively until chromosomal integrity is lost resulting in cell death. Conversely, cancer cells escape cell ageing by overexpressing telomerase an enzyme with the function of adding hexanucleotide repeats to telomeres thus preserving chromosome integrity. Tumour cells consume nutrients and oxygen like their non-tumour counterparts. However, due to the rapid growth of tumour cells, the demand for oxygen and nutrients becomes unsustainable. Tumour cells compensate for this insufficient blood supply by activating new blood vessel formation (angiogenesis) by activating growth factors such as vascular endothelial growth factor (VEGF) [58].

Metastases, which is the spread of cancer from one organ or tissue to surrounding tissues, is a characteristic of many cancers (Figure 1). An assessment of metastasis is used to diagnose cancer stage in patients. Stage I cancer is relatively small and contained at the site of origin. Stage II cancer usually has not spread to surrounding tissues but has grown larger in size than in Stage I. Conversely, Stage 3 cancer involves the spreading of cancer cells into surrounding tissues and lymph nodes. Stage IV is an advanced form of cancer where the initial cancer has spread to another organ within the body. This cancer is often referred to as metastatic cancer [59,60]. E-Cadherin is a transmembrane glycoprotein that establishes interactions with adjacent E-cadherin molecules and forms adherent junctions between epithelial cells. E-cadherin downregulation or deactivation in many cancers suggests its role in suppressing metastasis [61].

1.3.1 The onset and development of cancer

Cancer development is a multi-stage process. The concept of multi-stage cancer was first proposed in 1948 [62]. Cancer is divided into three distinct phases: initiation, promotion and progression. Underlying molecular events such as altered gene expression and cellular signalling are crucial in the formation of cancer and numerous genes and proteins have been implicated to have a role in cancer development. Initiation of cancer occurs where non-tumour cells experience DNA damage. This DNA damage is normally repaired by molecular DNA repair processes. However, when a cell is in a growth state, there is significantly less time to perform necessary DNA repairs. Consequently, these cells retain genetic alterations during cell division [63,64]. The second stage of cancer, promotion, is the process whereby tumour promoters encourage cells to divide. If these tumour promoters are present in tissues for a long time in high concentration, tumour formation can ensue without any other stimuli. On the other hand, if a tumour promoter is absent, then tumour regression can occur by means of apoptosis [49].

During the promotion stage, a series of cellular adaptions are necessary in cancer to survive the toxic effects of acidosis and hypoxia. Cancer cells are thought to switch to anaerobic respiration resulting in increased glycolysis and increased acid production. The third and final stage in cancer development is progression. This stage is characterised by increased growth rate and the development of a more aggressive malignant phenotype. At this stage, the tumour begins to migrate to surrounding tissues and enter the blood stream where it can spread to other organs within the body where there is the potential for the development of secondary tumours. Cancer cells now have a significant growth advantage having adapted to hypoxia and acidosis. Consequently, there is a large drop in competing non-tumour phenotypes due to the harsh growth environment. This decline of competing cell types is thought to be crucial in the evolution of a metastatic cancer type [65].

1.3.2 Cancer treatment

Surgery, radiation and chemotherapy are routinely used in combination to treat malignant tumours to improve patient outcome [66–70]. Tumour removal during surgery remains one of the most effective cancer treatments today [3]. However, surgery is limited due to the inaccessibility of some tumour types such as brain tumours and those which have spread to vital organs. Tumour debulking can be performed, in which some, but not all the tumour is removed to prevent damage to vital organs. leukaemia is present in the blood stream and does not form a tumour mass. Therefore, this cancer subtype cannot be removed surgically [71]. Furthermore, it is often difficult to remove all the tumour cells which lead to the cancer re-growing [3]. Metastatic cancers, which account for most cancer deaths, are not curable with surgery alone as they spread to different tissues and organs [72–74]. Radiotherapy is also utilised in cancer treatment and involves exposing cancer cells to ionising radiation which generates reactive oxygen species that cause DNA damage and apoptosis [75–78]. However, low oxygen concentrations typically present in areas within tumour mass are known to reduce the efficacy of radiotherapy [79]. In addition, radiotherapy has been associated with the development of secondary tumours in brain cancer patients [80].

Chemotherapy refers to the use of one or more anticancer drugs to kill cancer cells [81]. Great progress has been made in the development of novel anticancer drugs which often target specific mechanisms upregulated in cancer cells including DNA replication, angiogenesis, metastasis, proliferative signalling and resistance to cell death as illustrated in Figure 1 [82,83] . For example genomic instability has been targeted with poly(ADP-ribose) polymerase (PARP) inhibitors to prevent cancer cells initiating single stranded DNA repair [84]. Furthermore, most chemotherapies used in the clinic target DNA replication to target the rapid division of cancer cells [1]. Drugs which result in ROS generation, such as ARTs, are used to target the higher levels of oxidative stress and the compromised antioxidant systems often present in cancer cells [8586]. The importance of ROS generation and glutathione antioxidant response in cancer treatment are described in more detail in sections 5.4 and 5.5. VEGF has also been targeted using monoclonal antibodies to prevent cancer cells promoting angiogenesis and maintaining blood supply to the growing tumour [87]. Chemotherapy has proven

effective in treating several cancers but is limited by non-tumour cell toxicity. Rapidly dividing non-tumour cells such as and hair follicles, stomach epithelia and haemopoietic cells are susceptible to chemotherapy resulting in hair loss, ulcers and anaemia [3]. Therefore, there remains an urgent need to continue to develop improved and more targeted cancer therapies which will mitigate the cancer minimising toxic side effects in cancer patients.

Adjuvant (or adjunct) therapy involves the use of a pharmacological or immunological agent in combination with primary treatment to improve overall tumour destruction. For example, anticancer agents are commonly administered after surgery to ensure that any remaining tumour cells can be destroyed. This approach has been employed in the treatment of several cancers including colon, breast and lung cancer [88]. Radiation and surgery have also been combined to treat several cancers including breast and prostate cancer [89–91]. Neoadjuvant chemotherapy refers to the administration of a therapeutic agent prior to the main treatment to improve overall efficacy. This type of treatment is usually applied to reduce the tumour size before surgery and can include hormones, immune system modulators and chemotherapeutic agents [92,93]. Neoadjuvant chemotherapy has been applied successfully in combination with surgery and trastuzumab in HER2-positive breast cancer patients [94].

1.3.3 Multidrug resistance

The development of multidrug resistance (MDR) remains a major obstacle to successful cancer treatment. Anticancer drugs can fail to destroy cancer cells for several reasons. As most drugs are administered systemically, metabolism and absorption can impact drug efficacy. For example folate receptor mediated drug uptake can contribute to resistance in breast cancer cells [95]. Additionally, drug metabolising enzymes have a central role in drug metabolism which can lead to detoxification of an anticancer agent and thus can cause reduced drug efficacy [96]. Cancer cells also make genetic alterations to adapt to the toxic effects of chemotherapy (section 1.3). Upregulation of transport mechanisms in cancer cells is commonly implicated in the development of MDR. For example, ATP binding cassette transporters (ABC transporters) are a family of proteins which function to transport solute across the cellular membrane. During chemotherapy,

these transport proteins are upregulated resulting in an increased efflux and removal of the anticancer agent from within the cancer cell [97,98]. Consequently, drug efficacy is greatly reduced. Many anticancer agents are designed to kill proliferating cells, causing extensive DNA damage that eventually leads to cell cycle arrest and apoptosis.

However, the efficacy of these anticancer agents can be significantly reduced by the ability of cells to repair DNA [82]. DNA repair involves an intricate network of repair systems including the nucleotide excision repair (NER) [99] pathway, the base excision repair (BER) [100] pathway, the homologous recombination (HR) [101] pathway, and the nonhomologous end joining (NHEJ) pathway [101] (Discussed further in Chapter 5). These pathways have been linked to multidrug resistance from both platinum based and DNA alkylating anticancer agents [102–104]. p53 is a key transcription factor involved in cell cycle regulation, apoptosis and DNA repair. Mutations in this gene are common in cancer cells and have also been associated with multidrug resistance [105]. Apoptosis evasion can also contribute to resistance. For example, BCL-2 antiapoptotic protein (discussed further in section 5.3) activation was found to be upregulated in multidrug resistant lung cancer cells [106].

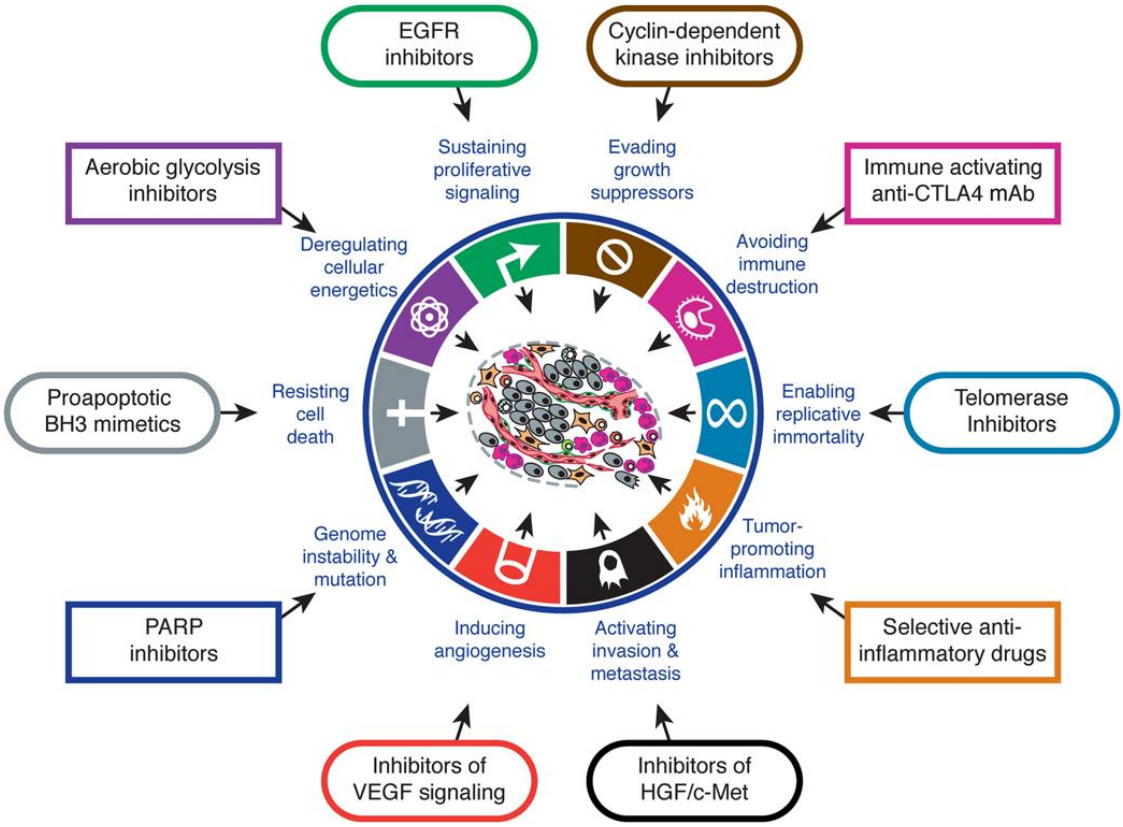

Figure 1 Characteristics of cancer cells and potential therapeutic targets

The diagram represents the most common characteristics of cancer cells including evading cell death, sustained growth, angiogenesis induction, evading immune destruction and metastasis. The diagram also highlights some promising therapies which have been designed to target these mechanisms; many of these therapies have reached advanced clinical trials [4].

1.4 Artemisinins- A family of endoperoxide containing antimalarial compounds

1.4.1 Artemisinin in malaria treatment

Artemisinin (ART) is a sesquiterpene lactone (a class of chemical compound which contains sesquiterpenoids and a lactone ring). ART was first isolated from the Chinese herb qinghaosu (*artemisia annua* or annual wormwood) in 1972 [15]. It was then discovered that artemisinin had excellent antimalarial properties with potent activity in multidrug resistant *P. falciparum* malaria strain *in vitro* and *in vivo* [107]. Naturally occurring artemisinin has low solubility in oil and water prompting several semi-synthetic derivatives to be produced [108]. The latter include dihydroartemisinin and artesunate which both contain an endoperoxide moiety (Figure 2).

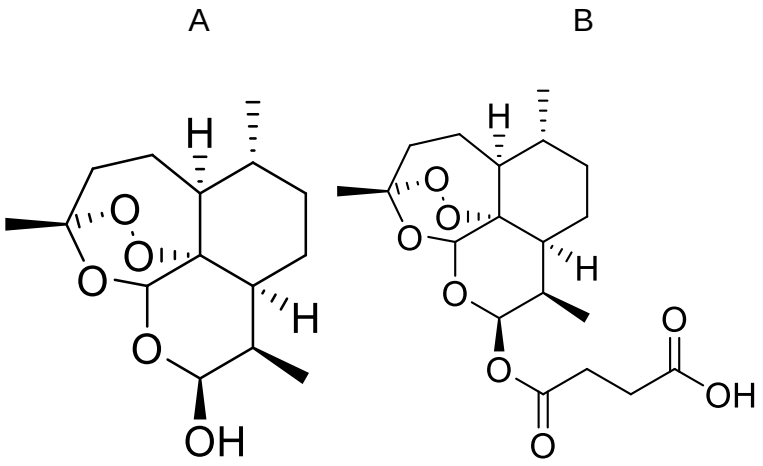

Figure 2 Chemical structure of (A) Dihydroartemisinin and (B) Artesunate

ARTs have been previously well tolerated in hundreds of thousands of malaria patients with little side-effects even at high doses [109]. Typical malaria treatment in humans require oral doses of 70 mg/kg/day [110]. It was demonstrated that the endoperoxide group in ART is essential for antimalarial activity [111]. Several derivatives of ART which lacked the endoperoxide bridge peroxide were found to have no antimalarial activity [111]. The exact mode of action of artemisinin in malaria remains under debate. However, most studies concur that ART and its

structurally similar derivatives require bioactivation through cleavage of the endoperoxide bond to produce toxic oxygen radicals. There is a large body of evidence suggesting that this bioactivation occurs through the reductive scission by the iron II centre of haem [111,112].

Malaria parasites infect erythrocytes and consume haemoglobin as a source of nutrients producing toxic haem as a by-product [113]. Nearly all this toxic haem is converted into a non-toxic insoluble polymer called haemozoin. Most of this haemozoin, often referred to as the malaria pigment, is stored in the food vacuole of infected erythrocytes [114]. Following haemoglobin degradation and haematin detoxification, iron is available in the form of Iron II (Haem) and iron III (Haematin). Haem and haematin are structurally very similar. They can be distinguished by different oxidative states. Haem is in the +2 oxidation state whereas haematin is in the +3 oxidation state and contains an additional hydroxyl ligand [115,116]. Other forms of iron are also available but it has not been fully elucidated which source of iron is utilised in ART activation within the parasite. This information is outside the scope of the current study but a detailed review has previously been performed [111]. ART activation by iron is then capable of producing toxic free radicals [117]. The involvement of haem in the bioactivation of ART could explain its selective toxicity since extensive haemoglobin catabolism and haem polymerisation are processes that only occur within infected red blood cells [111].

There is debate surrounding the way in which bioactivation of the endoperoxide occurs [111]. Two models of ART activation that were hypothesised include the reductive scission model and the open peroxide model. In the reductive scission model, iron II centre of haem binds to ART resulting in electron transfer and in turn the reductive scission of the peroxide bond. This reductive scission produces carbon centred radicals, which are thought to be responsible for antimalarial activity [118]. The open peroxide model, on the other hand, involves Iron II behaving as a Lewis acid resulting in an opening of the peroxide ring to produce an open hydroperoxide [119]. A Fenton reaction then occurs to produce hydroxyl radicals which are toxic to the parasite [120]. Both primary and secondary carbon centred

radicals have been detected *in vitro* following ART activation and are thought to result in protein alkylation and protein oxidation [111,121].

ART has been shown to alkylate haem to form adducts. ART has been combined with haem during *in vitro* Iron degradation studies which demonstrate the formation of ART-haem adducts [122,123]. ART alkylation of haem was detected in urine samples of malaria-infected mice following ART treatment [124]. Radiolabelled dihydroartemisinin (DHA), arteether and arteflene have been shown to alkylate several proteins in the malaria parasite which adds more evidence to support the proposed mechanism [125–127].

1.4.2 Artemisinins in cancer treatment

ART was first found to have anticancer properties in 1993 when several ART derivatives, including artesunate, were investigated in Ehrlich ascites tumour cells (cell line is derived from a mammary gland tumour in a mouse model). All compounds active in the tumour cell line with IC_{50} (inhibitory concentration 50%) values ranging from 12.2 to 29.8 μM [128]. However, IC_{50} values in the tumour cell line were markedly higher when compared to the activity of ART in malaria treatment (1.3 μM) suggesting that higher doses of ART are required for anticancer activity [128]. This promising study led to the evaluation of ART and its derivatives in several cancer cell lines *in vitro*. Artesunate and DHA are the most commonly investigated derivatives. Artesunate was tested against 55 different tumour cell lines. The results were encouraging with an IC_{50} value of less than 20 μM in most cell lines tested. Leukaemia and colon cancer cells were the most sensitive to artesunate with mean IC_{50} values of 1.11 μM and 2.13 μM respectively [18]. (The average IC_{50} of artesunate on NCI database across multiple cancer types is 4.7 μM [129]). Several other cancer cells were also sensitive including melanoma, prostate, breast and ovarian cancer. The author concluded that ART activity was comparable to other standard cytotoxic agents employed clinically in the treatment of several cancer cell types including leukaemia, breast and prostate cancer [18]. Artesunate was also effective in a panel of neuroblastoma cells with an IC_{50} of 5 μM or lower in nearly all cell lines tested. ROS generation and apoptosis were detected following drug treatment [130]. DHA was shown to be

effective in MOLT-4 leukaemia cells with rapid cell death after 8 hours with 27.5% of cells undergoing apoptosis.

ART compounds (primarily artesunate and DHA) have been examined *in vivo* employing several animal models of cancer including leukaemia [131], sarcoma [22] and cancers of the breast [21], pancreas [132,133], liver [134,135] and colon [136]. For example, ART was found to delay the development of 7,12-dimethylbenz[a]anthracene (DMBA)-induced breast cancer in a rat model at a dosage of approximately 8 mg/kg/day for 40 weeks [21]. Another study reported that artesunate (167 mg/Kg/day) effectively reduced tumour growth to approximately 30% of the untreated control group in Kaposi's sarcoma mouse model [22]. In mice bearing BxPC-3 xenograft tumours (pancreatic cancer), DHA inhibited tumour growth in a dose-dependent manner; DHA (50 mg/kg/day) resulted in a reduction in tumour size to 27% of the untreated tumour control by day 18 [137]. On the evidence of these studies, ARTs can significantly retard tumour growth *in vivo* at relatively high doses (50-200 mg/kg/day) with no significant side effects reported at these dosages. This *in vivo* research suggests that ART compounds have the potential to be utilised in the treatment of cancer patients. However, further clinical trials are needed before ARTs can be further developed.

ARTs have been investigated in a small number of clinical studies to date in the treatment of several cancer types including cervical [138], lung [139] and skin cancer [140]. The first case studies involving the treatment of cancer patients with ART related compounds was on a compassionate use basis, where standard chemotherapy had proven ineffective. A patient with laryngeal squamous cell carcinoma was treated with both oral (50mg) and interparental (60mg) doses of artesunate daily. The tumour size was reduced by approximately 70% after 2 months of treatment with a reported improvement in patient symptoms [140]. 2 patients with advanced metastatic uveal melanoma were also treated with artesunate in combination with standard chemotherapy [141]. The combination therapy was well tolerated with no additional side effects reported. Tumour growth stabilised in one of the patients following treatment with artesunate and

dacarbazine; this treatment also resulted in reduced metastasis. The patient was still alive 47 months after first diagnosis of stage IV uveal melanoma; the median survival for this advanced stage cancer is usually between 2-5 months [141].

These initial case studies led to development of more controlled clinical trials. A clinical trial in advanced non-small cell lung cancer investigated a combination treatment with artesunate [139]. Vinorelbine and cisplatin (standard chemotherapy) were administered with or without intravenous ART injections (120 mg). There were significant improvements in disease control rate of the trial group (88.2%) when compared to the control group (72.7%). Again, artesunate was well tolerated in all patients. A separate clinical study investigated oral artenimol, the succinate ester of DHA, in the treatment of cervical cancer. Symptoms of the disease subsided within three weeks of artenimol treatment (200 mg/day) in all patients. An increased survival time was also observed [138]. A double-blind, placebo-controlled trial was performed in 23 colorectal carcinoma patients. Patients were administered with oral artesunate (200 mg) or placebo. The results showed that after 42 months only one ART-treated patient developed refractory tumours when compared to six placebo-treated patients [142].

In conclusion, numerous studies have reported that ART and its derivatives are active against cancer *in vitro* and *in vivo.* This evidence suggests that ARTs could be utilised in chemotherapy, either as a monotherapy of adjuvant therapy. This point is reinforced by preliminary clinical results.

1.4.3 Artemisinins anticancer mode of action

ART's anticancer mode of action has been investigated *in vitro*. The endoperoxide bridge of ART is crucial for anticancer activity drawing comparisons to the malaria narrative [143]. When the endoperoxide moiety was removed from DHA, the result was a 50-130 fold decrease in cytotoxicity in HL60 and Jurkat leukaemia cells when compared to endoperoxide-containing DHA [143]. It is generally accepted that iron-mediated endoperoxide cleavage results in ROS production, DNA damage and cell death [144]. This theory has been supported by numerous studies [145–147]. An early study reported the artesunate caused growth inhibition, apoptosis and glutathione depletion in human KG-1a leukaemia cells

in response to ROS generation [145]. Intrinsic apoptosis, mediated by the mitochondria, is thought to be activated in response to this ROS generation [146]. For example, DHA treatment was found to induce apoptosis in hepatocellular carcinoma cells. Mitochondrial membrane depolarisation, cytochrome C release and caspase enzyme activation were reported [147].

The source of iron required for ART activity remains under debate. Two modes of action have been hypothesised (Figure 3) [148]; (A) ART accumulates in the endosome before being activated by unbound iron. This results in the generation of ROS causing lysosomal damage, disruption of endosomal transport and mitochondrial mediated apoptosis; and (B) an alternate mode of action involves the activation of ART by haem within the mitochondrion resulting in the production of carbon centered free radicals. These radicals then form adducts that may interfere with the electron transport chain by interacting with haem-bound proteins. This results in the generation of ROS, cytochrome C release from the mitochondria and caspase mediated apoptosis [146,149].

1.4.4 The role of Iron in artemisinin anticancer activity

Haem and Iron content are important to the anticancer activity of ART and its derivatives [150–152]. Activation of the endoperoxide bridge of ART is thought to be activated by cellular haem resulting in ROS production, DNA damage and apoptosis [149]. Cancer cells are known to have increased haem synthesis and thus increased intracellular iron to facilitate rapid growth and proliferation [153,154]. Transferrin (Tf) is a protein found in human serum which aids in iron transport within the cell [155]. Tf receptor expression can be up to 100-fold higher in cancer cells than non-tumour cells [156]. Furthermore, hypoxia is thought to enhance transferrin expression through the binding of HIF-1 transcription factor [157].

ART derivatives have shown to be selectively toxic in cancer cells due to the increased iron mediated bioactivation [158]. The stimulation of haem synthesis in tumour cells has been shown to increase the activity of ART [111]. Furthermore ART efficacy has shown to be improved with the addition of iron or Tf. An early study in 1995 reported that co-treatment of DHA with Tf was found to increase activity in molt-4 leukaemia cells [159]. Furthermore, this treatment proved to be

selective to cancer cells with 100 times more activity on molt-4 leukaemia cells than non-tumour lymphocytes [159]. Cells co-treated with Tf were hypothesised to increase the peroxide activation leading to increased anticancer activity [159]. Cancer cells often contain higher levels of Tf and Tf receptor expression to sustain cell growth [160,161]. It can be hypothesised that higher levels of these proteins, which are involved in iron uptake and transport, may increase susceptibility to ARTs. For example, breast cancer cells co-treated with DHA and Tf were shown to be selectively toxic to breast cancer cells[150].

Prostate cancer cells also have typically higher numbers of Tf receptor [162]. An ART-Tf conjugate successfully induced apoptosis in DU145 prostate cancer cells [156]. Furthermore, ART-Tf conjugate activity was significantly reduced when Tf receptors were blocked by short interfering RNA (siRNA) [156]. Another study reported the selective toxicity of a DHA-Tf conjugate against leukaemia cells as compared to their non-tumour counterparts [163]. To conclude, iron is central to ART anticancer activity and may explain why selectivity has been observed in cancer cells. There is excellent potential to exploit this Iron-mediated mechanism for the clinical treatment of cancer with ART by modulating haem synthesis and iron transport in target cells.

1.4.5 Artemisinins and multidrug resistance

The lack of resistance to artesunate is promising for the treatment of tumours which are resistant to standard chemotherapy. An *in vitro* study investigated artesunate on several multidrug-resistant cell lines differentially expressing the multidrug resistance gene-1 (MDR-1), multidrug resistance protein-1 (MRP-1) and breast cancer resistance protein (BCRP) genes. All cell lines tested displayed no cross-resistance to artesunate [164]. A separate study compared basal mRNA expression profiles in tumour cells in response to artesunate, arteether or artemether [16]. The results of hierarchical cluster analyses, which correlated IC_{50} values and the mRNA expression of over 400 genes, suggested that genes associated with cellular proliferation may play an important role in ART antitumour action [16]. .

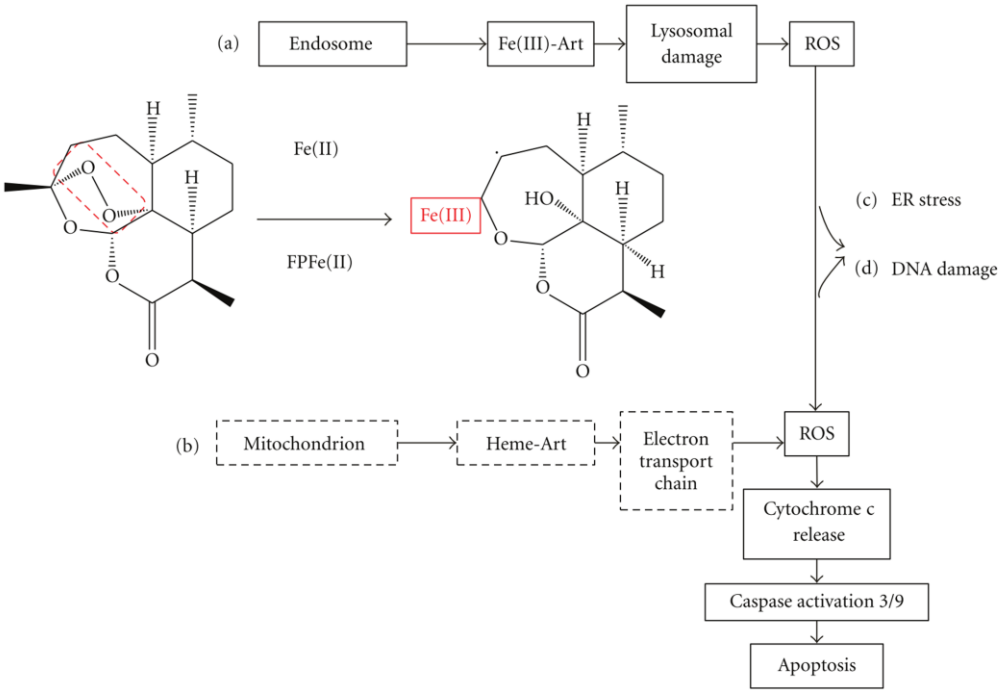

Figure 3 Artemisinin mode of action

ART is thought to induce cancer cell death through the iron mediated breakdown of the endoperoxide subunit (endoperoxide outlined with the broken red line). Two modes of action have been hypothesised; A) ART locates to the endosome where it is activated by free iron from the release of iron from transferrin. Endosome function is then disrupted and lysosomal damage occurs due to ROS production. This ROS production leads to the induction of intrinsic caspase mediated apoptosis; B) Alternatively, activation of ART by haem generates cytotoxic carbon-centered radicals in the mitochondrion. These adducts then may interfere with ETC by interacting with haem-bound proteins leading to generation of ROS and apoptosis [19].

1.5 Naphthalimides

1.5.1 Naphthalimides in cancer treatment

Naphthalimides (NAPs) are drugs containing an aromatic naphthalene system and an imide group and are known to induce apoptosis in tumour cells. NAPs were first synthesised as antitumour agents in 1977 by combining structural components of several anticancer drugs into a single molecule; the β-nitronaphthalene of aristochic acid, the glutarimide rings of cycloheximide and the basic side chain of tilorone [25]. These potent drugs exert their antitumour effects by DNA intercalation [26]. NAPs also disrupt topoisomerase II, enzymes which are essential in regulating DNA topology and coiling of DNA during replication and

transcription [165]. Therefore, NAPs are toxic to fast growing cancer cells with higher DNA replication and cell division as outlined in Figure 1. Two of the most well-known antitumour NAPs are amonafide and mitonafide (Figure 4). These drugs have shown good activity against HeLa cervical cancer cells with IC_{50} values of less than 10 µM [166].

Amonafide has reached phase II clinical trials against a number of cancer types including lung, prostate, cervix with advanced metastatic breast cancer being the most promising [27,167–172]. Amonafide has been reported to induce topoisomerase II-mediated DNA cleavage, which occurs independently of adenosine triphosphate (ATP) availability. This is in contrast to doxorubicin, etoposide, and mitoxantrone which require ATP [173–176]. In addition, amonafide is unaffected by P-glycoprotein-mediated efflux which can lead to resistance in alternate clinical topoisomerase II inhibitors [177]. Reported drawbacks of amonafide include haematological, gastrointestinal and neurological toxicity [178]. Mitonafide also reached clinical trials but was unsuccessful due to neurotoxicity issues [179–181]. Bis-NAPs, consisting of two naphthalimides connected by a covalent linker, were first synthesised in 1993 [182]. Bis-NAPs have been reported to have improved activity as compared to mono-NAP equivalents [182]. Bis-NAP elinafide was found to exhibit high activity against a number of human xenograft models including melanoma, lung and colon cancer [183]. Elinafide also reached phase I clinical trials [184,185].

Thirty patients with advanced malignancies were treated with elinafide at doses ranging from 2 to 24 mg/m^2/d. Although no dose-limiting events were noted in the first two courses of elinafide, cumulative muscular toxicity prevented the repeated treatment with elinafide at doses above 18 mg/m^2/d. The authors concluded that while the preliminary antitumor activity of elinafide was promising, the observed cumulative muscular toxicity warrants a rigorous long-term toxicologic monitoring for future clinical evaluations [184]. A separate study investigated elinafide mode of action by examining the chemical interactions with DNA. NMR studies were reported that elinafide intercalated into the DNA helix with the linker located in the major groove of the DNA helix [186].

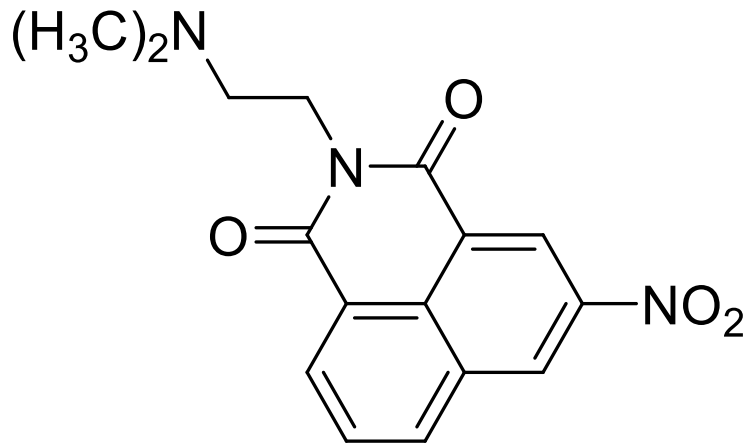

Figure 4 Mitonafide chemical structure

1.6 Anticancer hybrid chemotherapy

1.6.1 Anticancer conjugate drugs

The covalent binding of one drug to another chemical or biological molecule is a concept that has been employed for some time. The aim in this case is usually to target a specific mechanism and improve drug specificity. For example, antibody drug conjugates (ADCs) capable of site-selective drug delivery have proved successful in treating of several diseases [187,188]**.** Calicheamicin is an extremely potent anticancer antibiotic which targets DNA but is limited due to non-tumour toxicity [189,190]. One of the first clinical anticancer applications ADCs was calicheamicin-conjugated humanised anti-CD33 monoclonal antibody under brand name Mylotarg® [191]. This ADC was approved in 2000 for the treatment of elderly acute myeloid leukaemia patients who have who have experienced a relapse and are not suitable for standard chemotherapy. CD33 was chosen as a target in this case at is often highly expressed in cancer cells [192,193]. Specific proteins have also been utilised in conjugates targeting cancer cells [163]. Tf is a protein which has a role in binding iron and Tf receptors are reported to be more abundant on the surface of cancer cells compared to non-tumour cells [151].

Consequently, Tf conjugation has been utilised to direct drugs towards cancer cells. For example, ART derivatives conjugated to Tf have been investigated by several research groups with increased potency and cancer cell selectivity [158,163,194].

1.6.2 Anticancer hybrid drugs

Hybrid drugs are a novel class of chemotherapeutics in which two active drugs are covalently linked to deliver an improved response compared to either "parent" drug alone. The two parent drugs each have their own unique pharmacophore unlike the conjugates described in section 1.6.1. A significant driver for the hybrid approach is the ability to overcome development of resistance to treatment by employing a multimodal drug action. Improved efficacy and safety have been demonstrated in hybrid compounds when compared to their respective parent compounds [7]. Hybrid drugs have been in the treatment of several diseases including anticancer, antibacterial, transdermal and neurodegenerative disorders [7]. Natural products contribute to about half of the drugs currently being utilised in a clinical setting and therefore it is not surprising that many hybrid compounds under development contain natural compounds [12].

1.6.3 Hybrid drug design

Hybrid compounds can be designed by two main methods (1) merging of compatible drug moieties of two drugs and (2) combination of two or more drugs using a linker [195]. The two parent compounds can have either a common target or two distinct targets. In the case of merging of two drugs in a hybrid, there is a chemical bond formed without the use of a linker. Conversely, combination hybrids are connected through a linking arm [195]. Both cleavable or non-cleavable bonds can be employed. When a non-cleavable bond is employed, the objective is to retain the biological activity and target site affinity. On the other hand, the cleavable bond is employed to release two parent drugs under specific enzymatic or physiological conditions present at the target site [7,9,195]. For example, the tumour microenvironment is typically acidic prompting the design of bonds which will cleave upon entering acidic environments [196,197]. This allows anticancer drugs to be slowly delivered to the biological target and also can be utilised to improve

the selectivity of treatment to spare non-tumour cells [195]. In addition, hypoxia inducible prodrugs have also been utilised in cancer therapy [43,198]

1.6.4 Advances in anticancer hybrid research

There has been significant progress made in anticancer hybrid drug research over the past decade [199]. Many of the hybrids are designed to reach a specific target. This section will discuss the effective use of the hybrid approach in a diverse range of anticancer drugs. Microtubule inhibitors [200] and antioxidants [10] are the most commonly employed compounds in novel anticancer hybrids to date and will be discussed to give context to the hybrid approach. ARTs, NAPs and porphyrins have also been employed in hybrid drugs for the treatment of cancer. These hybrids will also be discussed.

Microtubule inhibitor hybrids

Microtubules have been one of the most prominent drug targets for cancer therapy in recent times due to their important role in cell division [201]. Microtubules are proteins compromised of heterodimers of α and β-tubulin, which will bind taxanes, vinca, alkaloids and colchicines in three separate tubulin binding sites [202]. During cell growth, these proteins are polymerised. Several natural products have proved effective in blocking microtubule binding sites and thus inhibiting polymerisation [203,204]. Furthermore, a semi-synthetic derivative of hemiasterlin entitled taltobulin has advanced to clinical trials [205].

Microtubule-targeting agents have been investigated in several novel hybrid drug combinations. By combining different microtubule-targeting agents, it is anticipated that they will work in synergy to deliver increased potency in cancer cells. Taltobulin was conjugated to dolastatin 10, or the dolastatin 15 derivative cemadotin. It was found that several of the hybrids were potent in KB-3-1 (cervical cancer) cells with up to 69% tubulin polymerisation inhibition [200]. A separate study investigated a hybrid containing discodermolide and dictyostatin (hybrid 38) was effective against the taxol-resistant ovarian cancer cell line with an IC_{50} of 8.2 nM [206].

Antioxidant hybrids

Antioxidant drugs can prevent the build-up of excessive ROS which are known to cause damage to lipids, proteins and DNA within the cell. Lipids are the most susceptible to oxidation; lipid peroxidation leads to the generation of lipid free radicals which further attack lipid molecules leading to cell death [207]. Protein damage can also occur with increased levels of ROS and oxidative stress. ROS can induce irreversible chemical reactions with protein backbone, and the side chains of nearly all amino acids. In addition some lipid peroxidation by-products, such as 4-hydroxy-nonenylaldehyde, can form protein adducts and impair their function [208]. DNA can also be damaged under severe oxidative stress by alteration of DNA bases by highly reactive hydroxyl radicals ($OH^{\bullet}$) [63]. Thus, antioxidants have been employed as chemoprotective agents [209,210]. Conversely, antioxidants have been employed as antitumour agents with cancer cell toxicity reported [211]. A potential strategy to improve cancer therapy is the conjugation of antioxidants with a known anticancer agent. For example, several dietary antioxidants were conjugated with paclitaxel to create a series of novel hybrid drugs [6]. The resulting hybrids were evaluated for cytotoxic activity against several human tumour cells as well as the corresponding non-tumour cells. Most drug hybrids were effective against tumour cell lines tested including prostate, lung and breast cancer [6]. A hybrid consisting of a glycinate ester salt conjugated with paclitaxel was particularly effective in reducing Panc-1 cell growth. In pancreatic cancer treatment, the same hybrid was shown to selectively toxic with less activity in E6E7 non-tumour cell line [6].

Both coumarin and chalcone are naturally occurring antioxidants with known anticancer activities [212–215]. Recently a series of coumarin-chalcone hybrids were synthesised [10]. Among 21 hybrids tested, the three most effective hybrid drugs produced IC_{50} range from 3.59 to 8.12 μM against four human cancer cell lines, KB (oral squamous cell carcinoma), C33A (cervical cancer), MCF-7 (breast cancer), A549 (lung cancer) [10]. One hybrid drug showed a 30-fold increase in activity towards C33A (cervical carcinoma) cells over non-tumour fibroblast NIH3T3 cells with an IC_{50} value of 3.59 μM [10].

Artemisinin hybrids

ART is a well-tolerated natural compound with both antimalarial and anticancer properties as discussed in section 1.4. ART derivatives have already been employed in hybrid compounds designed for malaria treatment [216]. Hybrid compounds are an attractive alternative to conventional malaria treatment with the potential to minimise the potential for drug resistance. For example, fast acting ART was combined in a hybrid with slow acting quinine were combined in a hybrid molecule and proved more effective in *plasmodium falciparum* strain of malaria [14]. The rationale was that quinine would act to kill off any remaining parasites which had evaded ART treatment. The hybrid was indeed more potent than ART alone [14]. More recently, arterolane was combined with piperaquine in a hybrid which showed excellent cure rate in *P. falciparum* malaria during phase II clinical trials [217,218]. This promising evidence suggests that future treatment of malaria may well involve hybrid drugs. The successful adaption of the hybrid approach in ART based malaria treatment has led to the hypothesis that such compounds may also be more effective in cancer treatment.

ART based hybrids have been previously developed and investigated for anticancer efficacy by our collaborators in this work. For example, ART-acridine hybrids showed a 2-4-fold increase in activity against HL60, MDA-MB-231 and MCF-7 cells when compared to DHA [8]. Artesunate has also been investigated as a combination therapy with tumour necrosis factor related apoptosis inducing ligand (TRAIL). This *in vitro* investigation involved pre-treatment of HeLa cervical cancer cells with artesunate for 3 h before incubation with TRAIL [24]. Pre-treatment of HeLa with artesunate was found to sensitise the cervical cancer cell line to TRAIL with increased apoptosis detected. The authors also reported that artesunate/TRIAL combination treatment inhibited the expression of X-linked inhibitor of apoptosis protein XIAP protein, which is involved in anti-apoptotic signalling by binding to active caspase-3 and caspase-7 and by preventing caspase-9 activation [24,219]. ART has also been combined with glycolipids in a conjugate which showed improved anticancer activity in oral cancer cells. Furthermore, this conjugate showed five times more anti-oral cancer activity than

either cisplatin or paclitaxel [220]. More recently, ART-chalcone hybrids were synthesised and investigated for anticancer activity in several cancer cell lines including Breast, colorectal and cervical cancer. Several hybrids showed improved activity and selectivity as compared to DHA [221]. The hybrid and conjugate examples discussed here highlight the potential to improve the properties of ART for improved cancer treatment. Reported drawbacks of short half-life and recrudescence in ARTs may well be improved upon hybridisation [222,223].

Naphthalimide hybrids

NAPs, previously discussed in section 1.5, are potent anticancer agents. They have also been incorporated into drug hybrids. For example, a study in 2002 investigated a group of Pyrrolobenzodiazepine (PBD)-NAP hybrids. The second parent, in this case, PBD, is known to bind to guanine residues in the minor groove of DNA and thus has been investigated as a potential anticancer agent [224]. The results of this study showed hybrids had significant DNA binding activity [225]. The same authors later developed coumarin linked NAPs which showed good anticancer activity against colon, breast and lung cancer cell lines [226]. Polyamines are ubiquitous small molecules essential in many functions in human health and are thought to be often dysregulated during cancer [227,228]. Polyamine-NAP conjugates were synthesised with the aim of improving tumour cell selectivity. They were then investigated in leukaemia and melanoma cells [229]. Interestingly, tumour cell selectivity was improved with hybrid compounds as demonstrated by higher activity in human hepatoma BEL-7402 as compared to non-tumour QSG-7701 cells [229].

Porphyrin hybrids

Photodynamic therapy (PDT) is based on the administration of a photosensitiser (PS), prior to external light activation. Upon light activation, toxic radicals such as singlet oxygen cause cell damage and toxicity [230]. Porphyrins are a group of heterocyclic organic compounds which are widely employed in PDT [231]. PDT and porphyrins are discussed in detail in Chapter 3. For over a decade, porphyrins

have been combined with other structures to improve anticancer efficacy. Conjugation of porphyrins with metal complexes has been investigated. In 1997, a series of porphyrin ligands were combined with platinum (II) complexes. The combination of cytostatic platinum with the cytotoxic porphyrin resulted in improved efficacy in MDA-MB-231 breast cancer cells [232]. This synergistic effect highlights the potential of porphyrin combinations as a promising anticancer strategy. There are several more recent examples of platinum-porphyrin hybrids with demonstrable anticancer effects [233–236]. Another metal, ruthenium, has also been utilised in porphyrin-based hybrids. Several ruthenium(II)–porphyrin hybrids were investigated in HeLa cells with hybrids 1–3 producing high singlet oxygen quantum yields and cytotoxicity upon light activation. The author also reported a correlation between cellular uptake and PDT efficacy [237].

Combining porphyrins with DNA crosslinking agents has also been investigated. A series of porphyrin-DNA cross linker/intercalator hybrids were investigated in human leukemic cell line TF-1. Porphyrin-chlorambucil combination was particularly effective in reducing TF- 1 cell growth at low concentrations [238]. However, it must be noted that steric hindrance was an issue reducing overall DNA binding activity compared to chlorambucil alone [238]. A more recent study reported the evaluation of porphyrin–DNA crosslinking hybrids against THP-1 leukaemia cells. The hybrids proved effective with IC_{50} values in the nM range [239,240]. The same author further examined porphyrin–DNA crosslinking conjugates in HeLa and HepG2 (liver cancer) cells. Again, excellent anticancer activity was observed with the tested compounds producing an IC_{50} range of 0.182-6.983 μM in HeLa cells and 0.293-3.308 μM in HepG2 cells. Apoptosis was confirmed by confocal microscopy and flow cytometry [240].

1.7 Aims and objectives of this study

The overall aim of the current study was to evaluate the cytotoxicity of ART-porphyrin hybrids and ART-NAP hybrids in both tumour and non-tumour cell lines. Hybrids were then examined further to investigate their mode of action and the potential for tumour cell selectivity. Oxygen availability is often crucial for effective chemotherapy and radiotherapy with hypoxia induced resistance reported to

adversely affect patient outcome. However, oxygen concentration remains overlooked during early drug development in which atmospheric oxygen levels have become the standard procedure. This study incorporated the maintenance of oxygen environment during *in vitro* evaluation to better mimic *in vivo* conditions.

The more specific objectives of the project are as follows:

1. Determine the effect of oxygen availability on anticancer drug efficacy *in vitro*: the anticancer efficacy of artesunate was investigated in HeLa cells at 3 different oxygen conditions; atmospheric oxygen, normoxia and hypoxia.

2. Perform a cytotoxic evaluation of novel anticancer hybrids across four cell lines: this was achieved through real-time cell analysis and cell count analysis of both hybrid compounds and their respective “parent drugs”. This analysis was performed at an *in vivo* relevant oxygen concentration of 4% (v/v).

3. Determine the tumour cell selectivity of hybrid drugs: by analysing the data generated during cytotoxic evaluation. Novel hybrid selectivity was evaluated by comparing activity in prostate tumour and non-tumour cell lines.

4. Investigate the mechanisms involved in hybrid drug action: Apoptosis, DNA damage/repair, ROS generation and glutathione antioxidant response were investigated in the most promising hybrid drug candidates to uncover the molecular mechanisms responsible for their drug action.

Chapter 2. In vitro oxygen availability modulates the effect of artesunate on HeLa cells

2.1 Introduction

Tissue hypoxia is defined as a decrease in oxygen availability below critical levels which compromises the function of cells tissues or organs [34]. This critical value has been identified in a previous clinical study as pO_2 of <10 mm Hg or <1.3%(v/v) oxygen [241]. Hypoxia often develops in tumours due to poor blood supply and inadequate oxygen diffusion. More than 50% of solid tumours exhibit areas of hypoxia throughout the tumour mass, with areas of anoxia (no oxygen availability) also occurring [35]. Tumour cell oxygenation was first shown to be a key factor in the efficacy of radiation treatment of cancer over 50 years ago [242]. Furthermore, many chemotherapeutic drugs are dependent on the oxygenation of the tumour mass for optimal efficacy. Tumour cells in normoxic conditions were shown to be more sensitive to melphalan, a DNA alkylating chemotherapeutic, when compared to cells under hypoxic conditions [243,244]. Hypoxia dramatically alters cell cycle distribution with the majority of cells in G1/S phase arrest [245].

Consequently, chemotherapeutics which target DNA may be susceptible to hypoxia-induced resistance due to a substantial reduction in cell division and DNA replication. DHA, an ART derivative discussed in Chapter 1, was shown to be 30% more effective in an oxygen rich environment when compared to a low oxygen environment in the treatment of *P. falciparum* strain of malaria. Furthermore, hypoxia was thought to increase DHA activity at lower concentrations in epithelial cells [246]. Despite the evidence suggesting that hypoxia is crucial in chemotherapy outcome, related *in vitro* assays in an oxygen-rich environment remain the norm [39,242–244]. Such levels are well beyond normoxic/hypoxic levels typically experienced by non-tumour tissues/tumour masses [42,43]. This chapter investigates the potential for these lower oxygen concentrations to potentiate the antitumor efficacy of artesunate *in vitro*. HeLa cell growth was measured in real-time in response to artesunate treatment in different oxygen environments; atmospheric oxygen (21%), normoxia (4%) and hypoxia (1%). Cell count analysis was performed to validate real-time data.

2.2 Hypoxia

2.2.1 Definition of hypoxia

Hypoxia occurs due to inadequate oxygen supply to cells and tissues of the body. Due to highly regulated processes in the body, increased blood flow occurs to meet oxygen demand and maintain homeostasis. However, when the oxygen demand is greater than supply, hypoxia can occur in a given tissue type [35]. Since the development of a commercially available oxygen electrodes in the 1990's, which enabled investigators to make accurate measurements of oxygen levels in human tumours, it is now understood that oxygen concentrations in human tumours are heterogeneous with many areas experiencing hypoxic conditions (>2%) [247,248]. More than 50% of solid tumours exhibit areas of hypoxia throughout the tumour mass [249]. In tumours, oxygen supply to cells can be reduced considerably and in some cases, cease completely. This is due to abnormal blood vessels, inadequate diffusion and anaemia [250]. When both tumour and non-tumour tissue oxygenation levels are compared, it is clear that the tumour tissue will often have lower oxygen levels [251]. Furthermore, hypoxia-induced changes in gene expression may result in tumour progression by allowing tumour cells to withstand nutrient deprivation and grow in an unregulated manner. Hence, hypoxic tumours may be associated with a more aggressive phenotype [34].

Tumour tissue derived from cervical cancer, prostate cancer, breast cancer, head and neck carcinoma, glioblastoma and soft tissue carcinoma displayed oxygen levels varying from 0.3-2.4% (v/v) (2-18 mmHg) [43]. Indeed, it is likely that oxygen levels fall even further during treatment with chemotherapeutic drugs and other cytotoxic agents [252]. While atmospheric oxygen concentrations range from 20-21% oxygen (160 mmHg), in lung alveoli, the oxygen level is reduced to about 14.5% oxygen (110 mmHg). It drops even further in the blood and, by the time it reaches peripheral tissues, the oxygen levels range from 3.4% to 6.8% with an average of about 6.1%.

Table 1 summarises oxygen levels typically present in the atmosphere, and in some human tissues and tumours. It is clear, from this table, that oxygen varies depending on tissue type and location. The atmosphere typically contains 21% (v/v) oxygen and is used as standard in most *in vitro* investigations. However,

tissue oxygen levels *in vivo* are much lower. For example, lung alveoli were found to contain 14.5 % oxygen [253]. The mid-range of oxygen in peripheral non-tumour tissues was reported to be 5.3%. On the other hand, solid tumours were found to have a lower mid-range of 1.1% oxygen [43]. The table also highlights that lower oxygen levels are present in prostate tumour tissue when compared to non-tumour tissue; 3.9% oxygen was detected in non-tumour prostate when compared to 0.8% in prostate tumour xenografts and 0.3% in prostate tumours *in situ* [251,252].

mm Hg	% (v/v) Oxygen	Description
760	100.0	Atmospheric pressure
160	21.1	Approx. oxygen in inspired air
110	14.5	Approx. oxygen in lung alveoli
40	5.3	Mid-range of oxygen levels in peripheral tissues
8.6	1.1	Mid-range of oxygen levels in solid tumours
30	3.9	Level in non-tumour prostate
6	0.8	LNCaP prostate tumour xenografts
2	0.3	Level in human prostate tumours *in situ*

Table 1 Oxygen levels in the atmosphere, non-tumour and tumour tissues

The table above summarises the varying oxygen levels in the atmosphere, human tissues and tumours. The data was obtained from several previous studies [43,247,251–253]. See [43] for a more detailed comparison of human tumour oxygenation studies.

2.2.2 Role of hypoxia in malignant progression

Non-tumour cells can survive brief periods of hypoxia through cell cycle arrest and energy conservation [254,255]. However, prolonged hypoxia is known to cause cell death [256,257]. Furthermore, Hypoxia has been implicated in malignant progression [248]. Solid tumours are understood to have poor blood vessel network with many defects [43] This leads to areas of hypoxia or anoxia within the tumour mass. While hypoxia is toxic to both tumour and non-tumour cells, tumour cells evade cell death by adapting to the adverse hypoxic environment. In this way, there is a natural selection for hypoxia-resistant cells [258].

There are many molecular mechanisms which must be activated in tumour cells to allow survival in hypoxia. These include changes in gene expression, regulation of tumour suppressor genes and activation of oncogenes and genetic instability [259]. Hypoxia is also known to induce changes in the proteome to overcome oxygen deprivation [260]. This is achieved through hypoxia stimulated angiogenesis, glycolysis and inhibition of apoptosis and up-regulation of growth factors. VEGF is a key growth factor in the promotion of blood vessel formation and is strongly up-regulated in hypoxia and in tumours [261,262]. In addition, erythropoietin (EPO) production is often up-regulated in hypoxia which stimulates the production of haemoglobin and red blood cells thus increasing the oxygen transport capacity of a growing tumour mass [263]. All of these changes support tumour cell survival [264].

2.2.3 Regulation of hypoxia and the HIF-1 pathway

Hypoxia is a potent mediator of gene expression with 20% of the entire genome thought to be affected [265]. Hypoxia-inducible factor (HIF) is the most important transcription factor associated with hypoxia-dependant changes in gene expression [266]. HIF is a heterodimer comprising of an oxygen-labile α subunit (HIF-1α) and a constitutively expressed β -subunit (HIF-1β). There are 3 different isoforms of HIFα present in the body: HIF-1α, HIF-2α and HIF-3α; all of these isoforms contain an oxygen-dependent degradation domain (ODD). HIF-1α and HIF-2α are the most structurally similar and are well characterised. HIF-3α exists as multiple splice variants, some of which inhibit HIF1α and HIF2α activity [267].

Under normoxia (Figure 5A), HIF-1α is hydroxylated by prolyl-hydroxylase domains (PHDs). Hydroxylated HIF-1α is then recognised by the Von Hippel-Lindau protein (pVHL) which triggers ubiquitylation by ubiquitin-ligase complex thereby marking HIF-1α for degradation by the 26S proteasome [268,269]. PHD enzymes require oxygen to catalyse their target substrates. Under hypoxia (Figure 5B), these enzymes are prevented from hydroxylating HIF-1α. This allows HIF-1α to escape hydroxylation, recognition and degradation. HIF-1α then accumulates and is translocated to the nucleus where it can combine with HIF-1β to form the HIF-1 complex. This complex, in turn, binds to small regions of DNA, termed hypoxia responsive elements (HRE), which are present in the promoter regions of oxygen-sensitive genes [259,266].

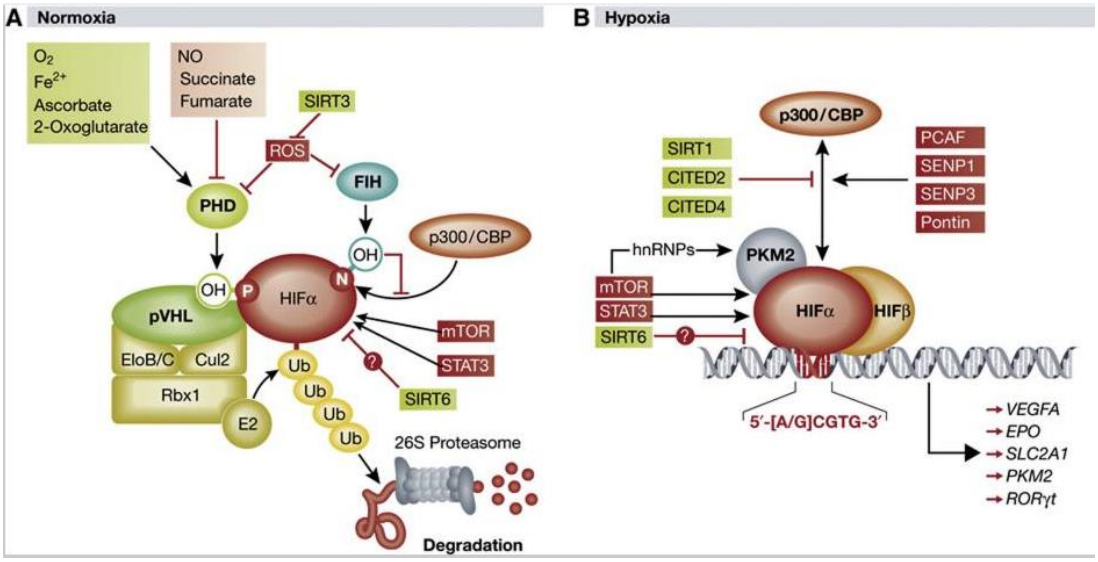

Figure 5: Expanded models for HIFα regulation in normoxia and hypoxia

(A) Under normoxia, HIFα is prolyl hydroxylated by PHDs, which allows for recognition by pVHL and its associated ubiquitin–ligase complex. Ubiquitylated HIFα is then degraded by the 26S proteasome. The prolyl-hydroxylase activity of PHDs is regulated by several intracellular factors, including ROS, which are negatively regulated by SIRT3. HIFα gene expression is upregulated by mTOR and STAT3, while SIRT6 negatively regulates HIFα protein levels. (B) Under hypoxia, HIFα escapes prolyl hydroxylation by PHDs and combines with HIFβ to avoid degradation. The heterodimer then binds to HRE's in oxygen-sensitive genes such as VEGFA and EPO to activate transcription and gene expression [270].

Hypoxia inducible genes are involved in several key cellular processes including angiogenesis, erythropoiesis, and glucose metabolism [266]. HIF-1 has been shown to initiate erythropoiesis by regulating the expression of multiple genes encoding proteins responsible for the uptake and delivery of iron and haemoglobin synthesis; these genes include transferrin ceruloplasmin [271] hepcidin [272] and EPO receptor [273]. HIF-1 has a key role in regulating angiogenesis in response to hypoxia by activating the expression of several genes which encode for angiogenic growth factors including vascular endothelial growth factor (VEGF) [266,274]. Interestingly, HIF-1α treatment was found to overcome limb ischemia in an older mice model by improving angiogenesis and the perfusion of growth factors and cytokines [275].

HIF-1 regulates glucose metabolism in response to hypoxia [258]. Under hypoxia, glucose metabolism switches from the oxygen-dependent tricarboxylic acid (TCA) cycle to glycolysis which does not require oxygen [264]. This metabolic switch is a fundamental characteristic of cancer cells (Figure 1) and thus hypoxia and HIF-1 have been implicated in tumorigenesis [276]. Pyruvate kinase (PK) enzymes are involved in the final rate-limiting step of glycolysis, which catalyses the transfer of a phosphate group from phosphoenolpyruvate (PEP) to ADP, producing pyruvate and ATP. Previous studies demonstrated that hypoxia induces PK mRNA expression through the HIF Pathway. Aldolase A, liver type phosphofructokinase, and phosphoglycerate kinase genes were all found to contain HIF-1 binding sites mediated by hypoxia-induced transcription in transient expression assays [277]. PKM2 was found to interact with HIF-1α in the nucleus and to function as a transcriptional coactivator in HeLa cervical cancer cells and Hep3B liver cancer cells. PKM2 was increased HIF-1 binding to HREs in target genes and the recruitment of the p300 coactivator. Subsequently, HIF-1 target genes were transactivated including glucose transporter 1 (SLC2A1) and phosphoinositide-dependent kinase-1 (PDK1) [278].

It has also been hypothesised that HIF-1 has a role in the immune response to hypoxia. RAR-related orphan receptor gamma t (RORγt) is a short isoform of the orphan nuclear receptor which is important in the development and function of interleukin (IL)-17 producing inflammatory effector T cells known as T_H17 cells. It has been shown that HIF-1 regulates the balance between T regulatory (T_{reg}) and T_H17 differentiation by enhancing T_H17 development through transcriptional activation of RORγt.

Sirtuins (SIRTs) are a family of NAD-dependent deacetylases which have several cellular localisations and functions. For example, SIRT1 and SIRT2 are found in both the nucleus and cytoplasm. SIRT1 is the most well studied and is involved in the regulation of metabolism, inflammation and tumorigenesis [279]. Recent reports have linked HIF to the SIRT proteins; SIRT1, SIRT3 and SIRT6 can regulate the activity of HIF proteins [280–283]. It was demonstrated that SIRT1 binds to and deacetylates HIF-1α which prevents p300 recruitment to the promoter regions of HIF-1 target genes. Consequently HIF-1 transcriptional activity is supressed [283]. This would indicate that SIRT1 functions to negatively regulate HIF mediated transcription. However, there has been debate with regards to SIRT1 interaction with HIF. Another report suggested that that SIRT1 does not target HIF-1α, but deacetylates HIF-2, promoting HIF-2 transcriptional activity [282]. Interestingly, increased ROS production has been shown to correlate with reduced levels of prolyl-hydroxylated HIF-1α [284,285]. This effect was later owed to the inhibition of PHD catalytic activity resulting in HIF-1α stabilisation and increased HIF mediated transcription [286].

In conclusion, HIF is a crucial transcription regulator affecting a vast array of target genes. The HIF pathway (Figure 5) plays an important role in cellular response to hypoxia with both positive and negative regulation mechanisms. It also has been suggested that increased levels of ROS may cause increased HIF mediated transcription. Therefore, this pathway may be important in the response of cancer cells to ROS inducing anticancer agents in hypoxia.

2.2.4 The impact of hypoxia on cancer treatment

For many years hypoxia has been observed as a therapeutic problem during cancer treatment due to the adverse impact on radiotherapy [36,37]. This adverse effect results from an insufficient supply of oxygen for reactive oxygen species production during radiotherapy. It is estimated that three times higher doses of ionising radiation are required to have similar biological effects when hypoxia develops [38]. Furthermore, many chemotherapy drugs are less effective for several reasons. Firstly, hypoxic cells are often distant from blood vessels which mean that anticancer drugs can often not reach the target site. This perfusion limitation also means that hypoxic tumour cells proliferate slower than normoxic counterparts leaving them less sensitive to anticancer drugs that target faster DNA replication in cancer cells [43]. Many anticancer drugs are oxygen dependent to facilitate production of toxic ROS. Finally, hypoxia initiates the selection of cells that have lost sensitivity to p53-mediated apoptosis. Examples of anticancer drugs that have shown resistance in hypoxia PDT agents and DNA intercalators such as porphyrins, doxorubicin and cisplatin [287,35].

On the other hand, hypoxia has the potential to be exploited for superior cancer treatments [43]. The main strategies to date include prodrugs activated by hypoxia, hypoxia-selective gene therapy, targeting HIF-1 and recombinant anaerobic bacteria based therapy [43,249,250]. In hypoxia prodrug design, the hypoxia-selective cytotoxicity requires one-electron reduction of a non-toxic prodrug to a free radical that then becomes a substrate for back-oxidation by oxygen to the original compound. Therefore, hypoxia-dependent cytotoxicity ensues for a more targeted drug action. 4-[3-(2-nitro-1-imidazolyl)-propylamino]-7-chloroquinoline hydrochloride (NLCQ-1) is a hypoxia-activated prodrug which has reached clinical trials. The prodrug, containing chloroquinoline DNA-targeting agent linked to 2-nitroimidazole, was found to be enhance the efficacy of in cyclophosphamide (CPM) against SCCVII murine tumours and PC-3 human xenografts. NLCQ-1 in combination with nontoxic CPM doses resulted in a delay of 4-12 days in tumour regrowth as compared to CPM alone. Furthermore no systemic toxicity was observed as a result of this combination treatment [288]. It was also found that NIPCQ enhances the antitumor effects of DNA alkylating agents, 5-fluorouracil, and paclitaxel against the same murine tumour model and PC-3 human

xenografts. Pre-treatment with NLCQ-1 was found to delay tumour growth by 11 days and 10.3 days in 5-fluorouracil and paclitaxel respectively [289,290].

2.2.5 Artemisinins and hypoxia

ART is the frontline therapy for malaria treatment globally and has also been found to have excellent anticancer properties [111]. ART has been discussed in detail in chapter 1. During anti-angiogenesis cancer therapy of solid tumours, areas of hypoxia can occur and cause resistance to chemotherapy [291]. However, it has been hypothesised that this “Achilles heel” can be transformed into an advantage during iron-mediated ART treatment [291]. Indeed, ART co-treatment with iron has proved effective in treating these hypoxic tissues in the past [292]. Hypoxia results in upregulation of hypoxia inducible factor-1 (HIF-1) which can then induce an increase in Tf receptor transcription. It has been hypothesised that the resulting increase in iron uptake may well increase ART activation and overcome hypoxia-induced resistance [291].

ART derivatives have been evaluated in different oxygen environments. ART was shown to be 30% more effective in an oxygen rich environment (21% oxygen, or 152 mm Hg) when compared to a low oxygen environment (1%, 7.6 mm Hg) in the treatment of *P. falciparum* strain of malaria [116]. In 2011 the activity of DHA was evaluated in human dermal microvascular endothelial cells at different oxygen concentrations [246]. DHA had significantly increased activity in hypoxia at low doses (0.01-0.8 μM). However, DHA was more effective in atmospheric oxygen at high doses (50-200 μM) [246]. The authors hypothesised that ROS production at low doses (0.5 μM) by DHA could be controlled by antioxidants present in the cells. However, at high doses (50 μM) the level of ROS produced is sufficient to overcome antioxidant defences [246]. While these endothelial cells are not cancerous, they are reported to exhibit some common responses when exposed to hypoxia, such as changes in cell growth and the induction of angiogenesis [246]. Consequently, the findings are useful to understand how ART compounds may act in hypoxia.

More recently DHA activity was analysed in several colorectal cancer cells in both atmospheric oxygen conditions (21 %(v/v)) and severe hypoxia (0.2 %(v/v)) utilising a hypoxic chamber [293]. DHA was found to be active in hypoxia but no

significant change in necrosis or apoptosis activity was observed as compared to normoxia. Interestingly, cytochrome c release from the mitochondria and caspase-activation were observed only under normoxic conditions, whereas, under hypoxic conditions DHA induced caspase-independent apoptosis. This may partly explain why DHA does not display resistance in hypoxia [293]. In 2014, artesunate was investigated against HepG2 (human) and BWTG3 (mouse) liver cancer cells in atmospheric (21 % (v/v) oxygen) or hypoxic conditions (1 % (v/v) oxygen). It was found that 50 μM artesunate significantly reduced cell viability and increased caspase-3 activity. Interestingly, artesunate efficacy was enhanced by hypoxia with a significant reduction in cell viability at concentrations of 12.5 μM and higher [294]. These studies involving artesunate and DHA add further evidence to the hypothesis that oxygen availability may improve artesunate anticancer efficacy *in vitro*. If this is the case, then artesunate may be even more potent than originally perceived during *in vitro* analyses.

In this chapter, real-time cell analysis (RTCA) software was employed to investigate HeLa cell sensitivity to artesunate in varying oxygen environments of atmospheric oxygen, normoxia and hypoxia. To our knowledge this is the first time that artesunate efficacy has been evaluated in HeLa cells in hypoxia. HeLa cervical cancer cells were employed as a tumour cell line model and are known to be sensitive to artesunate though notably when analysed in oxygen rich conditions [24,149]. For this study, it was necessary to choose a drug with known anticancer activity. Artesunate is a semi-synthetic derivative of ART with anti-malarial and anti-cancer activity and was chosen for this analysis [18]. The work in this chapter has been peer reviewed and published in 2014 [295].

As previously discussed in section 1.3.2, surgery, radiation and chemotherapy are routinely used in combination to cancer patients [66–70]. Chemotherapy usually involves drug administration at regular intervals to destroy the tumour. However, during *in vitro* analyses, the common approach is to administer the drug at one time point prior to measuring cell growth or cell viability [296]. For this work, an alternative drug addition schedule was applied where two doses of artesunate were added at 24 h and 48 h post seeding, rather than one, with the aim of improving artesunate anticancer efficacy *in vitro*.

2.3 Methodology

2.3.1 Cell culture

HeLa cervical cancer cells (European Collection of Cell Cultures) were cultured in Dulbecco's Modified Essential Medium (DMEM F12) (Sigma-Aldrich, UK) supplemented with 5% Foetal Bovine Serum (Sigma-Aldrich, UK) and 1% Penicillin /Streptomycin (Sigma-Aldrich, UK) and 1% L-Glutamine (Sigma-Aldrich, UK). Cells were maintained at 37°C, 95% humidity, 5% (v/v) CO_2.

2.3.2 Oxygen maintenance

In addition to the cell culture conditions, cells were maintained at oxygen concentrations of either 1% (v/v) (7.6 mm Hg), 4% (v/v) (30mm Hg) or 21% (v/v) (160 mm Hg) for a minimum of 24 h before any experiment was commenced and until analysis was completed. This was achieved using specialised Thermo 3110 CO_2 incubator (Thermo Fisher Scientific, UK). Nitrogen feed was used to maintain the incubator at the desired oxygen concentration [295].

2.3.3 Preparation and addition of artesunate

Artesunate was kindly provided by Dr Sarah Rawe, School of Chemical and Pharmaceutical Sciences, Dublin Institute of Technology. Artesunate was dissolved in dimethyl sulfoxide (DMSO) to make master stock solutions. DSMO was chosen as a the most commonly used solvent for *in vitro* cytotoxicity assays. Furthermore, artesunate is known to be soluble in DMSO at 100 mM concentration [297].These stock solutions were then further diluted in fresh complete medium to make working stock solutions, such that when added to cells, the desired final concentrations of artesunate were achieved with a final DMSO concentration of 0.1% (v/v) maintained in all cells.

2.3.4 Real-Time Cell Analysis

Real-Time Cell Analysis (RTCA) was employed to evaluate HeLa growth following artesunate treatment in varying oxygen environments (Figure 6). RTCA was chosen ahead of other cytotoxicity assays because it does not require dye metabolism which may be partially affected by varying oxygen availability (due to the function of oxygen as an electron acceptor during oxidative phosphorylation) [298]. In addition, RTCA allows for the measurement of cell growth in real time which

is advantageous in determining specific drug response profiles in treated cells [299]. Cells are seeded onto the specially designed E-plates which contain microelectrodes covering approximately 80% of the total surface area. Each E-plate well has approximately the growth surface area as in a 96 well plate (0.3165 cm^2/well). The electrodes measure the electrical impedance across each well. In the absence of cells, there are only background levels of electrical impedance at the electrode/solution interface. As cells attach and grow onto the well surface electrical impedance increases accordingly (Figure 6). The RTCA system quantifies cell status based on the measured cell-electrode impedance and converts this data to a parameter termed cell index (CI). CI is derived, according to the following equation:

$$CI = \max_{i = 1,\ldots,N} \left(\frac{R_{cell}(f_i)}{R_b(f_i)} - 1 \right)$$

$R_b(f_i)$ and $R_{cell}(f_i)$ are the frequency-dependent electrode resistances (function of impedance) without cells or with cells present, respectively, and N is the number of the frequency points at which the impedance is measured. Therefore, CI is a quantitative measure of the overall status of the cells incorporating changes in adhesion, growth, size, and morphology. In addition, the RTCA system allows CI to be normalised at the point of drug addition (i.e. 24 h after seeding). At a given time point, normalised CI is calculated by dividing the CI at the time point by the cell index at a reference time point. Thus, the normalised cell index is 1 at the reference time point. This allows for a more precise comparison of the cellular response to different treatments from the time of drug addition onwards. For further detail regarding the RTCA measurement principle, refer to Solly et al [300].

E-plates (ACEA Biosciences, USA) were seeded with $5x10^3$ HeLa cells per well 24 h before artesunate exposure. E-plates were placed within the cradle of an xCELLigence DP RTCA instrument that remained inside the incubator for the duration of the experiment. After 24 h incubation at 37 °C, half the culture medium was removed and replaced with an equal volume of fresh medium (control), DMSO (vehicle control) or artesunate working stock to achieve the desired final concentrations of 0, 10 or 50 µM. The final DMSO concentration was maintained

at 0.1% (v/v) in both vehicle control and treated samples. Artesunate was also investigated in a two-dose regime. In this case, cells were treated at 24 h and 48 h. Cell growth was measured every 15 min for the duration of the experiment, beginning 24 h before the first drug addition and continuing for further 48 h. Cell growth is expressed as CI. CI was normalised up until the point of drug addition allowing changes in cell growth to be analysed only after this point.

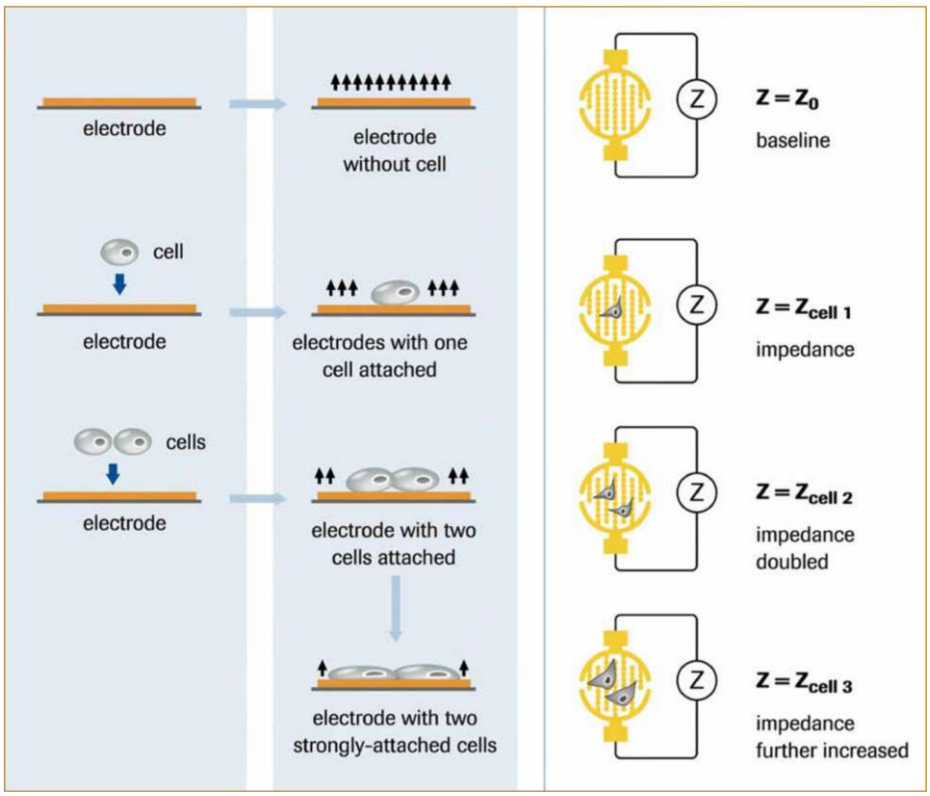

Figure 6 Real-time cell analysis (RTCA) principle

The principle of RTCA: As cells adhere to electrodes on the surface of the E-plate well, electrical impedance is increased. The more cells that attach and grow onto the microelectrodes, the larger the impedance signal. Conversely impeadance signal will be reduced as cells die and detach in response to different treatments. Impedance is measured every 15 minutes throughout analysis to measure cell growth In real time [301].

2.3.5 Cell count analysis

To validate RTCA data obtained, cell count analysis was performed using the Z2 particle analyser (Beckman Coulter® USA). This instrument was used to count cells based on size. HeLa cells were seeded on a 6 well plate (Sarstedt) at $1x10^5$ cells per well (equal density to real-time cell analysis). After 24 h incubation at 37 °C, half the culture medium was removed and replaced with an equal volume of fresh medium (control), DMSO (vehicle control) or artesunate to achieve the desired final concentrations of 0, 10 or 50 µM. The final DMSO concentration was maintained at 0.1% (v/v) in both vehicle control and treated samples. Artesunate was also investigated in a two-dose regime. In this case, cells were treated similarly at 24 h and 48 h after seeding. Cells were harvested and counted 0 (time 0), 24 or 48 h later using a Z2 Particle Analyser (Beckman Coulter, USA). Cell counts are expressed as a percentage of the time 0 control.

2.3.6 Statistical analysis

Data is representative of three independent experiments performed in triplicate ± standard deviation (SD). Data graphing and statistical analysis were performed using GraphPad Prism 5.0. Significant differences in a single parameter (i.e., treated versus untreated) between samples were determined by one-way ANOVA and Tukey's multiple comparison test. This test assumes a Gaussian distribution and compares every mean with every other mean. Significant differences in two parameters (i.e., cell lines) were determined by two-way ANOVA and Bonferroni post hoc test. Again, a Gaussian distribution is assumed, but in this test, a family of comparisons is compared rather than each individual treatment. In this work, the test is employed to detect a difference in response between two cell lines exposed to the same set of treatments. In both tests $p < 0.05$ was chosen as the criterion for significance. (*=$p \leq 0.05$, **= $p \leq 0.01$, ***= $p \leq 0.001$).

2.4 Results

2.4.1 Effect of oxygen concentration on artesunate efficacy in HeLa cells

In vitro RTCA was performed at three different oxygen concentrations, 21% (atmospheric oxygen), 4% (normoxia) and 1% (hypoxia). Cells were either exposed to control (fresh growth media), vehicle, 10 µM artesunate or 50 µM artesunate (Figure 7). In atmospheric oxygen conditions, 10 µM artesunate reduced cell growth more than 30% after 48 h and 50 µM artesunate reduced HeLa cell growth by over 80% after 48 h.

When oxygen availability was reduced to that of normoxic conditions, an increase in artesunate efficacy was observed. 10 µM artesunate reduced cell growth by 35.1% after 24 h and 73.2% after 48 h. In normoxia, 50 µM artesunate rapidly reduced cell growth from approximately12 h onwards with nearly a 95% reduction in cell growth at 48 h. When artesunate is analysed in hypoxic conditions, a similar increase in HeLa cell sensitivity to the drug was observed. 10 µM artesunate reduced cell growth by 52% and 70% after 24 and 48 h respectively. Furthermore, 50 µM artesunate treatment reduced cell growth from 10 h onwards, resulting in an 88% reduction in cell growth after 48 h.

Cell count analysis was also performed in oxygen concentrations of either 21% (atmospheric oxygen), 4% (normoxia) or 1% (hypoxia) to validate RTCA data. HeLa cells were either exposed to control (fresh growth media), vehicle, 10 µM artesunate or 50 µM artesunate 24 h after seeding. Cells were harvested and counted using a Beckman Coulter Z2 particle analyser at 0, 24 or 48 h post exposure (Figure 8). All data expressed as a percentage of cell numbers at time 0 (time of drug addition). In atmospheric oxygen, 10 µM artesunate significantly reduced cell number after 48 h ($p \leq 0.01$). Furthermore 50 µM artesunate reduced cell number even further at 24 h and 48h ($p \leq 0.01$, $p \leq 0.001$). In normoxia, an increase in artesunate efficacy was observed when compared to atmospheric oxygen levels. This is evident after 48 h treatment with 10 µM artesunate with a significant reduction in cell number observed ($p \leq 0.001$). 50 µM artesunate also causes a significant decrease in cell growth ($p \leq 0.001$). A similar HeLa cell response was observed in hypoxia with a significant reduction in cell growth detected after 48 h treatment with artesunate ($p \leq 0.001$).

A

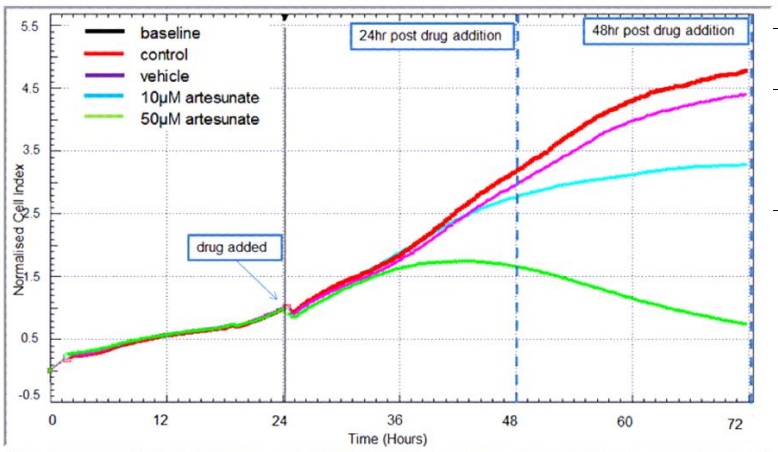

	Cell Index (% Control)	
	24 h	48 h
Control	100.0	100.0
Vehicle	94.0	93.8
10 μM artesunate	87.9	68.8
50 μM artesunate	54.5	16.7

B

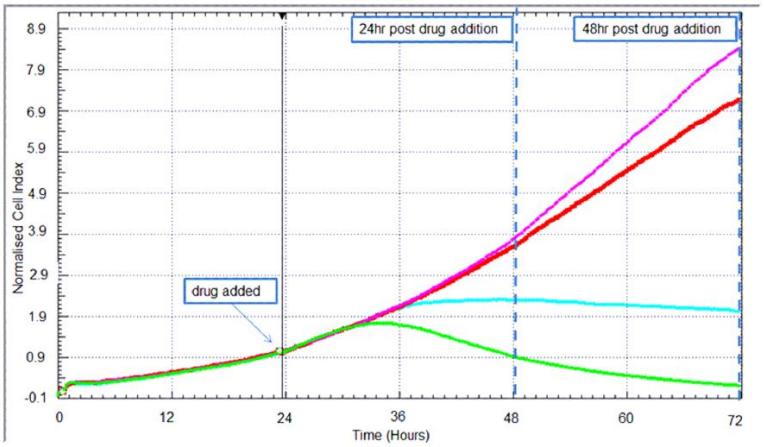

	Cell Index (% Control)	
	24 h	48 h
Control	100.0	100.0
Vehicle	102.7	115.4
10 μM artesunate	64.9	26.8
50 μM artesunate	24.3	4.2

C

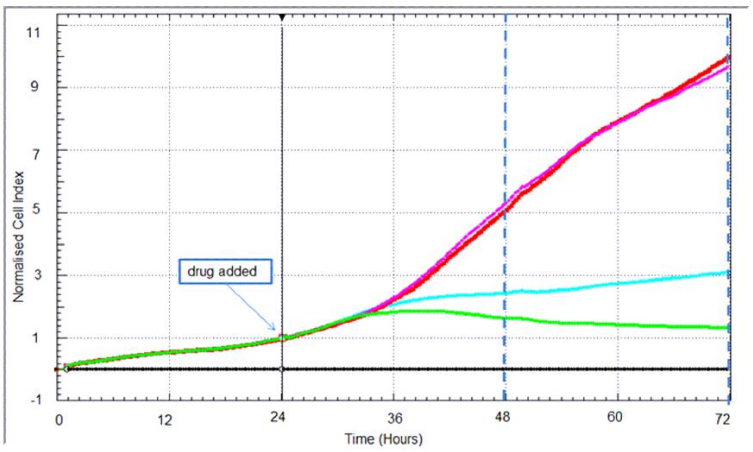

	Cell Index (% Control)	
	24 h	48 h
Control	100.0	100.0
Vehicle	102.0	98.0
10 μM artesunate	48.0	30.0
50 μM artesunate	32.0	12.0

Figure 7 Real-time cell analysis of HeLa cells in response to artesunate

Real-time cell analysis of HeLa cells in (A) 21% oxygen, (B) 4% oxygen or (C) 1% oxygen conditions. HeLa cells seeded at 5×10^3 cells/well, treated with drugs after 24 h growth and measured using RTCA instrument until experiment end at 72 h. Cell growth is plotted as cell index (CI) on the y-axis. On the right of each real time graph is a corresponding table sumarising the mean CI values recorded for each treatment at 24 h and 48 h (time points indicated by broken blue lines); CI values are expressed as % control. Each real-time experiment was performed three times in triplicate.

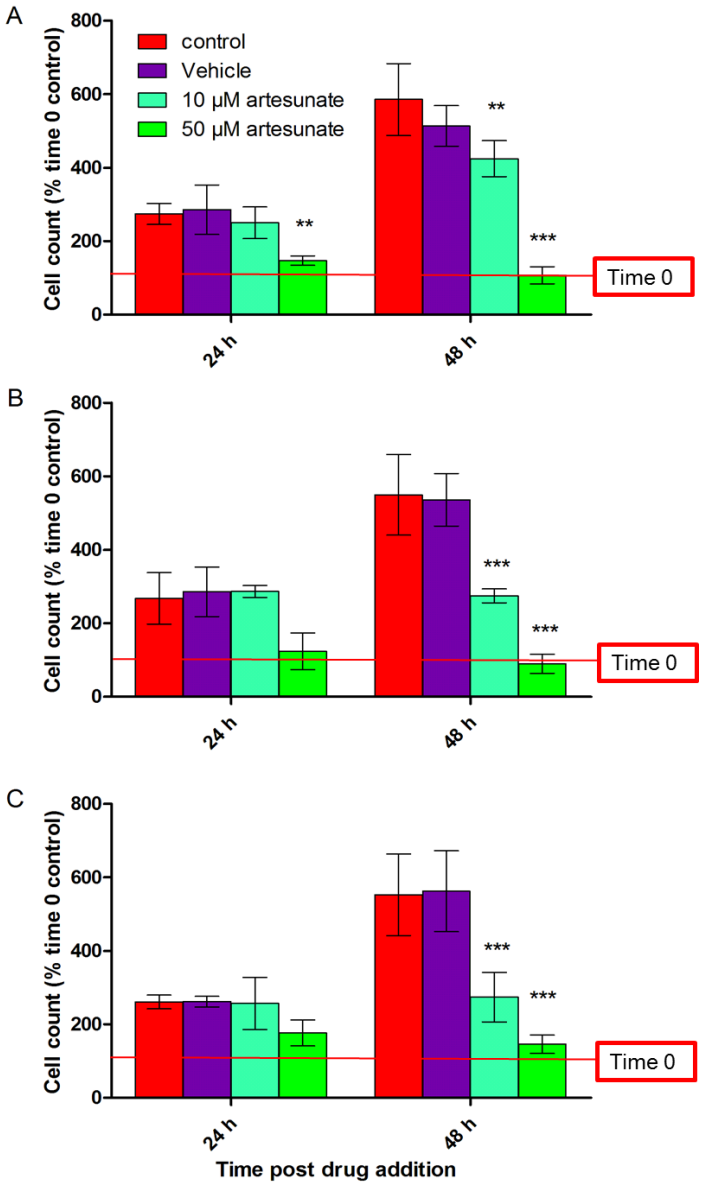

Figure 8 HeLa cell count analysis

HeLa cells maintained in either (A) 21% oxygen, (B) 4% oxygen or (C) 1% oxygen conditions. HeLa cells seeded in 6-well plates at a density of $1x10^5$ cells/well. 24 h later cells were exposed to either fresh growth media (control), 0 µM (vehicle), 10 µM or 50 µM artesunate. Cells were harvested and counted at 24 or 48 h post drug addition. Data is expressed as a percentage of cell numbers at time zero (drug addition). All data is representative of 3 experiments performed in triplicate (±SD). Differences between treated/exposed and sham-exposed/control cell populations were analysed using one-way ANOVA, with Tukey post hoc test using $p<0.05$ as the criterion for significance (*$p\leq0.05$, **$p\leq0.01$, ***$p\leq0.001$).

2.4.2 The effect of two separate administrations of artesunate in HeLa growth

HeLa cell growth was accessed in real-time for 48h after the first drug addition with 10 or 50 μM artesunate (Figure 9A). A second drug addition took place 24 h later in selected wells. The vehicle had no effect on cell growth following similar growth profile to the untreated control. Artesunate was effective against HeLa cells with 50 μM artesunate treatment resulting in an 87.9% reduction in cell growth after 48 h treatment. However, there was no significant improvement of artesunate efficacy in one verses two treatments of artesunate with similar growth profiles observed at equivalent concentrations. Cell number was also accessed 48 h after first drug addition (Figure 9B). A similar trend was observed with artesunate treatment resulting in a decrease in cell number at 10 and 50 μM. However, there was no significant difference in cell numbers observed between one treatment verses two treatments of artesunate.

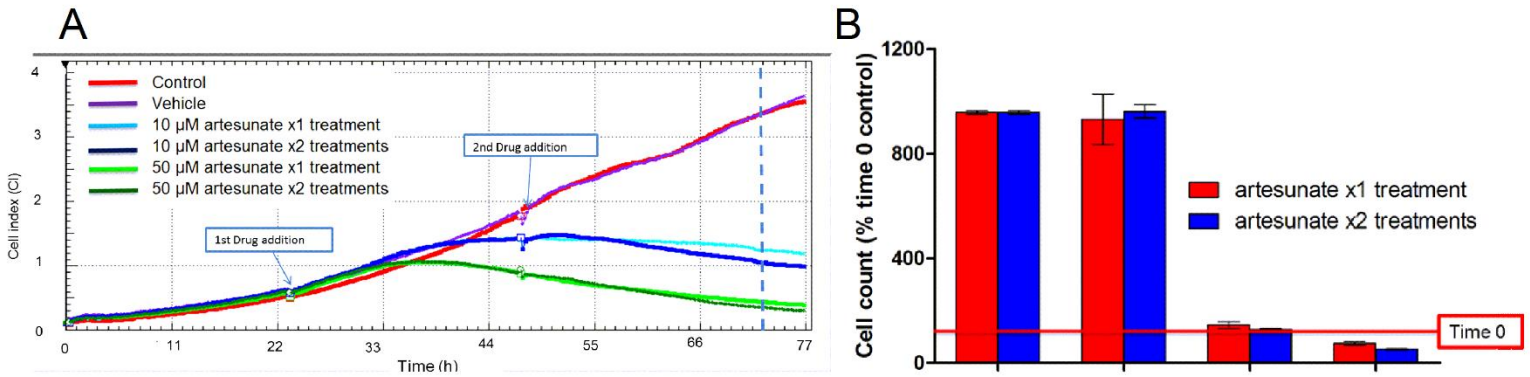

	Cell Index (% Control) 48 h (after first treatment)
Control	100.0
Vehicle	100.0
10 µM artesunate x1	36.4
10 µM artesunate x2	35.3
50 µM artesunate x1	12.1
50 µM artesunate x2	9.1

Figure 9 The effect of two separate artesunate treatments *in vitro*

(A) HeLa cells were seeded at $5x10^3$/well and maintained at 4% (v/v) oxygen. 24h later HeLa exposed to either fresh growth media (control), 0.1% DMSO (Vehicle), 10 µM artesunate or 50 µM artesunate. After a further 24 h, a second dose was added to selected wells by removal of all spent media followed by addition of the same treatments again. Cell growth was monitored using RTCA until experiment end at 72 h. Cell growth is plotted as cell index (CI) on y-axis. Below the real time graph is a corresponding table sumarising the mean CI values recorded for each treatment at 48 h (time point indicated by broken blue line); CI values are expressed as % control. (B) HeLa cells were seeded at $8x10^4$ cells/well onto 6 well plates and maintained at 4% (v/v) oxygen. 24 h later, HeLa were treated with either fresh growth media (control), 0.1% DMSO (Vehicle), 10 µM artesunate or 50 µM artesunate. After a further 24 h, a second dose was added to selected wells by removal of all spent media followed by addition of same treatments again. Cells were harvested and counted 48 h after the first drug addition. Data is expressed as a percentage of cell numbers at time 0 (time of first drug addition). Both data sets above are representative of a single experiment performed in triplicate.

2.5 Discussion

Hypoxic regions are typically present within solid tumour masses due to inadequate blood supply. Hypoxia is associated with a more aggressive tumour phenotype which often displays resistance to chemotherapy and radiotherapy [35,241,302]. Moreover, chemotherapeutic drugs are often dependent on oxygenation of the tumour mass for optimal efficacy [243,244] . However, despite the evidence that tissue oxygenation is important in response to chemotherapy, almost all *in vitro* cytotoxic assays to date have been performed in a standard oxygen-rich environment of 21% (v/v) or 160 mm Hg.

In this chapter, real-time cell analysis (RTCA) was employed to investigate the effect of oxygen in potentiating Hela cell response to artesunate; this assay responds to changes in cell growth, cell number, cellular adhesion, cell size and morphology thus giving an indication of overall cell status. RTCA data is generated every 15 minutes in real-time rather than at selected time-points on a bar graph [301,303]. The resulting data is automatically converted to cell index (CI) by the software as described in section 2.3.4. As cells detach and die (due to a cytotoxic agent) the surface area covered by cells is reduced and CI values decrease. HeLa cell growth was analysed in real-time at oxygen concentrations of 21% (atmospheric), 4% (normoxia) or 1% (hypoxia). In this study, it was demonstrated that artesunate potency against HeLa cervical cancer cells is enhanced as oxygen concentration is varied from atmospheric levels to *in vivo* relevant normoxia and hypoxia. In atmospheric oxygen conditions (Figure 7A), artesunate was shown to be effective against HeLa with 50 µM artesunate reducing HeLa cell growth by over 80% after 48 h.

However, when oxygen availability was reduced to in-vivo body relevant oxygen concentrations of 4% (normoxia) (Figure 7B) and 1% (hypoxia) (Figure 7C) a significant increase in artesunate efficacy was observed; this was evident in normoxia with 10 µM and 50 µM artesunate reducing cell growth by 73.2% and 88% after 48 h respectively. When artesunate is analysed in hypoxic conditions, a similar increase in HeLa cell sensitivity to the drug was observed compared to that of atmospheric oxygen. Cell count analysis was also performed to quantify cell numbers at 0, 24 or 48 h post drug addition (Figure 8). Again, an increase in

artesunate efficacy against HeLa cells can be observed when oxygen availability is lowered to either normoxia or hypoxia in agreement with the real-time data. This is evidenced by a significant reduction in cell numbers following 48 h treatment with either 10 µM or 50 µM artesunate in normoxia and hypoxia ($p \leq 0.001$). This is significant as many aggressive malignant tumours exhibit areas of hypoxic tissue. Therefore artesunate, and indeed many other chemotherapeutic agents, assessed at atmospheric oxygen may be more potent against cancer cells *in vivo* than originally thought. This highlights the need to consider the employment of lower oxygen levels such as normoxia or hypoxia during novel drug analyses *in vitro*.

Repeated exposures to the same drug are standard in chemotherapy with the patient administered the drug on a daily basis over a predetermined time course [304–308]. Conversely, during novel *in vitro* drug analyses treatment is often limited to a single drug addition [309,310]. It was hypothesised that two treatments of artesunate may be more effective in reducing HeLa cell growth and cell number when compared to a single treatment. To investigate this hypothesis, HeLa cell growth and cell number were quantified in response to one verses two treatments of artesunate (Figure 9). As expected, artesunate reduced HeLa cell growth and cell number in agreement with the previous experiments in normoxia (section 2.4.1). However, the second artesunate treatment did not appear to offer an advantage, with a similar growth profile recorded in HeLa treated once and those treated for a second time.

2.6 Conclusions

Oxygen levels were shown to potentiate the anticancer efficacy of artesunate *in vitro* with an increased reduction in HeLa cell growth and cell number in normoxia and hypoxia when compared to atmospheric oxygen levels. Consequently, there is a need to incorporate oxygen concentration as a key variable for future novel drug analyses *in vitro*. HeLa cells showed a similar response to artesunate regardless of whether one or two treatments of artesunate were employed suggesting that there is no advantage in administering more than one treatment *in vitro.*

Chapter 3. Analysis of porphyrin-based light activated hybrids

3.1 Introduction

Photodynamic therapy (PDT) is a clinically approved minimally invasive therapy. PDT involves 3 key components, a photosensitiser (PS), light, and oxygen. While none of these elements are independently toxic, when combined they produce highly toxic oxygen free radicals. The procedure involves either systemic or topical administration of a PS, followed by irradiation of the diseased area with light of a specific wavelength (which corresponds to the absorbance band of the PS) [30–32].

3.1.1 The history of PDT

The use of light to treat diseases dates back over 4000 years when the Egyptians treated vitiligo with a combination of sunlight and orally ingested plants containing light-activated psoralens [311]. Modern day PDT began in 1900 when Oscar Raab discovered that a combination of acridine and light were lethal to a species of *paramecia* [312]. Parenteral administration of a photosensitiser (PS) in humans was first performed in 1900 by a French neurologist, who used orally administered eosin to treat epilepsy. However, he discovered that this treatment caused dermatitis to develop in sun-exposed skin [29]. The first anticancer application of PDT in humans occurred in 1903 when topically applied eosin was combined with white light to treat skin tumours [313].

Porphyrin-based PDT began in 1913 when Mayer-Betz injected himself with haematoporphyrin (Hp) isolated from blood. He reported no toxic effects until he exposed himself to sunlight which resulted in severe swelling and pain [314]. In addition, prolonged photosensitivity was reported for two months after exposure. In the early 1950's, Schwartz showed that phototoxicity was caused by an oligomeric mixture of the material formed during the isolation of Hp from blood and not Hp as previously hypothesised [314]. Haematoporphyrin derivative (HpD) was first synthesised in 1960 by treating Hp with acetic acid and sulphuric acid to remove some of the non-active components. It was observed that HpD led to fluorescence of neoplastic lesions visualised during surgery [315].

Interestingly, developments in PDT research were slow to advance and it was not until many years later in 1975 when Dr Thomas Dougherty and co-workers at the Roswell Park Cancer Institute in Buffalo reported the first successful treatment of tumours in mice following administration of HpD and activation with red light. Mice and rats carrying mammary tumours were given 2.5–15 mg/kg HpD [316]. Tumours were then exposed to red light from a xenon arc lamp for three times in 5 days. Almost half of the transplanted mouse mammary tumours were cured. Similar results were observed with rat tumours induced via immunosuppression with a dose of 15 mg/kg HpD. Lower doses of HpD or light failed to induce tumour regression, and neither drug nor light alone had any effect [316]. Dougherty followed this animal study with the first controlled clinical trials involving PDT when he investigated HpD against 113 malignant tumours. He observed a complete or partial destruction of 111 tumours [317].

HpD was later purified to become Photofrin® which became the first clinically approved PS for PDT in 1993 when regulatory approval was secured in Canada for the treatment of bladder cancer [318,319]. Dougherty's success brought the concept of PDT to a wider audience and subsequently HpD based PDT was clinically investigated to treat several cancer types including lung [320], breast [321,322], gastrointestinal [323], brain [324], colorectal [325] and pancreatic cancer [326]. However, the use of Photofrin® in clinical cancer treatment has reported drawbacks of lack of specificity, dark toxicity and sub-optimal wavelength for tissue penetration. However, the success of Photofrin® has prompted the synthesis of several hundred second generation PSs with the aim of producing a PS with more desirable properties and thus a more effective treatment [327]. The most successful second generation PS's to date include 5-aminolevulinic acid (ALA), benzoporphyrin derivative (BPD) and m-tetrahydroxyphenylchlorin (mTHPC). All have proven effective clinically and are commercially available today [328–330].

3.1.2 PDT photochemistry

Absorption of energy by a PS occurs between the electronic energy levels of molecular orbitals [331]. A Jablonski energy diagram can be used to illustrate this process (Figure 10). PSs absorb light energy and therefore increase the energy of ground state electrons to the excited state [332]. PSs in the ground state contain electrons in a singlet state (no net spin, S=1). Following light activation one of these electrons is boosted to a higher energy level but remains in the singlet state. This singlet state is unstable, however, and quickly emits this energy through fluorescence or heat before returning to ground state. However, if one of the spin-paired electrons undergoes spin inversion via intersystem crossing (ISC), the result is a spin aligned pair of electrons [333] (Figure 10).

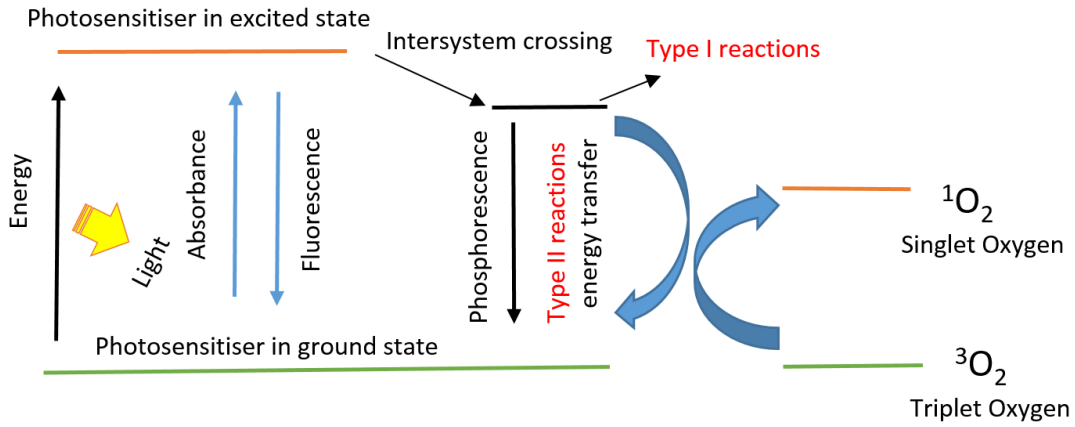

Figure 10: Jablonski diagram showing photochemical reactions which occur during PDT

Light activation during PDT converts a PS from a ground singlet state to an excited state. The molecule in this excited state (S1) can undergo intersystem crossing to form oxygen radicals from either type I or type II reactions. Type II reactions lead to the production of singlet oxygen which is thought to the major cytotoxic agent generated during PDT. Figure adapted from [33].

The PS is now in its triplet state (net spin of 3, S=3). This triplet state PS can undergo one of two possible reactions: Type I and Type II [334]. A type I reaction occurs when the PS reacts directly with a substrate molecule resulting in the removal of a hydrogen atom or electron transfer causing the production of free radicals and thus oxidative damage [335,336]. In Type II reaction a PS transfers its energy to the stable triplet state of molecular oxygen. The oxygen gains energy from excited PS causing one of the oxygen's unpaired electrons to undergo a spin inversion reducing net electronic spin to zero [33]. Thus, oxygen is now in its extremely reactive singlet excited state, referred to as singlet molecular oxygen ($^1O_2$) [337]. The type II mechanism and the cytotoxicity of singlet oxygen is thought to be the primary mechanism responsible for the cytotoxic effects of PDT [315]. However as low oxygen concentration and hypoxia is typical of the tumour microenvironment, this can result in a greater reliance on type I reaction during PDT [334].

Two-photon excitation (TPE) is a non-linear optical process in which a molecule is promoted to an excited state by simultaneous absorption of two photons. This concept has been successfully applied in confocal fluorescence microscopy for some time now [337,338]. TPE achieves the same effect as one-photon excitation at half the wavelength, promoting a molecule into its singlet excited state [339,340]. This means that optimal excitation of PSs can be achieved by deeply penetrating light (infrared region) of the electromagnetic spectrum thus maximising the PDT effect when employed for clinical purposes. Two-photon PDT has been explored since 1990 and has several potential advantages over conventional one-photon PDT including deeper penetration of tissues, reduced side effects and higher doses are achievable [341].

3.1.3 Light source

Many light sources have been adapted for use in PDT. They can be categorised into three main groups; broadband lamps, light omitting diodes (LEDs) and lasers [342]. The first light sources used in PDT were conventional lamps where the output was varied by use of filters which facilitated activation at specific wavelength range. These light sources were readily available and cheap but were limited by photosensitivity, the generation of high temperatures and the difficulty in

regulating light dose [343]. LEDs were also developed for use in PDT. LEDs are small solid-state semiconductors with emission in a narrow bandwidth of 20–50 nm without infrared emission and give a broad spectrum of illumination. They were an attractive alternative to lamps as they are compact, lightweight, user-friendly and require lower energy levels to produce the desired wavelengths of light [344,345]. Fluorescent lamps have also been employed successfully in PDT to treat skin cancer and keratosis where large surface areas require activation. In this case, the PS is topically administered and the limitation of light penetration is not a concern [346,347].

The development of lasers which emit light in focused beams at precise wavelengths signalled an important breakthrough in PDT. This light source is by far the most common methodology employed for light activation during PDT with the advantages of increased power output, better control of dosimetry and are compatible with fibre optic technology for more [342,343]. Several types of lasers have been developed for PDT. These include argon dye laser [348], potassium-titanyl-phosphate (KTP) dye laser [349] and diode lasers [350]. The argon dye laser has been widely used because it is possible to alter the wavelength of these systems to absorption wavelength of the PS by adjusting the filters inside the laser, thus allowing the flexibility of using it for activation of different PSs [348]. For example, the argon dye laser can easily produce wavelengths of 630 nm for HpD, 635 nm for the activation of ALA/PpIX and 652 nm for mTHPC. The next major advance in laser technology for PDT came with the invention of KTP:YAG/dye laser combination system [351]. This is a modular unit that uses a potassium titanyl phosphate (KTP) laser (pulsed wave as opposed to continuous wave) [352]. This system had advantages over other systems employed in PDT including portability, fine dose adjustment, and fibre optic compatibility [353]. The laser system used can be chosen depending on PS used and the depth of tumour within the tissue.

Another important potentiator of PDT response is the drug-light interval. The drug-light interval is usually between 1 and 7 days *in vivo* but this parameter varies between tumour type and tumour size [354,355]. Shorter drug-light intervals may also be desirable in some cases as the PS remains in blood vessels resulting in enhanced vascular damage depriving tumour tissue of nutrients [356]. The

influence of drug-light interval was investigated in nude mice bearing human malignant mesothelioma xenografts. Administration of 0.3 mg/kg mTHPC was performed at a light dose of 10 J/cm^2 at 650 nm for varying time intervals. The results demonstrated activity of mTHPC varied significantly with the time interval between drug administration and activation and was greatest at an interval of 3 days [354]. This highlights the dose-light interval as an important variable to investigate when evaluating a new PDT therapy.

3.2 PDT in cancer treatment

PDT has been investigated in the treatment of several cancer types *in vitro* and *in vivo* including skin [357], breast [358], prostate [359,360], bladder [361,362] and colorectal [363] cancers. Following these successful preclinical studies, numerous clinical trials were performed involving several different photosensitisers leading to the approval of PDT, using porfimer sodium (Photofrin®) for the treatment of bladder cancer in 1993 [327]. Other approvals of PDT for clinical use followed including ALA (Levulan®) [364] mTHPC (Foscan®) [328]. PDT has become useful as a non-invasive alternate therapy in the treatment of pre-cancerous lesions and localised cancers [313]. The PDT procedure begins when a photosensitiser (PS) is introduced into target tissue either by topical or parenteral administration. The PS is then allowed to accumulate in the diseased tissue over time. This PS should cause little or no toxicity prior to light activation (dark toxicity). A controlled light dose activates the drug resulting in the production of highly toxic singlet oxygen [315].

3.2.1 Photosensitiser development for cancer treatment

PSs are compounds which absorb light of a specific wavelength, and in combination with molecular oxygen, have the ability to generate highly cytotoxic singlet oxygen [331]. PSs are generally aromatic structures that are efficient at undergoing intersystem crossing and forming long-lived triplet excited states. The ideal PS have an absorption peak of 600-800nm to allow penetration through tissue *in vivo*. Additional desirable attributes include high purity, high singlet oxygen yield, photochemical reactivity, preferential retention by tumour cells, rapid excretion from the body and low dark toxicity [33]. There have been numerous efforts to synthesise new improved PSs for superior cancer therapy. They can be divided into three distinct generations.

HPDs including Photofrin® were the first PSs clinically employed. Photofrin® was used in the treatment of several cancers including esophageal [365], bladder [318], cervical [366], pancreas [367], brain[368] , lung [369], breast [370] and non-melanoma skin cancer [371]. Even though this Photofrin® satisfies some criterion for an ideal PS, it has several drawbacks such as having a long wavelength (does not penetrate further than 0.5cm), weak absorption band, and prolonged photosensitivity [372]. The success of Photofrin® did, however, lead to the intense development of new and improved PSs. HpD and its purified derivatives Photofrin®, Photoset® and Photoheme® are all classified as first generation PSs [372–374].

Second generation PSs were then developed with better properties and lower toxic side effects. Second generation PSs demonstrate higher absorption levels (650-800nm) facilitating deeper tissue penetration [328,375]. Their tissue accumulation is much shorter and therefore, the treatment can be carried out on the same day as the administration of the drug. Moreover, second-generation PSs are chemically pure and show lower toxicity and a lower photosensitivity than first generation PSs [376]. In addition, they have up to 100 times more activity reported than Photofrin® in animal models owing to their increased capability to generate toxic oxygen free radicals [80]. ALA, BPD, lutetium texaphyrin, temoporfin (mTHPC), talaporfin sodium (LS11) and Foscan® are examples of second generation PSs. ALA is a naturally occurring PS that is converted to PpIX in the haem biosynthetic pathway (discussed further in section 3.2.4). ALA has been employed in the clinical treatment of precancerous lesions [378], and non-melanoma skin cancers [379].

An improvement of the tumour selectivity of PSs remains a major challenge in PDT. Third generation PSs have been developed by conjugation of a PS to monoclonal antibodies or other protein carriers for a more targeted delivery [380–382]. Tumour surface markers including glucose transporters [383], growth factor receptors [384], transferrin receptors [385] and folic acid receptors [386] have been conjugated to PSs in the hope that they will direct the PS to tumour site. In addition, nanostructure delivery methods are being developed to increase PS concentrations at the tumour site [387,388].

3.2.2 PDT mode of action

PDT has three distinct mechanisms of action: (1) direct tumour cell toxicity; (2) damage to tumour cell vasculature and (3) robust inflammatory response that can induce systemic immunity [331]. At a cellular level, exposure to PDT generally results in one of two cell death pathways; necrosis or apoptosis [389]. In the necrotic pathway, PDT damages cellular and subcellular membranes which can trigger the release of organelle contents [390]. In the apoptosis pathway, cell death is achieved by cell signalling in response to PDT mediated stress [391,392]. PDT-induced apoptosis usually occurs through extrinsic or intrinsic pathways. Extrinsic apoptosis is initiated by death receptors of the TNFR superfamily. These receptors activate caspase-8, which in turn activates downstream caspases [393]. The activation of extrinsic apoptosis has been shown to occur following a number of PDT experiments *in vitro* [394,395].

The mitochondrial mediated intrinsic apoptosis pathway has also shown to be activated in response to PDT [396]. This pathway is characterised by depolarisation of the outer mitochondrial membrane. This membrane then becomes permeable leading to the release of cytochrome-c into the cytosol. Cytochrome-c then interacts with apoptotic protease activating factor 1 (Apaf-1) and deoxyadenosine triphosphate (dATP) forming the apoptosome. Once formed, the apoptosome triggers the activation of caspase-9 which then activates caspase-3. Caspase-3 subsequently activates the remainder of the caspase cascade resulting in PARP cleavage and finally apoptosis [393]. Most PSs are lipophilic and localise in the intracellular membrane systems such as the mitochondria; therefore, it is not surprising that PDT-mediated apoptosis is most often reported to occur through the intrinsic pathway [397].

The Bcl-2 family of pro-apoptotic and anti-apoptotic proteins (discussed in section 5.3.2) have been shown to play a role in PDT response. Bax was found to translocate to mitochondria during apoptosis in HeLa cells after PDT with zinc (II) phthalocyanine [398]. Another study showed the Bax expression was key to mono-L-aspartyl chlorin e6 (Npe6) mediated PDT in Lewis lung carcinoma cells. A time dependant increase in Bax expression was observed in response to PDT [399]. Phthalocyanine mediated PDT was found to damage antiapoptotic protein Bcl-2.

MCF-7c3 cells (human breast cancer cells expressing stably transfected procaspase-3) were transfected to overexpress wild-type Bcl-2 or Bcl-2 mutants. It was found that wild-type Bcl-2 protected cells from apoptosis caused by phthalocyanine -PDT. In contrast, Bcl-2 which lacks the C-terminal transmembrane domain (cannot be photodamaged) did not provide this protection [400.]

DNA damage (oxidative damage and strand breaks) has also been reported in response to PDT in vitro [401,402]. For example, metallophthalocyanine based PDT was investigated in A549 lung cancer cells, MCF-7 breast cancer cells and SNO esophageal cancer cells. DNA damage was quantified using a comet assay. The results indicated that PDT caused significant levels of DNA damage in all three cell lines tested [402]. PDT using a porphyrin-derivative has also been reported to cause direct DNA damage[403] and the production of 8-oxo-Guanine, a by-product of DNA oxidative damage [404]. A separate study also utilised the comet assay to evaluate DNA damage and repair in murine glioblastoma C6 cells after PDT with mTHPC. There were significant increases in DNA damage after light activation of mTHPC. However the cells appeared to recover from this DNA damage after 4 h and no DNA damage was evident after 24-h post-treatment [405]. The data generated to date indicates that DNA damage occurs after PDT but is not necessarily lethal to cells. The effect of PDT on DNA damage will also depend on the DNA repair mechanisms within the cell [406].

PDT is also known to cause damage to the tumour vasculature and induce a pro-inflammatory response [407]. Long-term tumour response to PDT was diminished or absent in immunocompromised mice suggesting that the immune response is important to PDT outcome. This immune response provoked by PDT is thought to be due to inflammation at the tumour site. While complete tumour destruction is not achieved, this response is thought to be beneficial for long-term tumour control [408]. Pre-clinical and clinical studies have demonstrated that PDT induces a response from both the innate and the adaptive immune system [409–411]. However the PDT-induced immune response depends on the area treated, and the photosensitizer type [381]. The immune stimulatory properties of PDT offer a promising approach to developing antitumour immunity involving memory T cells that can potentially prevent the recurrence of cancer [408].

3.2.3 Future perspectives for PDT

PDT remains a promising antitumor strategy but its full potential has yet to be discovered, and its range of applications has not been fully exhausted. PDT is an attractive alternative to surgery, chemotherapy, or radiotherapy and does not compromise future cancer treatment options. Despite great progress and a large body of research focused on developing new PSs with more desirable properties for clinical efficacy, some limitations still prevail. Poor solubility in water, low chemical purity high dark toxicity[412], photosensitivity[413], resistance[406], and non-homologous distribution of PS [315] have been reported.

PDT, by nature, is a localised therapy as only the target tissue is irradiated with light. This localised nature often limits complete destruction of metastatic lesions which is the leading cause of death in cancer patients [414]. Reduction in oxygen levels may also reduce the efficacy of PDT since singlet oxygen arises from ground state oxygen [340]. Light irradiation is known to cause a reduction in oxygen concentrations in tissues [242,415,416]. Consequently, PDT procedure can lead to low oxygen concentration and areas of hypoxia in the target site causing reduced singlet oxygen yield [417]. In addition, PDT efficacy may be reduced with lower concentrations of glucose which is known to occur in cancer cells and is referred to as the Warburg effect [418,419].

To overcome the shortcomings of current PDT, there must be a focus on bringing PS to the target site, improving tumour selectivity and closer monitoring PDT in real-time. Conjugation of a PS to an imaging agent may allow for accurate determination of PS localisation and better control of dosimetry [420,421]. Improved delivery systems are being investigated and offer huge potential for future PDT. The incorporation of PSs into various nanocarriers, including lipid vesicle carriers and polymeric carriers, is a popular strategy [422–424]. Conjugation of PS with monoclonal antibodies or other protein carriers is a promising approach to achieve increased tumour selectivity [380–382]. Tumour surface markers including glucose transporters [383], growth factor receptors [384], transferrin receptors [385] and folic acid receptors [386] have been conjugated to PSs with the aim of improving PDT outcome. The immune system is thought to be modulated by PDT [425]. This property could be exploited to activate a systemic immune response against the

tumour which may overcome metastatic cancer cells for a more complete PDT response [426–428].

3.2.4 Porphyrin-based PDT

Protoporphyrin IX (PpIX) is a naturally occurring organic compound belonging to the porphyrin family and a constituent of haemoglobin PpIX is produced in the body as an intermediate in the haem biosynthetic pathway [379]. PpIX has also become widely researched in PDT due to its light activation properties and is utilised in many of the porphyrin-based hybrids for this study. PpIX is typically excited with red light at an absorption band around 635 nm (Figure 11) [412,429]. PpIX based PDT has been employed *in vitro* against several cancers such as skin [430], prostate [431] oesophageal [432], cervical [433], leukaemia [434], bladder [361], and breast cancer [435]. The direct administration of PpIX to cancer patients during PDT has been limited by aggregation and low solubility in physiological medium [436]. Therefore, PpIX accumulation is commonly achieved by pre-treatment with ALA, a precursor of PpIX in the haem biosynthetic pathway.

ALA is water soluble and can be used in both oral and parenteral administration [364,379]. The ability to administer a PS in a tablet form means there is less risk of phototoxicity. ALAs use as a pro-drug has proven very effective in sensitising cells to PDT [379,429]. After pre-incubation with ALA, the PS then enters haem biosynthetic pathway and is metabolised to PpIX to maintain haem homeostasis. In this way, there is a preferential build-up of PpIX (cancer cells have increased haem synthesis) before light activation is performed. Studies of ALA-induced PDT in animal models have resulted in a decrease in metastases and tumour recurrence reinforcing its suitability for clinical use [437,438]. ALA has been investigated in phase III clinical trials and demonstrated its efficacy in Bowen's disease [439], actinic keratosis [440] and superficial basal cell carcinoma (BCC) [441].

This chapter investigates the antitumour efficacy of ART-porphyrin hybrid **AP433** in PC-3 prostate cancer cells. This hybrid was formed by linking the porphyrin derivative tetraphenylporphyrin (TPP) to DHA via an ester linker (Figure 12). DHA is an artemisinin derivative with both antimalarial and anticancer activity as discussed in Chapter 2. The rationale behind this drug design was to capitalise on the dual selectivity of PpIX which can preferentially accumulates in tumour

masses in a clinical context, and is selectively activated by light. By combining an ART derivative, DHA, it is anticipated that there will be a synergistic effect which will overcome the common drawbacks associated with the respective parent compounds. PDT has limited clinical use due to photosensitivity and the failure to fully irradiate metastatic cancer [442]. Furthermore, some tumours are not accessible for light activation [414]. DHA, while being well tolerated in patients, is limited by short half-life [443]. There is the potential that the porphyrin hybrid will direct DHA to the target site and, upon activation by light, both parents will exert their anticancer effects. Furthermore, PDT is an oxygen dependant therapy and is known to be less effective in hypoxic tissues [406]. The observed increase in artesunate efficacy at lower oxygen concentrations (Chapter 2) is promising and could potentially reduce or overcome the development of resistance to PDT in hypoxia [406]. Based on the findings in Chapter 2 an oxygen concentration of 4% (v/v) was maintained during analysis of novel hybrid **AP433** to better mimic *in vivo* conditions.

PC-3 were the chosen cancer cell line as they are known to be sensitive to both porphyrin mediated PDT [444] and ART derivatives [445,446]. In addition, prostate tumours are accessible for light activation during PDT in patients [447]. A novel light activation method was employed using Q-Sun solar simulator. PpIX is similar in structure to TPP, which is used in the synthesis of hybrid **AP433**. Therefore, PpIX was chosen as a suitable parent drug. PpIX has an absorption maxima of 635 nm but can also be activated in the UV range (Figure 11) [361]. The Q-Sun instrument has a wavelength range from 200-800nm set to irradiance of up to 0.68 W/cm^2 and thus can be employed for the light activation procedure (Figure 13) [448,449]. The RTCA instrument, used in chapter 2, was found to be unsuitable for Q-SUN light activation experiments due to the conductance of heat by gold plated electrodes within RTCA E-plates resulting in cell detachment. Therefore, RTCA was only employed to detect changes in cell growth in response to PS without light activation.

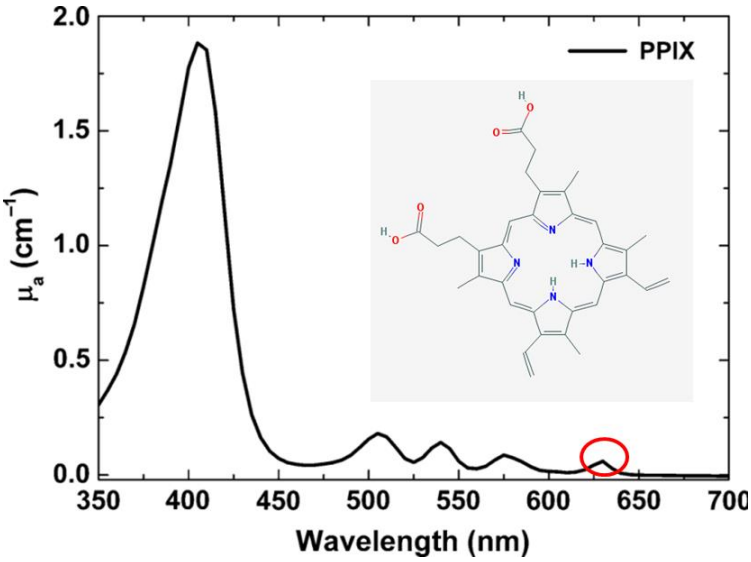

Figure 11 Protoporphyrin IX (PpIX) absorption spectrum

PpIX is typically excited at 635nm (highlighted by red circle) due to better penetration of red light through tissue at clinical stage. Graph adapted from [450]. Inset illustrates chemical structure of PpIX (Pub Chem).

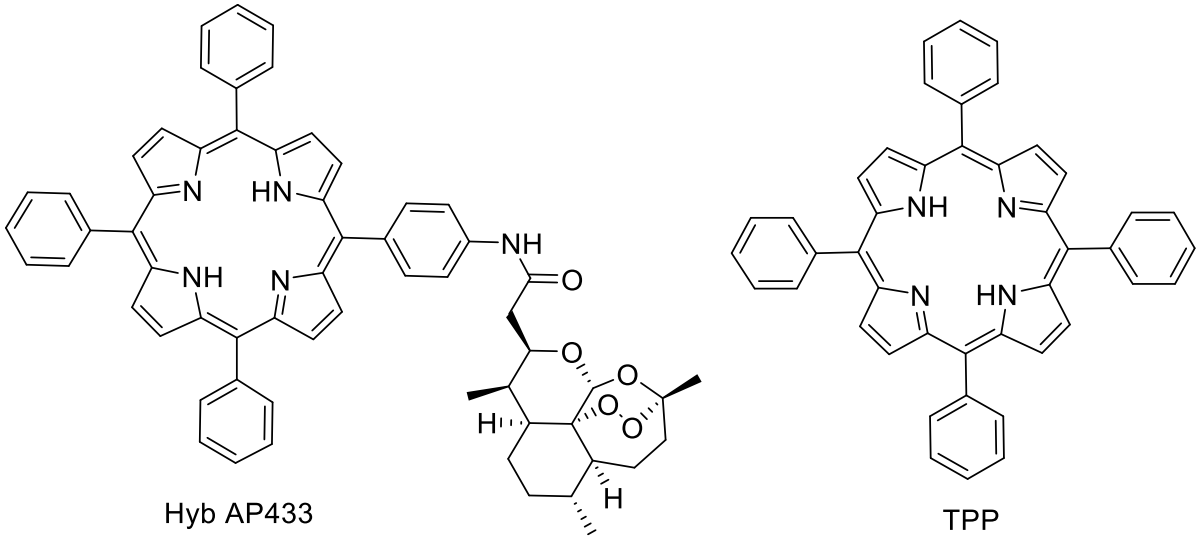

Figure 12: AP433 hybrid structure and parent compound

The structure of **AP433** hybrid and parent compound tetraphenylporphyrin (TPP). TPP is linked to DHA to form the hybrid.

3.3 Methodology

3.3.1 Cell Culture

PC-3 prostate tumour cells (ECACC) were cultured in RPMI 1640 (Sigma-Aldrich, UK) supplemented with 5% Foetal Bovine Serum (FBS) (Sigma-Aldrich, UK) and 1% Penicillin – Streptomycin (Sigma-Aldrich, UK) and 1% L-Glutamine (Sigma-Aldrich, UK). All cells were cultured at 37°C, 95% humidity, 5% (v/v) CO_2.

3.3.2 Oxygen maintenance

In addition to the cell culture conditions, cells were maintained at an *in vivo* relevant oxygen concentration of 4% (v/v) (30 mmHg) for a minimum of 24 h before any experiment was commenced and until analysis was completed using a Thermo 3110 CO_2 incubator (Thermo Fisher Scientific, UK)**.** An oxygen concentration of 4% (v/v) was chosen for analysis of novel hybrids based on the previous chapter in which artesunate was more effective against HeLa cells at in vivo relevant oxygen concentrations of 4%(v/v) and 1% (v/v) [295] .

3.3.3 Preparation and addition of drug compounds

AP433 hybrid (synthesised by Dr Sarah Rawe and colleagues Dublin Institute of Technology) and Protoporphyrin IX (Sigma-Aldrich, UK) were dissolved in the vehicle, DMSO to create the master stock. 20 µl aliquots of 10 mM or 50 mM concentrations were prepared for each compound and stored at -80 ˚C. Working stocks of 20 µM or 100 µM were prepared by diluting master stocks in RPMI to a final volume of 10 ml. During drug addition in each 16 well E-plate well, 100 µl of spent media was removed and replaced with an equal volume of working stock in a final volume of 200 µl. The dilution of stock solution results in a final compound concentration of 1 µM or 10 µM respectively. Final concentrations of DMSO were adjusted to 0.1% (v/v) for all drug concentrations and the vehicle control. Additional concentrations of drug compounds were achieved by a further dilution of working stocks and an adjustment of the vehicle concentration accordingly. A similar drug addition protocol was applied during the cell count analysis where cells were grown in 6 well plates (1.5 ml working stocks added to make final 3ml volume).

3.3.4 Real-Time Cell Analysis

RTCA was performed using the xCELLigence system as described in section 2.3.4. Briefly, E-plates were seeded with $4x10^3$ PC-3 cells per well (3 wells/treatment) 24 h before drug/compound exposure. Cell growth was measured every 15 minutes for a further 48 h post drug addition and is displayed by the built-in software as Cell Index (CI).

3.3.5 Cell count analysis

Cell count analysis was performed similarly to section 2.3.1. Briefly, PC-3 cells were seeded onto a 6 well plate (Sarstedt) at a density of $1x10^5$ cells per well. After 24 h incubation at 37 °C, half the culture medium was removed and replaced with an equal volume of fresh medium (control), DMSO (vehicle control) or drug working stock to achieve the desired final concentrations of 0, 10 or 50 µM. The final DMSO concentration was maintained at 0.1% (v/v) in both vehicle control and treated samples. Artesunate was also investigated in a two-dose regime. In this case, cells were treated similarly at 24 h and 48 h after seeding. Cells were harvested and counted 0 (time 0), 24 or 48 h later using a Z2 Particle Analyser (Beckman Coulter, USA). Cell counts are expressed as a percentage of time 0 control. Cell counts are expressed as a percentage of untreated control.

3.3.6 Photodynamic therapy

Protoporphyrin IX (PpIX) was employed as a PS in preliminary PDT experiments. PpIX is similar in structure to TPP used in the synthesis of hybrid **AP433** (Figure 12). A Q-Sun solar simulator (Q-LAB, FL, USA) was employed to light activate the PS/hybrid. The Q-Sun instrument operates at 0.68 W/m2 at 340-800 nm range (continuous green line in Figure 13) and mimics the typical solar spectrum at a latitude of 25" north (i.e. Florida USA) at solar noon mid-summer (dotted blue line) [448]. This instrument was deemed suitable for light activation as PpIX and other porphyrin derivatives are known to be activated at a wavelength of 635nm PpIX (Figure 11, Figure 13) [361]. This irradiance output was set to 0.68 W/m^2 and cells were irradiated for 1 or 2 minutes.

PC-3 prostate cancer cells were seeded in 6 well plates (Sarstedt) at densities of $1x10^5$ cells/well. 24 h later cells were exposed to vehicle (0.1% (v/v) DMSO in complete growth media), 1 or 10 µM PpIX/**AP433**. This is similar concentration range to that previously reported *in vitro* [329,375,451]. After a further 24 h incubation period, media was removed from cells and replaced with 2ml PBS before irradiation for 0 (Sham-exposed), 1 or 2 minutes. Cells to be "sham exposed" were covered in tin foil and placed in the Q-Sun solar simulator for 2 min (no light activation). Cells were harvested 48 h post irradiation and counted using a Z2 particle analyser (Beckman Coulter, USA). "Dark" toxicity of PpIX/**AP433** (no light irradiation) was also analysed in real-time utilising RTCA. PC-3 cells were seeded at $4x10^3$ cells/well in a specifically designed E-plate in a final volume of 200 µl (refer to 3.3.4). 24 h later 100 µl of the medium was removed and replaced with 100 µl of compound dissolved in media. Cells were exposed to PpIX/**AP433** at final concentrations 10 or 50 µM. Cell growth was analysed for a further 48 h. Cell growth was expressed as "cell index" (CI) by the RTCA software.

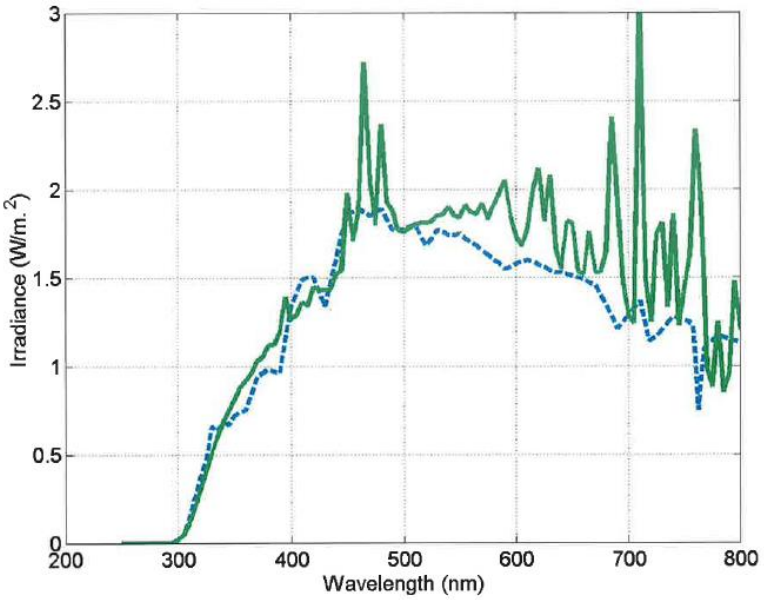

Figure 13 Q-Sun solar simulator and irradiance spectra

The figure illustrates the spectral irradiance for the Q-Sun solar simulator instrument utilised for light activation during PDT based experiments. The Q-Sun instrument operates at 0.68 W/m2 at 340-800 nm range (continuous green line) and the typical solar spectrum at a latitude of 25" north (i.e. Florida USA) at solar noon mid-summer (dotted blue line). Data provided by (Q-Lab, USA) and confirmed by in house calibration. The irradiance output is read and calibrated at 340 nm [448].

3.4 Results

3.4.1 Real-time analysis of PC-3 following exposure to protoporphyrin IX without light activation

PC-3 cells were exposed to 0, 10 or 50 µM PpIX 24 h after seeding and growth was measured in real-time for a further 48 h using xCELLigence software (Figure 14). 10 µM PpIX was not toxic to PC-3 in the dark with a similar growth profile to the untreated control. However, it is evident that at 50 µM, PpIX reduces cell growth shortly after treatment. After 48 h treatment 50 µM PpIX reduced cell growth by over 60% when compared to the vehicle control.

3.4.2 Effect of protoporphyrin IX based photodynamic therapy on PC-3 cell number

PC-3 cell count analysis was performed following PDT exposure with PpIX at concentrations of 0, 1 or 10 µM respectively (

Figure 15). For successful PDT, the PS should have minimal effect on cell growth prior to light activation. This concentration range was chosen based on real time cell analysis of PpIX in section 3.4.1 which showed that 50 µM PpIX reduced PC-3 growth without light activation (dark toxicity). Irradiation was performed using Q-Sun solar simulator for 0 (sham-exposed), 1 or 2 minutes. Dark toxicity is evident at 10 µM inducing a significant decrease in cell number after 48 h when compared to untreated control ($P \leq 0.01$). Light activation of PpIX can be observed with a significant reduction in PC-3 cell number 48 h post irradiation at 1 ($P \leq 0.05$) and 2 minutes ($P \leq 0.01$) when compared to sham-exposed control. However, the light activation procedure causes toxicity as evidenced by reduced cell numbers in the vehicle controls at light exposure times of 1 and 2 minutes.

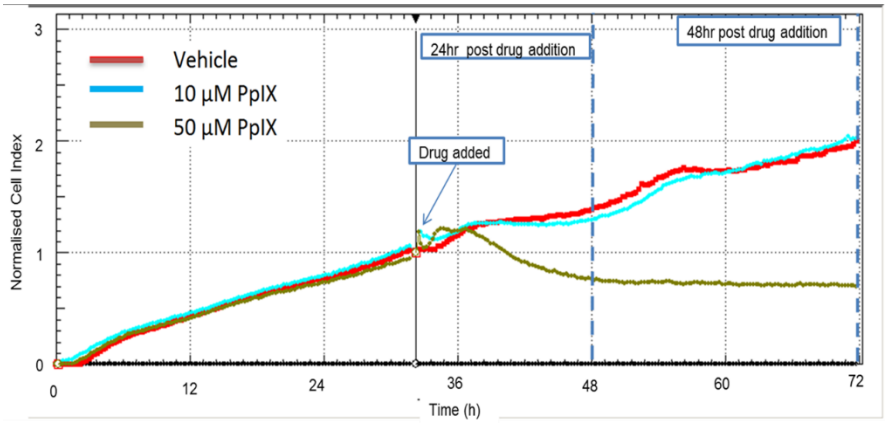

	Cell Index (% Vehicle)	
	24 h	48 h
Vehicle	100.0	100.0
1 µM PpIX	98.1	101.3
10 µM PpIX	57.3	35.5

Figure 14 Real-time analysis of dark toxicity in PC-3 following PpIX treatment

PC-3 cells were seeded at 4x10^3 cells/well. After a further 24 h incubation cells were exposed to either vehicle (0.1% DMSO), 10 or 50 µM PpIX. Cell growth was measured every 15 minutes for a further 48 h using xCELLigence RTCA system. Cell growth is expressed as cell index (CI) by the built-in software. The corresponding table below the RTCA graph summarises the mean CI values recorded for each treatment at 24 h and 48 h (time points indicated by broken blue lines); CI values are expressed as a % vehicle control. Each real-time experiment was performed three times in triplicate.

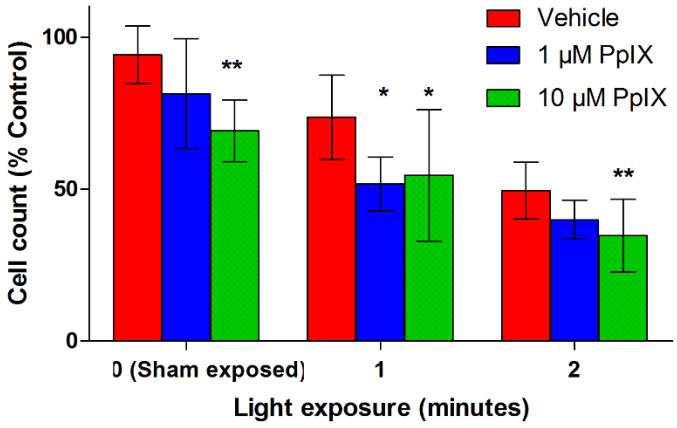

Figure 15 PC-3 cell number following PpIX PDT

PC-3 cells were seeded at 1x10^5 cells/well. 24 h later cells were exposed to either vehicle , 1 or 10 µM protoporphyrin IX (PpIX). After a further 24 h cells were irradiated with light using Q-Sun solar simulator for 0 (sham-exposed), 1 or 2 min. Cells were counted 48 h post treatment with Z2 particle analyser. All data is normalised as a percentage of untreated control. Statistical significance was measured using one-way ANOVA followed by Tukey post hoc test with P≤0.05 chosen as criterion for significance

3.4.3 Real-time analysis of PC-3 following exposure to AP433 hybrid without light activation

PC-3 cells were exposed to 0, 1 or 10 µM AP433 hybrid 24 h after seeding and cell growth was monitored in real-time for a further 48 h using xCELLigence system (Figure 16, Figure 17). This concentration range was chosen based on real time cell analysis of the parent compound PpIX in section 3.4.1 which showed that 50 µM PpIX reduced PC-3 growth without light activation (dark toxicity). To minimise dark toxicity due to the porphyrin component of the hybrid a concentration range of 10 µM and lower was used. 1 µM **AP433** did not reduce cell growth with a similar growth profile to the vehicle control. 10 µM **AP433** reduces cell growth by 25% after 48 h.

3.4.4 of AP433 hybrid based photodynamic therapy on PC-3 cell number

PC-3 cell count analysis was performed following PDT therapy with **AP433** hybrid (TTP-DHA) at concentrations of 0, 1 or 10 µM respectively (Figure 17). Light Irradiation was performed using Q-Sun solar simulator for 0 (sham-exposed), 1 or 2 minutes. **AP433** treatment without light activation did not result any significant loss in cell numbers at either 1 or 10 µM. Light activation of **AP433** can be observed at a higher concentration with a significant reduction in PC-3 cell number 48 h after light exposure for 1 minute ($P \leq 0.01$) and 2 minutes ($P \leq 0.001$). However, the light exposure alone also caused a significant reduction in PC-3 cell number after 2 minutes light exposure reducing the cell number below 30% of the untreated control.

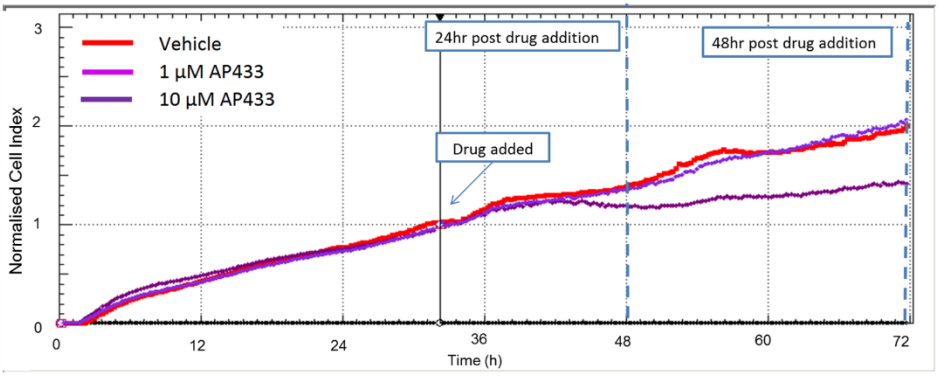

	Cell Index (% Vehicle)	
	24 h	48 h
Vehicle	100.0	100.0
1 µM AP433	100.0	102.5
10 µM AP433	92.3	75.0

Figure 16 Real-time analysis of dark toxicity in PC-3 following AP433 hybrid treatment

PC-3 cells were seeded at 4x10^3 cells/well. After a further 24 h incubation cells were exposed to either vehicle (0.1% DMSO), 1 or 10 µM **AP433**. Cell growth was measured every 15 minutes for a further 48 h using xCELLigence RTCA system. Cell growth is expressed as cell index (CI) by the built-in software. The corresponding table below the RTCA graph summarises the mean CI values recorded for each treatment at 24 h and 48 h (time points indicated by broken blue lines); CI values are expressed as a % vehicle control. Each real-time experiment was performed three times in triplicate.

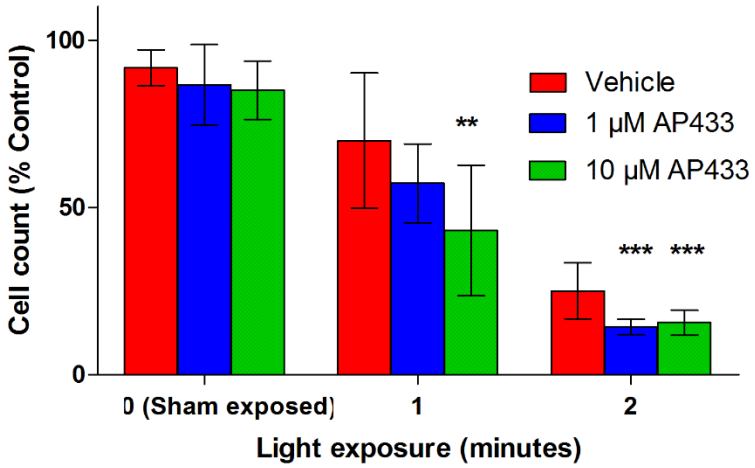

Figure 17 PC-3 cell number following AP433 PDT

PC-3 cells were seeded at 1X10^5 cells/well. 24 h later cells were exposed to 0, 1 or 10 µM **AP433** hybrid. After a further 24 h cells were irradiated with light using Q-Sun solar simulator for, 0 (sham-exposed), 1 or 2 minutes. Cells were counted 48 h post treatment with a Z2 particle analyser. All data is expressed as a percentage of untreated control. Statistical significance was measured using one-way ANOVA followed by Tukey post hoc test with P≤0.05 chosen as the criterion for significance.

3.5 Discussion

Porphyrin-based PDT has had demonstrable success in cancer treatment in a clinical setting [347,377,452]. PDT has become an attractive non-invasive alternative to conventional therapy in the treatment of pre-cancerous lesions and localised cancers. However, the full potential of PDT has not yet been revealed. Many studies are focused on the development of superior PSs which will be more potent and selective against cancer [453]. One potential strategy is to conjugate a PS to another anticancer agent in a hybrid compound. The hybrid approach has the potential to further improve the anticancer efficacy of PDT [238].

The current work investigates a novel DHA-TPP hybrid, **AP433**, in PC-3 cancer cells. TPP is a synthetic heterocyclic compound that resembles naturally occurring porphyrins such as PpIX [454]. DHA is an artemisinin derivative with both antimalarial and anticancer activity as discussed in Chapter 2. It is anticipated that hybrid **AP433** will combine DHA's iron mediated ROS production with the singlet oxygen production from the light activated TPP resulting in increased levels of oxidative stress and cancer cell death. PDT can lead to the development of hypoxia in the target tissue which in turn can reduce PDT efficacy. The artemisinin derivative artesunate (which metabolises to form DHA *in vivo*) was discovered to be more effective at lower oxygen levels in Chapter 2 [295]. By incorporating an ART derivative into a hybrid with a PS agent, there is the potential to overcome hypoxia induced resistance following PDT.

Before examining hybrid **AP433** efficacy, it was important to optimise light activation of PpIX and determine the potential for dark toxicity. PpIX did reduce PC-3 cell growth without light exposure at concentrations above 10 μM (Figure 14). PC-3 cells were then exposed to PDT using porphyrin parent drug PpIX (Figure 15). PpIX reduced cell growth significantly 48 h after exposure to light for 1 minute ($P \leq 0.05$) and 2 minutes ($P \leq 0.01$). However, the light activation alone also contributed to a loss in cell numbers with a 50% reduction detected in vehicle controls after light exposure for 2 minutes. Furthermore, 10 μM PpIX was found to reduce cell number significantly ($P \leq 0.01$) suggesting dark toxicity. This data suggests that the Q-Sun light doses required for activation of PpIX are toxic to PC-3.

AP433 was then investigated at the same concentration range and light activation procedure. **AP433** induced dark toxicity with a notable reduction in cell growth observed during RTCA (Figure 16). In this case, dark toxicity is expected as DHA activity is not dependent on light activation. However, the effects of the hybrid on cell growth are dramatically increased when light activation occurs. **AP433** induced a significant reduction in cell number 48 h after light exposure ($P \leq 0.001$) (Figure 17). However, it must be noted that light exposure alone reduced cell growth with a loss of cell numbers below 30% of untreated control after 2 minutes light exposure. This light mediated toxicity also has the potential to cause gene mutations and secondary tumours [455]. Therefore, the PDT procedure will need to be further optimised to enable light activation without causing unwanted cell toxicity. Once this is achieved, porphyrin-based hybrids can be evaluated effectively.

Perhaps employing a laser diode system for light activation would be more effective for evaluating PDT. This would allow for the use of higher light doses and also could be used to analyse cell growth in real time in response to PDT [456]. Cellular uptake of PpIX may also have affected PDT efficacy in PC-3. PpIX is a hydrophobic molecule and the reduced solubility in aqueous solutions make delivery of sufficient doses of the drug to malignant tissue or cells challenging [457]. The efficient intracellular localisation of a PS is largely dependent on hydrophobicity [457]. There is the potential to make these hybrids more soluble by means of the addition of hydrophilic groups [458].

3.6 Conclusions

A novel DHA-TPP hybrid, **AP433**, was investigated against PC-3 prostate cancer cells. Hybrid **AP433** was found to reduce PC-3 cell number following PDT ($P \leq 0.001$). However, the novel light activation procedure (using Q-Sun solar simulator) did account for a loss in cell numbers particularly at a light exposure time of 2 minutes. There is a need to optimise the PDT procedure to eliminate this unwanted toxicity before the porphyrin based hybrids can be effectively evaluated.

Chapter 4. Biological evaluation of artemisinin-naphthalimide hybrids

4.1 Introduction

Chemotherapy, radiation, and surgery are the standard methods of cancer treatment today. However, chemotherapy is limited by the development of multidrug resistance and non-tumour toxicity. Therefore, the search is ongoing for novel compounds with the potential for more effective chemotherapy. One strategy currently being investigated is the development of hybrid drugs. The term hybrid in the context of drug design refers to a single compound in which two active 'parent' drugs are linked to afford a single molecular entity with dual activity [5]. The two parent compounds from which the hybrid is prepared each have their own unique pharmacophore. By combining two compounds in this way several potential advantages are possible including simultaneous delivery of the parent drugs, enhanced uptake, a multimodal mechanism of action that could prevent or stall the development of drug resistance, and an improved side effects profile [6,7].

This chapter investigates the antitumour efficacy of novel ART-NAP or tetraoxane-NAP hybrids (Figure 18, Figure 19). Hybrids **MK129, SG76, SG77** and **SG81** contain an ART derivative, DHA, inked to a NAP while hybrid **MK134** contains a NAP group linked to a tetraoxane. Based on the findings in chapter 2, these novel hybrids were analysed in 4% (v/v) oxygen conditions to better mimic in vivo environment. ARTs (discussed in detail in section 1.4) are endoperoxide containing compounds with anticancer and antimalarial activity. ARTs lack of cross-resistance observed during malaria treatment is promising for their future development as anticancer agents [459]. This lack of cross resistance has also been observed in cancer treatment; for example, artesunate was shown to be effective against multidrug-resistant small cell lung cancer (SCLC) cell line, H69VP, when preloading of cells with transferrin was performed [460]. A separate study demonstrated that artesunate was just as potent against multidrug resistant cell lines that overexpress MDR1/P glycoprotein, MRP1 and BCRP (all associated with resistance to conventional chemotherapy) [108]. Furthermore the activity of ARTs may be improved in hypoxia [295], conditions under which many chemotherapies are rendered much less effective [461–463] .

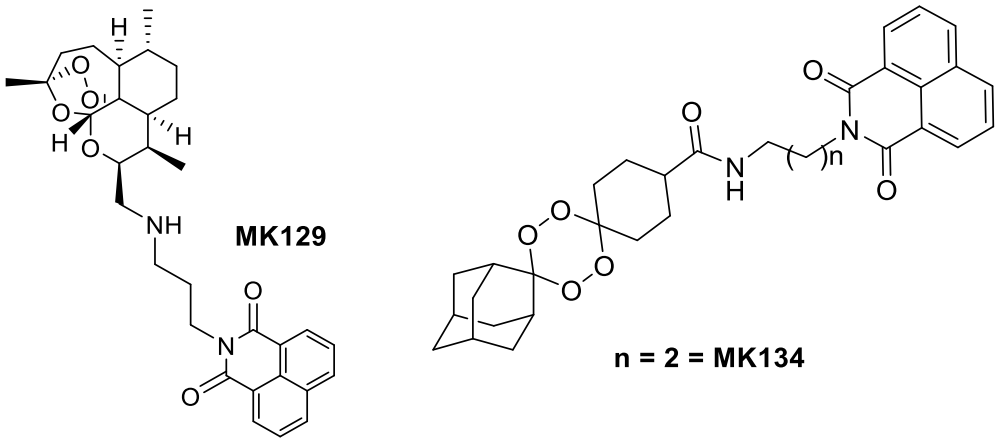

Figure 18 Artemisinin-naphthalimide and tetraoxane-naphthalimide hybrids

Figure above shows ART-NAP hybrid **MK129** and tetraoxane-NAP hybrid **MK134.** Both hybrids are linked via stable amido linker.

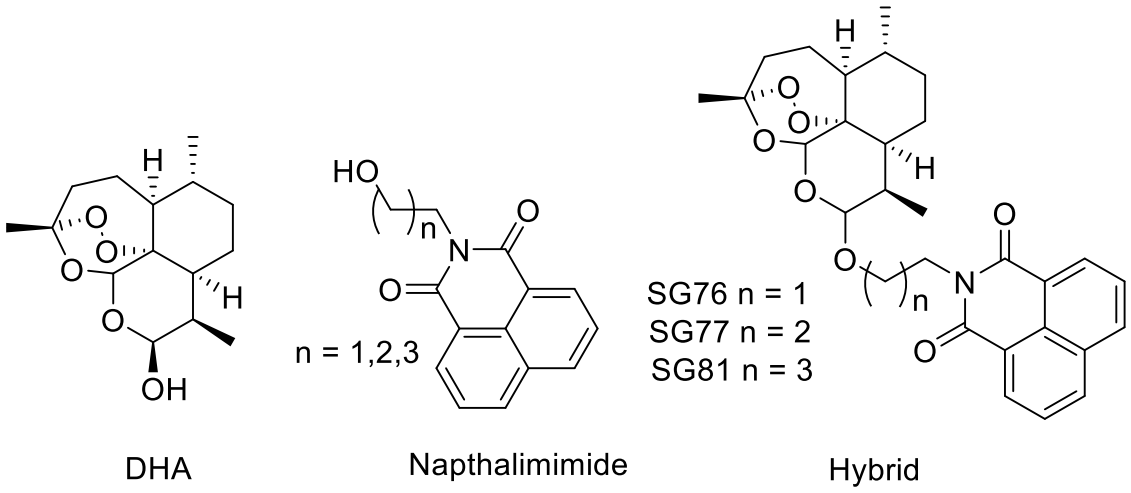

Figure 19 Artemisinin-naphthalimide hybrids

Artemisinin derivative, DHA, was covalently linked to the naphthalimide moiety via an ether linker in which linker length was incrementally increased by inclusion of additional methylene groups (Hybrids **SG76, SG77, SG81**)

NAPs (discussed in detail in section 1.5) are potent anticancer agents containing an aromatic naphthalene system fused to an imide group which are thought to act on cancer cells by intercalation of DNA or by inhibiting topoisomerase II [165,464]. NAPs have reached advanced clinical trials against several cancer types but have been limited by severe toxicity in non-tumour tissue [178,179]. It must be stated that the NAP component within the hybrid does not have the same structure of mitonafide. Furthermore, our collaborators have shown that similar ART-NAP hybrids **119**, and **129** do not localise specifically in the nucleus of cells suggesting that DNA may not necessarily be a direct target despite the DNA intercalation properties of NAPs [465].

Hybrid **MK134** contains a NAP group linked to a tetraoxane. Tetraoxanes are fully synthetic ART derivatives which were first synthesised in the 1990s as an attractive more cost-effective alternative to naturally sourced ART in the treatment of malaria [466]. These compounds were found to have antimalarial activity *in vitro* but none of the compounds had better antimalarial activity than ART [467]. These compounds have not been well studied against cancer to date. However, a recent study did report the synthesis of tetraoxane dimers with excellent activity in HT29-AK colon cancer and HL60 leukaemia cells. Compound **29** was particularly effective against the cancer cell lines with generated IC_{50} values of 3.8 μM in HT29-AK cells and 12.2 μM in HL60 cells.

It is anticipated that by linking ART and NAP derivatives in a hybrid, there will be a synergistic effect, with the hybrid exerting a multimodal drug action in cancer cells (Figure 20). There is the potential that ART induced ROS generation coupled with NAPs DNA intercalation properties will result in increased DNA damage, oxidative stress and cell death. It is also possible that glutathione antioxidant response will be up regulated in response to hybrid treatment.

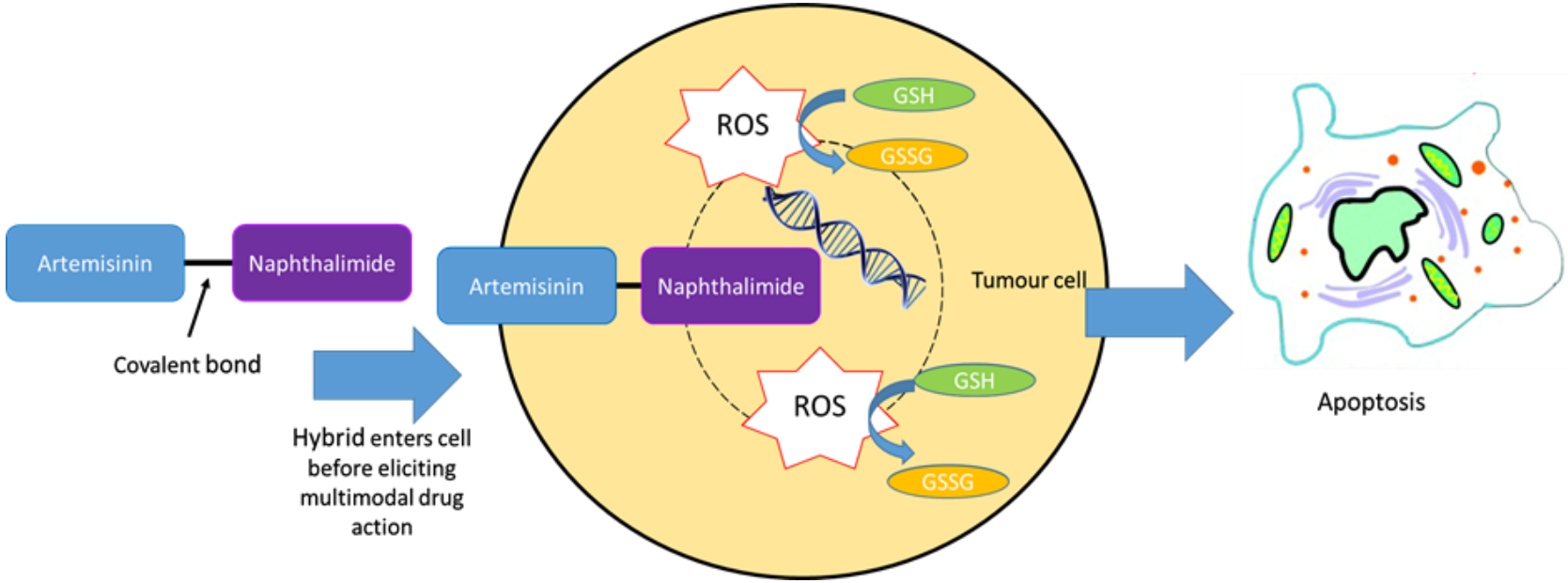

Figure 20: Graphical abstract

ART and NAP are covalently linked to form hybrid compound. This hybrid then enters cell upon administration. It is anticipated that a multimodal action will take place resulting in ROS production, DNA damage and cell death

4.2 Methodology

4.2.1 Cell Culture.

PC-3, PNT1A and HL60 (ECACC) were maintained in RPMI 1640 (Sigma-Aldrich, UK) supplemented with 5% FBS (Sigma-Aldrich, UK), 1% Penicillin-Streptomycin (Sigma-Aldrich, UK) and 1% L-glutamine (Sigma-Aldrich, UK). MCF-7 breast cancer cells (ECACC) were cultured in DMEM (Sigma-Aldrich, UK) supplemented with 5% (v/v) FBS, 1% (v/v) Penicillin/Streptomycin and 1%(v/v) L-glutamine. All cells were maintained at 37°C, 95% humidity, 5% (v/v) CO_2 for a minimum of 24 h before any experiment was commenced and maintained until the end of analysis.

4.2.2 Oxygen maintenance

In addition to the cell culture conditions, cells were maintained at *in vivo* relevant oxygen concentration of 4% as described in section 3.3.2.

4.2.3 Preparation and addition of drug compounds.

Hybrid compounds and mitonafide were synthesised by Prof. Paul O'Neill, Dr Sarah Rawe and colleagues at the School of Chemistry, University of Liverpool, UK and at the School of Chemical and Pharmaceutical Sciences, Dublin Institute of Technology, Ireland. Artesunate was purchased from Tokyo Chemical Industry Co. Ltd. All compounds were dissolved in the vehicle, DMSO (100%), to create the master stock. 20 µl aliquots of 10 mM or 50 mM concentrations were prepared for each compound and stored at -80 ˚C. Working stocks of 20 µM or 100 µM were prepared by diluting master stocks in fresh growth medium to a final volume of 10 ml. Additional concentrations of drug compounds were achieved by further dilution of working stocks and adjustment of the vehicle concentration accordingly. The further dilution of drug stock solutions during drug addition resulted in final compound concentrations of 0.01, 0.1, 1, 10 or 50 µM respectively. Final concentrations of DMSO were adjusted to 0.1% (v/v) for all drug concentrations and vehicle control. During RTCA, drug addition was performed by removing 100 µl of spent media from each 16 well E-plate well, and replacing with an equal volume of working stock in a final volume of 200 µl.

A similar drug addition protocol was applied during the cell count analysis where cells were grown in 6 well plates (1.5 ml working stocks added to each well to make final 3ml volume).

4.2.4 Real-time cell analysis.

RTCA was performed in a similar manner to that described in section 2.2. Briefly, E-plates (ACEA Biosciences, San Diego, CA, USA) were seeded with either 5,000 PNT1A, 5,000 MCF-7 or 4,000 PC-3 cells per well, 24 h before drug addition. E-plates were placed within the cradle of an xCELLigence DP Real Time Cell Analyser that remained inside the incubator for the duration of the experiment. 24 h post seeding, the hybrid drugs were added. Cell growth was measured every 15 min for the duration of the experiment (beginning 24 h before drug addition and continuing for a further 48 h) and is displayed by the RTCA software as “Cell Index”.

4.2.5 Cell count analysis.

$1x10^5$ PNT1A, $8x10^4$ PC-3, $1x10^5$ MCF-7 or $3x10^5$ HL60 cells were seeded per well in a 6 well plate (Sarstedt, Germany) achieving the same seeding density as utilised in real-time cell analysis). Cells were harvested and counted 48 h post drug addition using a Z2 Particle Analyser (Beckman Coulter, Miami, FL, USA). Cell counts are expressed as a percentage of untreated control ±SD. IC_{50} (the concentration of drug required to reduce cell number by 50%) values were calculated for each drug by plotting a sigmoidal dose response curve fit using GraphPad Prism 5 (GraphPad Software, San Diego, CA, USA). Log_{10} of the drug concentration was plotted on x axis while cell count (% of untreated control) was plotted on the y axis. IC_{50} analysis was not possible in Chapter 2 and Chapter3 because a broader concentration is required for an accurate IC_{50} estimation [468].

4.2.6 Statistical analysis.

Statistical analysis performed as in section 2.3.6 .

4.3 Results

4.3.1 Initial screening of endoperoxide-naphthalimide hybrid compounds in PC-3 cells

Several ART-NAP hybrids and tetraoxane-NAP hybrids were selected for initial screening at a concentration of 50 μM to determine activity in PC-3 cancer cells. All hybrids tested reduced cell growth during RTCA (Figure 21). Despite a 30% reduction in cell growth after 48 h, **MK134** was least effective in PC-3. **MK129** and **SG76** were both found to reduce cell growth by approximately 50% after 48 h. PC-3 cell growth did appear to recover from 24 h after drug addition in the case of **SG76**. **SG77** and **SG81** were most active in PC-3 with 50 μM treatment resulting in an 83.7 % and 79.6% reduction in cell growth after 48 h respectively. Cell count analysis was also performed to validate RTCA results (Figure 22). A similar trend can be observed with all hybrids reducing cell number 48 h after drug addition. **SG77** and **SG81** again were the most effective hybrids reducing cell number by more than 50% after 48 h.

4.3.2 Effects of endoperoxide-naphthalimide hybrids on tumour and non-tumour cell number

Based on preliminary data above, ART-NAP hybrids **SG76, SG77** and **SG81** were most active hybrids in PC-3. The next phase of the *in vitro* investigation involved the evaluation of most active hybrids at a wider concentration range against four different cell types. In Chapter 2, HeLa were selected for analysis based on the criteria that they are a well-studied adherent cancer cell line sensitive to artesunate [24]. In this case, the focus was to highlight the potential of oxygen to modulate drug activity *in vitro*. However, for this chapter it was elected to limit the study to three more commonly diagnosed cancer types including prostate cancer, breast cancer and leukaemia. Prostate cancer is one of the most common cancers diagnosed in men [90,431]. PNT1A cells (non-tumour prostate) were employed as a marker of non-tumour prostate cells and have been used for this purpose in a previous study [469]. PC-3 cells (prostate cancer) are known to be sensitive to ART derivatives [446] and DNA targeting agents similar to NAPs [470]. PNT1A and PC-3 were chosen for this work to access the potential for novel hybrid drugs to induce selective toxicity in prostate cancer. MCF-7 and HL60 were chosen to access the potential of novel hybrids to treat breast cancer

and leukaemia. These cancer types are also very prevalent worldwide [72]. Both cell lines have also shown to be sensitive to NAPs [471,472] and ARTs [146,473]. By investigating both hybrids and the parent drugs in four cell lines, the overall anticancer activity and tumour cell selectivity of can be accessed. Cell count analysis was employed to detect changes in cell number in response to both hybrid compounds and parent drugs (Figure 23, Figure 24). Cells were treated with either artesunate, mitonafide, **SG76**, **SG77** or **SG81** at concentrations of 0, 0.01, 0.1, 1, 10 or 50 µM. Cells were harvested and counted 48 h after drug addition.

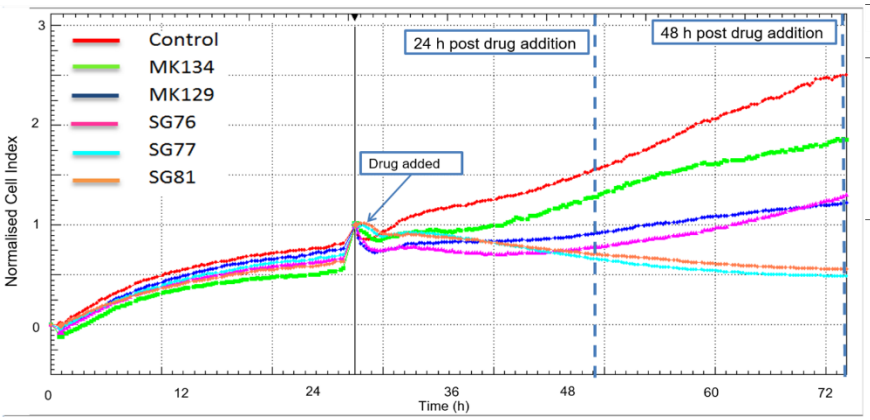

	Cell Index (% Control)	
	24 h	48 h
Control	100.0	100.0
MK134	85.7	71.4
MK129	64.3	53.1
SG76	50.0	49.0
SG77	46.4	16.3
SG81	47.9	20.4

Figure 21 Real-time cell analysis of PC-3 cells in response to endoperoxide-naphthalimide hybrids

PC-3 were seeded onto E-plate at 5,000/well. 24 h later, the hybrid drugs were added at a single concentration of 50 µM. Cell growth was then measured for a further 48 h and is plotted as CI. The corresponding table on the right of the RTCA graph summarises the mean CI values recorded for each treatment at 24 h and 48 h (time points indicated by broken blue lines); CI values are expressed as % control. Each real-time experiment was performed three times in triplicate.

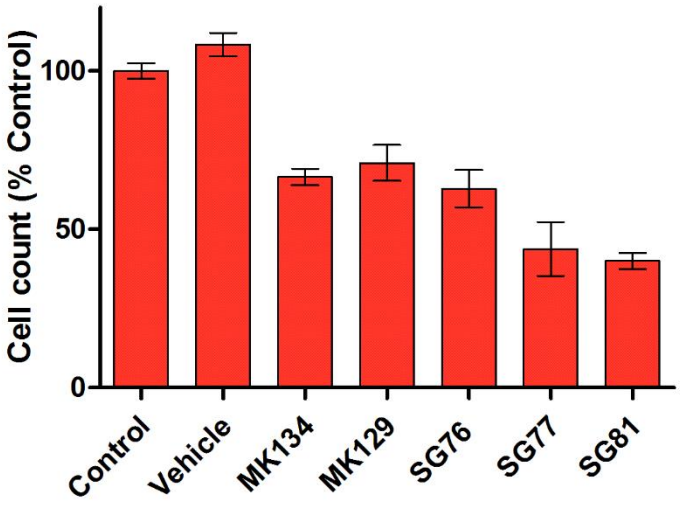

Figure 22 cell count analysis of PC-3 in response to several endoperoxide-naphthalimide hybrids

PC-3 were seeded onto a 6 well plate at $8x10^4$ cells/well. 24 h later, the hybrid drugs were added at a single concentration of 50 µM. Cell count analysis was performed 48 h post drug exposure. All data is normalised as a percentage of untreated control.

Parent drugs artesunate and mitonafide were potent against all 4 cell lines with significant reductions in cell number detected at concentrations of 1, 10 and 50 µM ($P \leq 0.001$) (Figure 23). ART-NAP hybrids **SG76, SG77** and **SG81** all reduced tumour cell number significantly at concentrations above 1 µM in all 4 cell lines ($P \leq 0.001$) (Figure 24). To summarise the cell count data more effectively, an IC_{50} was generated for each drug by plotting log concentration vs cell number (expressed as % control) as described in 4.2.5. This sigmoidal dose response curve was then used to calculate the concentration required to reduce cell number by 50% (non-linear regression model). This data shows that HL60 was most sensitive to the hybrid drugs with IC_{50} ranging from 2.0-3.9 µM (Table 2). Hybrid **SG76** was the most effective hybrid against HL60 with 5 times more activity than artesunate. None of the hybrids evaluated were more active in MCF-7 cells when compared to parent drugs. Artesunate and mitonafide produced IC_{50} values of 17.5 µM and 4.8 µM while hybrids **SG76, SG77** and **SG81** were somewhat less effective in MCF-7 producing higher IC_{50} values ranging from 23.0 µM-74.0 µM. PC-3 cells were particularly sensitive to mitonafide with an IC_{50}

value of 0.4 µM. All three hybrids also showed anticancer activity in PC-3 with IC_{50} values ranging from 1.7-15.8 µM.

PNT1A were more tolerant to the hybrids than artesunate and mitonafide with IC_{50} values ranging from 2.9 µM to 23.3 µM in the parent drugs and from 15.9 µM to 68.3 µM in the hybrids. Furthermore, hybrids **SG76**, **SG77** and **SG81** were selectively toxic in PC-3 compared to PNT1A with IC_{50} values ranging from 1.7 - 15.8 µM in PC-3 compared to 15.9-68.3 µM (highlighted in bold font in Table 2). Prostate tumour PC-3 were also compared directly to their non-tumour counterparts PNT1A. The IC_{50} values generated in prostate tumour and non-tumour cell lines (Table 2) were used to calculate non-tumour/tumour ratio for each drug/compound tested. Higher non-tumour/tumour ratio is indicative of higher tumour cell selectivity and can be ranked from 1-5 as shown in Table 3. Hybrid **SG77** was the most selective with 11 times more activity in tumour cells. Artesunate was the least selective hybrid with only three times more activity in tumour cell line. PNT1A vs. PC-3 cellular response to both parent drugs and hybrids was compared statistically using a two-way ANOVA (Figure 25). This analysis was performed using data generated during cell count analysis (Figure 21, Figure 22). PNT1A were found to be less sensitive than PC-3 in the case of both hybrids and parent drugs with significant differences in cell response detected at concentrations of 0.1 µM and higher ($P \leq 0.001$).

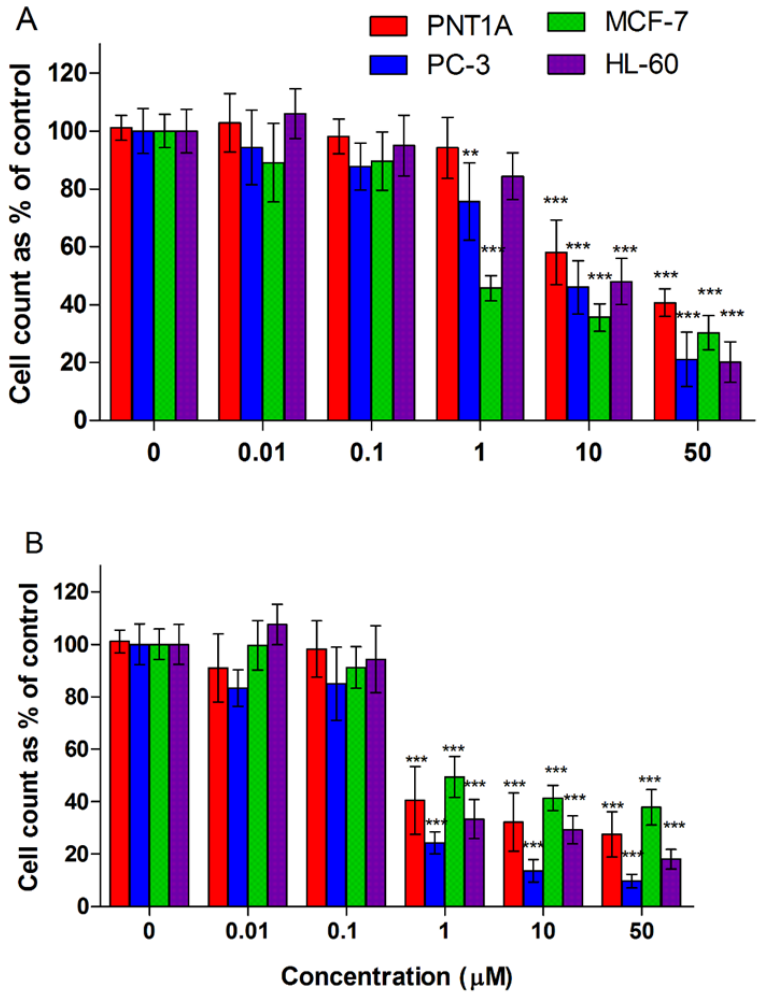

Figure 23: Effect of artesunate and mitonafide on tumour and non-tumour cell number

$1X10^5$ (PNT1A), $8X10^4$ (PC-3 and MCF-7) or $3X10^5$ (HL60) cells were seeded per well in a 6 well plate. After further incubation for 0 h (HL60) or 24 h (PNT1A, PC-3 and MCF-7) cells were exposed to (A) artesunate or (B) mitonafide at concentrations of 0- 50 µM as indicated. Cell count was performed 48 h post compound addition. All treatments normalised against vehicle control (0.1% DMSO). The above data is representative of triplicate experiments (+/-SEM). One way ANOVA, followed by Tukey post-hoc test was utilised to analyse differences between treated/exposed and control cell populations of same cell type.

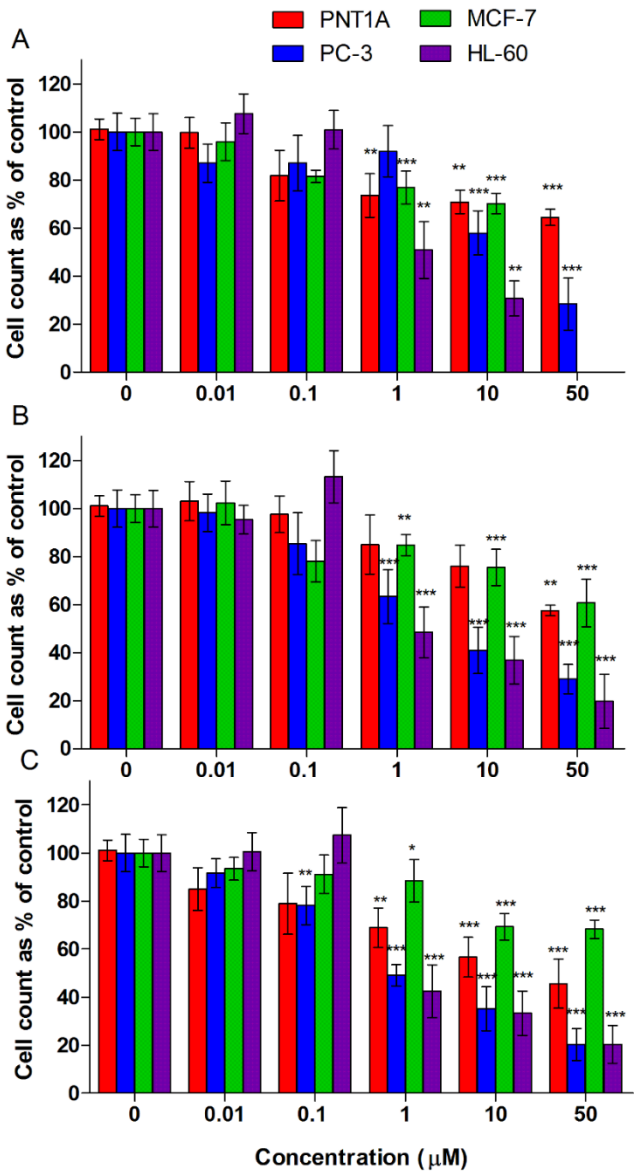

Figure 24: Effect of artemisinin-naphthalimide hybrids on tumour and non-tumour cell number

$1X10^5$ (PNT1A), $8X10^4$ (PC-3 and MCF-7) or $3X10^5$ (HL60) cells were seeded per well on a 6 well plate. After further incubation for 0 h (HL60) or 24 h (PNT1A, PC-3 and MCF-7) cells were exposed to (A) **SG76** (B) **SG77** or (C) **SG81** at concentrations of 0- 50 µM as indicated. Cell count was performed 48 h post compound addition. All treatments normalised against vehicle control (0.1% DMSO). The above data is representative of triplicate experiments (+/-SEM). One way ANOVA, followed by Tukey post-hoc test was utilised to analyse differences between treated/exposed and control cell populations of same cell type.

	IC_{50} (μM)			
	PNT1A	PC-3	MCF-7	HL60
Parents				
ART	23.3±10.2	7.5±6.7	17.5±5.1	9.3±2.9
MIT	2.9±3.3	0.4±0.2	4.8±4.5	1.1±0.2
Hybrids				
SG76	**68.3±24.5**	**15.8±3.9**	23.0±14.7	2.0±0.6
SG77	**54.9±8.4**	**4.9±2.4**	40.4±5.6	3.9±2.9
SG81	**15.9±9.1**	**1.7±0.7**	74.0±21.6	3.4±3.3

Table 2: IC_{50} summary

IC_{50} (Inhibitory concentration 50%) was calculated for parent compounds (artesunate and mitonafide) and hybrid compounds (**SG76**, **SG77** and **SG81**) using data generated during cell count analysis 48 h after drug addition. All data is presented as the mean ± SD of three independent experiments. IC_{50} was calculated using GraphPad Prism software. Hybrid compounds were more active in PC-3 compared to non-tumour PNT1A (values highlighted in bold)

Drug/Compound	Ranking	Non-tumour/ tumour ratio
SG77	**1**	**11.2**
SG76	2	9.4
mitonafide	3	7.3
SG81	4	4.3
artesunate	5	3.3

Table 3 Tumour cell selectivity

IC_{50} values generated in prostate tumour and non-tumour cell lines (Table 2) were used to calculate non-tumour/tumour ratio for each drug/compound tested. Higher non-tumour/tumour ratio is indicative of higher tumour cell selectivity. Each drug tested can be ranked from 1-5 as shown above. **SG77** highlighted in bold was the most selective hybrid tested.

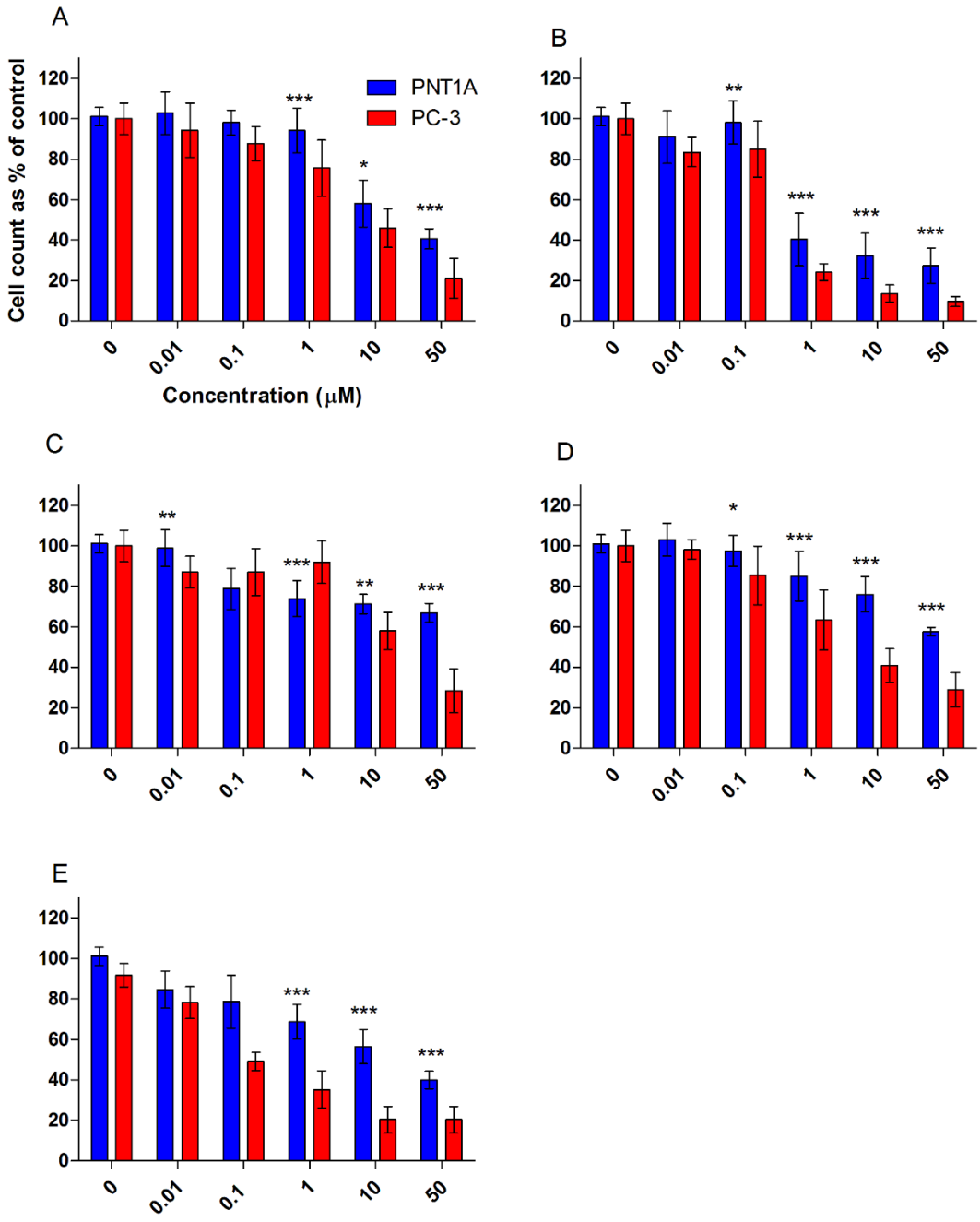

Figure 25: Prostate cell sensitivity to hybrids and parent compounds

1X10^5 PNT1A or 8X10^4 PC-3 cells were seeded per well in a 6 well plate. After a further 24 h incubation, cells were exposed to (A) artesunate (B) mitonafide (C) **SG76** (D) **SG77** or (E) **SG81** at concentrations of 0- 50 µM as indicated. Cell count was performed 48 h post drug addition. All treatments normalised against vehicle control (0.1% DMSO). Significant differences between cell response were evaluated using two-way ANOVA, followed by Bonferroni post hoc test (*=p ≤ 0.05, **= p ≤ 0.01, ***= p≤ 0.001). IC_{50} values were also calculated at 48 h using the above data.

4.3.3 Effects of endoperoxide-naphthalimide hybrids on tumour and non-tumour cell growth

RTCA system was employed as a dynamic method for biological evaluation of antitumour hybrids in real-time. As discussed in chapter 2, this impedance based assay will detect changes in cell growth, cell death, adhesion, and morphology to give an indication of overall cellular status. Artesunate and mitonafide both reduced PNT1A cell growth (Figure 26). It could be observed that 10 µM artesunate inhibited cell growth from 20 h after drug addition with 50 µM reducing cell growth by 93.3% after 48 h. Mitonafide also reduced PNT1A cell growth by 3.3% and 56.7% at concentrations of 10 µM and 50 µM respectively. PNT1A were more tolerant to hybrid **SG76** with 10 µM reducing cell growth by 20% after 48 h (Figure 26). 50 µM **SG77** reduced cell growth by 45.7% and 76.4% after 24 h and 48 h respectively. PNT1A cells showed a similar response to **SG81** with 50 µM reducing cell growth by over 60% after 48 h.

Artesunate reduced PC-3 growth after 24 h at concentrations of 1 µM and higher (Figure 27). Cells exposed to 1 µM artesunate appear to recover towards 48 h mark. 10 and 50 µM artesunate reduced PC-3 by 41.2% and 70% respectively. Mitonafide was also effective against PC-3 with a reduction in cell growth evident from 24 h. 10 µM and 50 µM mitonafide reduced PC-3 cell growth by 60.8% and 92.2% respectively after 48 h. **SG76** reduced PC-3 growth from 12 h onwards with 50 µM resulting in nearly a 50%reduction in cell growth after just 24 h. However, it appears that PC-3 cells begin to recover from 24 h to 48 h (Figure 28). **SG77** was also effective in reducing PC-3 growth with a 26.1% and 39.1% reduction in cell growth recorded after 24 h. 10 and 50 µM **SG81** reduced PC-3 growth within 24 h resulting in a 37.8% and 66.2% reduction in cell growth after 48 h. MCF-7 cells were the most sensitive to parent drugs and hybrids during RTCA. Artesunate and mitonafide both reduced MCF-7 growth by more than 80% after 48h (Figure 28). Mitonafide was particularly potent with 50 µM treatment resulting in a 61.9% reduction in cell growth after 24 h. MCF-7 cells were more tolerant to hybrid **SG76** (Figure 28) with 10 µM reducing cell growth by 34.9% after 48 h. **SG77** and **SG81** were effective against MCF-7 with 1, 10 and 50 µM reducing cell growth from 12 h onwards. Both hybrids resulted in more than an 85% reduction in cell growth after 48 h.

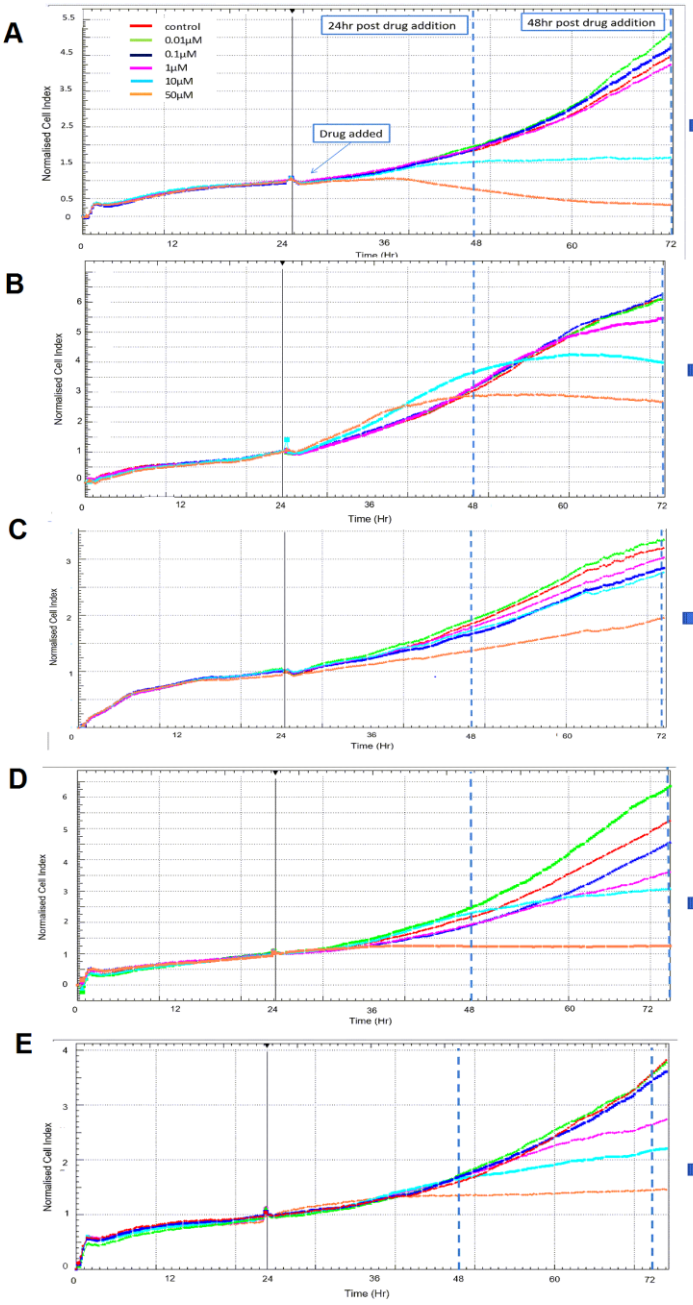

Artesunate

Cell Index (% Control)	24 h	48 h
Control	100.0	100.0
0.01 µM	102.6	113.3
0.1 µM	102.6	104.4
1 µM	97.4	95.6
10 µM	76.9	35.6
50 µM	41.0	6.7

Mitonafide

Cell Index (% Control)	24 h	48 h
Control	100.0	100.0
0.01 µM	103.3	103.3
0.1 µM	106.7	100.0
1 µM	107.7	91.7
10 µM	116.7	66.7
50 µM	93.3	43.3

SG76

Cell Index (% Control)	24 h	48 h
Control	100.0	100.0
0.01 µM	102.6	103.0
0.1 µM	91.1	81.8
1 µM	94.7	90.9
10 µM	92.1	78.8
50 µM	73.7	60.6

SG77

Cell Index (% Control)	24 h	48 h
Control	100.0	100.0
0.01 µM	108.7	118.9
0.1 µM	87.0	84.9
1 µM	87.0	67.9
10 µM	104.3	56.6
50 µM	54.3	23.6

SG81

Cell Index (% Control)	24 h	48 h
Control	100.0	100.0
0.01 µM	106.3	100.0
0.1 µM	104.4	97.0
1 µM	103.8	71.6
10 µM	103.1	59.5
50 µM	87.5	39.2

Figure 26: PNT1A response to parent drugs and hybrids in real-time

PNT1A cells were seeded at 5,000 cells/well. After 24 h growth, cells were treated with 0, 0.01, 0.1, 1, 10 or 50 µM of (A) artesunate, (B) mitonafide, (C) **SG76**, (D) **SG77** or (E) **SG81**. Cell growth was measured every 15 min using RTCA instrument for a further 48 h after drug addition. The corresponding tables on right of each RTCA graph summarises the mean CI values recorded for each treatment at 24 h and 48 h (time points indicated by broken blue lines); CI values are expressed as % of untreated control. Each real-time experiment was performed three times in triplicate.

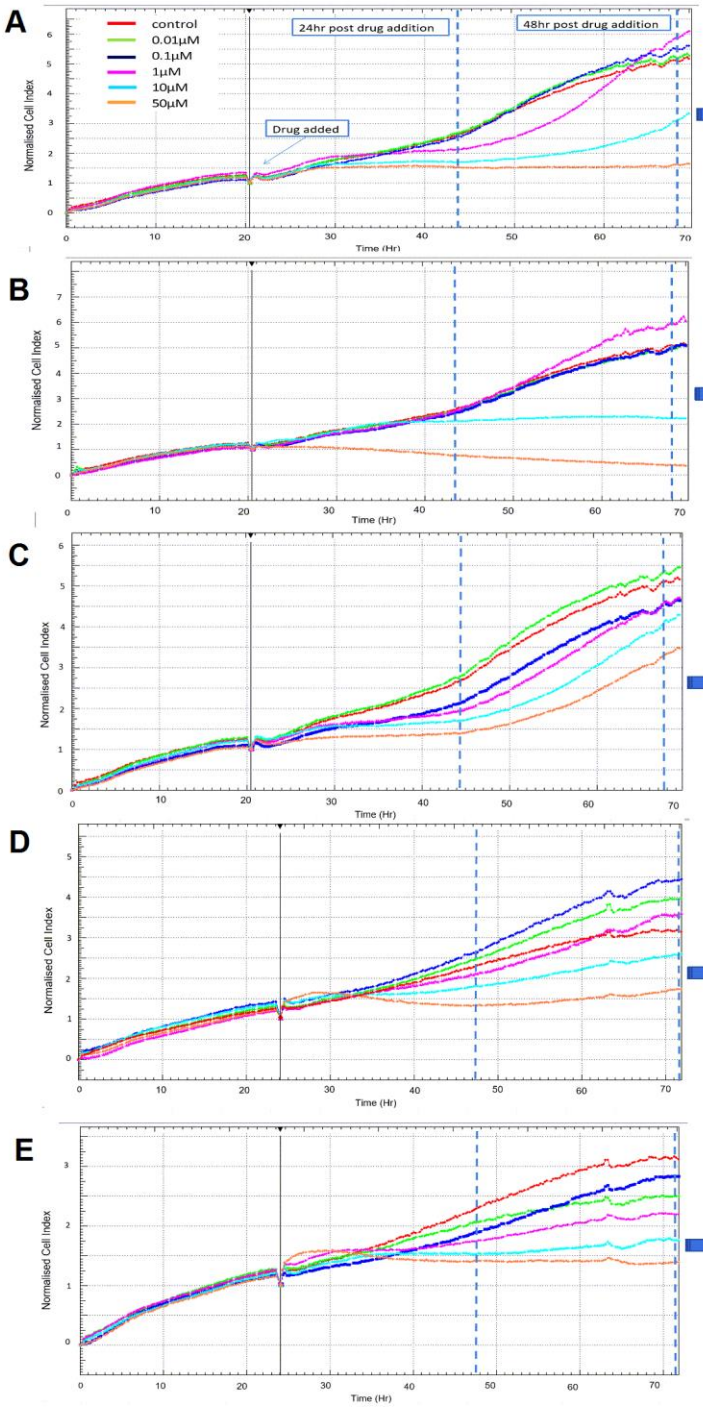

Artesunate

Cell Index (% Control)	24 h	48 h
Control	100.0	100.0
0.01 µM	102.0	106.0
0.1 µM	99.2	110.0
1 µM	82.4	118.0
10 µM	62.7	60.0
50 µM	58.8	30.0

Mitonafide

Cell Index (% Control)	24 h	48 h
Control	100.0	100.0
0.01 µM	99.2	98.0
0.1 µM	98.0	99.0
1 µM	99.6	115.7
10 µM	84.0	39.2
50 µM	32.0	7.8

SG76

Cell Index (% Control)	24 h	48 h
Control	100.0	100.0
0.01 µM	105.8	103.8
0.1 µM	84.6	84.6
1 µM	76.9	86.5
10 µM	65.4	76.9
50 µM	53.8	63.5

SG77

Cell Index (% Control)	24 h	48 h
Control	100.0	100.0
0.01 µM	108.7	125.0
0.1 µM	113.0	140.6
1 µM	87.0	109.4
10 µM	73.9	78.1
50 µM	60.9	54.7

SG81

Cell Index (% Control)	24 h	48 h
Control	100.0	100.0
0.01 µM	88.9	78.1
0.1 µM	80.0	81.3
1 µM	71.1	71.9
10 µM	66.7	54.7
50 µM	62.2	43.8

Figure 27: PC-3 response to parent drugs and hybrids in real-time

PC-3 cells seeded at 4,000 cells/well. After 24 h growth, cells were treated with 0, 0.01, 0.1, 1, 10 or 50 µM of (A) artesunate, (B) mitonafide, (C) **SG76**, (D) **SG77** or (E) **SG81**. Cell growth was measured every 15 min using RTCA instrument for a further 48 h after drug addition. Each experiment was performed three times in triplicate. The corresponding tables on right of each RTCA graph summarises the mean CI values recorded for each treatment at 24 h and 48 h (time points indicated by broken blue lines); CI values are expressed as % of untreated control. Each real-time experiment was performed three times in triplicate.

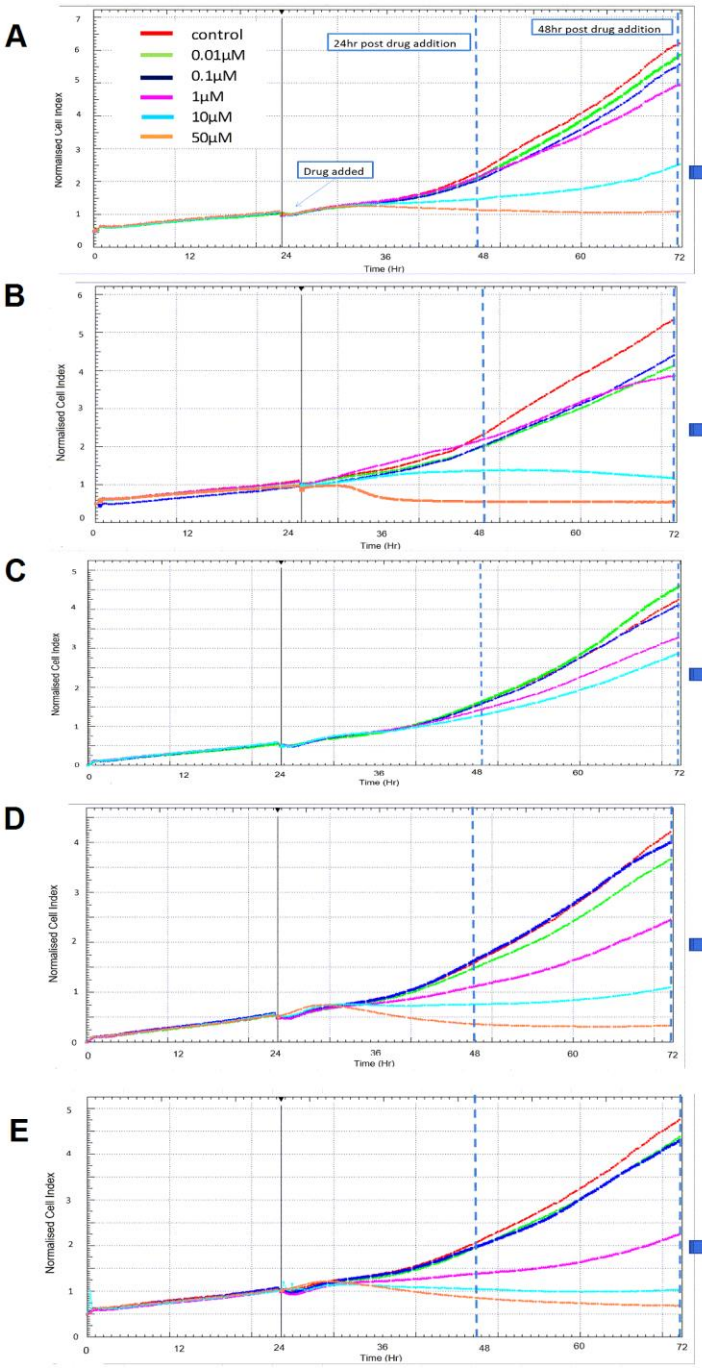

Artesunate

Cell Index (% Control)	24 h	48 h
Control	100.0	100.0
0.01 µM	95.7	93.5
0.1 µM	93.5	90.3
1 µM	91.3	64.5
10 µM	63.0	58.1
50 µM	50.0	17.7

Mitonafide

Cell Index (% Control)	24 h	48 h
Control	100.0	100.0
0.01 µM	87.0	77.8
0.1 µM	87.0	82.4
1 µM	95.7	70.4
10 µM	56.5	22.2
50 µM	26.1	9.3

SG76

Cell Index (% Control)	24 h	48 h
Control	100.0	100.0
0.01 µM	101.2	104.7
0.1 µM	99.4	95.3
1 µM	87.9	81.4
10 µM	81.8	65.1

SG77

Cell Index (% Control)	24 h	48 h
Control	100.0	100.0
0.01 µM	91.5	84.9
0.1 µM	100.6	93.0
1 µM	67.1	57.0
10 µM	42.7	25.6
50 µM	28.0	9.3

SG81

Cell Index (% Control)	24 h	48 h
Control	100.0	100.0
0.01 µM	95.2	91.5
0.1 µM	95.2	90.9
1 µM	66.7	48.9
10 µM	47.6	21.3
50 µM	38.1	14.5

Figure 28: MCF-7 response to parent drugs and hybrids in real-time

MCF-7 cells were seeded at 5,000 cells/well. After 24 h growth, cells were treated with 0, 0.01, 0.1, 1, 10 or 50 µM of (A) artesunate, (B) mitonafide, (C) **SG76**, (D) **SG77** or (E) **SG81**. Cell growth was measured every 15 min using RTCA instrument for a further 48 h after drug addition. Each experiment was performed three times in triplicate.

4.4 Discussion

In this chapter, ART-NAP hybrids were investigated for antitumour efficacy. To our knowledge, this is the first time such hybrids have been synthesised and investigated. The anticancer activity of the hybrids was compared with the parent drugs artesunate and mitonafide. Both parent drugs have known anticancer properties *in vitro* and *in vivo* [18,474–476].

ART-NAP hybrids were initially investigated in PC-3 cells at a single concentration of 50 µM to determine the best performing hybrids for further investigation. ART-NAP hybrids **SG76**, **SG77** and **SG81** were then nominated for a more in depth *in vitro* investigation. Firstly, cell count analysis was performed 48 h after drug addition in all cell lines tested; these included PC-3, MCF-7 and HL60 tumour cells and non-tumour PNT1A. Artesunate and mitonafide were potent in all 4 cell lines with significant reductions in cell number detected at concentrations of 1,10 and 50 µM ($P \leq 0.001$) (Figure 23). All three hybrids evaluated were also effective against tumour cells with significant reductions in cell number detected at concentrations of 1,10 and 50 µM ($P \leq 0.001$) (Figure 24). It was clear that PNT1A were less sensitive to hybrid treatment despite significant reductions in cell number at higher concentrations ($P \leq 0.001$).

To summarise the cell count data more effectively, an IC_{50} was generated for each drug by plotting log concentration vs cell number (expressed as % control) as described in 4.2.5. This data shows that HL60 was most sensitive to the hybrid drugs with IC_{50} ranging from 2.0 µM to 3.9 µM (Table 2). Furthermore, hybrids were generally more active than artesunate in HL60 and PC-3. However, the hybrids appeared to be less effective than parent drugs in reducing MCF-7 cell number with IC_{50} values ranging from 23.0 µM to 74.0 µM. This reason for the reduced efficacy in MCF-7 is yet to be determined but may involve MDR proteins which facilitate the efflux of drugs from the cell [477]. From the generated IC_{50} data it was clear that PC-3 cells were more sensitive to ART-NAP hybrids than non-tumour PNT1A. **SG76** and **SG77** generated IC_{50} values of 68.3 µM and 54.9 µM in PNT1A when compared to 15.8 µM and 4.9 µM in PC-3 respectively (Table 2). PC-3 and PNT1A response was also compared directly using two-way ANOVA (Figure 25). Mitonafide was significantly more effective in the tumour cell line. The

improved selectivity of mitonafide and similar DNA-targeting drugs is likely to be due to the rapid growth of and compromised DNA repair mechanisms in cancer cells [4]. PC-3 cells were more sensitive to the hybrids than their non-tumour counterparts with significant differences in cell response detected at concentrations of 0.1 µM and higher.

Furthermore, PNT1A were more tolerant to hybrid compounds than to the parent drugs with IC_{50} ranging from 2.9-23.3 µM in the parents and from 15.9-68.3 µM for the hybrids. All compounds tested were also ranked in terms of tumour cell selectivity (Table 3). **SG77** was shown be most selective drug tested with 11 times more activity in PC-3 cells. Artesunate is the least selective with only three times more activity in in tumour cells. The reason for this observed selective toxicity is yet to be determined. Although it has been suggested that the selectivity of artesunate in cancer cells could be due to higher iron (II) levels which mediate endoperoxide cleavage [158]. Furthermore, the correlation between the mRNA expression of glutathione-related genes and the IC_{50} values of artesunate has been reported. The authors concluded that glutathione-related enzymes contribute to the resistance of tumour cells to artesunate and also to reduced toxicity in non-tumour organs [474]. This data highlights a potential advantage of utilising ART-NAP hybrids to reduce toxicity in non-tumour cells and tissues while still maintaining efficacy in tumour cells.

ART-NAP hybrids and their parent drugs were further investigated in PNT1A, PC-3 and MCF-7 using the xCELLigence RTCA system for a dynamic evaluation of cell growth in real-time. This assay is not compatible with suspension cell lines and therefore HL60 cells were not analysed by this method. Artesunate and mitonafide were both active in PC-3 and PNT1A in agreement with cell count analysis (Figure 26, Figure 27). Hybrid drugs also reduced PNT1A and PC-3 cell growth particularly at higher concentrations 10 µM and 50 µM. it was apparent that both parent drugs and hybrids take effect earlier in PC-3 compared to PNT1A with increased reduction in cell growth within 24 h of treatment. For example, 10 µM **SG76** reduced PNT1A cell growth by only 7.9% after 24 h when compared to a reduction of 34.6% observed in PC-3 cells. It must also be noted that PC-3 cells do appear to mount a recovery from 24-48 h in the case of both artesunate and **SG76** treatment (Figure 27). This highlights the advantage of quantifying cell

growth in real time to detect instances of cell recovery which may otherwise be overlooked.

MCF-7 cells were the least sensitive tumour cell line during cell count analysis. Interestingly, RTCA data (Figure 28) suggests that parent compounds and two of the hybrids are very effective in reducing MCF-7 growth. **SG77** and **SG81** were very effective against MCF-7 with both 10 µM and 50 µM reducing cell growth by more than 80%. This is in contrast with IC_{50} values of 40 and 74 µM generated during cell count analyses (Table 2). MCF-7 are known to be sensitive to both ART [146] and NAP [471] derivatives with ROS production, lysosomal damage and apoptosis reported. This observed difference across the two methodologies is likely due to the improved sensitivity of the xCELLigence system to detect more subtle changes such as reduction in adherence and change in morphology as compared to cell number [299,456]. It is, therefore, possible that hybrids are active in MCF-7 but cell detachment does not occur in all cells within 48 h after treatment.

Based on these findings, the hybrid approach may result in a more targeted cancer therapy with non-tumour cell line more tolerant to hybrids while retaining antitumour activity in three cancer cell lines. This is particularly evident in hybrids **SG77** and **SG81** which were 8 and 11 times more active in PC-3 than their non-tumour counterparts. While mitonafide is more than 7 times more effective in PC-3, which is likely owed to DNA targeting properties, the NAP is also very potent in PNT1A. This is in agreement with previous NAP studies which have reported non-tumour cell toxicity [166,181,478]. The endoperoxide artesunate was only three times more active in tumour cell line which highlights the improvement and potential merits of the hybrid approach. Perhaps physiochemical properties contribute to this observed specificity in hybrid compounds, with slower drug uptake previously highlighted as a potential challenge of hybrid therapy [195,479]. It is also possible that endoperoxide cleavage is increased in cancer cells due to inherently higher iron levels [151,158]. Further research is needed to determine the detailed pharmacological anticancer mechanism(s) responsible for hybrid cytotoxicity.

4.5 Conclusions

Hybrids **SG76**, **SG77** and **SG81** were evaluated in both tumour and non-tumour cell lines**.** HL60 and PC-3 were the most sensitive cells with IC_{50} values ranging from of 2.0-3.9 µM and 1.7-15.8 µM respectively. Hybrids **SG76** and **SG77** were more potent in PC-3 when compared to non-tumour PNT1A suggesting selective toxicity. Furthermore, PNT1A cells were more tolerant to hybrids when compared to artesunate and mitonafide. Hybrid **SG77** was the most selective hybrid with 11 times more activity in PC-3. Based on these findings ART-NAP hybrids may result in more potent and targeted cancer therapy which may overcome the common drawbacks of severe toxicity in non-tumour tissue and development of resistance.

Chapter 5. Role of oxidative stress in SG77 hybrid drug action

5.1 Introduction

The work described in this chapter builds upon chapter 4 evaluating some of the suspected underlying mechanisms responsible for the efficacy of NAP-ART hybrid **SG77** (Figure 19). This hybrid was shown to induce selective cell growth inhibition in several cancer types when compared to non-tumour PNT1A. Furthermore, PNT1A were more tolerant to this hybrid treatment than either parent compound. The objective of this work was to investigate the mechanisms accounting for **SG77** drug action and tumour cell selectivity. Gene expression analysis was performed to determine the potential for **SG77** to induce oxidative stress, DNA damage and apoptosis. In addition, ROS generation, glutathione levels and apoptosis was measured in response to **SG77.** HL60 cells were the most sensitive to the novel hybrid drugs in the previous chapter and were therefore selected for this mechanistic evaluation.

5.2 DNA damage/repair

5.2.1 Cellular DNA repair mechanisms

DNA damage is unavoidable during the lifetime of a cell and can occur from a range of internal and external factors [480]. For example, oxygen radicals, ionising radiation and chemotherapeutic drugs are known to cause DNA damage [481,482]. Internal processes such as cellular respiration can also lead to DNA damage. The cell is equipped with a DNA damage response (DDR) mechanism to cope with or eliminate damaged DNA [483]. Damaged DNA can be removed from the cell or DNA can be repaired [483]. Cell cycle progression is also slowed down to facilitate DNA repair [480]. Furthermore, changes in gene expression can allow the cell to cope with DNA damage [484–486]. However, if DNA damage is excessive, or the cell becomes deregulated then apoptosis will be activated to eliminate the damaged cell [487]. ATM and ATR are checkpoint protein kinases which are key in detecting DNA damage in the DNA damage response [488]. They activate transducer protein kinases such as Chk1 and Chk2 checkpoint regulators. Once transducers reach their downstream targets or effectors they can initiate several processes including cell cycle arrest, DNA repair and apoptosis [489,490]. In the cell, the main modes of DNA repair are (a) single stranded break repair (base excision repair (BER) and

nucleotide excision repair (NER)) and (B) double-strand break repair [40,491]. BER involves the removal of a damaged base by a DNA glycosylase to generate an abasic (AP) site. The 3' sugar residue is then removed by an AP endonuclease inserting a 5' to the abasic sugar. This forms a gap that is filled by DNA polymerase which assembles the corresponding nucleotide sequence to repair the nick [492,493]. NER excision is the main DNA repair system utilised in response to radiation or chemotherapy [494]. This method involves the removal of bulky DNA lesions. The damaged bases are removed by an enzyme called a nuclease [495]. This enzyme has several components capable of making two incisions surrounding the damaged nucleotides for repair [495]. Double-strand breaks (DSBs) are more serious lesions that threaten a loss of chromosomal content and are produced by severe insults such as ROS and ionising radiation [494,496]. DSBs are repaired either by homologous recombination (HR) or nonhomologous end-joining (NHEJ) mechanisms [101].

5.2.2 PARP-mediated DNA repair

PARPs are an enzyme family capable of catalysing the transfer of ADP-ribose to proteins (poly-ADP-ribosylation), a post-translational modification (PTM) that was discovered over 40 years ago [497,498]. PARP-1 and PARP-2 the most well-studied due to their involvement in DNA repair [499–501]. However, PARPs may also be involved in other key cellular processes such as proliferation and apoptosis [497]. PARPs function in DNA repair was first discovered when DNA damaging agents and radiation-induced DNA damage were found to correlate with increased PARP activity [502]. The accumulation of DNA fragmentation has also been found to result in a significant increase in PARP levels in cells [503].

PARP is involved in BER and NER repair pathways in response to single-stranded DNA breaks (SSBs) [100,504,505]. PARP also plays a role in DSB repair during NHEJ pathway [506]. It has been shown that the PARP enzyme binds tightly to DNA strand breaks following poly-ADP-ribosylation. This process then allows for a repair enzyme to access the damaged section of DNA [507,508]. PARP-1 and PARP-2 can interact with many of the same downstream effectors in SSB repair and BER pathways [509]. PARP-1 is also involved in NER and when PARP-1 is inhibited NER is adversely affected [510]. Furthermore, PARP knockdown in a

mouse model resulted in increased sensitivity to alkylating agents such as gamma radiation [511]. DNA repair mechanisms have been shown to induce resistance to chemotherapeutic agents [512,513]. Furthermore, PARP inhibitors have also been shown to sensitise cancer cells to chemotherapy and radiation [514,515].

Both ART and NAP compounds, similar to the compound investigated in the current study, have been shown to involve PARP upregulation [516,517]. For example, a 3-Nitro-naphthalimide and nitrogen mustard conjugate, NNM-25, was shown to be very potent against liver cancer cells. The antitumor mechanism was thought to be p53 mediated apoptosis. Furthermore, NNM-25 inhibited PARP-1 activity suggesting the suppression of DNA repair [516]. Another study investigated the cytotoxicity of ART, DHA, artemether, and artesunate in liver cancer cell lines HepG2 (p53 wild-type), Huh-7 and BEL-7404 (p53 mutant), and Hep3B (p53 null), and a normal human liver cell line, 7702. Artesunate and DHA were found to be the most potent in liver cancer cell lines with selective toxicity observed. The authors also reported increased levels of cleaved PARP protein expression following a western blot analysis. This indicates that PARP mediated DNA repair may be crucial in the cellular response to both ART and NAP compounds [134].

5.2.3 NHEJ pathway in Double strand DNA repair

Intercellular repair of DSBs can be problematic because bringing two DNA molecules together increases the risk of mutations and chromosome rearrangements if the ends are incorrectly joined [518–520]. The NHEJ pathway is most commonly employed in DSB repair although several other “backup” pathways are possible [521]. The initial step in NHEJ pathway is the recognition and binding of the Ku heterodimer to the DSB [522,523]. The Ku heterodimer is composed of Ku70 and Ku80 subunits [524]. These two Ku subunits are both composed of three domains: an amino-terminal (also called von Willebrand domain (vWA)), a central Ku core , and a carboxyl-terminal region [524,525]. The vWA and Ku core domains are involved in the heterodimerisation of Ku complex. The carboxyl-terminal region is likely where a DNA molecule will bind [526,527].

Ku80 is thought to be involved in several protein-protein interactions [528]. Ku70/80 has also been shown to rapidly localise DSBs when they arise and bind with extremely high affinity [529,530]. The Ku70/80 heterodimer is thought to produce a ring-shaped structure which can house a double strand DNA helix [530]. Furthermore, Ku binds to the sugar backbone of DNA and not to the nucleotide bases which explains the ability of Ku to bind to DNA regardless of the sequence composition [531,532]. Once the Ku heterodimer is bound to the DSB ends, other NHEJ factors are recruited to the DNA damage site including DNA dependent protein kinases, X-ray cross-complementing protein 4 (XRCC4), DNA Ligase IV and NHEJ-1 [533–535].

Several studies have investigated Ku and its interaction with other NHEJ factors [533,536,537]. DNA Ligase IV catalyses the ATP-dependent transfer of phosphate bonds resulting in strand ligation and DNA repair like other DNA ligases [538]. However, DNA Ligase IV is unique in that it can repair large nucleotide gaps and incompatible DSB ends [536,539]. NHEJ-1 (also called XLF (XRCC4 like factor) interacts with XRCC4 to form extensive filaments [540–542]. XLF stimulates the activity of LIGIV in joining non-compatible DNA ends, indicating that XLF can mediate the activity of XRCC4:LIGIV and may induce end joining by promoting the re-adenylation of LIGIV [543–545].

5.3 Cell death and apoptosis

There are several forms of cell death which can be categorised in different ways including by morphological features (blebbing, cell shrinkage, swelling of cellular organelles), enzymatic processes (nuclease and protease activity such as caspase enzymes) and functional properties (physiological, programmed, immune stimulated). The Nomenclature Committee on Cell Death (NCCD) has published several papers detailing the most suitable ways for identifying the different types of apoptosis and cell death [546–548]. Autophagic cell death is a process of cell death by which damaged cellular materials are engulfed by double membraned organelles called autophagosomes signalling them for degradation. This form of cell death is characterised by the vacuolisation of the cytoplasm and the accumulation of autophagic vacuoles [549]. Necrosis is characterised by increases in cell size swelling of cellular organelles and the loss of intracellular

contents. Necrotic cell death was generally thought to be an accidental or uncontrolled form of cell death but several studies have now shown that necrosis can be regulated by transduction pathways and catabolic events [550,551].

Apoptosis is a mechanism of cell death first discovered in 1972 [552,553]. Apoptosis is characterised by the rounding up of the cell, retraction of pseudopodes, reduction of cell size, condensation of chromatin and nuclear fragmentation. Typically, apoptosis will not result in plasma membrane blebbing or engulfment by phagocytes [550]. Apoptosis can be activated by the cell in response to excessive DNA damage, chemotherapy or where a cell becomes dysregulated [554,555]. DNA fragmentation and the presence of activated caspase proteins are often associated with apoptosis but it must be noted that both events can occur independently of apoptosis.

It is now known that the term apoptosis encompasses several different and complex biochemical pathways. These include extrinsic apoptosis (receptor mediated) and intrinsic apoptosis (mitochondria mediated) and the Perforin Granzyme pathway [393,556]. Caspase enzymes are involved in all of these apoptotic pathways and are important for maintaining homeostasis through regulating cell death and inflammation. They can be divided in to two subtypes; Initiator caspases and executioner caspases. The initiator caspases-8 and -9 normally exist as inactive procaspase monomers that are activated by dimerization [557,558]. Executioner caspases -3, -6, and -7 occur as inactive procaspase dimers that must be cleaved by initiator caspases to be activated. This cleavage allows a conformational change that brings the two active sites of the executioner caspase dimer together to form a mature protease [557]. Once activated, a single executioner caspase can cleave and activate other neighbouring executioner caspases resulting in an accelerated response.

5.3.1 Extrinsic apoptosis pathway

The extrinsic pathway is initiated through several death receptors including tumour necrosis factor (TNF), Fas receptor, death receptor -3 (DR3), death receptor-4 (DR4), and death receptor-5 (DR-5) [550,559–561]. These death receptors all contain an amino acid sequence known as a “death domain”. This domain is key in transmitting signals from outer cell membrane to the cytoplasm [562]. There

have been several death receptor/ligand combinations which have been identified. TNF-α and Fas pathways are the most well understood of the death receptor pathways [559,563]. In these two models of extrinsic apoptosis, there is a clustering of receptors to their corresponding ligands.

Cytoplasmic proteins are then recruited which bind to the death domains [564]. When Fas ligand binds to its receptor, this results in binding of Fas associated protein with death domain (FADD) [357]. On the other hand, binding of TNF-α to its corresponding receptor triggers the binding of the adaptor protein TNF-1 associated death receptor domain (TRADD) [565,566]. TRADD then recruits FADD and receptor interacting protein kinase (RIP) proteins which interact with procaspase-8 to form death-inducing signalling complex (DISC) [567]. DISC then cleaves procaspase-8 to form active caspase-8 which marks the beginning of the execution phase of apoptosis (Figure 29). Extrinsic apoptosis can also be inhibited through a protein called c-FLIP which can bind to FADD and caspase-8 to render them inactive [568,569]. A protein called Toso, has also been shown to block Fas-induced apoptosis by inhibiting caspase-8 [570,571]. Activated Caspase-8 is known to activate caspase 3, a crucial executioner caspase [572]. Once activated caspase 3 is known to act on multiple proteins leading to apoptosis. These proteins are involved in chromatin condensation and migration, DNA fragmentation, cellular shrinkage and blebbing [573,574].

5.3.2 Intrinsic apoptosis pathway

Intrinsic apoptosis involves a diverse array of signalling processes initiated in the mitochondria that then act on specific cellular targets [393] (Figure 29) . Both pro-apoptotic and anti-apoptotic proteins play a role in controlling the cells fate [393]. Hypoxia, free radicals and viral infections are all known to induce apoptosis, while growth factors and hormones are known to down regulate or prevent apoptosis [575] . When apoptosis is activated, there is a loss in mitochondrial outer membrane potential resulting mitochondrial outer membrane permeabilisation (MOMP) [576]. Subsequently, proapoptotic proteins such as cytochrome C and a second mitochondria-derived activator of caspases (SMAC/DIABLO) [577]. Both of these proteins are known to initiate caspase dependent apoptosis [577]. Cytochrome C binds to apoptosis protease activating factor 1 (APAF-1) and procaspase 9 to

form the apoptosome (Figure 29) [578]. Caspase-9 then triggers the cleavage of caspase-3 and apoptosis ensues [578].

Further downstream of the caspase cascade, apoptosis inducing factor (AIF), endonuclease G and CASP-activated deoxyribonuclease (CAD) are released from the mitochondria and translocated to the nucleus to facilitate DNA degradation and chromatin condensation [579–581]. The B cell lymphoma-2 (Bcl-2) family of proteins, identified over 30 years ago as crucial regulators of cell death are thought to play an important role in regulating intrinsic apoptosis [582]. The Bcl-2 family of proteins consist of both pro and anti-apoptotic proteins. Pro-apoptotic proteins include Bax, Bad, Bak and Bid while anti-apoptotic proteins include Bcl-2, BCL-xL and BCL-xS [583–585]. Bax induces the release of cytochrome c from the mitochondria into the cytosol of the cell while Bcl-2 is involved in the inhibition of apoptosis by blocking cytochrome c release [586]. An increase in the Bax/Bcl-2 ratio is known to cause the release of cytochrome c triggering the activation of caspase-9 which cleaves procaspase 3. Active caspase-3 then initiates a cascade of enzymatic reactions resulting in apoptosis [587].

It must be noted that the intrinsic and extrinsic pathways are not completely independent. A protein called BID plays a role in the crosstalk between the two pathways (Figure 29). In this case, caspase 8 cleaves a BH3 only protein BID generating a truncated fragment known as truncated BID that can permeabilise the mitochondrion resulting in MOMP. ART and NAP based compounds have both been found to induce intrinsic apoptotic pathway in cancer cells For example a novel amonafide analogue, 7-b, was shown induce mitochondrial mediated intrinsic apoptosis with the production of reactive oxygen species (ROS) and alteration of the MOMP in a lymphoma cell line [588]. A separate study showed that artesunate treatment resulted in intrinsic apoptosis in breast cancer cells via Iron-mediated ROS production in the lysosome [146]. Artesunate was also shown to induce apoptosis in doxorubicin resistant leukemic T cells through the intrinsic pathway via the generation of ROS [296].

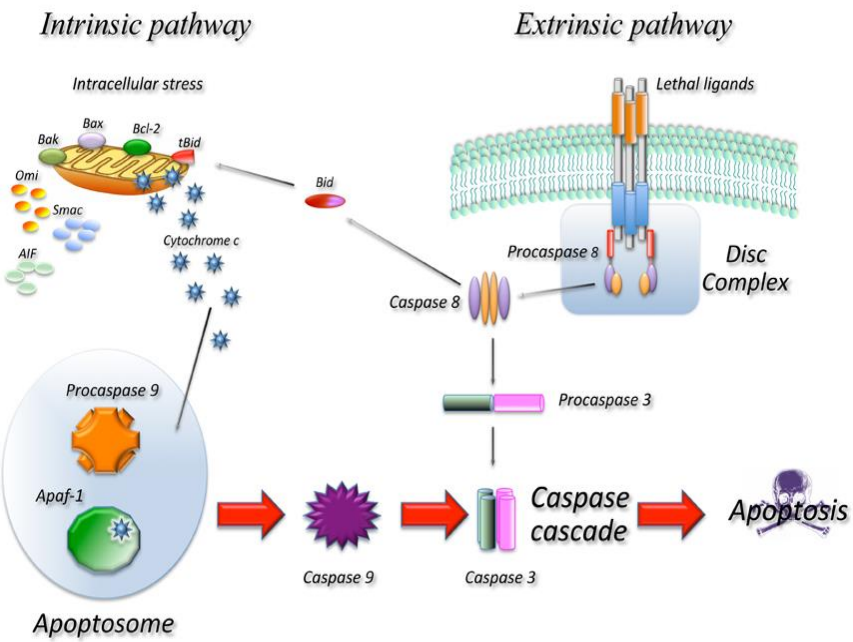

Figure 29 Intrinsic and extrinsic apoptotic pathways

Schematic of both intrinsic (mitochondria-mediated) and extrinsic (receptor mediated) apoptotic pathway. The extrinsic pathway is activated upon ligand binding to specific receptors. This results in the formation of the DISC complex which then activates procaspase-8 trigering the activation of executioner caspase-3. In the intrinsic pathway release of cytochrome c from the mitochondria results in the formation of the apoptosome and the activation of caspase 9. Caspase 8 and 9 then activate downstream caspases such as caspase 3 resulting in cell death.The two pathways are connected through the cleavage of the BH3 only protein BID by activated caspase-8 [589].

5.3.3 Perforin/granzyme apoptosis pathway

T-cell mediated cytotoxicity occurs through the recruitment of CD8+ cells to kill antigen-bearing cells. CTLs are able to kill target cells via the extrinsic pathway and the Fas ligand/ Fas receptor interaction is the predominant method of cytotoxic T cells -induced apoptosis [590]. However, they are also able to exert their cytotoxic effects on tumour cells and virus-infected cells via the perforin/granzyme apoptotic pathway [556]. Granzymes are serine proteases that are released by cytoplasmic granules within cytotoxic T cells (CTLs) and natural killer (NK) cells of the immune system [591] . Perforins are proteins released by killer cells and function to create pores in target cells. Perforins and granzymes induce target-cell apoptosis cooperatively. Granzymes are required for triggering apoptosis in antigen presenting target cells but the delivery of granzymes to the target cells is facilitated by perforins [592]. Granzyme A and granzyme B are the most important components in apoptosis activation. Granzyme B will cleave proteins such as pro-caspase-10 and factors such as ICAD (Inhibitor of Caspase Activated DNase) [593]. Granzyme B can utilise the intrinsic pathway via BID cleavage and induction of cytochrome c release [594]. However, granzyme B can also directly activate caspase-3 triggering the execution phase of apoptosis [594].

5.4 Reactive oxygen species

5.4.1 What are reactive oxygen species?

Reactive oxygen species (ROS) are oxygen containing species which may be radicals, ions or molecules that have a single unpaired electron in their outermost shell of electrons making them extremely reactive [595]. ROS interact with biological molecules, including DNA, proteins and lipids. Mild increases in ROS can activate cellular signalling processes such as cell growth and inflammation , whereas a large increase of ROS would likely induce irreversible cellular damage, leading to cell death [595]. ROS are generated from the metabolism of molecular oxygen and occurs in many forms including superoxide ($O_2^{\bullet -}$), hydroxyl radical ($^{\bullet}OH$), nitric oxide ($NO^{\bullet}$) and singlet oxygen ($_1O^2$). Superoxide, hydrogen peroxide and hydroxyl radicals are the most common ROS associated with cancer research

[595]. The majority of cellular ROS is produced in the mitochondria via oxidative phosphorylation [596].

5.4.2 Effects of ROS

ROS are essential for regulating many biological functions including cell growth, enzyme activity, inflammation and removal of toxins and pathogens [595]. ROS regulate several signal transduction pathways by modifying the function of proteins, transcription factors and genes [597]. Low doses of ROS are required in non-tumour cells to modulate these vital processes while excessive ROS lead to cell damage and the onset of cancer [598,599]. Mitochondria-derived ROS regulate both cell growth and quiescence. These processes are mediated by manganese superoxide dismutase (MnSOD) activity and this enzyme functions as a ROS activator [597]. Decreased MnSOD activity induces growth, due to increased superoxide and low hydrogen peroxide levels, while increasing MnSOD activity induces quiescence, due to increased generation of hydrogen peroxide [600].

Severe increases in ROS can cause cancer cell cycle arrest, senescence and apoptosis. Apoptosis has been linked to an increase in mitochondrial oxidative stress that causes cytochrome C release in caspase-mediated cell death [601]. Superoxide generation through the Rac-1/NADPH oxidase pathway can also signal apoptosis [602]. In response to ROS, c-Jun N-terminal kinases (JNK) catalyse the phosphorylation and downregulation of anti-apoptotic proteins such as Bcl-2 [603]. JNK also play a role in stimulating pro-apoptotic Bax production and thus altering Bax/Bcl-2 ratio [604]. p38, another MAPK family member, has been shown to signal apoptosis in response to increased ROS levels [243]. Both p38 and JNK are activated through ASK-1 (apoptosis signal-regulating kinase-1) [604,605].

5.4.3 ROS in cancer progression

ROS has been implicated for some time in malignant transformation [606,607]. Some cancer cells have been reported to use ROS to suppress apoptosis, accelerate growth, metastasis and angiogenesis, and promote genetic instability by increased oxidative DNA damage [608]. Many cancer cells produce higher levels of ROS than their non-tumour counterparts *in vitro* and *in vivo* [609–611]. Compared with non-tumour cells, cancer cells are also more resistant to oxidative stress [612]. DNA damage and lipid peroxidation, by-products of oxidative stress, have been

found to occur at higher levels in cancer cells. For example, levels of 8-hydroxydeoxyguanosine (8-OHdG) which has been identified as a possible marker for cancer and oxidative stress [613].

Lipid peroxidation products such as 4-hydroxynonenal (HNE) have also been detected in response to ROS in cancer cells [207]. Cancer cells are thought to adapt to ROS and evade apoptosis by genetic mutations [92]. Activation of oncogenes, abnormal metabolism, mitochondrial dysfunction and loss of functional p53 are intrinsic factors known to cause increased ROS production in cancer cells [554,614]. These events cause more genomic instability, mutations and ROS formation as the process repeats itself leading to cancer progression. ROS can also be produced in response to chemotherapy and hypoxia. This ROS build up can cause DNA damage which in turn may activate p53 to protect non-tumour cells from oxidative stress [86]. However, in cancer cells, p53 can be defective resulting in an accumulation of DNA damage and genetic instability. This instability gives rise to further oncogene activation, mitochondrial dysfunction and compromised antioxidant systems. ROS is generated due to these events and the “vicious cycle” repeats itself [86]. ROS induced gene mutations can then result in resistance to chemotherapy [615]. It must be noted that oxidative stress responses are very complex with several molecular signalling pathways already identified involving key factors such as HSF-1 [616], p53 [617], NF-kB [618] and p13K [619].

5.4.4 ROS in cancer treatment

Therapeutic selectivity is an important concern in cancer treatment. An ideal anticancer agent should be toxic to cancer cells with minimum toxicity in non-tumour cells. However, there are limited numbers of selective agents available for clinical use. A common biochemical target in cancer therapy is increased ROS generation exhibited by cancer cells [595]. There is an opportunity to exploit higher ROS in cancer cells by overcoming antioxidant defences in favour of apoptosis [620]. For example, leukaemia cells with intrinsic oxidative stress were highly sensitive to ROS induced stress by 2-methoxyestradiol (2-ME) when compared to non-tumour primary cell line [621]. This selectivity was thought to occur due to an increased reliance of the cancer cell line on superoxide dismutase (SOD) antioxidant defence [621].

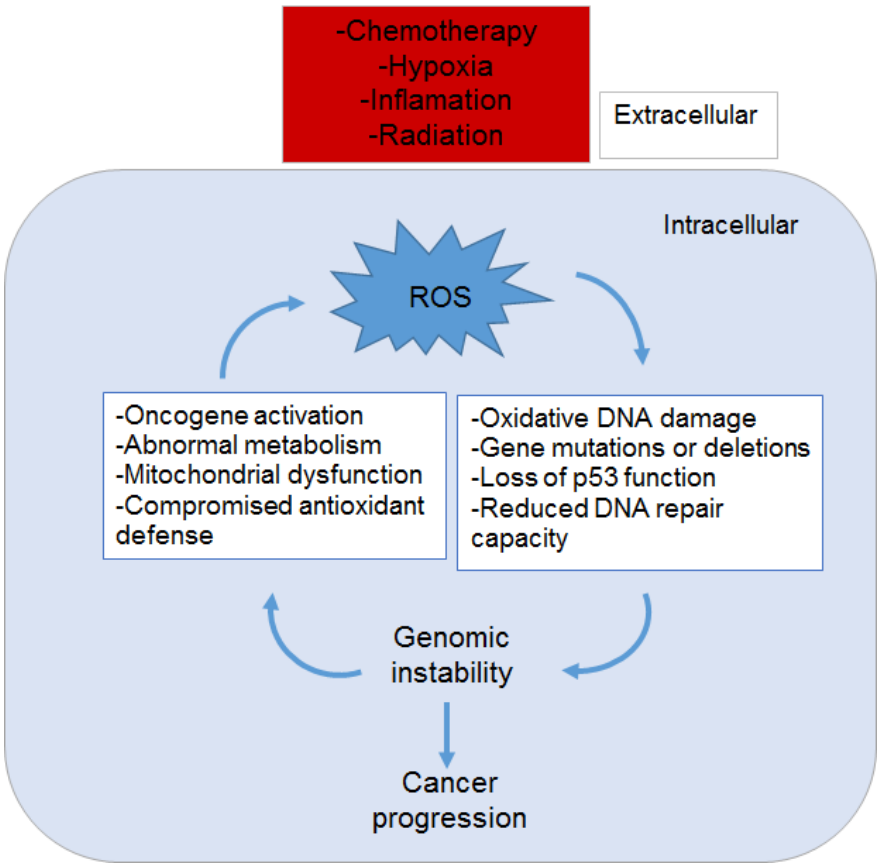

Figure 30 The vicious cycle of ROS stress in cancer therapy

ROS can be produced both from intracellular processes or can be induced through extracellular sources such as chemotherapy and hypoxia. ROS build up can cause DNA damage which in turn may activate p53 to protect non-tumour cells from oxidative stress. However, in cancer cells, p53 can be defective resulting in an accumulation of DNA damage and genetic instability. This instability gives rise to further oncogene activation, mitochondrial dysfunction and compromised antioxidant systems. Further ROS is generated due to these events and the "vicious cycle" repeats itself. This is often the reason why cancer cells can adapt to ROS and become resistant to chemotherapy. Figure adapted from [86]

Many frontline chemotherapeutic agents promote ROS production while attempting to disable the antioxidant system. The reoccurring drawback of ROS-based treatment is non-tumour cell toxicity. However innovative new delivery methods which employ more selective macromolecular techniques or nanoparticles are currently being developed which may increase retention in target tissues [622–624]. To conclude, cancer cells exhibit increased ROS generation that may promote cell growth, cell survival and drug resistance. This highlights the crucial role of ROS stress in tumour development and drug resistance. Targeting these biochemical properties of cancer cells with redox-modulating strategies is a promising therapeutic approach.

5.5 Glutathione

5.5.1 Glutathione synthesis and functions

Glutathione (GSH) is a three-amino-acid peptide formed by glutamic acid, cysteine, and glycine which is found in eukaryotic cells [625]. GSH is expressed in a broad range of organisms highlighting its major biological importance. GSH exists in both the reduced form (GSH) and the oxidised form (GSSG), reduced GSH is the more abundant, reaching a millimolar concentration in the intracellular compartment, the oxidised form (GSSG) is estimated to be less than 1% of the total GSH. GSH is primarily found in the cytosol of the cell (about 90%),while mitochondria contain nearly 10%, with the endoplasmic reticulum containing a very small percentage [626] .

GSH has several key functions including maintaining redox balance, detoxification, protein modulation and gene regulation [627]. GSH has a role in the detoxification of xenobiotics [628]. These substances are electrophiles and form conjugates with GSH in reactions catalysed by glutathione-s-transferases (GST) [627]. GSH is also involved in the maintenance of the thiol status of proteins. GSH maintains cysteinyl thiol groups of proteins in their reduced form which is often vital for protein functionality [616]. The balance of this reaction depends on the concentrations of GSH and GSSG. Through this protein modification, GSH is thought regulate several biological processes including enzyme activity, signal transduction and gene expression through redox-sensitive nuclear transcription factors such as AP-1, nuclear factor-kappa B (NF- κB) and p53 [598,629–631].

The biosynthesis of GSH from its constituent amino acids involves two ATP-requiring enzymatic steps. The first and rate-limiting step involves joining of L-glutamine and L-cysteine to form L-γ-glutamyl-L-cysteine and is catalysed by γ -glutamylcysteine synthetase (γ-GCS). γ-GCS consists of two subunits; heavy or catalytic subunit (GCLC) and a light or modifier subunit (GCLM). GCLC is subject to feedback inhibition by GSH thus regulating GSH synthesis. The second step catalysed by GSH synthetase (GSS) involves a bond formation between L-γ-glutamyl-L-cysteine and glycine to form GSH (Figure 31) [632,633]. The rate of cellular GSH synthesis is dependent on γ-GCS enzyme levels (rate limiting step

of glutathione synthesis) and the availability of its GSH substrates including L-cysteine [632].

5.5.2 Glutathione depletion and oxidative stress

Oxidative stress results when there is an imbalance between the production of excessive ROS and a biological system's ability to detoxify these harmful metabolites to prevent damage to cells, including proteins, lipids, and DNA [634]. Hence, the cell is equipped with antioxidant defence mechanisms which serve to scavenge harmful ROS. GSH is one of the most abundant antioxidants within the cell. When synthesised, GSH acts as a ROS scavenger, converting hydrogen peroxide and other ROS to water and non-toxic metabolites in the glutathione redox cycle (Figure 31). During this redox cycle, GSH is converted into an oxidised form, GSSG, as two GSH molecules form a disulphide bond. This step is catalysed by glutathione peroxidase (GPX). GSSG is then converted back to reduced GSH by glutathione reductase (GSR) at the expense of NADPH. This cycle is repeated to maintain redox balance in the body [635]. However, when ROS levels are excessive the depletion of GSH can occur resulting in a marked increase in GSSG. Therefore a reduction in GSH:GSSG ratio is a good indicator of oxidative stress [625,626]. In a resting cell, the molar GSH:GSSG ratio exceeds 100:1. However, when severe oxidative stress persists, this ratio can decrease to values of 10:1 and even 1:1 [636].

Oxidative stress can also induce the expression of GSH synthetic enzymes γ-GCS and GSS [626]. GSR regulates cellular GSH homeostasis by catalysing the reduction of GSSG to GSH using NADPH [637]. GSR expression, regulated by nuclear factor-erythroid 2 p45-related factor 2 (Nrf2), has been shown to be critical for cell survival during oxidative stress [638] . Furthermore, lower GSR levels in both cells and tissues may sensitise them to oxidative damage [639]. GPx is an 80 kDa protein with the function of reducing lipid hydroperoxides to corresponding alcohols, and free hydrogen peroxide to water. GPx expression is known to be important in alleviating oxidative stress *in vitro* and *in vivo* [640–642]. Furthermore, knockout of cellular glutathione peroxidase gene in mice caused increased sensitivity to diquat-induced oxidative stress [643].

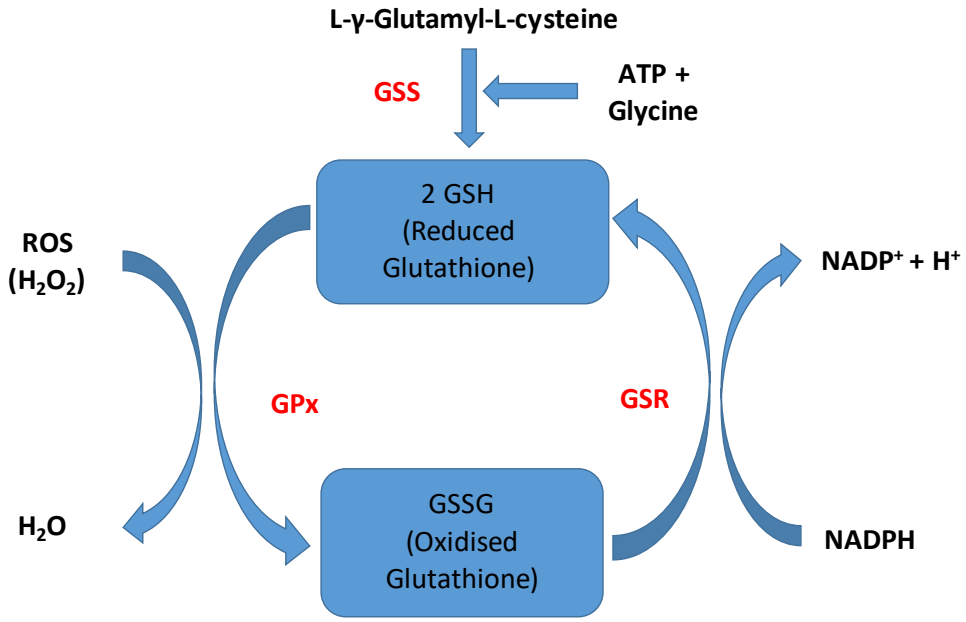

Figure 31 Glutathione redox cycle

Illustration of the final steps in glutathione synthesis. Glutathione acts as a ROS scavenger converting hydrogen peroxide and other ROS to water and non-toxic metabolites. In this process, GSH is converted into an oxidised form, GSSG, as two GSH molecules form a disulphide bond. This GSSG is then converted back to reduced GSH at the expense of NADPH. This redox cycle is repeated to regulate redox balance in the body. During chemotherapy, often the ROS burden is increased resulting in depletion of GSH and increase in GSSG. Figure adapted from [635].

5.5.3 Glutathione in cancer progression

In both non-tumour and tumour cells, an increased GSH level is associated with an increased growth and is necessary for cell cycle progression. GSH modulation of DNA synthesis is thought to involve the maintenance of reduced glutaredoxin or thioredoxin, which is required for the activity of ribonucleotide reductase, a key enzyme in DNA synthesis [644,645]. GSH status has correlated with both growth and metastasis in cancer cells [646,647]. GSH levels and expression of GSH synthetic enzymes were shown to be increased in hepatocellular carcinoma (HCC). Injection of B16M melanoma cells into C57BL/6J mice with high GSH content (exponentially growing cultures) showed higher metastatic activity in the liver than cells with low GSH content [646]. This study indicated that higher GSH status could be important for cancer metastasis. Moreover, maintenance of mitochondrial GSH homeostasis may be a limiting factor for the survival of metastatic cells.

GSH is released by cells via gamma-glutamyl transferase (GGT), before GSH redox cycle is initiated, which is associated with tumour development [646,648]. Furthermore, increased levels of GGT have been detected in several tumour types in animal studies including cancers of the liver [649] ovary [650] and colon [651]. B16 melanoma cells with elevated GGT activity has been found to strongly correlate with an increased metastasis [652]. Higher GGT expression was also demonstrated to correlate with poor prognostic signs of lymph node metastases and absence of oestradiol receptors in human breast cancer [653].

5.5.4 Glutathione depletion in cancer treatment

Tumour cells with low or depleted GSH levels have been demonstrated to be much more sensitive than control cells to the effect of irradiation [654]. Buthionine sulfoximine (BSO) is an inhibitor of glutamate cysteine ligase (GCL) and induces glutathione depletion [655]. BSO has been employed to sensitise cancer cells to oxidative stress in combination with chemotherapeutic agents. For example, it was reported that a combination therapy of arsenic trioxide with BSO effectively enhanced growth inhibition in several cancer cell lines including prostate, breast, cervix, bladder, and kidney, compared with arsenic trioxide treatment alone [656].

Another study showed that BSO-mediated GSH depletion could be employed to overcome resistance in neuroblastoma cell lines [657]. A combination of BSO and anticancer drug melphalan has reached phase I clinical trials to determine safety and tolerability of the combination treatment. It was found that BSO alone produced minimal side effects but the combination treatment did cause nausea and occasional severe myelosuppression. Continuous infusion of BSO at a concentration of 15mg/m^2 was very effective with more than a 90% reduction in GSH compared to pre-treatment levels [658]. Furthermore, BSO in combination with melphalan has proven effective at reaching advanced clinical trials in the treatment of neuroblastoma [659,660]. The same combination was effective against melanoma cells *in vitro* with electroporation improving efficacy [661].

DNA damage and apoptosis triggered via JNK activation have been reported as a result of BSO combination therapies [662–667]. BSO therapy is limited for clinical applications due to short half-life, with prolonged infusions required for 30% reduction in GSH compared to basal levels [662,668,669]. Due to these limitations,

new strategies have focused on a more selective approach in the process of targeting specific enzymes. For example, GSH phosphono analogues were developed and successfully inhibited a subgroup of GST enzymes in colon and gastric cancer cells [670]. Specially designed prodrugs which can be activated under oxidative stress have also been developed. Telcyta® is a prodrug that is selectively activated by GST P1-1 which in turn releases active cytotoxic fragment [671]. This drug targets cancer cells overexpressing GST P1-1 which are locally exposed upon release of an alkylating agent with limited toxicity to the surrounding non-tumour tissues. Telcyta® has had promising results in phase II and III clinical trials for the treatment of ovarian cancer, non-small cell lung cancer, and breast cancer [672].

5.5.5 Role of glutathione in chemoresistance

GSH can be a double-edged sword in cancer therapy, with induction of chemoresistance a reoccurring problem [209]. An increase in GSH levels, GCL activity and γ-GCS gene transcription is often associated with drug resistance in tumour cells [673–677]. Furthermore γ-glutamyl transferase (GGT) was shown to accelerate tumour growth and increase the resistance of tumours to cisplatin *in vivo* [678]. Human multidrug resistance protein (MRP) can lead to resistance to multiple classes of chemotherapeutic agents [97]. Synchronised overexpression of GCLC and MRP has been demonstrated in several drug-resistant tumour cells [679–681]. Many chemotherapeutics are dependent on ROS generation [615]. GSH contributes to drug resistance interacting with ROS, preventing damage to proteins or DNA and aiding in DNA repair processes. In Instances of GSH depletion, increased anticancer drug efficacy has been observed [682]. Artesunate, which is utilised in this study, may also be affected by GSH mediated resistance. Higher expression of several GST enzymes were found to correlate with higher artesunate IC_{50} in a broad study encompassing data from 55 different cancer cell lines including HL60, PC-3 and MCF-7 cells which are employed in the current study [474].

5.6 Methodology

5.6.1 Cell culture and oxygen maintenance

The cell lines used for the work described in this chapter were HL-60 (leukaemia), PNT1A (prostate non-tumour) and PC-3 (prostate tumour). Cell culture conditions and oxygen maintenance are previously described in sections 4.2.1 and 3.3.2.

5.6.2 Preparation and addition of drug compounds

Hybrid **SG77** and mitonafide were synthesised by Prof. Paul O'Neill, Dr Sarah Rawe and colleagues at the School of Chemistry, University of Liverpool, UK and at the School of Chemical and Pharmaceutical Sciences, Dublin Institute of Technology, Ireland. Artesunate was purchased from Tokyo Chemical Industry Co. Ltd. All compounds were dissolved in the vehicle, DMSO (100%), to create the master stock. 20 µl aliquots of 10 mM were prepared for each compound and stored at -80 ˚C. Working stocks of 20 µM concentration were prepared by diluting the master stocks in fresh growth medium to a final volume of 10 ml.

Additional drug concentrations were achieved by a further dilution of working stocks in fresh growth media to achieve a final compound concentration of 0, 1 or 10 µM respectively. Final concentrations of DMSO were adjusted to 0.1% (v/v) for all drug concentrations and vehicle control. During RTCA, drug addition was performed by removing 100 µl of spent media from each 16 well E-plate well, and replacing with an equal volume of working stock in a final volume of 200 µl. A similar drug addition protocol was applied during the cell count analysis where cells were grown in 6 well plates (1.5 ml working stocks added to each well to make final 3ml volume).

5.6.3 Glutathione (GSH/GSSG) detection assay

$1.2x10^5$ PNT1A or $1x10^5$ PC-3 cells were seeded onto 6 well culture plates (Sarstedt). Cells were exposed to either fresh growth media (control), 0.1% DMSO (vehicle) or hybrid **SG77** at concentrations of 1 or 10 µM for 24 or 48 h. Cells were then harvested, counted and re-suspended in metaphosphoric acid before total glutathione was quantified as per manufactures instructions using a glutathione detection kit (Enzo life sciences). Briefly, a 1:10 (total glutathione detection) or 1:3 (GSSG detection) dilution of samples was performed using

freshly prepared assay buffer to achieve an appropriate dynamic range of detection. Samples were then dispensed into 96 well plate alongside varying known concentrations of glutathione to produce a standard curve. Freshly prepared reaction mix containing glutathione reductase was then added to each sample and standard. Absorbance was read immediately at 420 nm to detect total glutathione using FLOUstar optima microplate reader (BMG Labtech, UK). GSSG detection was achieved with the similar protocol with the addition of a 1h 2-vinylpyridine (2-VP) incubation step before reaction mix was added. This removes any reduced GSH molecules within samples to leave only oxidised form. GSH/GSSG levels were expressed as pM/1x10^5 cells. Each experiment was repeated three times in triplicate.

5.6.4 ROS assay

ROS generation was determined using OxiSelect™ intracellular ROS assay kit (Cell Biolabs, USA). 2x10^4 PNT1A or 1.5x10^4 cells were seeded onto black-walled 96-well cell culture plate. 24 h later cells were pre-incubated with H_2O_2 specific dye specific 2', 7'-Dichlorodihydrofluorescin diacetate (DCFH-DA) dissolved in serum-free RPMI for 45 min at 37 °C. Medium containing DCFH-DA was discarded and the cells were gently washed with PBS. Subsequently, cells were treated with phenol red free RPMI (control), vehicle (0.1%DMSO), artesunate, mitonafide or **SG77** hybrid at concentrations of 1, 10 or 50 µM (all dissolved in RPMI without phenol red). Cells exposed to 100 µM H_2O_2 were used as positive control. ROS generation results in cleavage of DCFDA to 2', 7' Dichlorodihydrofluorescein (DCF). DCF florescence intensity was read at 420 nm using FLOUstar optima microplate reader (BMG Labtech, UK) at 1, 4, 24 and 48h after drug addition. A DCF standard curve was prepared before ROS experiments to ensure a linear relationship between DCF concentration and fluorescence intensity at 420nm. Each experiment was performed three times.

5.6.5 Reverse transcription PCR

Total RNA was extracted from control and treated cells using Direct-zol RNA miniprep kit (Zymo Research) in a final volume of 80 µl RNase and DNase-free water. The resulting RNA was then quantified using a nanospectrophotometer (DeNovix DS-11, USA) and stored in -80°C freezer. RNA (1 µg) was reverse

transcribed to first strand cDNA using qScript™ Flex cDNA kit (Quanta biosciences, USA) using 2 µl Random primer and 2 µ Oligo dT in a mixed primer strategy. For RT-PCR, 5 µl of 1:50 dilution of the cDNA was used per well in a 20 µl reaction mixture. Real-time ready hydrolysis probes (Roche, UK), summarised in Table 4, were used to quantify the relative expression of selected target genes. PCR was performed using a LightCylcer 1.5 instrument (Roche, UK).

For quantification of relative gene expression, the cycle of threshold (Ct) for each gene transcript was determined. Ct is the point at which the fluorescence rises appropriately above the background fluorescence. The baseline signal and threshold signal of fluorescence were determined automatically by the PCR instrument (Figure 32). Calculation of fold change in gene expression was performed according to the delta delta-Ct method [683] using the following formula (where FC = fold change in gene expression compared to control sample; ΔCt sample = Ct difference of target-reference genes in treated samples; ΔCt control = Ct difference of target-reference genes in control sample)

$$\mathbf{FC} = \mathbf{2} \text{ ^ } (-(\mathbf{\Delta Ct\ sample\ (target - reference)} - \mathbf{\Delta Ct\ control\ (target - reference)}))$$

GAPDH and Beta actin expression (reference/housekeeper genes) was analysed in all samples in triplicate. Both genes are expressed in all nucleated cell types as they are vital for cell survival. Because of their stable expression and abundance they are among the most commonly used housekeeping genes in RT-PCR [684,685]. The resulting Ct values were plotted for each sample (Figure 48). Both reference genes tracked each other in terms of changes in Ct values between samples. This indicates that both genes are stably expressed across all samples regardless of treatment. Therefore, either beta actin or GAPDH could be used as suitable housekeeper genes. Beta actin expression was then quantified in all samples for a further two experiments in triplicate. Average Ct values for beta actin expression were then used as the reference gene in the delta delta Ct formula above. The mean and SD of fold change values were calculated from three experiments performed in triplicate for each treatment. One-way ANOVA was performed as described in 5.6.7 to detect significant differences in fold change between the treated samples and the control samples.

5.6.6 Annexin V/ propidium iodide assay

Apoptosis mediated cell death of PNT1A and PC-3 cells were examined using FITC-labelled Annexin V/PI apoptosis detection kit (BD Bioscience, UK) as per the manufacturer's instructions. Briefly, cells were exposed to either fresh growth media (control), 0.1% DMSO (vehicle), 100 µM vincristine sulphate (VS) (positive control), or hybrid **SG77** at concentrations of 1 or 10 µM for 72 h. Spent media was removed from each sample and centrifuged to collect floating cells. Remaining cells were then detached by trypsinisation and collected in centrifuge tubes before being washed twice in cold phosphate-buffered saline (PBS). Cells were then re-suspended in 1x binding buffer to a final concentration of ~$1x10^6$ cells/ml. 100 µl of this each cell solution (~$1x10^5$ cells) was then transferred to new labelled Eppendorf tube. Staining was then performed by adding 5 µl of Annexin V FITC and 5 µl of PI to each sample and centrifuging for 10s to mix. Samples were then incubated for 15min at RT in dark. Unstained cells, PI and Annexin V controls were also prepared for the correct gating of the flow cytometer channels. 400 µl of 1x binding buffer was then added to each Eppendorf and mixed prior to flow cytometry analysis. The externalisation of phosphatidylserine and the permeability to PI were evaluated by flow cytometry using a BD Accuri™ C6 flow cytometer (BD Bioscience, UK). Data from 10,000 gated events per sample were collected. Cells in early stages of apoptosis were positively stained with Annexin V; whereas, cells in late apoptosis were positively stained with both Annexin V and PI.

5.6.7 Statistical analysis

All data is representative of three independent experiments performed in triplicate ± standard deviation (SD) unless otherwise stated. Data graphing and statistical analysis were performed using GraphPad Prism 5.0. Significant differences between untreated and treated samples were determined by one-way ANOVA and Tukey's multiple comparison test. This test assumes a Gaussian distribution and compares every mean with every other mean. $p< 0.05$ was chosen as the criterion for significance. (*=$p \leq 0.05$, **= $p \leq 0.01$, ***= $p \leq 0.001$).

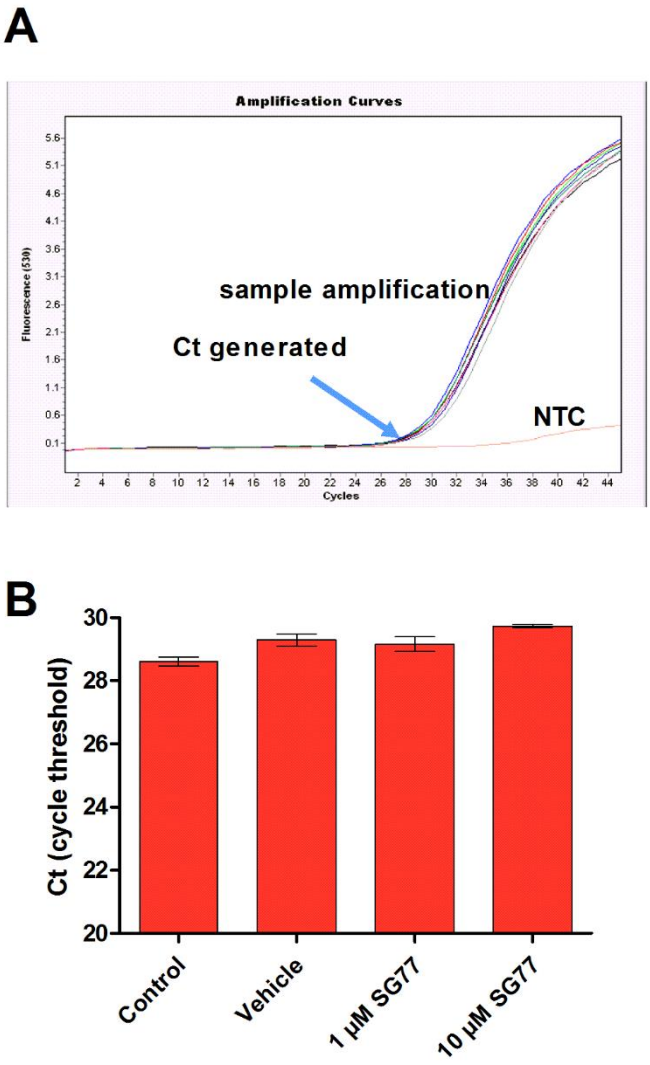

Figure 32 Quantification of gene expression using RT-PCR

Short hydrolysis probes (Roche UK) were used to quantify target gene expression during RT-PCR. (A) A typical RT-PCR plot of fluresecence vs cycles as (generated by the LightCycler 1.5 software). Sample amplification and no template control (NTC) are highlighted. The NTC contains all reaction mix reagents without cDNA sample. The Ct is generated when flurorescent signal increases beyond backround levels. (B) The mean Ct +/- SD for each treatment can then be plotted. This data is then converted in to fold change in gene expression using the formula described in 5.6.5.

Name	Abbrev.	Category	Description	Assay ID (Roche UK)
Beta actin	ACTB	Housekeeper	This gene encodes one of six different actin proteins. Actins are highly conserved proteins that are involved in cell motility, structure, and integrity.	143636
Glyceraldehyde 3-phosphate dehydrogenase	GAPDH	Housekeeper	The product of this gene catalyses an important energy-yielding step in carbohydrate metabolism, the reversible oxidative phosphorylation of glyceraldehyde-3-phosphate.	102052
Glutathione reductase	GSR	Antioxidant	This enzyme is a central to cellular antioxidant defence, and reduces oxidized glutathione disulphide (GSSG) to the sulfhydryl form GSH, which is an important cellular antioxidant.	111427
Glutathione synthetase	GSS	Antioxidant	GSH is important antioxidant. The protein encoded by this gene functions to catalyse the second step of glutathione biosynthesis; the conversion of gamma-L-glutamyl-L-cysteine to glutathione.	117723
Poly (ADP-ribose) polymerase	PARP-1	DNA repair/damage	PARP-1 encodes for poly(ADP-ribosyl) transferase, an enzyme which modifies various nuclear proteins by poly(ADP-ribosyl)ation. The modification is dependent on DNA. PARP is involved in single stranded DNA repair.	111143
non-homologous end-joining-1	NHEJ1	DNA repair/damage	Double-strand breaks in DNA result from genotoxic stresses and are among the most damaging of DNA lesions. NHEJ1 encodes a DNA repair factor essential for the non-homologous end-joining pathway, which mediates repair of double-stranded breaks.	117472
B-cell lymphoma 2	BCL-2	Apoptosis	This gene encodes an important outer mitochondrial membrane protein that blocks the apoptotic death. Important cell survival protein.	100083
BCL2-Associated X Protein	BAX	Apoptosis	The protein encoded by this gene forms a heterodimer with BCL2, and functions as an apoptotic activator. This protein is reported to interact with, the mitochondrial voltage-dependent anion channel (VDAC), which leads to the loss in membrane potential and the release of cytochrome c.	142318

Table 4 Genes selected for RT-PCR

The table above summarises genes selected for RT-PCR analysis. They fall under the categories of housekeeper, antioxidant, DNA damage/repair and apoptosis. Taqman probes (Roche UK) were utilised for RT-PCR. The assay ID above can be used to identify specific nucleotide sequences on Roche website

5.7 Results

5.7.1 HL60 gene expression analysis post artesunate, mitonafide or SG77 treatment

RT-PCR was performed on HL60 samples after exposure to artesunate, mitonafide or **SG77**. Genes involved in DNA damage repair, glutathione redox cycle and apoptosis were investigated to determine some of the underlying mechanisms responsible for **SG77** drug action (Table 4). RT-PCR was split into three phases; Phase 1: time point optimisation, phase 2: parent compound analysis and phase 3: PNT1A vs PC-3 gene expression. ACTB was chosen as the housekeeping gene due to the stable expression across all samples tested (Figure 48). 24 h exposure to hybrid/parent compounds was determined to be optimal for detecting changes in gene expression (Figure 33).

HL60 cells were selected for Phase 1 of the RT-PCR experiments as the cell line was the most sensitive to both parent and hybrid drugs in Chapter 4. Firstly, Bax and Bcl-2 expression was quantified in in HL60 cells following **SG77** exposure (Figure 34). Bax is pro-apoptotic protein while Bcl-2 is an anti-apoptotic protein. Ct values were converted to fold change in gene expression compared to untreated control samples. The results show that there is no significant changes Bax or Bcl-2 expression after 4 h. However, Bax expression is significantly reduced after 12 h after 1 μM **SG77** treatment ($P \leq 0.01$) (Figure 34). After 24 h, 10 μM **SG77** resulted in a significant reduction in BCL-2 expression ($P \leq 0.05$). This data was manipulated to form Bax/Bcl-2 ratio. From the generated result, a significant increase in Bax/Bcl-2 ratio can be observed in HL60 exposed to 10 μM **SG77** after 24 h ($P \leq 0.001$).

GSS, GSR, PARP or NHEJ1 expression were analysed in HL60 after 24 h treatment with artesunate, mitonafide or **SG77** to determine the effect of both hybrid and parent drugs on DNA damage/repair mechanisms and GSH antioxidant response (Figure 35). GSS and GSR are involved in GSH synthesis and reduction in the glutathione redox cycle. PARP and NHEJ1 are involved in single stranded and double stranded DNA repair respectively.

Artesunate induced a significant increase in PARP expression at 1 µM concentration ($P \leq 0.001$). However, no such increase was observed in HL60 exposed to 10 µM artesunate. Mitonafide induced a more pronounced effect in PARP expression with more than a ten-fold increase when compared to untreated cells ($P \leq 0.001$). **SG77** exposure also induced a significant increase in PARP expression ($P \leq 0.05$). NHEJ1 expression was not affected by **SG77** or parent compounds. Artesunate treatment did not result in any significant changes in GSS or GSR expression. However, mitonafide significantly increased GSS expression at 1 and 10µM ($P \leq 0.001$). A reduction of GSR expression and an increase in GSS expression was observed in HL60 cells exposed to 10 µM **SG77** for 24 h ($P \leq 0.05$).

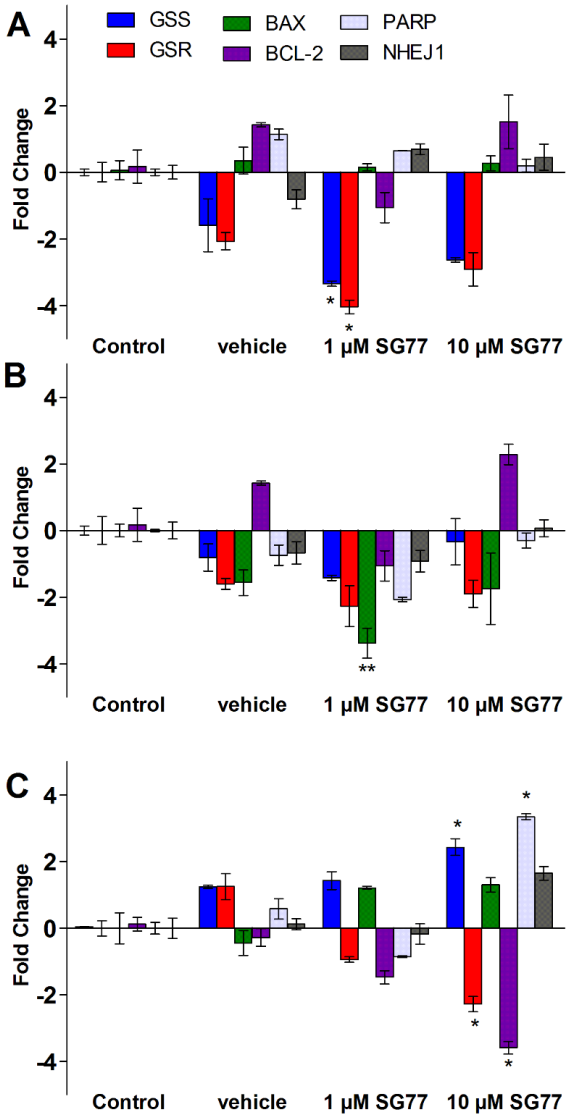

Figure 33: HL60 gene expression following hybrid SG77 treatment at multiple time points

The relative changes in HL60 gene expression following **SG77** treatment were analysed using RT-PCR. Briefly, $6x10^5$ HL60 were seeded per petri dish. 24 h later cells were exposed to either complete fresh growth media (control), 0.1% DMSO (vehicle), artesunate, mitonafide or hybrid **SG77** at indicated final concentrations. After a further 4, 12 or 24 h incubation cells were harvested. RNA was extracted from each sample before conversion to cDNA. Approximately 20 ng of the resulting cDNA was added per PCR reaction. Data is expressed as log fold change in expression compared to untreated control and is normalised to beta-actin expression (housekeeper gene). Statistical significance was measured using one-way ANOVA followed by Tukey post hoc test with $P \leq 0.05$ chosen as the criterion for significance.

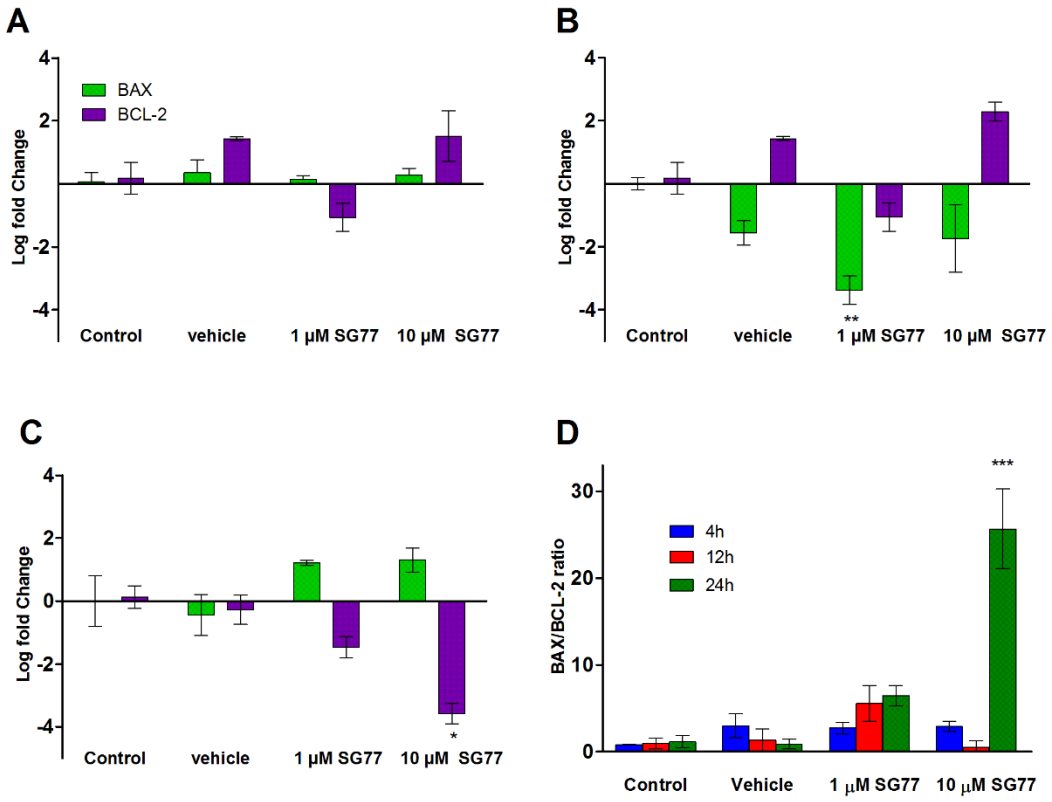

Figure 34: Bax and Bcl-2 gene expression in HL60 following SG77 hybrid exposure.

The relative changes in Bax and Bcl-2 gene expression was analysed in HL60 following **SG77** exposure for (**A**) 4 h, (**B**) 12 h and (**C**) 24 h. Briefly, $6x10^5$ HL60 were seeded per petri dish. 24 h later cells were exposed to either complete fresh growth media (control), 0.1% DMSO (vehicle), or **SG77** hybrid at indicated final concentrations. After a further 4, 12 or 24 h incubation, cells were harvested. RNA was extracted from each sample before conversion to cDNA. Approximately 20 ng of the resulting cDNA was added per PCR reaction. Data is expressed as log fold change in expression compared to untreated control and is normalised to beta-actin expression (housekeeper gene). (**D**) Bax/BCL-2 ratio was calculated for each treatment for 4 h, 12 h and 24 h using the data from graphs A, B and C. Statistical significance was measured using one-way ANOVA followed by Tukey post hoc test with $P \leq 0.05$ chosen as the criterion for significance.

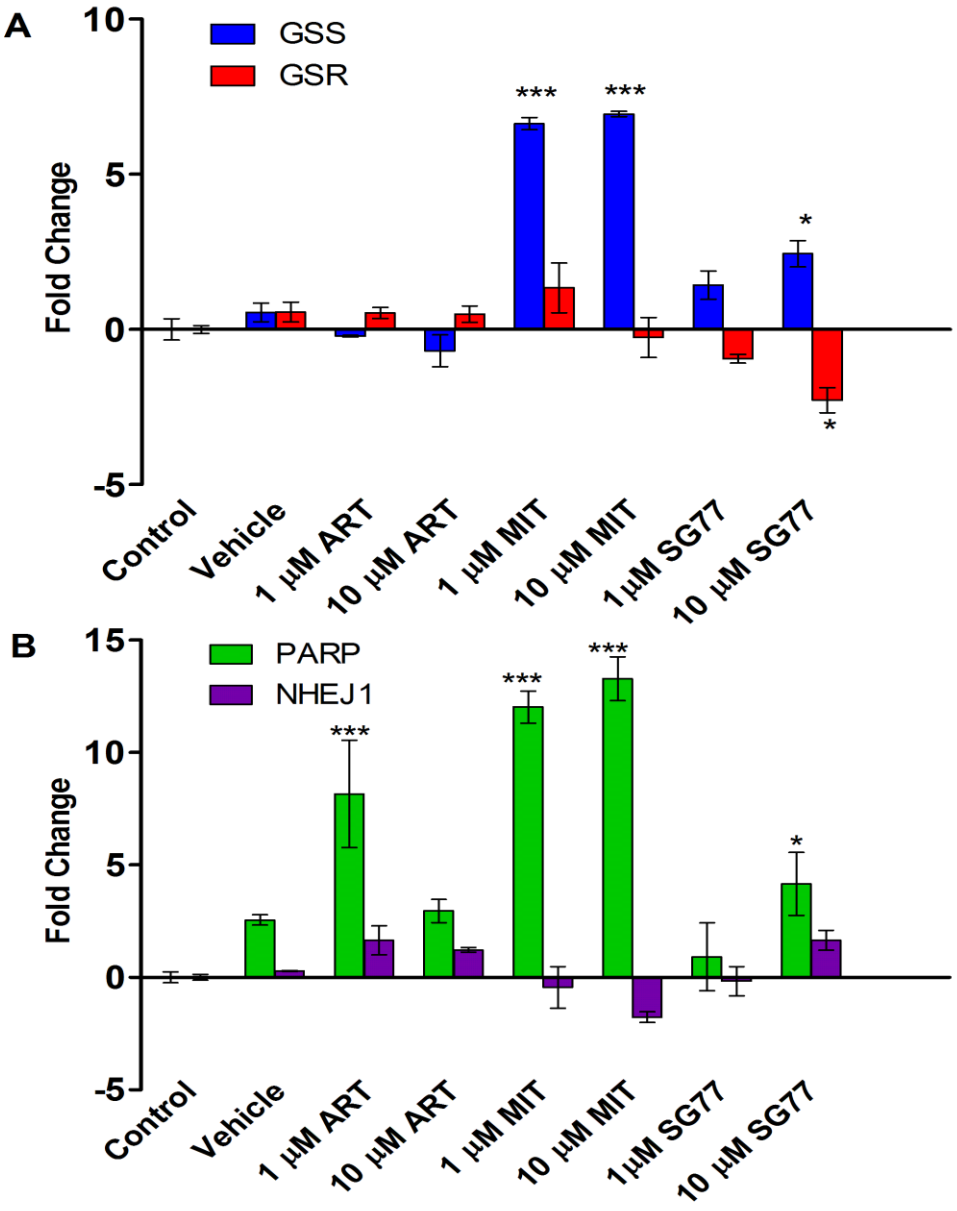

Figure 35: HL60 gene expression following hybrid/parent compound treatment

HL60 gene expression was analysed following treatment. (A) GSS and GSR and (B) PARP and NHEJ1 were analysed using RT-PCR after 24 h drug treatment. Briefly, $6x10^5$ HL60 were seeded per petri dish. 24 h later cells were exposed to either complete fresh growth media (control), 0.1% DMSO (vehicle), artesunate, mitonafide or **SG77** hybrid at indicated final concentrations. After a further 24 h incubation cells were harvested. RNA was extracted from each sample before conversion to cDNA. Approximately 20 ng of the resulting cDNA was added per PCR reaction. Data is expressed as log fold change in expression compared to untreated control and is normalised to beta-actin expression (housekeeper gene). Statistical significance was measured using one-way ANOVA followed by Tukey post hoc test with $P \leq 0.05$ chosen as the criterion for significance.

5.7.2 PNT1A vs. PC-3 gene expression following SG77 exposure

To compare prostate cell response to **SG77** hybrid, gene expression of GSS, GSR, PARP and NHEJ1 were analysed after 24 h treatment (Figure 36, Figure 37). GSS expression was unchanged in PNT1A. Conversely, GSS expression was significantly reduced in PC-3 (P≤0.05). GSR was significantly reduced in response to 10 µM **SG77** treatment with an almost four-fold reduction in expression (P≤0.001). No significant difference in PARP was detected in either cell line at 24 h. NHEJ1 expression was unchanged in PNT1A but significantly up-regulated in PC-3 (P≤0.05).

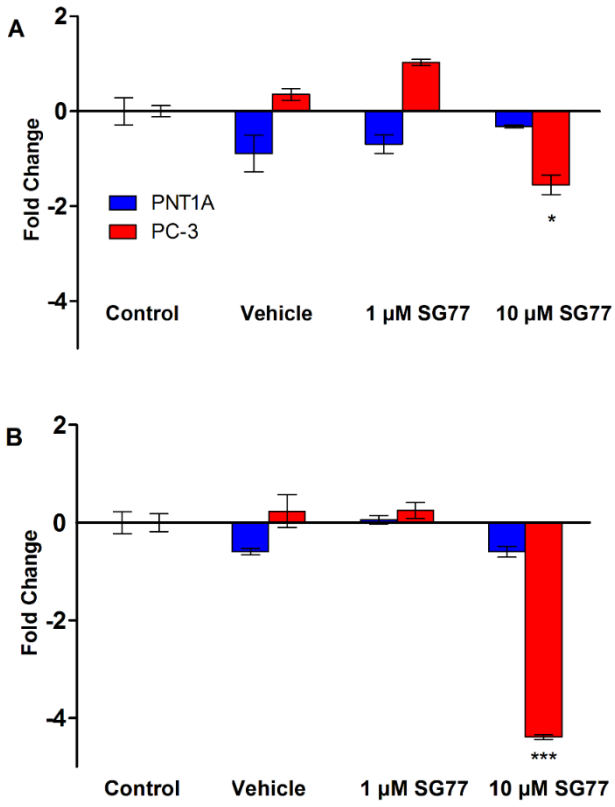

Figure 36: Glutathione-related gene expression following hybrid SG77 treatment

The relative changes in PC-3 or PNT1A gene expression were quantified in the case of (**A**) GSS (**B**) GSR Briefly 4x10^5 PC-3 or 5 x10^5 PNT1A were seeded per petri dish. 48 h later cells were exposed to either complete fresh growth media (control), 0.1% DMSO (vehicle), or **SG77** hybrid at indicated final concentrations. After a further 24 h incubation cells were harvested. RNA was extracted from each sample before conversion to cDNA. Approximately 20 ng of the resulting CDNA was added per PCR reaction. Data is expressed as log fold change in expression compared to untreated control and is normalised to beta-actin expression (housekeeper gene). Statistical significance was measured using one-way ANOVA followed by Tukey post hoc test with P≤0.05 chosen as the criterion for significance.

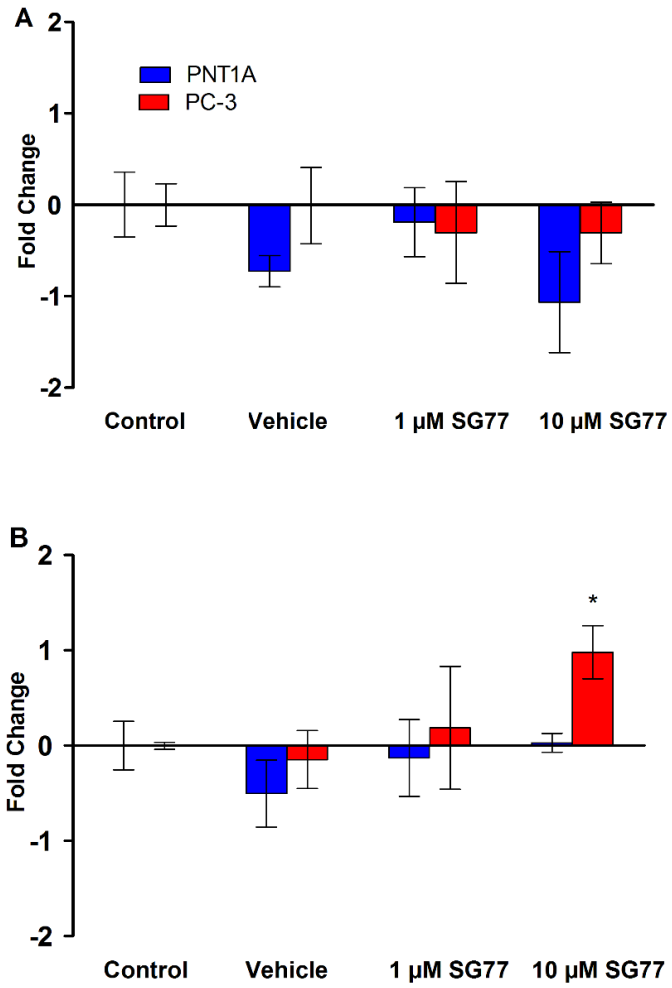

Figure 37: DNA damage related gene expression following hybrid SG77 treatment.

The relative changes in PC-3 or PNT1A gene expression were quantified in the case of (A) PARP and (B) NHEJ1. Briefly 4x10^5 PC-3 or 5 x10^5 PNT1A were seeded per petri dish. 48 h later cells were exposed to either complete fresh growth media (control), 0.1% DMSO (vehicle), or **SG77** hybrid at indicated final concentrations. After a further 24 h incubation cells were harvested. RNA was extracted from each sample before conversion to cDNA. Approximately 20 ng of the resulting CDNA was added per PCR reaction. Data is expressed as log fold change in expression compared to untreated control and is normalised to beta-actin expression (housekeeper gene). Statistical significance was measured using one-way ANOVA followed by Tukey post hoc test with $P \leq 0.05$ chosen as the criterion for significance.

5.7.3 ROS generation in PNT1A and PC-3 following SG77 treatment

ROS generation was analysed in PNT1A and PC-3 using OxiSelect™ Intracellular ROS Assay Kit. ROS generation was quantified at 1, 4, 24 or 48 h post **SG77** treatment. A significant increase in ROS generation were observed in PNT1A exposed to 50 μM artesunate for 48 h (P≤0.05) (Figure 38). However, artesunate treatment resulted in a more pronounced increase in ROS generation after 24 h and 48 h (P≤0.001) (Figure 39). 50 μM mitonafide treatment resulted in significant increases in ROS at 4, 24 and 48 h in PNT1A (P≤0.05) and PC-3 (P≤0.001). However, mitonafide was more effective in increasing ROS levels in PC-3 with significant ROS generation observed after just 1 h at the highest concentration tested (P≤0.05). In addition, 10 and 50 μM mitonafide caused significant increases in ROS after 24 h and 48 h (P≤0.001). Interestingly, no significant increase in ROS was observed in PNT1A following **SG77** hybrid treatment (Figure 38). However, a dose dependent increase in ROS generation could be observed. **SG77** was a more effective ROS inducer in PC-3 with 10 μM causing a significant increase in ROS from 4h onwards (P≤0.001). 1 μM **SG77** also induced significant ROS generation after 24 h (P≤0.01) (Figure 39).

5.7.4 Total and oxidised glutathione levels in PNT1A and PC-3 following SG77 treatment

The effect of anticancer hybrid **SG77** on intracellular levels of oxidised and total glutathione (GSH) was assessed using glutathione detection kit (Figure 40). PNT1A had a lower basal level of total GSH with untreated cells having less than 200 pm/10^5 cells as compared to over 300 pm/10^5 cells in PC-3. Both prostate cells displayed a significant reduction in total glutathione when treated with 10 μM **SG77** for 48 h (P≤0.01) with PNT1A also showing a significant reduction at 24 h (P≤0.05). Interestingly, 10 μM **SG77** resulted in a significant increase in oxidised glutathione (GSSG) after 24 h (Figure 41) (P≤0.001). GSSG levels in PNT1A remained unchanged after 24 h but a significant increase in GSSG was detected after exposure to 10 μM **SG77** for 48 h (P≤0.05).

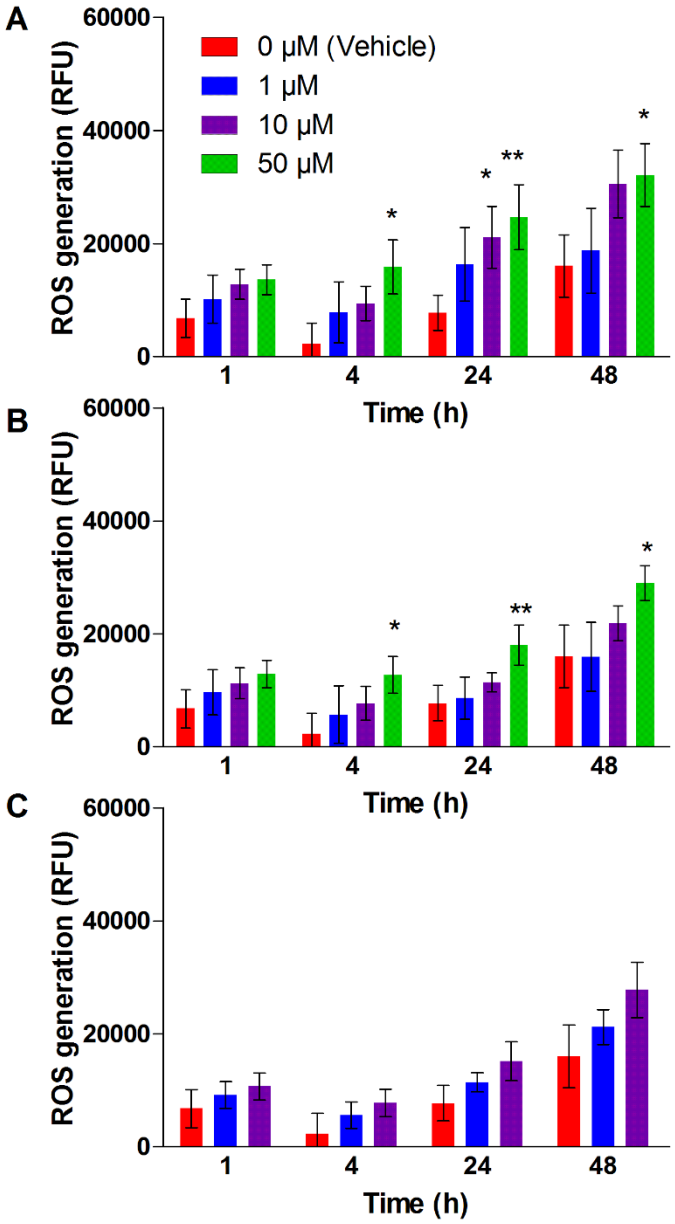

Figure 38: ROS generation in PNT1A cells exposed to hybrid SG77

ROS activity was determined using OxiSelect™ ROS assay kit (Cell Biolabs, USA). Briefly, 20,000 PNT1A cells per well were seeded onto black-walled 96-well cell culture plate. 24 h later cells were pre-incubated with H_2O_2 specific dye DCFH-DA for 45 min at 37 °C. Medium containing DCFH-DA was discarded and the cells were gently washed with PBS. Subsequently, cells were treated with vehicle (0.1%DMSO) or (**A**) artesunate, (**B**) mitonafide or (**C**) **SG77** hybrid at indicated concentrations. DCF fluorescence intensity was read using microplate reader at indicated time points. The above data is representative of triplicate experiments (+/-SD). One way ANOVA, followed by Tukey post-hoc test was utilised to analyse differences between treated/exposed and control cell populations (*=$p \leq 0.05$, **= $p \leq 0.01$, ***= $p \leq 0.001$).

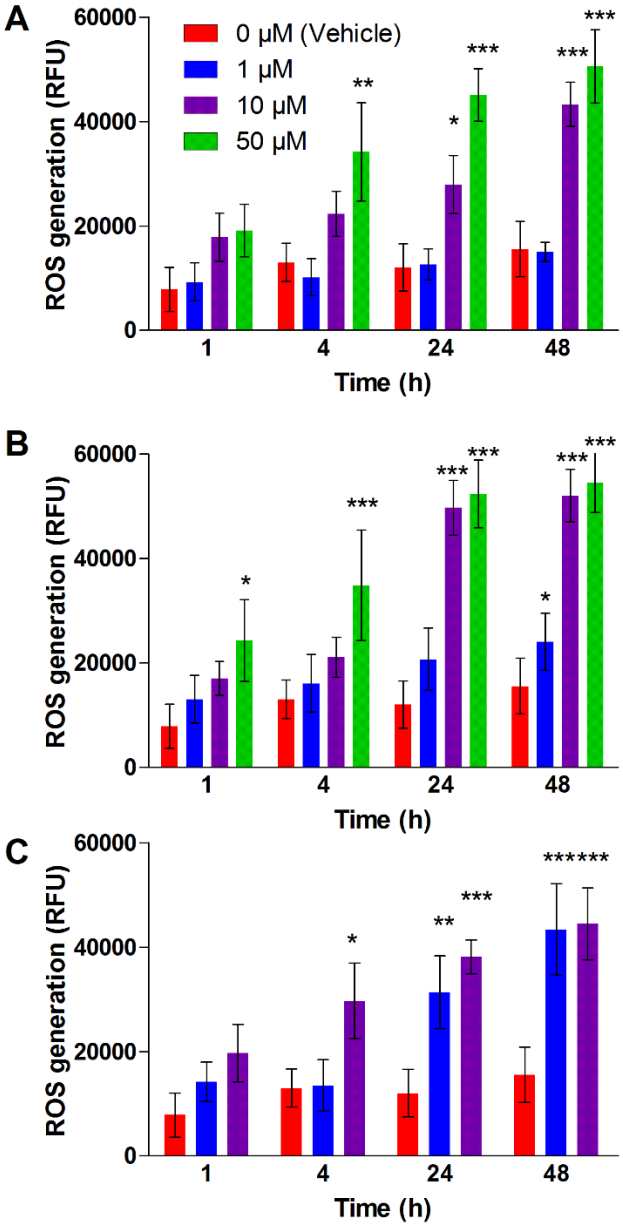

Figure 39: ROS generation in PC-3 cells exposed to hybrid SG77

ROS activity was determined using OxiSelect™ intracellular ROS assay kit (Cell Biolabs, USA). Briefly, 15,000 PC-3 cells per well were seeded onto black-walled 96-well cell culture plate. 24 h later cells were pre-incubated with H_2O_2 specific dye DCFH-DA for 45 min at 37 °C. Medium containing DCFH-DA was discarded and the cells were gently washed with PBS. Subsequently, cells were treated with vehicle (0.1%DMSO) or (**A**) artesunate, (**B**) mitonafide or (**C**) **SG77** hybrid at indicated concentrations. DCF fluorescence intensity was read using microplate reader at indicated time points. The above data is representative of triplicate experiments (+/-SD). One way ANOVA, followed by Tukey post-hoc test was utilised to analyse differences between treated/exposed and control cell populations (*=$p \leq 0.05$, **= $p \leq 0.01$, ***= $p \leq 0.001$).

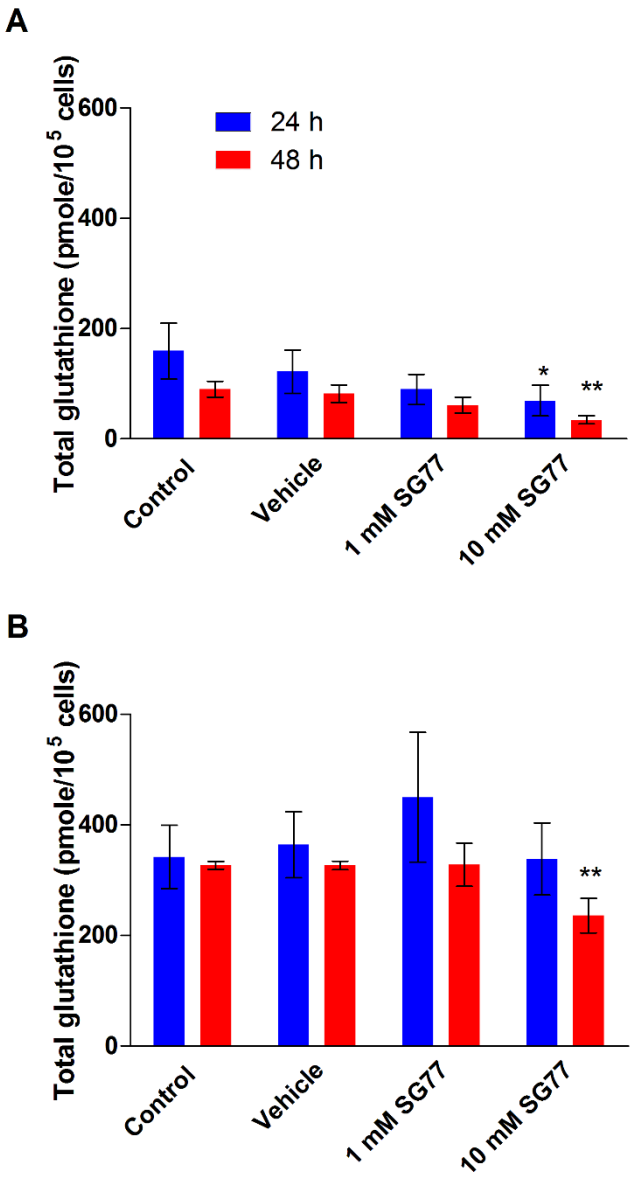

Figure 40: Glutathione levels in prostate cells exposed to hybrid SG77

A) PNT1A and B) PC-3 cells were exposed to either fresh growth media (control), vehicle or hybrid **SG77** at the indicated concentrations for (**A)** 24 or (**B**) 48 h. Cells were then scraped, counted and re-suspended in metaphosphoric acid before total glutathione was quantified as per manufactures instructions using glutathione detection kit (Enzo life sciences). The above data is representative of triplicate experiments (+/-SD). One way ANOVA, followed by Tukey post-hoc test was utilised to analyse differences between treated/exposed and control cell populations (*=$p \leq 0.05$, **= $p \leq 0.01$, ***= $p \leq 0.001$).

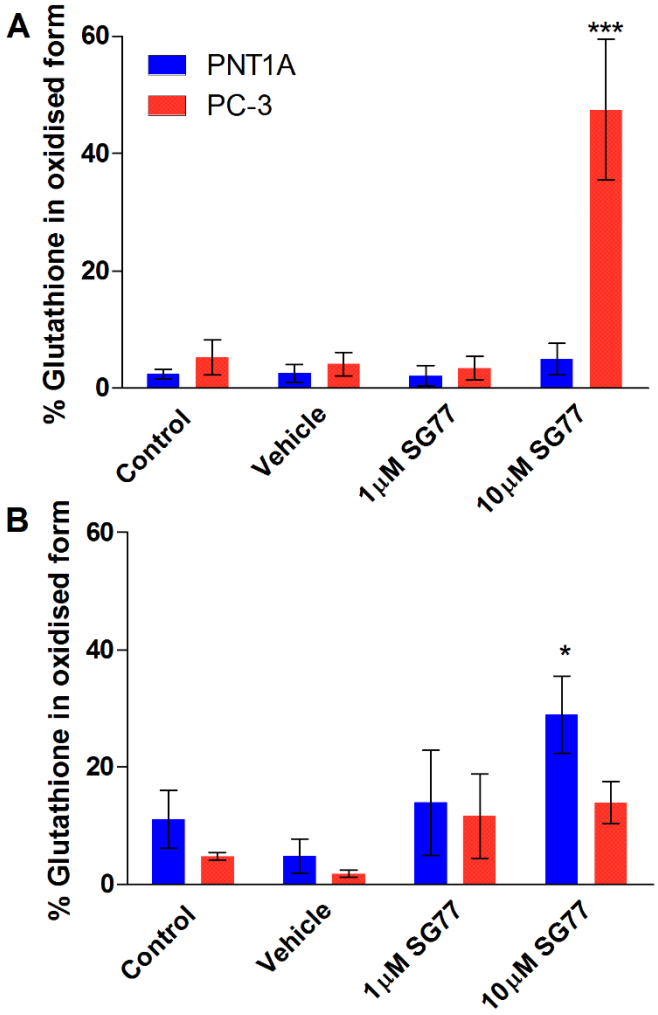

Figure 41: GSSG levels in prostate cells exposed to hybrid SG77

PNT1A or PC-3 cells were exposed to fresh growth media (control), vehicle (0.1% DMSO) or hybrid **SG77** at the indicated concentrations for (**A**) 24h or (**B**) 48h. Cells were then scraped and re-suspended in metaphosphoric acid before oxidised glutathione was quantified as per manufactures instructions using Glutathione detection kit (Enzo life sciences). All data is expressed as GSSG as a percentage of total glutathione. The above data is representative of triplicate experiments (+/-SD). One-way ANOVA, followed by Tukey post-hoc test was utilised to analyse differences between treated/exposed and control cell populations (*=p ≤ 0.05, **= p ≤ 0.01, ***= p≤ 0.001).

5.7.5 Induction of apoptosis by SG77 in PNT1A and PC-3 cells

FITC-labelled Annexin V/PI apoptosis detection kit was employed to detect apoptosis induction in PNT1A and PC-3 after 72 h **SG77** treatment (Figure 42, Figure 43). 100 µM VS was utilised as a positive control. Untreated PNT1A were found to contain 83.3% live cells. PNT1A exposed to vehicle (0.1% DMSO) had a 77.5% live cell population. **SG77** was shown to induce apoptosis at both concentrations tested. More than half of the PNT1A cell population were in an early apoptotic state following 1 µM **SG77** treatment. 10 µM **SG77** induced a further increase in apoptosis with 42% of cells progressing to late apoptosis. More than 80% of PNT1A cells were in apoptotic state following exposure to the positive control (100 µM VS).

PC-3 cells were very sensitive to **SG77** induced apoptosis after 72 h. 85.4 % of untreated PNT1A were live. However, the vehicle treatment did appear to induce apoptosis with 27% of the cell population in late apoptosis. However, PC-3 exposed to both 1 and 10 µM **SG77** showed a dramatic increase apoptosis compared to the vehicle with more than 80% of cell population either in late apoptotic stage or dead. More than 65% of PC-3 cells exposed to the positive control were either in late apoptosis or dead.

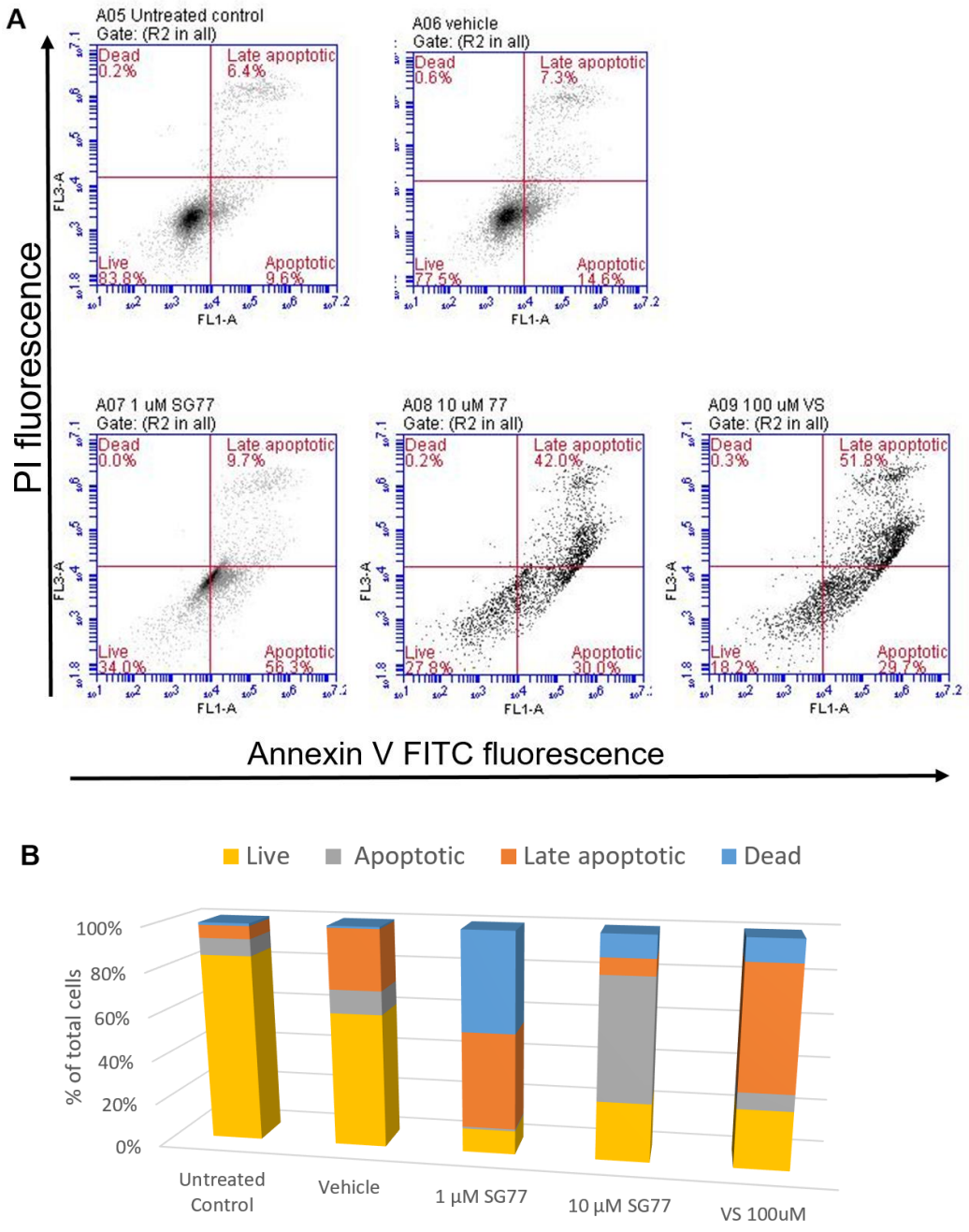

Figure 42: SG77 hybrid induces apoptosis in PNT1A.

PNT1A cells were seeded at 1.2 x10^5 cells/ 6 well plate. After a further 24 h, cells were treated with fresh media (untreated control), 0.1%DMSO in fresh media (Vehicle) 1µM **SG77**, 10µM **SG77** or 100 µM vincristine sulphate (positive control). Apoptosis was measured 72 h post treatment using Annexin V FITC Assay kit. Dot plots (**A**) and corresponding stacked column graph (**B**) are representative of a single experiment.

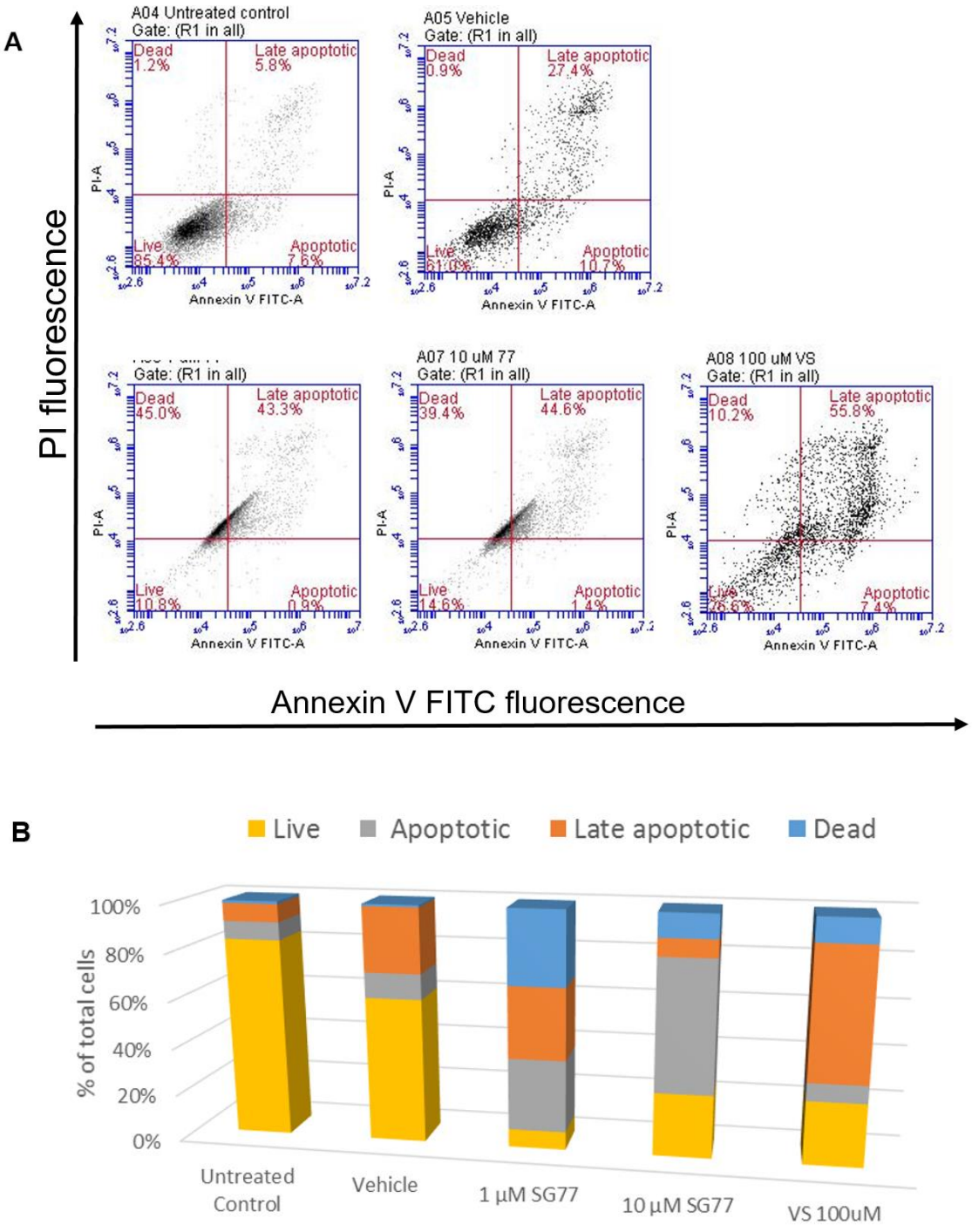

Figure 43: SG77 hybrid induces apoptosis in PC-3.

PC-3 cells were seeded at 1 x10^5 cells/ 6 well plate. After a further 24 h, cells were treated with fresh media (untreated control), 0.1%DMSO in fresh media (Vehicle) 1µM **SG77**, 10µM **SG77** or 100 µM vincristine sulphate (positive control). Apoptosis was measured 72 h post treatment using Annexin V FITC Assay kit. Dot plots (**A**) and corresponding stacked column graph (**B**) are representative of a single experiment.

5.8 Discussion

Hybrid anticancer drugs are gaining increasing therapeutic interest due to potentially overcoming the most common drawbacks experienced during chemotherapy such as multidrug resistance and non-tumour cell toxicity. Improved efficacy and safety have been successfully demonstrated in hybrid compounds when compared to their parent compounds [195]. Indeed, the future of hybrid anticancer drugs is very promising for the discovery of highly potent and selective molecules, that activate two or more pharmacological mechanisms of action, acting in synergy to inhibit tumour growth [195]. However, before a novel drug can reach clinical use the mode of action must be well understood.

Hybrid **SG77** was selected for further investigation based on promising anticancer activity in HL60 and PC-3. Furthermore, **SG77** was shown to be selectively toxic in PC-3 prostate tumour cells when compared to non-tumour PNT1A (Chapter 4). Perhaps even more significant was the observed tolerance of PNT1A to the hybrids compared to parent drugs. This increased tolerance has been reported with previous hybrid strategies [10,686,687]. The objective of this chapter was to determine some of the underlying mechanisms behind **SG77** drug action and selective toxicity. Gene expression was first investigated in HL-60 as they were the most sensitive cell line to both ART-NAP hybrids and parent drugs in Chapter 4. Genes involved in DNA damage repair, glutathione redox cycle and apoptosis were investigated (Table 4). Again, cells were maintained in a normoxic oxygen environment of 4 % (v/v) throughout this analysis to better mimic in vivo environment. It is possible that lower oxygen environments, which are typically present *in vivo*, may potentiate ROS production and the antioxidant response within cancer cells through HIF-1 hypoxia mediated pathway [688,689].

Artesunate and mitonafide (parent compounds) and their derivatives have previously shown to induce mitochondria-mediated intrinsic apoptosis resulting in tumour cell death [185,296,690] . To determine whether ART-NAP hybrid **SG77** also induced intrinsic apoptosis, Bax and Bcl-2 expression was investigated (Figure 34). Both genes belong to a family involved in apoptosis regulation [691,692]. Bcl-2 is anti-apoptotic protein and Bax is an pro-apoptotic [582]. A significant reduction in Bcl-2 expression was observed after 24 h ($P \leq 0.05$). An increase of Bax/Bcl-2

ratio is indicative of increased apoptosis level [61,690,693]. 10 µM **SG77** treatment for 24 h resulted in a significant increase in Bax/Bcl-2 ratio (P≤0.001) suggesting that **SG77** treatment promotes the induction of intrinsic apoptosis. Furthermore, both PC-3 and PNT1A exposed to **SG77** showed an increase in apoptosis induction during preliminary experiments (Figure 42, Figure 43). The induction of apoptosis was more pronounced in PC-3 with increased levels of late apoptotic and dead cells. It must be noted that flow cytometry data was representative of a single experiment. Repeat experiments are required to confirm apoptosis.

Oxidative stress and DNA damage are important to artesunate and mitonafide efficacy and therefore they may also be involved in hybrid **SG77** drug action [694–697]. GSS and GSR are involved in the synthesis and reduction of GSH respectively (Figure 35). Mitonafide treatment resulted in a significant up-regulation in GSS expression (P≤0.001), with no change in the case of GSR, indicating that GSH synthesis has been activated in response to oxidative stress. No significant change in either GSS or GSR expression was observed following artesunate treatment. This data suggests that HL60 have not yet mounted an antioxidant response to artesunate after 24 h. It has been reported that elevated levels of GSH related gene expression correlate with the resistance to artesunate *in vitro* [474]. **SG77** induced a significant up-regulation in GSS (P≤0.05) and a significant down-regulation of GSR (P≤0.05) indicating an increase in GSH synthesis.

Artesunate, mitonafide and **SG77** all induced up-regulation of PARP which codes for an enzyme involved in single strand break (SSB) DNA repair [84]. Mitonafide and its derivatives are known to be potent DNA intercalators and therefore it is not surprising that 1 and 10 µM mitonafide elicited the greatest response in PARP gene expression with more than 10-fold increase detected compared to untreated cells (Figure 35). NHEJ1 expression is a key in the non-homologous end-joining pathway, which preferentially mediates repair of double-stranded breaks preventing DNA damage and gene mutations [698]. NHEJ1 was unchanged across all HL60 samples tested. Therefore, double strand breaks are unlikely to account for cytotoxicity observed following **SG77** treatment.

As discussed in Chapter 4, **SG77** was selectively toxic to PC-3 (prostate tumour) when compared to PNT1A (prostate non-tumour). To determine the reason for tumour cell selectivity, DNA damage repair and oxidative stress were investigated in both cell lines and compared (Figure 37). Fluctuations in gene expression are much less pronounced in prostate cell lines as compared to HL60 in the previous graph (Figure 35). This may be explained by the higher sensitivity of HL60 to **SG77** induced cytotoxicity. PC-3 treated with 10 µM **SG77** for 24 h showed a significant reduction in GSS expression ($P \leq 0.05$) and greater than four-fold reduction in GSR expression ($P \leq 0.001$) indicating that GSR activity is reduced in response to **SG77**. This was unexpected due to the potential of **SG77** to induce oxidative stress and thus initiate GSH synthesis and reduction. However, previous cytotoxicity studies have reported a dose dependent decrease in GSR enzyme activity resulting in cell death [699,700]. Perhaps **SG77** is interfering with GSR activity in PC-3 resulting in compromised antioxidant defence.

NHEJ1 up-regulation was observed in PC-3 ($P \leq 0.05$) with no significant change in PARP. This data indicates that double stranded DNA repair may be initiated after 24 h treatment with 10 µM **SG77** but is not enough to induce significant single-strand DNA damage. PNT1A treated with **SG77** for 24 h showed no significant changes in gene expression indicating that PNT1A are more tolerant to **SG77** at the tested concentration range in agreement with cytotoxicity data in Chapter 4. To further investigate the involvement of oxidative stress in **SG77** hybrid drug action, both intracellular glutathione levels and ROS generation were quantified (Figure 38, Figure 39). Artesunate and mitonafide significantly increased ROS generation in both prostate cell lines from 4h onwards. 50 µM mitonafide was particularly effective with ROS production detected in PC-3 after just 1 h ($P \leq 0.05$). Interestingly, PNT1A treated with 10 µM **SG77** did not have any significant increases in ROS production after 24 h. In contrast, PC-3 cells treated with **SG77** showed a significant increase in ROS from 4h onwards ($P \leq 0.001$). This data suggests that PC-3 are more sensitive to **SG77** mediated ROS generation than PNT1A. Increased ROS and oxidative stress are often present in cancer cells. This trait has been targeted by several chemotherapy agents [622,701]. Furthermore, basal levels of ROS are thought to be higher in PC-3 when compared to prostate non-tumour cells [69]. It is possible that PC-3 are therefore

more susceptible to **SG77** mediated increases in ROS which act to tip the redox balance resulting in apoptosis induction [595,702].

This accumulation of excessive ROS will trigger antioxidant pathways of the cell. Once synthesised GSH reacts with oxygen radicals to ensure that they are removed from the body with minimal damage to cells [628]. However, when ROS levels are excessive GSH becomes overwhelmed and depleted resulting in a marked increase in GSSG. Therefore a reduction in GSH/GSSG ratio is a good indicator of oxidative stress [625,626,703]. To compare antioxidant response in prostate cells, both total glutathione (GSH) and oxidised glutathione (GSSG) were quantified using enzymatic recycling method [704]. PNT1A had a lower basal level of total GSH with untreated cells having less than 200 pm/10^5 cells as compared to over 300 pm/10^5 cells in PC-3 (Figure 40). Both prostate cells displayed a significant reduction in total glutathione when treated with 10 μM **SG77** for 48 h ($P \leq 0.001$). Interestingly, 10 μM **SG77** resulted in a significant increase in percentage GSSG after 24 h (Figure 41) ($P \leq 0.001$). No such increase was observed at 48 h suggesting that this antioxidant response subsided after initial drug-induced response.

GSSG levels in PNT1A remained unchanged after 24 h. PNT1A did, however, show a significant increase in GSSG after 48 h exposure to 10 μM **SG77**. This data suggests that PC-3 are under severe oxidative stress after 24 h with depletion of GSH and an increase in GSSG to more than 40% of total glutathione. PNT1A, on the other hand, were less susceptible to **SG77** induced ROS production and do not mount an antioxidant response until 48 h. It must also be noted that this response at 48 h is far less pronounced than that observed in PC-3 at 24 h. ROS production in lower oxygen environments has been shown to correlate with HIF-1α stabilisation and increased HIF mediated transcription [284–286]. This transcriptional activity usually involves the stimulation of growth, angiogenesis, and antioxidant production to promote cell survival [705]. It is interesting to note that PC-3 cells were sensitive to **SG77** mediated ROS generation and GSH depletion even at normoxic oxygen levels (4%v/v). The ROS generation from both ART and NAP components of **SG77** work in synergy to

increase oxidative stress in the cancer cell line preventing the development of resistance.

5.9 Conclusions

Based on the data generated, intrinsic apoptosis, DNA repair and glutathione antioxidant response may be important in **SG77** drug action. Furthermore PC-3 were more sensitive to **SG77** than non-tumour PNT1A with increased ROS generation, rapid glutathione depletion and the induction of intrinsic apoptosis. **SG77** should be considered as a promising candidate for animal trials with the potential for a potent and selective cancer therapeutic agent.

Chapter 6. Overall discussion

The current study evaluated the antitumour efficacy of ART-porphyrin hybrids and ART-NAP hybrids in both tumour and non-tumour cell lines. The development of anticancer hybrid drugs is an approach that can potentially improve current cancer therapy. Indeed this approach has found to improve potency and tumour cell selectivity with a reduction in the development of resistance [5–7]. ART, NAP and porphyrin derivatives were the primary parent drugs used to synthesise novel hybrids. ARTs are endoperoxide-containing compounds with antimalarial and anticancer activity [15,18]. The high clinical tolerance and lack of cross-resistance observed in ART derivatives have made them an attractive target for future development. NAPs are potent anticancer compounds which exert their antitumour effects by DNA intercalation [25,26]. Porphyrins are light activated compounds used in the treatment of cancer during PDT [29].. To our knowledge, this is the first time such hybrids have been investigated *in vitro*.

Before the cytotoxic evaluation of novel hybrid drugs, the effect of oxygen availability on artesunate anticancer efficacy in HeLa cells was investigated (Chapter 2). Artesunate is a well-studied semisynthetic ART derivative with known anticancer activity. Hypoxic regions are typically present within solid tumour masses due to the inadequate blood supply and chemotherapeutic drugs are often adversely affected by hypoxia [243,244] . However, despite the evidence, related *in vitro* cytotoxic assays in oxygen rich environment remain the norm [39]. Such oxygen levels are well beyond that typically present in non-tumour tissues/tumour masses [42,43,247]. HeLa cervical cancer cells were employed as a tumour cell line model and are known to be sensitive to artesunate [24,149]. The results showed that artesunate potency against HeLa cervical cancer cells is enhanced as oxygen concentration is varied from atmospheric levels to *in-vivo* relevant normoxia and hypoxia (Figure 7, Figure 8). Therefore artesunate, and indeed many other chemotherapeutic agents accessed at atmospheric oxygen may be more potent against cancer cells *in vivo* than originally thought.

The next phase of the study involved the evaluation of a novel ART-porphyrin hybrid **AP433** in PC-3 prostate cancer cells. Oxygen was maintained at a concentration of 4% (v/v) to better mimic *in vivo* conditions. This hybrid composes

of TPP linked to DHA. TPP is a synthetic porphyrin compound that resembles naturally occurring PpIX. The ART derivative, artesunate, was shown to more effective in lower oxygen concentrations in Chapter 2. By linking a porphyrin to DHA (the active metabolite of artesunate) in hybrid **AP433**, DHA may overcome the development of hypoxia mediated resistance which has been reported in response to PDT [406]. In addition, the porphyrin may enhance hybrid accumulation in the tumour cells and increase cancer cell death upon light activation. A Q-Sun solar simulator was employed as a novel method for light activation. To our knowledge, this is the first time this instrument has been employed for PDT. PpIX induced dark toxicity in PC-3 at concentrations above 10 µM after 48 h. This is similar toxicity range as previously reported although activity will vary considerably depending on cell type and incubation time [329,375,451]. Cell count results showed light activation of PpIX and **AP433**. However, after light exposure for 2 minutes, there was more than a 50% reduction in cell number in sham-exposed controls. This could be owed to heat generation or loss of cells through detachment during PDT. Based on these initial results, **AP433** mediated PDT was not more effective than PpIX mediated PDT in PC-3 cells. PDT treatment will need to be further optimised to determine suitable light activation without causing unwanted cell toxicity. Perhaps a laser diode system would be more effective for looking at cell growth in real-time with less heat generation and cell detachment allowing more scope for higher activation doses [456].

ART-NAP hybrids **SG76**, **SG77** and **SG81** were investigated in detail across four cell lines; PNT1A (non-tumour prostate), PC-3 (prostate cancer), MCF-7 (breast cancer) and HL60 (leukaemia). The anticancer activity of the hybrids was compared with artesunate and mitonafide (parent drugs). Cell count analysis showed that HL60 cells were very sensitive to the hybrid drugs with IC_{50} ranging from 2.0 µM to 3.9 µM after 48 h (Table 2). Furthermore, hybrids were generally more active than artesunate in HL60 and PC-3. However, the hybrids appeared to be less effective than parent drugs in reducing MCF-7 cell number with IC_{50} values ranging from 23.0 µM to 74.0 µM. it also emerged that PC-3 cells were more sensitive to the ART-NAP hybrids than non-tumour PNT1A. **SG76** and **SG77** generated IC_{50} values of 68.3 µM and 54.9 µM in PNT1A when compared to 15.8 µM and 4.9 µM in PC-3 respectively (Table 2). **SG77** was shown be most

selective drug tested with 11 times more activity in PC-3 cells (Table 3). Furthermore, PNT1A were more tolerant to hybrid compounds than to the parent drugs with IC_{50} ranging from 2.9-23.3 µM in the parents and from 15.9-68.3 µM for the hybrids. This data highlights a potential advantage of utilising ART-NAP hybrids to reduce toxicity in non-tumour cells and tissues while still maintaining efficacy in tumour cells.

Hybrid **SG77** was selected for further investigation as the most selective anticancer hybrid tested in Chapter 4. The aim was to determine some of the underlying mechanisms involved in **SG77** drug action. Artesunate and mitonafide (parent drugs) and their derivatives have previously been shown to induce mitochondria-mediated intrinsic apoptosis resulting in tumour cell death [164,185,296,472,690]. **SG77** treatment may also promote the induction of intrinsic apoptosis as evidenced by a significant increase in Bax/Bcl-2 expression ratio after 24 h($P \leq 0.001$). Furthermore, increased levels of late apoptosis and cell death were observed in both PC-3 and PNT1A after 72 h exposure to SG77 (Figure 42, Figure 43).

Oxidative stress and DNA damage are important to artesunate and mitonafide efficacy and therefore they may also be involved in hybrid **SG77** drug action [694–697]. Both mitonafide and **SG77** treatment was found to significantly increase GSS expression ($P \leq 0.001$, $P \leq 0.05$). This data indicates that both mitonafide and **SG77** trigger increased GSH synthesis in HL60. **SG77** induced a significant up-regulation of PARP expression (Figure 35) suggesting the occurrence of single stranded DNA damage [84]. DNA damage repair, oxidative stress and apoptosis were investigated in both prostate cell lines. PC-3 exposed to **SG77** showed a significant reduction in GSS expression ($P \leq 0.05$) and more than a four-fold reduction in GSR expression ($P \leq 0.001$). This was unexpected due to the potential of **SG77** to induce oxidative stress and thus initiate GSH reduction. However, previous cytotoxicity studies have reported a decrease in GSR enzyme activity resulting in cell death [699,700]. It is possible that **SG77** may interfere GSR activity in PC-3 cells resulting in a compromised antioxidant defence. Interestingly, PNT1A treated with **SG77** for 24 h showed no significant changes in gene expression indicating that PNT1A are more tolerant to **SG77** at the tested concentration range in agreement with cytotoxicity data.

To further investigate the involvement of oxidative stress in **SG77** hybrid drug action, both intracellular glutathione levels and ROS generation were quantified (Figure 38, Figure 39). Artesunate and mitonafide significantly increased ROS generation in both prostate cell lines from 4h onwards ($P \leq 0.05$). This was expected as both ART and NAP derivatives have been shown to cause the production of ROS *in vitro* [690,706]. Interestingly, PNT1A treated with 10 µM **SG77** did not have any significant increases in ROS production after 24 h. In contrast, PC-3 cells treated with **SG77** showed a significant increase in ROS from 4h onwards ($P \leq 0.001$). This data suggests that PC-3 are more sensitive to **SG77** mediated ROS generation than PNT1A. Increased ROS and oxidative stress are often present in cancer cells [622,701]. Furthermore, basal levels of ROS are higher in PC-3 when compared to prostate non-tumour cells [69]. It is possible that PC-3 are therefore more susceptible to **SG77** mediated increases in ROS which act to tip the redox balance resulting in apoptosis induction [595,702].

This accumulation of excessive ROS will trigger the antioxidant pathways of the cell including the GSH antioxidant response. Once synthesised GSH reacts with oxygen radicals to ensure that they are removed from the body to minimise cell damage [628]. However, excessive ROS generation can result in GSH depletion and a marked increase in GSSG. Both total and oxidised GSH levels were quantified in PNT1A and PC-3 following **SG77** treatment. PNT1A had a lower basal level of total GSH with untreated cells having less than 200 pm/10^5 cells as compared to over 300 pm/10^5 cells in PC-3 (Figure 40). Both prostate cells displayed a significant reduction in total glutathione when treated with 10 µM **SG77** for 48 h ($P \leq 0.001$). Interestingly, 10 µM **SG77** resulted in a significant increase in percentage GSSG in PC-3 after 24 h (Figure 41) ($P \leq 0.001$). GSSG levels in PNT1A remained unchanged after 24 h. This data suggests that PC-3 are under severe oxidative stress after 24 h with depletion of GSH and an increase in GSSG to more than 40% of total glutathione. PNT1A, on the other hand, were less susceptible to **SG77** induced ROS production and therefore do not mount an antioxidant response until 48 h. Apoptosis levels were also more pronounced in PC-3 with increased levels of late apoptotic and dead cells. PC-3 cells were very sensitive to **SG77** induced apoptosis after 72 h with more than 80% of cell population either in late apoptotic stage or dead. **SG77** mediated

apoptosis was also observed in PNT1A to a lesser extent with 42% of cells progressing to late apoptosis.

Overall this study has uncovered some important and novel findings. Firstly, oxygen concentration has the potential to modulate the anticancer efficacy of anticancer agents *in vitro*. It is important to factor oxygen into the preclinical evaluation of novel chemotherapeutics. Several ART-NAP hybrids were effective in reducing tumour cell number while sparing non-tumour cells. Furthermore, **SG77** was selectively toxic in PC-3 with 11 times more activity when compared to non-tumour PNT1A. The data generated indicates that intrinsic apoptosis, DNA damage and glutathione antioxidant response may be important in **SG77** drug action. **SG77** should be considered as a promising candidate for animal trials with the potential for a potent and selective cancer treatment which may improve patient outcome.

6.1 Future directions

In Chapter 2, it was discovered that oxygen modulates the anticancer activity of artesunate [295]. To date, almost all *in vitro* cytotoxicity assays employ an oxygen rich environment despite evidence that oxygenation is vital to chemotherapy outcome [243,244]. It is therefore proposed that future *in vitro* assays should employ oxygen levels which better mimic *in vivo* environments of non-tumour cells or tumour cell masses. While outside the scope of the current study, it would be worthwhile to investigate the molecular mechanisms responsible for this improved efficacy in a lower oxygen environment. This could be achieved by investigation of caspase enzyme expression at different oxygen concentrations. For example, DHA was shown to induce caspase independent apoptosis upon exposure to hypoxic conditions in colorectal cancer cells [293]. Furthermore, HIF-1 activation during hypoxia may also be suppressed by DHA [707]. Therefore, it may be beneficial to quantify HIF-1 expression in response to artesunate in varying oxygen environments.

While **SG77** hybrid has shown promising anticancer activity and tumour cell selectivity, there is a need to expand the current study by investigating **SG77** efficacy on several other non-tumour cell lines such as HTB 125 breast cells and a primary cell line such as lymphocytes. Indeed, these cell lines have been more

tolerant to DHA treatment than their tumour counterparts in previous studies [163,708]. Furthermore, it would be interesting to map cellular uptake and localisation of **SG77** which may also account for observed selective toxicity in PC-3. This could be achieved by developing a LC-MS assay to detect for hybrid metabolites in cell lysates following treatment [709]. Alternatively, the hybrid could be fluorescently labelled before treatment of cancer cells and detected by either fluorescent microscopy or flow cytometry [111]. Indeed, structurally related compounds (which are autofluorescent due to NAP component) and can be viewed in combination with organelle-specific dyes to map sub-cellular localisation (Appendix B). Cellular uptake studies at several time points would also allow estimation of hybrid half-life and comparison to parent drugs. PARP-1 and NHEJ1 expression indicated that DNA damage is likely initiated following **SG77** treatment. This could be confirmed with follow-up molecular assays such as the comet assay. In addition, it would be interesting to investigate the effect of **SG77** on cell cycle distribution using flow cytometry [78,710]. The role of DNA repair enzymes could be further investigated in response to **SG77** treatment by blocking gene expression using siRNA technology.

6.2 Concluding remarks

The first major finding of this study was that oxygen modulates the anticancer activity of artesunate. Increased anticancer efficacy of artesunate was observed in HeLa cells as oxygen concentration was lowered to normoxic or hypoxic levels [295]. This finding demonstrates that oxygen is a key variable which remains overlooked in most novel drug analyses. It is recommended that future *in vitro* assays should employ oxygen levels which better mimic *in vivo* environs. Several ART-NAP hybrids showed excellent activity in HL-60 and PC-3 cancer cells following *in vitro* evaluation. Perhaps even more significant was the greater tolerance of PNT1A non-tumour cells to hybrids **SG76** and **SG77** as compared to their parent drugs.

SG77 was evaluated further to investigate the mode of action. Bax/Bcl-2 ratio was significantly increased in HL60 indicating the activation of intrinsic apoptosis activation. In addition, significant up-regulation of PARP was detected thus indicating DNA damage could be involved in **SG77** drug action. It was apparent

that PC-3 were more sensitive to **SG77** than PNT1A from generated cytotoxicity data. A differential response was also observed when ROS production and GSH antioxidant response and apoptosis. ROS production and GSH depletion occurred more rapidly and at higher levels in PC-3. Because of this promising data, **SG77** must be considered as an excellent candidate for animal trials with the potential for a potent and selective cancer therapy.

Appendices

Appendix A: optimisation of HeLa cell density and vehicle concentration

HeLa cell growth was analysed at different starting cell densities ranging from 500-4500 cells per well (Figure 44). The experiment was run for over 100 h post seeding. Increased starting cell density correlated with an increase in growth. Cell densities above 2500 resulted in linear growth from 24-72h. The effect of vehicle concentration on HeLa cell number was accessed at 24 and 48h. Concentrations of 0.05, 0.15 and 0.25 % (v/v) were tested. No significant change in cell number was observed in DMSO-exposed cells when compared to control (Figure 45).

To optimise artesunate antitumour activity on HeLa cells, an alternative drug addition schedule was trialled where two doses of artesunate were added at 24 and 48 h post cell seeding in Chapter 2. A preliminary experiment was performed to determine the effect of two separate vehicle (0.1% (v/v) DMSO) exposures on HeLa cell number. Cell count analysis revealed no significant reduction in cell number was observed at any of the tested seeding densities (Figure 46).

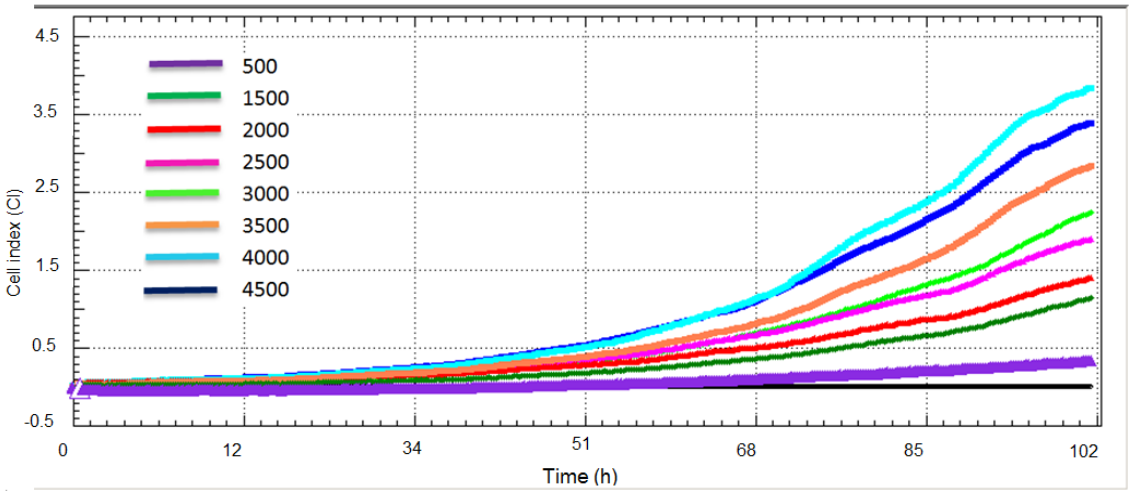

Figure 44 HeLa seeding density optimisation

HeLa cells seeded at indicated densities ranging from 500 to 4500/well in 1% (v/v) oxygen conditions. Cell proliferation was monitored in real time using RTCA DP instrument until experiment end at 102 h.

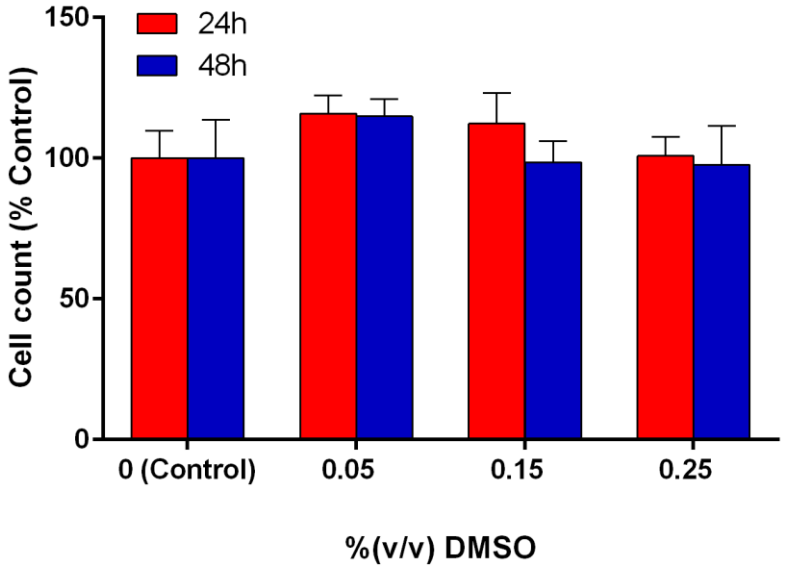

Figure 45 HeLa cell count analysis in response to varying vehicle concentration

HeLa cells seeded in 6 well plates at 80000/ well. 24 h indicated concentrations of DMSO were added. Cell count analysis was performed at both 24 and 48 h. Relative cell count is expressed as a percentage untreated control. The data above is representative of a single experiment.

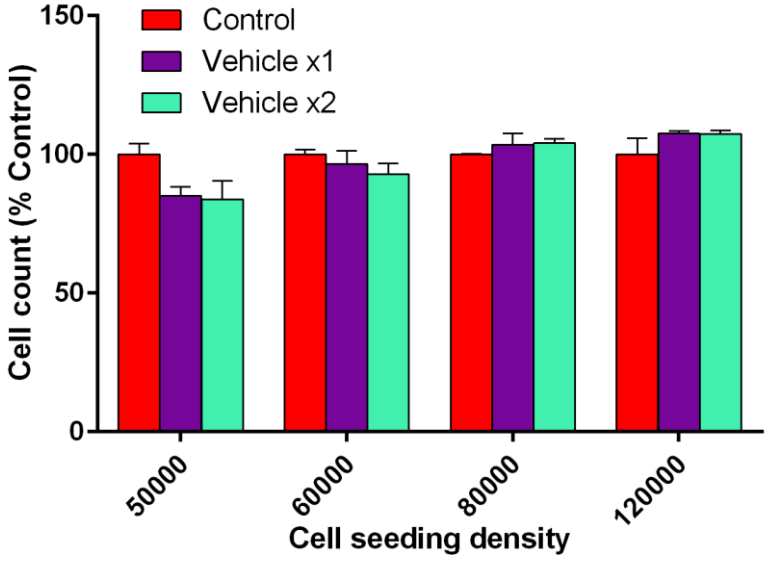

Figure 46 HeLa cell count analysis after vehicle treatment at varying cell density

HeLa cells seeded in 6 well plates at varying cell densities were exposed to either 1 or 2 doses of vehicle (0.1%DMSO). The first treatment was at 24 h after seeding with second treatment after a further 24 h. cell count analysis was then performed 24 h after second treatment and is expressed as a percentage of untreated control. The data above is representative of a single experiment.

Appendix B: cell count analysis raw data

A

	PNT1A			PC-3			MCF-7			HL-60		
Concentration (uM)	Mean (% control)	SD	N	Mean (% control)	SD	N	Mean (% control)	SD	N	Mean (% control)	SD	N
0	101.08	4.30	3	100.00	7.75	3	100.00	5.80	3	100.00	7.59	3
0.01	102.84	10.12	3	94.29	12.84	3	89.06	13.63	3	105.99	8.57	3
0.1	98.12	5.92	3	87.69	8.05	3	89.60	10.05	3	94.91	10.46	3
1	94.19	10.56	3	75.62	13.34	3	45.70	4.32	3	84.40	8.07	3
10	58.13	11.11	3	45.97	9.17	3	35.54	4.73	3	47.99	7.93	3
50	40.67	4.81	3	21.11	9.40	3	30.29	5.91	3	20.20	6.99	3

B

	PNT1A			PC-3			MCF-7			HL-60		
Concentration (uM)	Mean (% control)	SD	N	Mean (% control)	SD	N	Mean (% control)	SD	N	Mean (% control)	SD	N
0	101.08	4.30	3	100.00	7.75	3	100.00	5.80	3	100.00	7.59	3
0.01	90.98	12.99	3	83.30	6.92	3	99.58	9.43	3	107.55	7.69	3
0.1	98.19	10.68	3	84.97	13.90	3	91.15	7.94	3	94.27	12.78	3
1	40.47	12.99	3	24.26	4.23	3	49.38	7.87	3	33.34	7.43	3
10	32.23	11.10	3	13.63	4.29	3	41.38	4.86	3	29.21	5.28	3
50	27.48	8.68	3	9.73	2.54	3	37.85	6.74	3	18.03	3.75	3

C

	PNT1A			PC-3			MCF-7			HL-60		
Concentration (uM)	Mean (% control)	SD	N	Mean (% control)	SD	N	Mean (% control)	SD	N	Mean (% control)	SD	N
0	101.08	4.30	3	100.00	7.75	3	100.00	5.80	3	100.00	7.59	3
0.01	99.74	6.37	3	87.03	7.94	3	95.96	7.91	3	107.54	8.30	3
0.1	81.82	10.51	3	87.07	11.57	3	81.56	2.54	3	100.97	7.90	3
1	73.56	9.09	3	91.98	10.59	3	76.86	6.91	3	50.85	11.76	3
10	70.89	4.81	3	57.97	9.17	3	70.21	4.20	3	30.72	7.29	3
50	64.47	3.37	3	28.40	10.78	3						

D

	PNT1A			PC-3			MCF-7			HL-60		
Concentration (uM)	Mean (% control)	SD	N	Mean (% control)	SD	N	Mean (% control)	SD	N	Mean (% control)	SD	N
0	101.08	4.30	3	100.00	7.75	3	100.00	5.80	3	100.00	7.59	3
0.01	103.08	8.14	3	98.24	7.81	3	102.34	9.08	3	95.35	6.01	3
0.1	97.59	7.68	3	85.38	12.79	3	78.06	8.60	3	113.24	10.86	3
1	84.99	12.29	3	63.42	11.14	3	84.77	4.39	3	48.49	10.61	3
10	76.03	8.70	3	40.91	9.65	3	75.49	7.52	3	36.82	9.94	3
50	57.59	2.11	3	28.98	6.16	3	60.71	9.85	3	19.71	11.30	3

E

	PNT1A			PC-3			MCF-7			HL-60		
Concentration (uM)	Mean (% control)	SD	N	Mean (% control)	SD	N	Mean (% control)	SD	N	Mean (% control)	SD	N
0	101.08	4.30	3	100.00	7.75	3	100.00	5.80	3	100.00	7.59	3
0.01	84.93	8.85	3	91.68	5.92	3	93.49	4.70	3	100.51	7.88	3
0.1	78.98	12.69	3	78.20	7.90	3	91.20	7.95	3	107.43	11.56	3
1	68.88	8.16	3	49.09	4.46	3	88.42	8.78	3	42.48	10.93	3
10	56.63	8.25	3	35.18	9.15	3	69.30	5.45	3	33.32	9.18	3
50	45.66	10.18	3	20.27	6.57	3	68.31	3.87	3	20.40	7.79	3

Figure 47 Chapter 4 cell count data

The tables above summarise the cell cound analysis data generated during Chapter 4 in PNT1A, PC-3, MCF-7 and HL60 cell lines. Each table represents a different drug treatment; (A) Artesunate, (B) Mitonafide, (C) **SG76**, D) **SG77** and (E) **SG81**. at concentrations of 0, 0.01, 0.1, 10 or 50 µM. The mean cell count values (expressed as % of untreated control), SD and the number of experiments (N) are displayed.

Appendix C: housekeeper gene expression at all 3 phases of RT-PCR

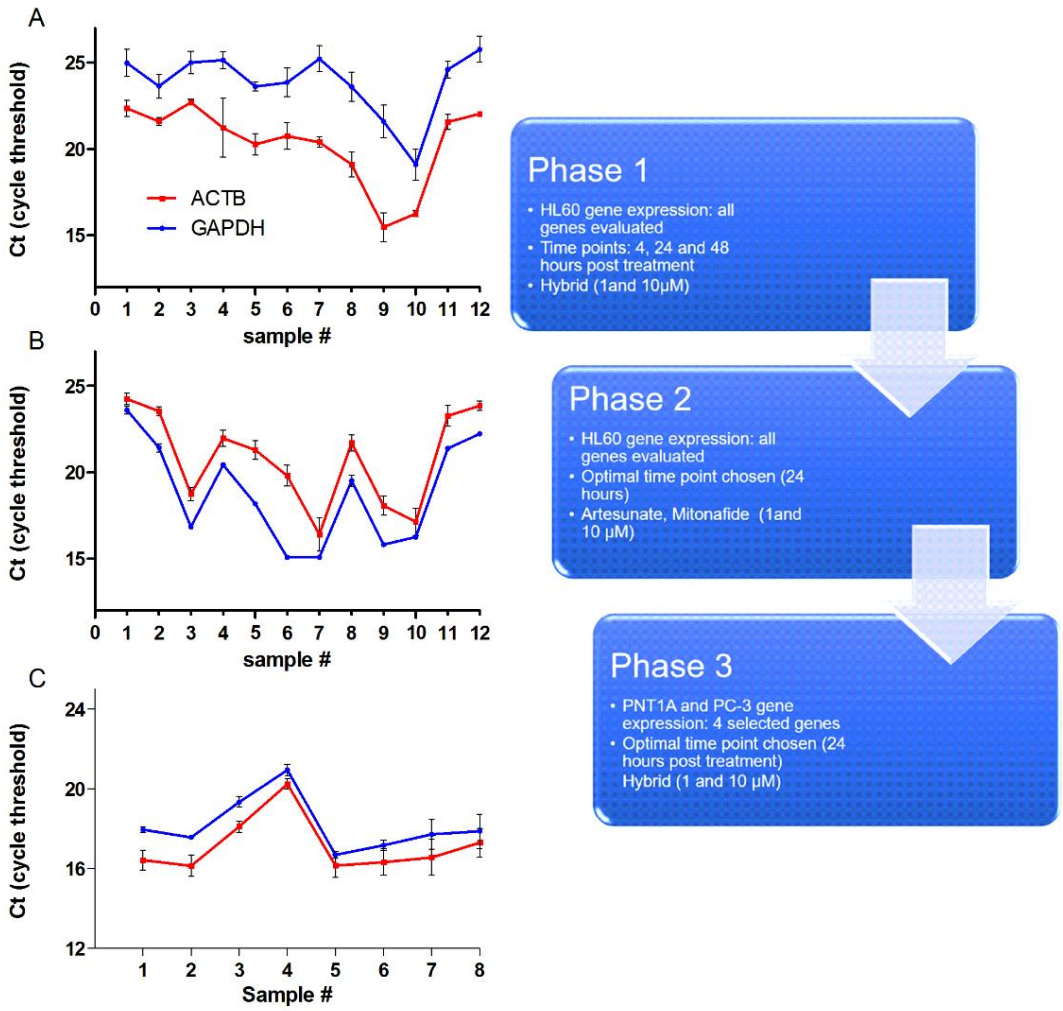

Figure 48 Housekeeper gene expression at all 3 phases of RT-PCR

Housekeeper gene expression (ACTB and GAPDH) was analysed across all samples using RT-PCR. Data is expressed as Ct values +/- SD for each sample. RT-PCR was performed as described in 5.6.5. in samples from (A) Phase 1, (B) Phase 2, and (C) Phase 3.

Appendix D: RT-PCR raw data

	Ct Values GSR						
	TREATMENT		1	2	3	**AVERAGE**	**SD**
	Control	exp 1	24.32	24.67	24.07	**24.35**	**0.30**
	Control	exp 2	24.67	24.72	24.45	**24.61**	**0.14**
	Control	exp 3	24.16	24.17	24.43	**24.25**	**0.15**
	Vehicle	exp 1	23.68	23.62	23.52	**23.61**	**0.08**
	Vehicle	exp 2	23.63	23.97	23.88	**23.83**	**0.18**
PNT1A	Vehicle	exp 3	24.55	24.15	24.09	**24.26**	**0.25**
	1 µM SG77	exp 1	25.8	25.89	26.03	**25.91**	**0.12**
	1 µM SG77	exp 2	25.79	25.92	26.26	**25.99**	**0.24**
	1 µM SG77	exp 3	26.26	26.26	25.67	**26.06**	**0.34**
	10 µM SG77	exp 1	33.07	32.27	32.61	**32.65**	**0.40**
	10 µM SG77	exp 2	32.06	32.34	33.63	**32.68**	**0.84**
	10 µM SG77	exp 3	32.61	33.63	32.52	**32.92**	**0.62**
	TREATMENT	EXP	REP 1	REP 2	REP 3	**AVERAGE**	**SD**
	Control	exp 1	21.91	22.86	22.99	**22.59**	**0.59**
	Control	exp 2	23.17	22.96	23.08	**23.07**	**0.11**
	Control	exp 3	22.77	22.56	22.36	**22.56**	**0.21**
	Vehicle	exp 1	24.18	24.17	24.19	**24.18**	**0.01**
	Vehicle	exp 2	23.79	23.81	23.84	**23.81**	**0.03**
PC3	Vehicle	exp 3	23.39	23.41	23.44	**23.41**	**0.03**
	1 µM SG77	exp 1	23.7	23.68	23.74	**23.71**	**0.03**
	1 µM SG77	exp 2	23.8	23.72	23.8	**23.77**	**0.05**
	1 µM SG77	exp 3	24.01	24.05	24.16	**24.07**	**0.08**
	10 µM SG77	exp 1	24.28	24.22	24.12	**24.21**	**0.08**
	10 µM SG77	exp 2	24.17	24.21	24.37	**24.25**	**0.11**
	10 µM SG77	exp 3	24.01	24.37	24.16	**24.18**	**0.18**

Figure 49 Ct values generated for GSR expression in PNT1A and PC-3

The table above shows individual Ct values generated by RT-PCR instrument. In this example, GSR is the target gene. Each experiment was repeated three times in triplicate. The indivdual Ct values from each of the 3 experiments were then averaged and the SD was calculated. These averages were then used to calculate fold change in gene expression as shown in Figure 50.

					targets	ref								
CELL LINE	sample n	Sample Name	Targets	References	Mean Cp	Mean Cp	Delta Cp	Rel ratio	Delta Delta Cp	Normalised rel ratio	Log BASE 2	average	average fold change	SD
PC-3	1	Control	GSR	Beta actin	24.35	16.42	7.93	0.00	0.05	1.0377	0.0533	1.0054	0.0000	0.1858
PC-3	1	Control	GSR	Beta actin	24.61	16.42	8.19	0.00	-0.21	0.8665	-0.2067			
PC-3	1	Control	GSR	Beta actin	24.25	16.42	7.83	0.00	0.15	1.1121	0.1533			
PC-3	2	Vehicle	GSR	Beta actin	23.61	16.15	7.46	0.01	0.53	1.4400	0.5261	1.1966	0.2339	0.3342
PC-3	2	Vehicle	GSR	Beta actin	23.83	16.15	7.68	0.00	0.31	1.2364	0.3061			
PC-3	2	Vehicle	GSR	Beta actin	24.26	16.15	8.12	0.00	-0.13	0.9135	-0.1306			
PC-3	3	1 µM SG77	GSR	Beta actin	25.91	18.11	7.79	0.00	0.19	1.1430	0.1928	1.0824	0.1128	0.0784
PC-3	3	1 µM SG77	GSR	Beta actin	25.99	18.11	7.88	0.00	0.11	1.0788	0.1094			
PC-3	3	1 µM SG77	GSR	Beta actin	26.06	18.11	7.95	0.00	0.04	1.0253	0.0361			
PC-3	4	10 µM SG77	GSR	Beta actin	32.65	20.25	12.40	0.00	-4.41	0.0471	-4.4094	0.0441	-4.5083	0.1488
PC-3	4	10 µM SG77	GSR	Beta actin	32.68	20.25	12.42	0.00	-4.44	0.0462	-4.4361			
PC-3	4	10 µM SG77	GSR	Beta actin	32.92	20.25	12.67	0.00	-4.68	0.0390	-4.6794			
PNT1A	5	Control	GSR	Beta actin	22.59	16.15	6.43	0.01	0.15	1.1121	0.1533	1.0126	0.0000	0.2860
PNT1A	5	Control	GSR	Beta actin	23.07	16.15	6.92	0.01	-0.33	0.7955	-0.3300			
PNT1A	5	Control	GSR	Beta actin	22.56	16.15	6.41	0.01	0.18	1.1303	0.1767			
PNT1A	6	Vehicle	GSR	Beta actin	24.18	16.33	7.85	0.00	-1.27	0.4161	-1.2650	0.5535	-0.8872	0.3835
PNT1A	6	Vehicle	GSR	Beta actin	23.81	16.33	7.49	0.01	-0.90	0.5365	-0.8983			
PNT1A	6	Vehicle	GSR	Beta actin	23.41	16.33	7.09	0.01	-0.50	0.7079	-0.4983			
PNT1A	7	1 µM SG77	GSR	Beta actin	23.71	16.56	7.14	0.01	-0.56	0.6801	-0.5561	0.6190	-0.7006	0.1953
PNT1A	7	1 µM SG77	GSR	Beta actin	23.77	16.56	7.21	0.01	-0.62	0.6494	-0.6228			
PNT1A	7	1 µM SG77	GSR	Beta actin	24.07	16.56	7.51	0.01	-0.92	0.5275	-0.9228			
PNT1A	8	10 µM SG77	GSR	Beta actin	24.21	17.30	6.90	0.01	-0.32	0.8026	-0.3172	0.7997	-0.3228	0.0353
PNT1A	8	11 µM SG77	GSR	Beta actin	24.25	17.30	6.95	0.01	-0.36	0.7789	-0.3606			
PNT1A	8	12 µM SG77	GSR	Beta actin	24.18	17.30	6.88	0.01	-0.29	0.8176	-0.2906			

Figure 50 Conversion of average Ct values in to fold change

The table above shows the conversion of average Ct values to fold change in Microsoft Excel 2016. The table shows GSR expression in both PNT1A and PC-3. The difference in Ct values between the target gene (yellow) and refereence gene (green) was first calculated for each treatment. This delta Ct is then normalised against control treatment to give delta delta Ct. This value is then expressed as LOG to the base 2 to convert in to fold change.

References

1. Laviano, A. & Rossi Fanelli, F. Toxicity in Chemotherapy — When Less Is More. *N. Engl. J. Med.* **366,** 2319–2320 (2012).

2. Chabner, B. A. & Roberts, T. G. Timeline: Chemotherapy and the war on cancer. *Nat. Rev. Cancer* **5,** 65–72 (2005).

3. Lauren, P. *Molecular Biology of Cancer: Mechanisms, targets, and therapeutics*. *Oxford University Press* (2012).

4. Hanahan, D. & Weinberg, R. A. Hallmarks of cancer: the next generation. *Cell* **144,** 646–74 (2011).

5. Meunier, B. Hybrid molecules with a dual mode of action: dream or reality? *Acc. Chem. Res.* **41,** 69–77 (2008).

6. Nakagawa-Goto, K. *et al.* Antitumor agents. 258. Syntheses and evaluation of dietary antioxidant--taxoid conjugates as novel cytotoxic agents. *Bioorg. Med. Chem. Lett.* **17,** 5204–9 (2007).

7. Das, N., Dhanawat, M., Dash, B., Nagarwal, R. C. & Shrivastava, S. K. Codrug: an efficient approach for drug optimization. *Eur. J. Pharm. Sci.* **41,** 571–88 (2010).

8. Jones, M. *et al.* Antitumour and antimalarial activity of artemisinin-acridine hybrids. *Bioorg. Med. Chem. Lett.* **19,** 2033–7 (2009).

9. Srivastava, V. & Lee, H. Chloroquine-based hybrid molecules as promising novel chemotherapeutic agents. *Eur. J. Pharmacol.* **762,** 472–86 (2015).

10. Sashidhara, K. V, Kumar, A., Kumar, M., Sarkar, J. & Sinha, S. Synthesis and in vitro evaluation of novel coumarin-chalcone hybrids as potential anticancer agents. *Bioorg. Med. Chem. Lett.* **20,** 7205–11 (2010).

11. Duan, Y.-C. *et al.* Design and synthesis of novel 1,2,3-triazole-dithiocarbamate hybrids as potential anticancer agents. *Eur. J. Med. Chem.* **62,** 11–9 (2013).

12. Decker, M. Hybrid molecules incorporating natural products: applications in cancer therapy, neurodegenerative disorders and beyond. *Curr. Med. Chem.* **18,** 1464–75 (2011).

13. Singh, K., Kaur, H., Chibale, K. & Balzarini, J. Synthesis of 4-aminoquinoline-pyrimidine hybrids as potent antimalarials and their mode of action studies. *Eur. J. Med. Chem.* **66C,** 314–323 (2013).

14. Walsh, J. J., Coughlan, D., Heneghan, N., Gaynor, C. & Bell, A. A novel artemisinin-quinine hybrid with potent antimalarial activity. *Bioorg. Med. Chem. Lett.* **17,** 3599–602 (2007).

15. Klayman, D. L. Qinghaosu (artemisinin): an antimalarial drug from China. *Science* **228,** 1049–55 (1985).

16. Efferth, T., Olbrich, A. & Bauer, R. mRNA expression profiles for the response of human tumor cell lines to the antimalarial drugs artesunate, arteether, and artemether. *Biochem. Pharmacol.* **64,** 617–623 (2002).

17. Krungkrai, S. R. & Yuthavong, Y. The antimalarial action on Plasmodium falciparum of qinghaosu and artesunate in combination with agents which modulate oxidant stress. *Trans. R. Soc. Trop. Med. Hyg.* **81,** 710–714 (1987).

18. Efferth, T., Dunstan, H., Sauerbrey, A., Miyachi, H. & Chitambar, C. R. The anti-malarial artesunate is also active against cancer. *Int. J. Oncol.* **18,** 767–73 (2001).

19. Crespo-Ortiz, M. P. & Wei, M. Q. Antitumor activity of artemisinin and its derivatives: from a well-known antimalarial agent to a potential anticancer drug. *J. Biomed. Biotechnol.* **2012,** 247597 (2012).

20. Nakase, I., Lai, H., Singh, N. P. & Sasaki, T. Anticancer properties of artemisinin derivatives and their targeted delivery by transferrin conjugation. *Int. J. Pharm.* **354,** 28–33 (2008).

21. Lai, H. & Singh, N. P. Oral artemisinin prevents and delays the development of 7,12-dimethylbenz[a]anthracene (DMBA)-induced breast cancer in the rat. *Cancer Lett.* **231,** 43–8 (2006).

22. Dell'Eva, R. *et al.* Inhibition of angiogenesis in vivo and growth of Kaposi's sarcoma xenograft tumors by the anti-malarial artesunate. *Biochem. Pharmacol.* **68,** 2359–2366 (2004).

23. Bachmeier, B. *et al.* Development of resistance towards artesunate in MDA-MB-231 human breast cancer cells. *PLoS One* **6,** e20550 (2011).

24. Thanaketpaisarn, O., Waiwut, P., Sakurai, H. & Saiki, I. Artesunate enhances TRAIL-induced apoptosis in human cervical carcinoma cells through inhibition of the NF-κB and PI3K/Akt signaling pathways. *Int. J. Oncol.* **39,** 279–85 (2011).

25. Braña, M. F. *et al.* Chromophore-modified bis-naphthalimides: synthesis and antitumor activity of bis-dibenz[de,h]isoquinoline-1,3-diones. *J. Med. Chem.* **40,** 449–54 (1997).

26. M. F. Brana, B. S. P., M. Cacho, B. S. P., A. Gradillas, B. S. P., B. de Pascual-Teresa, B.

S. P. & A. Ramos, B. S. P. Intercalators as Anticancer Drugs. *Curr. Pharm. Des.* **7,** 1745–1780 (2001).

27. Asbury, R., Blessing, J. A., Look, K. Y., Buller, R. & Lucci, J. A. A phase II trial of amonafide in patients with nonsquamous cell carcinoma of the cervix. A Gynecologic Oncology Group study. *Am. J. Clin. Oncol.* **20,** 626–7 (1997).

28. Ratain, M. J. *et al.* Population pharmacodynamic study of amonafide: a Cancer and Leukemia Group B study. *J. Clin. Oncol.* **13,** 741–7 (1995).

29. Ackroyd, R., Kelty, C., Brown, N. & Reed, M. The history of photodetection and photodynamic therapy. *Photochem. Photobiol.* **74,** 656–669 (2001).

30. Dougherty, T. J., Gomer, C. J. & Weishaupt, K. R. Energetics and efficiency of photoinactivation of murine tumor cells containing hematoporphyrin. *Cancer Res.* **36,** 2330–3 (1976).

31. Moan, J., Johannessen, J. V, Christensen, T., Espevik, T. & Mcghie, J. B. Porphyrin-Sensitized Photoinactivation of Human Cells in Vitro.

32. Gomer, C. J., Rucker, N., Ferrario, A. & Wong, S. Properties and applications of photodynamic therapy. *Radiat. Res.* **120,** 1–18 (1989).

33. Pushpan, S. K. *et al.* Porphyrins in photodynamic therapy - a search for ideal photosensitizers. *Curr. Med. Chem. Anticancer. Agents* **2,** 187–207 (2002).

34. Hockel, M. & Vaupel, P. Tumor Hypoxia: Definitions and Current Clinical, Biologic, and Molecular Aspects. *JNCI J. Natl. Cancer Inst.* **93,** 266–276 (2001).

35. Vaupel, P. & Mayer, A. Hypoxia and anemia: effects on tumor biology and treatment resistance. *Transfus. Clin. Biol.* **12,** 5–10 (2005).

36. Aebersold, D. M. *et al.* Expression of Hypoxia-inducible Factor-1{{alpha}}: A Novel Predictive and Prognostic Parameter in the Radiotherapy of Oropharyngeal Cancer. *Cancer Res.* **61,** 2911–2916 (2001).

37. Brizel, D. M., Sibley, G. S., Prosnitz, L. R., Scher, R. L. & Dewhirst, M. W. Tumor hypoxia adversely affects the prognosis of carcinoma of the head and neck. *Int. J. Radiat. Oncol.* **38,** 285–289 (1997).

38. Rockwell, S., Dobrucki, I. T., Kim, E. Y., Marrison, S. T. & Vu, V. T. Hypoxia and radiation therapy: past history, ongoing research, and future promise. *Curr. Mol. Med.* **9,** 442–58 (2009).

39. Lelong-Rebel, I., Brisson, C., Fabre, M., Bergerat, J.-P. & Rebel, G. Effect of pO2 on antitumor drug cytotoxicity on MDR and non-MDR variants selected from the LoVo

metastatic colon carcinoma cell line. *Anticancer Res.* **28,** 55–68 (2008).

40. Preston, T. J., Henderson, J. T., McCallum, G. P. & Wells, P. G. Base excision repair of reactive oxygen species-initiated 7,8-dihydro-8-oxo-2'-deoxyguanosine inhibits the cytotoxicity of platinum anticancer drugs. *Mol. Cancer Ther.* **8,** 2015–26 (2009).

41. Panda, D., Rathinasamy, K., Santra, M. K. & Wilson, L. Kinetic suppression of microtubule dynamic instability by griseofulvin: implications for its possible use in the treatment of cancer. *Proc. Natl. Acad. Sci. U. S. A.* **102,** 9878–83 (2005).

42. Papandreou, I., Powell, A., Lim, A. L. & Denko, N. Cellular reaction to hypoxia: sensing and responding to an adverse environment. *Mutat. Res.* **569,** 87–100 (2005).

43. Brown, J. M. & Wilson, W. R. Exploiting tumour hypoxia in cancer treatment. *Nat. Rev. Cancer* **4,** 437–47 (2004).

44. Hanahan, D. & Weinberg, R. A. The hallmarks of cancer. *Cell* **100,** 57–70 (2000).

45. National Cancer Registry Ireland. *Cancer in Ireland 1994-2014: Annual Report of the National Cancer Registry*. (2016).

46. National Cancer Registry Ireland. *Cancer projections for Ireland 2015- 2040*. (2014).

47. Silvenberg, E. & Lubera, J. Cancer Statistics. *CA Cancer J Clin.* **37,** 2–19 (1987).

48. Ferlay, J. *et al.* Cancer incidence and mortality worldwide: Sources, methods and major patterns in GLOBOCAN 2012. *Int. J. Cancer* **136,** E359–E386 (2015).

49. Yokota, J. Tumor progression and metastasis. *Carcinogenesis* **21,** 497–503 (2000).

50. Hecht, S. S. Tobacco smoke carcinogens and lung cancer. *J. Natl. Cancer Inst.* **91,** 1194–210 (1999).

51. de Gruijl, F. R. *et al.* Skin cancer and solar UV radiation. *Eur. J. Cancer* **35,** 2003–2009 (1999).

52. Kripke, M. L. Immunologic Mechanisms in UV Radiation Carcinogenesis. *Adv. Cancer Res.* **34,** 69–106 (1981).

53. Goustin, A. S., Leof, E. B., Shipley, G. D., Moses, H. L. & Moses2, H. L. Growth Factors and Cancer. **46,** 1015–1029 (1986).

54. Fernández-Medarde, A. & Santos, E. Ras in cancer and developmental diseases. *Genes Cancer* **2,** 344–58 (2011).

55. Maertens, O. & Cichowski, K. An expanding role for RAS GTPase activating proteins (RAS GAPs) in cancer. *Adv. Biol. Regul.* **1,** 1–14 (2014).

56. Goodsell, D. S. The molecular perspective: the ras oncogene. *Oncologist* **4,** 263–4 (1999).

57. Aubert, G. & Lansdorp, P. M. Telomeres and Aging. *Physiol. Rev.* **88,** 557–579 (2008).

58. Keramaris, N. C., Calori, G. M., Nikolaou, V. S., Schemitsch, E. H. & Giannoudis, P. V. Fracture vascularity and bone healing: A systematic review of the role of VEGF. *Injury* **39,** S45-57 (2008).

59. Cancer Research UK. Stages of cancer. (2014). Available at: http://www.cancerresearchuk.org/about-cancer/what-is-cancer/stages-of-cancer. (Accessed: 27th April 2017)

60. Edge, S. B. & Compton, C. C. The American Joint Committee on Cancer: the 7th Edition of the AJCC Cancer Staging Manual and the Future of TNM. *Ann. Surg. Oncol.* **17,** 1471–1474 (2010).

61. Weifeng, T. *et al.* Artemisinin inhibits in vitro and in vivo invasion and metastasis of human hepatocellular carcinoma cells. *Phytomedicine* **18,** 158–62 (2011).

62. Berenblum, I. & Shubik, P. A New, Quantitative, Approach to the Study of the Stages of Chemical Carcinogenesis in the Mouse's Skin*. *Br. J. Cancer* **1,** 383–391 (1947).

63. Ziech, D., Franco, R., Pappa, A. & Panayiotidis, M. I. Reactive oxygen species (ROS)--induced genetic and epigenetic alterations in human carcinogenesis. *Mutat. Res.* **711,** 167–73 (2011).

64. Traverso, N. *et al.* Role of Glutathione in Cancer Progression and Chemoresistance. *Oxid. Med. Cell. Longev.* **2013,** 1–10 (2013).

65. Vincent, T. L. & Gatenby, R. A. An evolutionary model for initiation, promotion, and progression in carcinogenesis. *Int. J. Oncol.* **32,** 729–37 (2008).

66. Fisher, B. *et al.* Postoperative adjuvant chemotherapy or radiation therapy for rectal cancer: results from NSABP protocol R-01. *J. Natl. Cancer Inst.* **80,** 21–9 (1988).

67. Corrie, P. G. Cytotoxic chemotherapy: clinical aspects. *Medicine (Baltimore).* **36,** 24–28 (2008).

68. Hayden, E. C. Cutting off cancer's supply lines. *Nature* **458,** 686–687 (2009).

69. Subotic, S., Wyler, S. & Bachmann, A. Surgical Treatment of Localised Renal Cancer. *Eur. Urol. Suppl.* **11,** 60–65 (2012).

70. Sawyers, C. Targeted cancer therapy. *Nature* **432,** 294–297 (2004).

71. National Cancer Institute. Surgery for Cancer. Available at: https://www.cancer.gov/about-cancer/treatment/types/surgery#WHS. (Accessed: 10th April 2017)

72. World Health Organisation. *Latest world cancer statistics Global cancer burden rises to 14.1 million new cases in 2012: Marked increase in breast cancers must be addressed*. *Press release 223* (2013).

73. Bailar, J. C. & Gornik, H. L. Cancer undefeated. *N. Engl. J. Med.* **336,** 1569–74 (1997).

74. Ferlay, J., Parkin, D. M. & Steliarova-Foucher, E. Estimates of cancer incidence and mortality in Europe in 2008. *Eur. J. Cancer* **46,** 765–81 (2010).

75. Moncharmont, C. *et al.* Targeting a cornerstone of radiation resistance: Cancer stem cell. *Cancer Lett.* **322,** 139–147 (2012).

76. Wallner, K. E. & Li, G. C. Effect of cisplatin resistance on cellular radiation response. *Int. J. Radiat. Oncol.* **13,** 587–591 (1987).

77. Louie, K. G. *et al.* Radiation Survival Parameters of Antineoplastic Drug-sensitive and -resistant Human Ovarian Cancer Cell Lines and Their Modification by Buthionine Sulfoximine. *Cancer Res.* **45,** (1985).

78. Azzam, E. I., Jay-Gerin, J.-P. & Pain, D. Ionizing radiation-induced metabolic oxidative stress and prolonged cell injury. *Cancer Lett.* **327,** 48–60 (2012).

79. Barker, H. E., Paget, J. T. E., Khan, A. A. & Harrington, K. J. The tumour microenvironment after radiotherapy: mechanisms of resistance and recurrence. *Nat. Rev. Cancer* **15,** 409–425 (2015).

80. Relling, M. V. *et al.* High incidence of secondary brain tumours after radiotherapy and antimetabolites. *Lancet* **354,** 34–39 (1999).

81. Bonadonna, G. *et al.* Combination Chemotherapy as an Adjuvant Treatment in Operable Breast Cancer. *N. Engl. J. Med.* **294,** 405–410 (1976).

82. Tacar, O., Sriamornsak, P. & Dass, C. R. Doxorubicin: an update on anticancer molecular action, toxicity and novel drug delivery systems. *J. Pharm. Pharmacol.* **65,** 157–170 (2013).

83. Cepeda, V. *et al.* Biochemical Mechanisms of Cisplatin Cytotoxicity. *Anticancer. Agents Med. Chem.* **7,** 3–18 (2007).

84. D'Arcangelo, M., Drew, Y. & Plummer, R. The role of PARP in DNA repair and its therapeutic exploitation. *DNA Repair Cancer Ther. Mol. Targets Clin. Appl. Second Ed.* **105,** 115–134 (2016).

85. Estrela, J. M., Ortega, A. & Obrador, E. Glutathione in Cancer Biology and Therapy. *Crit. Rev. Clin. Lab. Sci.* (2008).

86. Trachootham, D., Alexandre, J. & Huang, P. Targeting cancer cells by ROS-mediated mechanisms: a radical therapeutic approach? *Nat. Rev. Drug Discov.* **8,** 579–591 (2009).

87. Manley, P. W. *et al.* Advances in the structural biology, design and clinical development of VEGF-R kinase inhibitors for the treatment of angiogenesis. *Biochim. Biophys. Acta - Proteins Proteomics* **1697,** 17–27 (2004).

88. Thierry Le Chevalier a, *, T. L. b. Adjuvant treatment of tung cancer: current status and potentiat apptications of new regimens.

89. Spitler, L. E. *et al.* Adjuvant therapy of stage III and IV malignant melanoma using granulocyte-macrophage colony-stimulating factor. *J. Clin. Oncol.* **18,** 1614–21 (2000).

90. Thompson, I. M. *et al.* Adjuvant radiotherapy for pathological T3N0M0 prostate cancer significantly reduces risk of metastases and improves survival: long-term followup of a randomized clinical trial. *J. Urol.* **181,** 956–62 (2009).

91. Fiorica, F. *et al.* Adjuvant radiotherapy on older and oldest breast cancer patients after conservative surgery: A retrospective analysis. *Arch. Gerontol. Geriatr.* **55,** 283–288 (2012).

92. Kimura, H. & Yamaguchi, Y. A phase III randomized study of interleukin-2 lymphokine-activated killer cell immunotherapy combined with chemotherapy or radiotherapy after curative or noncurative resection of primary lung carcinoma. *Cancer* **80,** 42–49 (1997).

93. Colleoni, M. & Montagna, E. Neoadjuvant therapy for ER-positive breast cancers. *Ann. Oncol.* **23,** 243–248 (2012).

94. Buzatto, I. P. C. *et al.* Neoadjuvant chemotherapy with trastuzumab in HER2-positive breast cancer: pathologic complete response rate, predictive and prognostic factors. *Brazilian J. Med. Biol. Res.* **50,** e5674 (2017).

95. Worm, J., Kirkin, A. F., Dzhandzhugazyan, K. N. & Guldberg, P. Methylation-dependent Silencing of the Reduced Folate Carrier Gene in Inherently Methotrexate-resistant Human Breast Cancer Cells. *J. Biol. Chem.* **276,** 39990–40000 (2001).

96. Michael, M. & Doherty, M. M. Tumoral drug metabolism: overview and its implications for cancer therapy. *J. Clin. Oncol.* **23,** 205–29 (2005).

97. Ween, M. P., Armstrong, M. A., Oehler, M. K. & Ricciardelli, C. The Role of ABC Transporters in Ovarian Cancer Progression and Chemoresistance. *Crit. Rev. Oncol. Hematol.* **96,** 220–256 (2015).

98. Kelter, G. *et al.* Role of Transferrin Receptor and the ABC Transporters ABCB6 and ABCB7 for Resistance and Differentiation of Tumor Cells towards Artesunate. *PLoS One*

2, 7 (2007).

99. de Laat, W. L., Jaspers, N. G. & Hoeijmakers, J. H. Molecular mechanism of nucleotide excision repair. *Genes Dev.* **13,** 768–85 (1999).

100. Prasad, R. *et al.* DNA polymerase beta -mediated long patch base excision repair. Poly(ADP-ribose)polymerase-1 stimulates strand displacement DNA synthesis. *J. Biol. Chem.* **276,** 32411–4 (2001).

101. Takata, M. *et al.* Homologous recombination and non-homologous end-joining pathways of DNA double-strand break repair have overlapping roles in the maintenance of chromosomal integrity in vertebrate cells. *EMBO J.* **17,** 5497–508 (1998).

102. Goode, E. L., Ulrich, C. M. & Potter, J. D. Polymorphisms in DNA repair genes and associations with cancer risk. *Cancer Epidemiol. Biomarkers Prev.* **11,** 1513–30 (2002).

103. Selvakumaran, M., Pisarcik, D. A., Bao, R., Yeung, A. T. & Hamilton, T. C. Enhanced cisplatin cytotoxicity by disturbing the nucleotide excision repair pathway in ovarian cancer cell lines. *Cancer Res.* **63,** 1311–1316 (2003).

104. Bonanno, L., Favaretto, A. & Rosell, R. Platinum drugs and DNA repair mechanisms in lung cancer. *Anticancer Res.* **34,** 493–501 (2014).

105. Keshelava, N. *et al.* Loss of p53 Function Confers High-Level Multidrug Resistance in Neuroblastoma Cell Lines. *Cancer Res.* **61,** (2001).

106. Fennell, D. A. Bcl-2 as a target for overcoming chemoresistance in small-cell lung cancer. *Clin. Lung Cancer* **4,** 307–13 (2003).

107. Phillips, R. S. Current status of malaria and potential for control. *Clin. Microbiol. Rev.* **14,** 208–26 (2001).

108. Efferth, T. Mechanistic perspectives for 1,2,4-trioxanes in anti-cancer therapy. *Drug Resist. Updat.* **8,** 85–97 (2005).

109. van Agtmael, M. A., Eggelte, T. A. & van Boxtel, C. J. Artemisinin drugs in the treatment of malaria: from medicinal herb to registered medication. *Trends Pharmacol. Sci.* **20,** 199–205 (1999).

110. Boareto, A. C. *et al.* Toxicity of artemisinin [Artemisia annua L.] in two different periods of pregnancy in Wistar rats. *Reprod. Toxicol.* **25,** 239–246 (2008).

111. O'Neill, P. M., Barton, V. E. & Ward, S. A. The molecular mechanism of action of artemisinin--the debate continues. *Molecules* **15,** 1705–21 (2010).

112. Golenser, J., Waknine, J. H., Krugliak, M., Hunt, N. H. & Grau, G. E. Current perspectives

on the mechanism of action of artemisinins. *Int. J. Parasitol.* **36,** 1427–1441 (2006).

113. Haldar, K. & Mohandas, N. Malaria, erythrocytic infection, and anemia. *Hematology* **2009,** 87–93 (2009).

114. Coronado, L. M., Nadovich, C. T. & Spadafora, C. Malarial hemozoin: from target to tool. *Biochim. Biophys. Acta* **1840,** 2032–41 (2014).

115. Egan, T. J. *et al.* Structure-function relationships in aminoquinolines: Effect of amino and chloro groups on quinoline-hematin complex formation, inhibition of ??- hematin formation, and antiplasmodial activity. *J. Med. Chem.* **43,** 283–291 (2000).

116. Parapini, S. *et al.* Evidence that haem iron in the malaria parasite is not needed for the antimalarial effects of artemisinin. *FEBS Lett.* **575,** 91–4 (2004).

117. Wang, J. *et al.* Artemisinin directly targets malarial mitochondria through its specific mitochondrial activation. *PLoS One* **5,** e9582 (2010).

118. Shandilya, A. *et al.* A plausible mechanism for the antimalarial activity of artemisinin: A computational approach. *Sci. Rep.* **3,** 214–217 (2013).

119. Olliaro, P. L., Haynes, R. K., Meunier, B. & Yuthavong, Y. Possible modes of action of the artemisinin-type compounds. *Trends Parasitol.* **17,** 122–126 (2001).

120. Kamchonwongpaisan, S. & Meshnick, S. R. The Mode of Action of the Antimalarial Artemisinin and its Derivatives. *Gen. Pharmac* **27,** 587–592 (1996).

121. Haynes, R. K. & Vonwiller, S. C. The behaviour of qinghaosu (artemisinin) in the presence of heme iron(II) and (III). *Tetrahedron Lett.* **37,** 253–256 (1996).

122. Creek, D. J. *et al.* Relationship between antimalarial activity and heme alkylation for spiro- and dispiro-1,2,4-trioxolane antimalarials. *Antimicrob. Agents Chemother.* **52,** 1291–6 (2008).

123. Cazelles, J., Robert, A. & Meunier, B. Alkylation of heme by artemisinin, an antimalarial drug. *Comptes Rendus l'Académie des Sci. - Ser. IIC - Chem.* **4,** 85–89 (2001).

124. Robert, A., Benoit-Vical, F., Claparols, C. & Meunier, B. The antimalarial drug artemisinin alkylates heme in infected mice. *Proc. Natl. Acad. Sci. U. S. A.* **102,** 13676–80 (2005).

125. Dhingra, V., Rao, K. V. & Narasu, M. L. Current status of artemisinin and its derivatives as antimalarial drugs. *Life Sci.* **66,** 279–300 (1999).

126. Haynes, R. K. & Krishna, S. Artemisinins: activities and actions. *Microbes Infect.* **6,** 1339–1346 (2004).

127. Barton, V., Ward, S. A., Chadwick, J., Hill, A. & O'Neill, P. M. Rationale Design of

Biotinylated Antimalarial Endoperoxide Carbon Centered Radical Prodrugs for Applications in Proteomics. *J. Med. Chem.* **53,** 4555–4559 (2010).

128. Woerdenbag, H. J. *et al.* Cytotoxicity of artemisinin-related endoperoxides to Ehrlich ascites tumor cells. *J. Nat. Prod.* **56,** 849–56 (1993).

129. Burger, A. M. & Fiebig, H. *Handbook of Anticancer Pharmacokinetics and Pharmacodynamics*. (2014).

130. Michaelis, M. *et al.* Anti-cancer effects of artesunate in a panel of chemoresistant neuroblastoma cell lines. *Biochem. Pharmacol.* **79,** 130–136 (2010).

131. Gao, N. *et al.* Interruption of the MEK/ERK signaling cascade promotes dihydroartemisinin-induced apoptosis in vitro and in vivo. *Apoptosis* **16,** 511–23 (2011).

132. Du, J. H., Zhang, H. De, Ma, Z. J. & Ji, K. M. Artesunate induces oncosis-like cell death in vitro and has antitumor activity against pancreatic cancer xenografts in vivo. *Cancer Chemother. Pharmacol.* **65,** 895–902 (2010).

133. Aung, W., Sogawa, C., Furukawa, T. & Saga, T. Anticancer effect of dihydroartemisinin (DHA) in a pancreatic tumor model evaluated by conventional methods and optical imaging. *Anticancer Res.* **31,** 1549–58 (2011).

134. Hou, J., Wang, D., Zhang, R. & Wang, H. Experimental therapy of hepatoma with artemisinin and Its derivatives: In vitro and in vivo activity, chemosensitization, and mechanisms of action. *Clin. Cancer Res.* **14,** 5519–5530 (2008).

135. Jin, M. *et al. In vivo* study of effects of artesunate nanoliposomes on human hepatocellular carcinoma xenografts in nude mice. *Drug Deliv.* **20,** 127–133 (2013).

136. Noh, J. *et al.* Amplification of oxidative stress by a dual stimuli-responsive hybrid drug enhances cancer cell death. *Nat. Commun.* **6,** 6907 (2015).

137. Chen, H., Sun, B., Pan, S., Jiang, H. & Sun, X. Dihydroartemisinin inhibits growth of pancreatic cancer cells in vitro and in vivo. *Anticancer. Drugs* **20,** 131–140 (2009).

138. Jansen, F. H. *et al.* First study of oral Artenimol-R in advanced cervical cancer: clinical benefit, tolerability and tumor markers. *Anticancer Res.* **31,** 4417–22 (2011).

139. Zhang, Z.-Y. *et al.* Artesunate combined with vinorelbine plus cisplatin in treatment of advanced non-small cell lung cancer: a randomized controlled trial. *J. Chinese Integr. Med.* **6,** 134–8 (2008).

140. Singh, N. P. & Verma, K. B. Case report of a laryngeal squamous cell carcinoma treated with artesunate. *Arch. Oncol.* **10,** 279–280 (2002).

141. Berger, T. G. *et al.* Artesunate in the treatment of metastatic uveal melanoma--first experiences. *Oncol. Rep.* **14,** 1599–603 (2005).

142. Krishna, S. *et al.* A Randomised, Double Blind, Placebo-Controlled Pilot Study of Oral Artesunate Therapy for Colorectal Cancer. *EBioMedicine* **2,** 82–90 (2015).

143. Mercer, A. E. *et al.* Evidence for the involvement of carbon-centered radicals in the induction of apoptotic cell death by artemisinin compounds. *J. Biol. Chem.* **282,** 9372–82 (2007).

144. Das, A. K. Anticancer Effect of AntiMalarial Artemisinin Compounds. *Ann. Med. Health Sci. Res.* **5,** 93–102

145. Efferth, T. *et al.* Detection of apoptosis in KG-1a leukemic cells treated with investigational drugs. *Arzneimittelforschung.* **46,** 196–200 (1996).

146. Hamacher-Brady, A. *et al.* Artesunate Activates Mitochondrial Apoptosis in Breast Cancer Cells via Iron-catalyzed Lysosomal Reactive Oxygen Species Production. *J. Biol. Chem.* **286,** 6587–6601 (2010).

147. Zhang, C. Z., Zhang, H., Yun, J., Chen, G. G. & Lai, P. B. S. Dihydroartemisinin exhibits antitumor activity toward hepatocellular carcinoma in vitro and in vivo. *Biochem. Pharmacol.* **83,** 1278–89 (2012).

148. Klonis, N. *et al.* Artemisinin activity against Plasmodium falciparum requires hemoglobin uptake and digestion. *Proc. Natl. Acad. Sci. U. S. A.* **108,** 11405–10 (2011).

149. Mercer, A. E., Copple, I. M., Maggs, J. L., O'Neill, P. M. & Park, B. K. The role of heme and the mitochondrion in the chemical and molecular mechanisms of mammalian cell death induced by the artemisinin antimalarials. *J. Biol. Chem.* **286,** 987–96 (2011).

150. Ba, Q. *et al.* Dihydroartemisinin exerts its anticancer activity through depleting cellular iron via transferrin receptor-1. *PLoS One* **7,** e42703 (2012).

151. Nakase, I., Lai, H., Singh, N. P. & Sasaki, T. Anticancer properties of artemisinin derivatives and their targeted delivery by transferrin conjugation. *Int. J. Pharm.* **354,** 28–33 (2008).

152. Efferth, T. *et al.* Enhancement of cytotoxicity of artemisinins toward cancer cells by ferrous iron. *Free Radic. Biol. Med.* **37,** 998–1009 (2004).

153. Weinberg, E. D. The role of iron in cancer. *Eur. J. Cancer Prev.* **5,** 19–36 (1996).

154. Torti, S. V & Torti, F. M. Iron and cancer: more ore to be mined. *Nat. Rev. Cancer* **13,** 342–55 (2013).

155. Aisen, P. & Listowsky, I. Iron Transport and Storage Proteins. *Annu. Rev. Biochem.* **49,** 357–393 (1980).

156. Nakase, I. *et al.* Transferrin receptor-dependent cytotoxicity of artemisinin–transferrin conjugates on prostate cancer cells and induction of apoptosis. *Cancer Lett.* **274,** 290–298 (2009).

157. Rolfs, A., Kvietikova, I., Gassmann, M. & Wenger, R. H. Oxygen-regulated transferrin expression is mediated by hypoxia-inducible factor-1. *J. Biol. Chem.* **272,** 20055–62 (1997).

158. Singh, N. P. & Lai, H. Selective toxicity of dihydroartemisinin and holotransferrin toward human breast cancer cells. *Life Sci.* **70,** 49–56 (2001).

159. Lai, H. & Singh, N. P. Selective cancer cell cytotoxicity from exposure to dihydroartemisinin and holotransferrin. *Cancer Lett.* **91,** 41–46 (1995).

160. Daniels, T. R., Delgado, T., Helguera, G. & Penichet, M. L. The transferrin receptor part II: Targeted delivery of therapeutic agents into cancer cells. *Clin. Immunol.* **121,** 159–176 (2006).

161. Prost, A. C. *et al.* Differential transferrin receptor density in human colorectal cancer: A potential probe for diagnosis and therapy. *Int. J. Oncol.* **13,** 871–5 (1998).

162. Keer, H. N. *et al.* Elevated transferrin receptor content in human prostate cancer cell lines assessed in vitro and in vivo. *J. Urol.* **143,** 381–5 (1990).

163. Lai, H., Sasaki, T., Singh, N. P. & Messay, A. Effects of artemisinin-tagged holotransferrin on cancer cells. *Life Sci.* **76,** 1267–79 (2005).

164. Efferth, T. *et al.* Molecular modes of action of artesunate in tumor cell lines. *Mol. Pharmacol.* **64,** 382–94 (2003).

165. Hsiang, Y. H., Jiang, J. B. & Liu, L. F. Topoisomerase II-mediated DNA cleavage by amonafide and its structural analogs. *Mol. Pharmacol.* **36,** 371–6 (1989).

166. Braña, M. F. & Ramos, A. Naphthalimides as anti-cancer agents: synthesis and biological activity. *Curr. Med. Chem. Anticancer. Agents* **1,** 237–255 (2001).

167. Chang, A. Y. *et al.* Phase II trial of gallium nitrate, amonafide and teniposide in metastatic non-small cell lung cancer. An Eastern Cooperative Oncology Group study (E2588). *Invest. New Drugs* **13,** 137–41 (1995).

168. Malviya, V. K. *et al.* Evaluation of amonafide in cervical cancer, phase II. A SWOG study. *Am. J. Clin. Oncol.* **15,** 41–4 (1992).

169. Marshall, M. E. *et al.* Phase II trial of amonafide for the treatment of advanced, hormonally refractory carcinoma of the prostate. A Southwest Oncology Group study. *Am. J. Clin. Oncol.* **17,** 514–5 (1994).

170. Higano, C. *et al.* Phase II evaluation of amonafide in renal cell carcinoma. *Invest. New Drugs* **9,** (1991).

171. Levitt, R. *et al.* Phase II study of amonafide in patients with recurrent glioma. *J. Neurooncol.* **23,** 87–93 (1995).

172. Scheithauer, W. *et al.* Phase II study of amonafide in advanced breast cancer. *Breast Cancer Res. Treat.* **20,** 63–7 (1991).

173. Shen, K. *et al.* A ROS-mediated lysosomal-mitochondrial pathway is induced by a novel Amonafide analogue, 7c, in human Hela cervix carcinoma cells. *Cancer Lett.* **333,** 229–38 (2013).

174. Freeman, C. L., Swords, R. & Giles, F. J. Amonafide: a future in treatment of resistant and secondary acute myeloid leukemia? *Expert Rev. Hematol.* **5,** 17–26 (2012).

175. Li, Y. *et al.* E2F1-dependent pathways are involved in amonafide analogue 7-d-induced DNA damage, G2/M arrest, and apoptosis in p53-deficient K562 cells. *J. Cell. Biochem.* **113,** 3165–77 (2012).

176. Shao, J. *et al.* 7b, a novel amonafide analog, inhibited proliferation and phorbol 12-myristate 13-acetate/phytohemagglutinin-induced inflammatory responses of Jurkat T cells via p73-dependent pathway and decrease of nuclear factor-κB DNA-binding, respectively. *Leuk. Lymphoma* **54,** 359–71 (2013).

177. Chau, M., Christensen, J. L., Ajami, A. M. & Capizzi, R. L. Amonafide, a topoisomerase II inhibitor, is unaffected by P-glycoprotein-mediated efflux. *Leuk. Res.* **32,** 465–73 (2008).

178. Rosen, F. *et al.* Phase II study of amonafide in the treatment of patients with advanced squamous cell carcinoma of the head and the neck. An Illinois Cancer Center study. *Invest. New Drugs* **13,** 249–52 (1995).

179. Díaz-Rubio, E., Martín, M., López-Vega, J. M., Casado, A. & Benavides, A. Phase I study of mitonafide with a 3-day administration schedule: early interruption due to severe central nervous system toxicity. *Invest. New Drugs* **12,** 277–281 (1994).

180. Rosell, R. *et al.* Phase I study of mitonafide in 120 hour continuous infusion in non-small cell lung cancer. *Invest. New Drugs* **10,** 171–175 (1992).

181. Abad, A. *et al.* Phase II study of Mitonafide in advanced and relapsed colorectal cancer. *Invest. New Drugs* **14,** 223–5 (1996).

182. Braña, M. F. *et al.* Bis-naphthalimides: a new class of antitumor agents. *Anticancer. Drug Des.* **8,** 257–68 (1993).

183. Bousquet, P. F. *et al.* Preclinical Evaluation of Lu-79553 - A Novel Bis-Naphthalimide with Potent Antitumor-Activity. *Cancer Res.* **55,** 1176–1180 (1995).

184. Villalona-Calero, M. A. *et al.* Phase I and Pharmacokinetic Study of LU79553, a DNA Intercalating Bisnaphthalimide, in Patients With Solid Malignancies. *J. Clin. Oncol.* **19,** 857–869 (2001).

185. Braña, M. F. *et al.* New analogues of amonafide and elinafide, containing aromatic heterocycles: synthesis, antitumor activity, molecular modeling, and DNA binding properties. *J. Med. Chem.* **47,** 1391–9 (2004).

186. González-Bulnes, L. & Gallego, J. Analysis of mixed DNA-bisnaphthalimide interactions involving groove association and intercalation with surface-based and solution methodologies. *Biopolymers* **97,** 974–87 (2012).

187. Alley, S. C., Okeley, N. M. & Senter, P. D. Antibody-drug conjugates: targeted drug delivery for cancer. *Curr. Opin. Chem. Biol.* **14,** 529–37 (2010).

188. Scott, A. M., Wolchok, J. D. & Old, L. J. Antibody therapy of cancer. *Nat. Rev. Cancer* **12,** 278–87 (2012).

189. Hinman, L. M. *et al.* Preparation and Characterization of Monoclonal Antibody Conjugates of the Calicheamicins : A Novel and Potent Family of Antitumor Antibiotics Preparation and Characterization of Monoclonal Antibody Conjugates of the Calicheamicins : A Novel and Potent Fam. *Cancer Res.* **53,** 3336–3342 (1993).

190. Zein, N., Sinha, A., McGahren, W. & Ellestad, G. Calicheamicin gamma 1I: an antitumor antibiotic that cleaves double-stranded DNA site specifically. *Science (80-.).* **240,** 1198–1201 (1988).

191. Giles, F. J. *et al.* Mylotarg (gemtuzumab ozogamicin) therapy is associated with hepatic venoocclusive disease in patients who have not received stem cell transplantation. *Cancer* **92,** 406–13 (2001).

192. Laszlo, G. S., Estey, E. H. & Walter, R. B. The past and future of CD33 as therapeutic target in acute myeloid leukemia. *Blood Rev.* **28,** 143–153 (2014).

193. Walter, R. B., Appelbaum, F. R., Estey, E. H. & Bernstein, I. D. Acute myeloid leukemia stem cells and CD33-targeted immunotherapy. *Blood* **119,** (2012).

194. Nakase, I. *et al.* Transferrin receptor-dependent cytotoxicity of artemisinin–transferrin conjugates on prostate cancer cells and induction of apoptosis. *Cancer Lett.* **274,** 290–

298 (2009).

195. Fortin, S. & Bérubé, G. Advances in the development of hybrid anticancer drugs. *Expert Opin. Drug Discov.* **8,** 1029–47 (2013).

196. Qiu, L. *et al.* cRGDyK modified pH responsive nanoparticles for specific intracellular delivery of doxorubicin. *Acta Biomater.* **30,** 285–98 (2016).

197. Scheeren, L. E. *et al.* PEGylated and poloxamer-modified chitosan nanoparticles incorporating a lysine-based surfactant for pH-triggered doxorubicin release. *Colloids Surf. B. Biointerfaces* **138,** 117–27 (2016).

198. Yin, H., Xu, Y., Qian, X., Li, Y. & Liu, J. Novel N-oxide of naphthalimides as prodrug leads against hypoxic solid tumor: synthesis and biological evaluation. *Bioorg. Med. Chem. Lett.* **17,** 2166–70 (2007).

199. Fortin, S. & Bérubé, G. Advances in the development of hybrid anticancer drugs. *Expert Opin. Drug Discov.* **8,** 1029–1047 (2013).

200. Zask, A., Kaplan, J., Musto, S. & Loganzo, F. Hybrids of the hemiasterlin analogue taltobulin and the dolastatins are potent antimicrotubule agents. *J. Am. Chem. Soc.* **127,** 17667–71 (2005).

201. Jordan, M. A. & Wilson, L. Microtubules as a target for anticancer drugs. *Nat. Rev. Cancer* **4,** 253–265 (2004).

202. Lodish, H. *et al.* Microtubule Structures. (2000).

203. Bai, R. *et al.* Interaction of dolastatin 10 with tubulin: induction of aggregation and binding and dissociation reactions. *Mol. Pharmacol.* **47,** 965–76 (1995).

204. Anderson, H. J., Coleman, J. E., Andersen, R. J. & Roberge, M. Cytotoxic peptides hemiasterlin, hemiasterlin A and hemiasterlin B induce mitotic arrest and abnormal spindle formation. *Cancer Chemother. Pharmacol.* **39,** 223–6 (1997).

205. Tsogoeva, S. B. Recent progress in the development of synthetic hybrids of natural or unnatural bioactive compounds for medicinal chemistry. *Mini Rev. Med. Chem.* **10,** 773–93 (2010).

206. Paterson, I., Naylor, G. J. & Wright, A. E. Total synthesis of a potent hybrid of the anticancer natural products dictyostatin and discodermolide. *Chem. Commun. (Camb).* **6,** 4628–30 (2008).

207. Barrera, G. Oxidative stress and lipid peroxidation products in cancer progression and therapy. *ISRN Oncol.* **2012,** 137289 (2012).

208. Bergamini, C., Gambetti, S., Dondi, A. & Cervellati, C. Oxygen, Reactive Oxygen Species and Tissue Damage. *Curr. Pharm. Des.* **10,** 1611–1626 (2004).

209. Schumacker, P. T. Reactive oxygen species in cancer cells: live by the sword, die by the sword. *Cancer Cell* **10,** 175–6 (2006).

210. Offen, D., Gilgun-Sherki, Y. & Melamed, E. The role of oxidative stress in the pathogenesis of multiple sclerosis: The need for effective antioxidant therapy. *J. Neurol.* **251,** 261–268 (2004).

211. Jaakkola, K. *et al.* Treatment with antioxidant and other nutrients in combination with chemotherapy and irradiation in patients with small-cell lung cancer. *Anticancer Res.* **12,** 599–606 (1991).

212. Teiten, M.-H., Dicato, M. & Diederich, M. Hybrid Curcumin Compounds: A New Strategy for Cancer Treatment. *Molecules* **19,** 20839–20863 (2014).

213. Orlikova, B., Tasdemir, D., Golais, F., Dicato, M. & Diederich, M. Dietary chalcones with chemopreventive and chemotherapeutic potential. *Genes Nutr.* **6,** 125–47 (2011).

214. Bubols, G. B. *et al.* The antioxidant activity of coumarins and flavonoids. *Mini Rev. Med. Chem.* **13,** 318–34 (2013).

215. Anto, R. J. *et al.* Anticancer and antioxidant activity of synthetic chalcones and related compounds. *Cancer Lett.* **97,** 33–7 (1995).

216. Muregi, F. W. & Ishih, A. Next-generation antimalarial drugs: hybrid molecules as a new strategy in drug design. *Drug Dev. Res.* **71,** n/a-n/a (2009).

217. Toure, O. A. *et al.* Efficacy and safety of fixed dose combination of arterolane maleate and piperaquine phosphate dispersible tablets in paediatric patients with acute uncomplicated Plasmodium falciparum malaria: a phase II, multicentric, open-label study. *Malar. J.* **14,** 469 (2015).

218. Dong, Y. *et al.* The Structure−Activity Relationship of the Antimalarial Ozonide Arterolane (OZ277). *J. Med. Chem.* **53,** 481–491 (2010).

219. Srinivasula, S. *et al.* A conserved XIAP-interaction motif in caspase-9 and Smac/DIABLO regulates caspase activity and apoptosis. *Nature* **410,** 112–116 (2001).

220. Ricci, J., Kim, M., Chung, W.-Y., Park, K.-K. & Jung, M. Discovery of artemisinin-glycolipid hybrids as anti-oral cancer agents. *Chem. Pharm. Bull. (Tokyo).* **59,** 1471–5 (2011).

221. Xie, L. *et al.* Anti-Tumor Activity of New Artemisinin-Chalcone Hybrids. *Arch. Pharm. (Weinheim).* **344,** 639–647 (2011).

222. Lombard, M. C. *et al.* Potent in vivo anti-malarial activity and representative snapshot pharmacokinetic evaluation of artemisinin-quinoline hybrids. *Malar. J.* **12,** 71 (2013).

223. Ferreira, J. F. S., Luthria, D. L., Sasaki, T. & Heyerick, A. Flavonoids from Artemisia annua L. as Antioxidants and Their Potential Synergism with Artemisinin against Malaria and Cancer. *Molecules* **15,** 3135–3170 (2010).

224. Kamal, A., Reddy, B. S. N., Reddy, G. S. K. & Ramesh, G. Design and synthesis of C-8 linked pyrrolobenzodiazepine–naphthalimide hybrids as anti-tumour agents. *Bioorg. Med. Chem. Lett.* **12,** 1933–1935 (2002).

225. Kamal, A., Srinivas, O., Ramulu, P., Ramesh, G. & Kumar, P. P. Synthesis of novel C2 and C2–C8 linked pyrrolo[2,1-c][1,4]benzodiazepine-naphthalimide hybrids as DNA-binding agents. *Bioorg. Med. Chem. Lett.* **13,** 3577–3581 (2003).

226. Kamal, A., Adil, S., Tamboli, J., Siddardha, B. & Murthy, U. Synthesis of Coumarin linked Naphthalimide Conjugates as Potential Anticancer and Antimicrobial Agents. *Lett. Drug Des. Discov.* **6,** 201–209 (2009).

227. Scalabrino, G. & Ferioli, M. E. Polyamines in mammalian ageing: An oncological problem, too? A review. *Mech. Ageing Dev.* **26,** 149–164 (1984).

228. Nowotarski, S. L., Woster, P. M., Casero, R. A. & Jr. Polyamines and cancer: implications for chemotherapy and chemoprevention. *Expert Rev. Mol. Med.* **15,** e3 (2013).

229. Tian, Z. *et al.* Synthesis, cytotoxicity and apoptosis of naphthalimide polyamine conjugates as antitumor agents. *Eur. J. Med. Chem.* **44,** 393–9 (2009).

230. Dougherty, T. J. *et al.* Photoradiation Therapy for the Treatment of Malignant Tumors. *Cancer Res.* **38,** (1978).

231. Chandrashekar, T. K. & Venkatraman, S. Core-modified expanded porphyrins: New generation organic materials. *Acc. Chem. Res.* **36,** 676–691 (2003).

232. Brunner, H., Schellerer, K.-M. & Treittinger, B. Synthesis and in vitro testing of hematoporphyrin type ligands in platinum (II) complexes as potent cytostatic and phototoxic antitumor agents. *Inorganica Chim. Acta* **264,** (1997).

233. Lottner, C., Bart, K. C., Bernhardt, G. & Brunner, H. Soluble tetraarylporphyrin-platinum conjugates as cytotoxic and phototoxic antitumor agents. *J. Med. Chem.* **45,** 2079–2089 (2002).

234. Lottner, C., Bart, K. C., Bernhardt, G. & Brunner, H. Hematoporphyrin-derived soluble porphyrin-platinum conjugates with combined cytotoxic and phototoxic antitumor activity. *J. Med. Chem.* **45,** 2064–2078 (2002).

235. Brunner, H. & Schellerer, K. M. New porphyrin platinum conjugates for the cytostatic and photodynamic tumor therapy. *Inorganica Chim. Acta* **350,** 39–48 (2003).

236. Song, R., Kim, Y.-S., Lee, C. O. & Sohn, Y. S. Synthesis and antitumor activity of DNA binding cationic porphyrin-platinum(II) complexes. *Tetrahedron Lett.* **44,** 1537–1540 (2003).

237. Zhang, J.-X. *et al.* Comparative Studies of the Cellular Uptake, Subcellular Localization, and Cytotoxic and Phototoxic Antitumor Properties of Ruthenium(II)–Porphyrin Conjugates with Different Linkers. *Bioconjug. Chem.* **23,** 1623–1638 (2012).

238. Viola, A. *et al.* Phototoxicity of some novel porphyrin hybrids against the human leukemic cell line TF-1. *J. Photochem. Photobiol. B Biol.* **40,** 263–272 (1997).

239. He, H. *et al.* Porphyrin–DNA cross-linking agent hybrids: chemical synthesis and biological studies. *Bioorg. Med. Chem. Lett.* **14,** 3013–3016 (2004).

240. He, H. *et al.* Combination of porphyrins and DNA-alkylation agents: synthesis and tumor cell apoptosis induction. *Bioorg. Med. Chem.* **14,** 1068–77 (2006).

241. Höckel, M. *et al.* Intratumoral pO2 predicts survival in advanced cancer of the uterine cervix. *Radiother. Oncol.* **26,** 45–50 (1993).

242. Gray, L. H., Conger, A. D., Ebert, M., Hornsey, S. & Scott, O. C. A. The Concentration of Oxygen Dissolved in Tissues at the Time of Irradiation as a Factor in Radiotherapy. *Br. J. Radiol.* **26,** 638–648 (1953).

243. Teicher, B. A., Lazo, J. S. & Sartorelli, A. C. Classification of antineoplastic agents by their selective toxicities toward oxygenated and hypoxic tumor cells. *Cancer Res.* **41,** 73–81 (1981).

244. Teicher, B. A., Holden, S. A. & Jacobs, J. L. Approaches to defining the mechanism of enhancement by Fluosol-DA 20% with carbogen of melphalan antitumor activity. *Cancer Res.* **47,** 513–8 (1987).

245. Krtolica, a, Krucher, N. a & Ludlow, J. W. Molecular analysis of selected cell cycle regulatory proteins during aerobic and hypoxic maintenance of human ovarian carcinoma cells. *Br. J. Cancer* **80,** 1875–83 (1999).

246. D'Alessandro, S. *et al.* Hypoxia modulates the effect of dihydroartemisinin on endothelial cells. *Biochem. Pharmacol.* **82,** 476–84 (2011).

247. Movsas, B. *et al.* Hypoxia in human prostate carcinoma: an Eppendorf PO2 study. *Am. J. Clin. Oncol.* **24,** 458–61 (2001).

248. Hockel, M. *et al.* Association between tumor hypoxia and malignant progression in

advanced cancer of the uterine cervix. *Cancer Res.* **56,** 4509–15 (1996).

249. Brown, J. M. & Giaccia, A. J. The unique physiology of solid tumors: opportunities (and problems) for cancer therapy. *Cancer Res.* **58,** 1408–16 (1998).

250. Shannon, A. M., Bouchier-Hayes, D. J., Condron, C. M. & Toomey, D. Tumour hypoxia, chemotherapeutic resistance and hypoxia-related therapies. *Cancer Treat. Rev.* **29,** 297–307 (2003).

251. McKeown, S. R. Defining normoxia, physoxia and hypoxia in tumours-implications for treatment response. *Br. J. Radiol.* **87,** 20130676 (2014).

252. Ming, L. *et al.* Androgen deprivation results in time-dependent hypoxia in LNCaP prostate tumours: informed scheduling of the bioreductive drug AQ4N improves treatment response. *Int. J. Cancer* **132,** 1323–32 (2013).

253. Carreau, A., Hafny-Rahbi, B. El, Matejuk, A., Grillon, C. & Kieda, C. Why is the partial oxygen pressure of human tissues a crucial parameter? Small molecules and hypoxia. *J. Cell. Mol. Med.* **15,** 1239–1253 (2011).

254. Koumenis, C. *et al.* Regulation of Protein Synthesis by Hypoxia via Activation of the Endoplasmic Reticulum Kinase PERK and Phosphorylation of the Translation Initiation Factor eIF2. *Mol. Cell. Biol.* **22,** 7405–7416 (2002).

255. Vaupel, P. The Role of Hypoxia-Induced Factors in Tumor Progression. *Oncologist* **9,** 10–17 (2004).

256. Taraseviciene-Stewart, L. *et al.* Inhibition of the VEGF receptor 2 combined with chronic hypoxia causes cell death-dependent pulmonary endothelial cell proliferation and severe pulmonary hypertension. *FASEB J.* **15,** 427–38 (2001).

257. Greijer, A. E. & van der Wall, E. The role of hypoxia inducible factor 1 (HIF-1) in hypoxia induced apoptosis. *J. Clin. Pathol.* **57,** 1009–14 (2004).

258. Semenza, G. L. Hypoxia, clonal selection, and the role of HIF-1 in tumor progression. *Crit. Rev. Biochem. Mol. Biol.* **35,** 71–103 (2000).

259. Rademakers, S. E. *et al.* Molecular aspects of tumour hypoxia. *Mol. Oncol.* **2,** 41–53 (2008).

260. HOCKEL, M. Biological consequences of tumor hypoxia. *Semin. Oncol.* **28,** 36–41 (2001).

261. Mukhopadhyay, D. *et al.* Hypoxic induction of human vascular endothelial growth factor expression through c-Src activation. *Nature* **375,** 577–81 (1995).

262. Cross, M. J. & Claesson-Welsh, L. FGF and VEGF function in angiogenesis: signalling

pathways, biological responses and therapeutic inhibition. *Trends Pharmacol. Sci.* **22,** 201–7 (2001).

263. Maxwell, P. H. *et al.* The tumour suppressor protein VHL targets hypoxia-inducible factors for oxygen-dependent proteolysis. *Nature* **399,** 271–5 (1999).

264. Harris, A. L. Hypoxia--a key regulatory factor in tumour growth. *Nat. Rev. Cancer* **2,** 38–47 (2002).

265. Mole, D. R. *et al.* Genome-wide association of hypoxia-inducible factor (HIF)-1alpha and HIF-2alpha DNA binding with expression profiling of hypoxia-inducible transcripts. *J. Biol. Chem.* **284,** 16767–75 (2009).

266. Semenza, G. L. Hypoxia-inducible factor 1: master regulator of O2 homeostasis. *Curr. Opin. Genet. Dev.* **8,** 588–594 (1998).

267. Kaelin, W. G. & Ratcliffe, P. J. Oxygen Sensing by Metazoans: The Central Role of the HIF Hydroxylase Pathway. *Mol. Cell* **30,** 393–402 (2008).

268. Ohh, M. *et al.* Ubiquitination of hypoxia-inducible factor requires direct binding to the beta-domain of the von Hippel-Lindau protein. *Nat. Cell Biol.* **2,** 423–427 (2000).

269. Maxwell, P. H. *et al.* The tumour suppressor protein VHL targets hypoxia-inducible factors for oxygen-dependent proteolysis. *Nature* **399,** 271–275 (1999).

270. Greer, S. N., Metcalf, J. L., Wang, Y. & Ohh, M. The updated biology of hypoxia-inducible factor. *EMBO J.* **31,** 2448–60 (2012).

271. Mukhopadhyay, C. K., Mazumder, B. & Fox, P. L. Role of hypoxia-inducible factor-1 in transcriptional activation of ceruloplasmin by iron deficiency. *J. Biol. Chem.* **275,** 21048–54 (2000).

272. Peyssonnaux, C. *et al.* Regulation of iron homeostasis by the hypoxia-inducible transcription factors (HIFs). *J. Clin. Invest.* **117,** 1926–1932 (2007).

273. Manalo, D. J. *et al.* Transcriptional regulation of vascular endothelial cell responses to hypoxia by HIF-1. *Blood* **105,** 659–69 (2005).

274. Forsythe, J. O. A. *et al.* Activation of vascular endothelial growth factor gene transcription by hypoxia-inducible factor 1. *Mol. Cell. Biol.* **16,** 4604–4612 (1996).

275. Bosch-Marce, M. *et al.* Effects of aging and hypoxia-inducible factor-1 activity on angiogenic cell mobilization and recovery of perfusion after limb ischemia. *Circ. Res.* **101,** 1310–8 (2007).

276. Kunz, M. & Ibrahim, S. M. Molecular responses to hypoxia in tumor cells. *Mol Cancer* **2,**

23. (2003).

277. Semenza, G. L., Roth, P. H., Fang, H. M. & Wang, G. L. Transcriptional regulation of genes encoding glycolytic enzymes by hypoxia-inducible factor 1. *J. Biol. Chem.* **269,** 23757–63 (1994).

278. Luo, W. *et al.* Pyruvate Kinase M2 Is a PHD3-Stimulated Coactivator for Hypoxia-Inducible Factor 1. *Cell* **145,** 732–744 (2011).

279. Li, L.-N. *et al.* Artesunate attenuates the growth of human colorectal carcinoma and inhibits hyperactive Wnt/β-catenin pathway. *Int. J. Cancer* **121,** 1360–1365 (2007).

280. Finley, L. W. S. *et al.* SIRT3 Opposes Reprogramming of Cancer Cell Metabolism through HIF1α Destabilization. *Cancer Cell* **19,** 416–428 (2011).

281. Zhong, L. *et al.* The Histone Deacetylase Sirt6 Regulates Glucose Homeostasis via Hif1α. *Cell* **140,** 280–293 (2010).

282. Dioum, E. M. *et al.* Regulation of Hypoxia-Inducible Factor 2 Signaling by the Stress-Responsive Deacetylase Sirtuin 1. *Science (80-.).* **324,** 1289–1293 (2009).

283. Lim, J.-H. *et al.* Sirtuin 1 Modulates Cellular Responses to Hypoxia by Deacetylating Hypoxia-Inducible Factor 1α. *Mol. Cell* **38,** 864–878 (2010).

284. Mansfield, K. D. *et al.* Mitochondrial dysfunction resulting from loss of cytochrome c impairs cellular oxygen sensing and hypoxic HIF-α activation. *Cell Metab.* **1,** 393–399 (2005).

285. Brunelle, J. K. *et al.* Oxygen sensing requires mitochondrial ROS but not oxidative phosphorylation. *Cell Metab.* **1,** 409–414 (2005).

286. Pan, Y. *et al.* Multiple Factors Affecting Cellular Redox Status and Energy Metabolism Modulate Hypoxia-Inducible Factor Prolyl Hydroxylase Activity In Vivo and In Vitro. *Mol. Cell. Biol.* **27,** 912–925 (2007).

287. Song, X. *et al.* Hypoxia-induced resistance to cisplatin and doxorubicin in non-small cell lung cancer is inhibited by silencing of HIF-1alpha gene. *Cancer Chemother. Pharmacol.* **58,** 776–84 (2006).

288. Papadopoulou, M. V, Ji, M., Bloomer, W. D. & Hollingshead, M. G. Enhancement of the antitumor effect of cyclophosphamide with the hypoxia-selective cytotoxin NLCQ-1 against murine tumors and human xenografts. *J. Exp. Ther. Oncol.* **2,** 298–305

289. Papadopoulou, M., Ji, M., Ji, X. & Bloomer, W. Therapeutic advantage from combining 5-fluorouracil with the hypoxia-selective cytotoxin NLCQ-1 in vivo; comparison with tirapazamine. *Cancer Chemother. Pharmacol.* **50,** 291–298 (2002).

290. Papadopoulou, M. V., Ji, M., Ji, X., Bloomer, W. D. & Hollingshead, M. G. Therapeutic advantage from combining paclitaxel with the hypoxia-selective cytotoxin NLCQ-1 in murine tumor- or human xenograft-bearing mice. *Cancer Chemother. Pharmacol.* **50,** 501–508 (2002).

291. McCarty, M. . Turning an 'Achilles' Heel' into an asset – activation of HIF-1α during angiostatic therapy will increase tumor sensitivity to iron-catalyzed oxidative damage. *Med. Hypotheses* **61,** 509–511 (2003).

292. Zhang, S. & Gerhard, G. S. Heme mediates cytotoxicity from artemisinin and serves as a general anti-proliferation target. *PLoS One* **4,** e7472 (2009).

293. Ontikatze, T., Rudner, J., Handrick, R., Belka, C. & Jendrossek, V. Dihydroartemisinin is a Hypoxia-Active Anti-Cancer Drug in Colorectal Carcinoma Cells. *Front. Oncol.* **4,** 116 (2014).

294. - Paul Vandewynckel, Y. *et al.* Therapeutic effects of artesunate in hepatocellular carcinoma: repurposing an ancient antimalarial agent. *Eur. J. Gastroenterol. Hepatol.* **26,** 861–70 (2014).

295. Murray, J., Gannon, S., Rawe, S. & Murphy, J. E. J. In Vitro Oxygen Availability Modulates the Effect of Artesunate on HeLa cells. *Anticancer Res.* **34,** 7055–60 (2014).

296. Efferth, T., Giaisi, M., Merling, A., Krammer, P. H. & Li-Weber, M. Artesunate induces ROS-mediated apoptosis in doxorubicin-resistant T leukemia cells. *PLoS One* **2,** e693 (2007).

297. Konkimalla, V. B. *et al.* Effect of artemisinins and other endoperoxides on nitric oxide-related signaling pathway in RAW 264.7 mouse macrophage cells. *Nitric Oxide* **19,** 184–91 (2008).

298. Weir, L., Robertson, D., Leigh, I. M. & Panteleyev, A. a. The reduction of water-soluble tetrazolium salt reagent on the plasma membrane of epidermal keratinocytes is oxygen dependent. *Anal. Biochem.* **414,** 31–7 (2011).

299. Atienzar, F. a *et al.* The use of real-time cell analyzer technology in drug discovery: defining optimal cell culture conditions and assay reproducibility with different adherent cellular models. *J. Biomol. Screen.* **16,** 575–87 (2011).

300. Solly, K., Wang, X., Xu, X., Strulovici, B. & Zheng, W. Application of Real-Time Cell Electronic Sensing (RT-CES) Technology to Cell-Based Assays. *Assay Drug Dev. Technol.* **2,** 363–372 (2004).

301. Urcan, E. *et al.* Real-time xCELLigence impedance analysis of the cytotoxicity of dental composite components on human gingival fibroblasts. *Dent. Mater.* **26,** 51–8 (2010).

302. Höckel, M., Schlenger, K., Höckel, S. & Vaupel, P. Hypoxic cervical cancers with low apoptotic index are highly aggressive. *Cancer Res.* **59,** 4525–8 (1999).

303. Hammerová, J., Uldrijan, S., Táborská, E. & Slaninová, I. Benzo[c]phenanthridine alkaloids exhibit strong anti-proliferative activity in malignant melanoma cells regardless of their p53 status. *J. Dermatol. Sci.* **62,** 22–35 (2011).

304. Takatsuki, M. *et al.* Evaluation of resectability after neoadjuvant chemotherapy for primary non-resectable colorectal liver metastases: A multicenter study. *Eur. J. Surg. Oncol.* **42,** 184–9 (2016).

305. Beaver, K., Williamson, S. & Briggs, J. Exploring patient experiences of neo-adjuvant chemotherapy for breast cancer. *Eur. J. Oncol. Nurs.* **20,** 77–86 (2016).

306. Lu, S. *et al.* Co-delivery of peptide-modified cisplatin and doxorubicin via mucoadhesive nanocapsules for potential synergistic intravesical chemotherapy of Non-muscle-invasive bladder cancer. *Eur. J. Pharm. Sci.* **84,** 103–115 (2016).

307. Huo, Y. R., Richards, A., Liauw, W. & Morris, D. L. Hyperthermic intraperitoneal chemotherapy (HIPEC) and cytoreductive surgery (CRS) in ovarian cancer: A systematic review and meta-analysis. *Eur. J. Surg. Oncol.* **41,** 1578–89 (2015).

308. Fuh, K. C. *et al.* Comparison of bevacizumab alone or with chemotherapy in recurrent ovarian cancer patients. *Gynecol. Oncol.* **139,** 413–8 (2015).

309. Zhang, L., Chen, F., Zhang, Z., Chen, Y. & Wang, J. Synthesis and biological evaluation of a novel artesunate-podophyllotoxin conjugate as anticancer agent. *Bioorg. Med. Chem. Lett.* **26,** 38–42 (2016).

310. Yaseen, S. *et al.* Synthesis, characterization and urease inhibition, in vitro anticancer and antileishmanial studies of Co(III) complexes with N,N,N′-trisubstituted acylthioureas. *Inorganica Chim. Acta* **443,** 69–77 (2016).

311. FITZPATRICK, T. B. & PATHAK, M. A. Historical aspects of methoxsalen and other furocoumarins. *J. Invest. Dermatol.* **32,** 229–31 (1959).

312. Mitton, D. & Ackroyd, R. History of photodynamic therapy in Great Britain. *Photodiagnosis Photodyn. Ther.* **2,** 239–246 (2005).

313. Dolmans, D. E. J. G. J., Fukumura, D. & Jain, R. K. Photodynamic therapy for cancer. *Nat. Rev. Cancer* **3,** 380–7 (2003).

314. Brlickner, C. Porhyrin-based Photosensitizers for Use in Photodynamic Therapy. **54,** (1998).

315. Dougherty, T. J. *et al.* Photodynamic Therapy. *JNCI J. Natl. Cancer Inst.* **90,** 889–905

(1998).

316. Dougherty, T. J., Gomer, C. J. & Weishaupt, K. R. Energetics and Efficiency of Photoinactivation of Murine Tumor Cells Containing Hematoporphyrin. *Cancer Res.* **36,** 2330–2333 (1976).

317. Dougherty, T. J. *et al.* Photoradiation therapy for the treatment of malignant tumors. *Cancer Res.* **38,** 2628–35 (1978).

318. Walther, M. M. *et al.* Phase I trial of photo dynamic therapy in the treatment of recurrent superficial transitional cell carcinoma of the bladder. *Urology* **50,** 199–206 (1997).

319. Nseyo, U. O., Shumaker, B., Klein, E. A. & Sutherland, K. Photodynamic therapy using porfimer sodium as an alternative to cystectomy in patients with refractory transitional cell carcinoma in situ of the bladder. Bladder Photofrin Study Group. *J. Urol.* **160,** 39–44 (1998).

320. Balchum, O. J., Doiron, D. R. & Huth, G. C. Photoradiation therapy of endobronchial lung cancers employing the photodynamic action of hematoporphvrin derivative. *Lasers Surg. Med.* **4,** 13–30 (1984).

321. TS, M., Allison, R., Hewson, G., Snider, W. & Moskowitz, R. A phase ii/iii clinical study of tin ethyl etiopurpurin (purlytin)--induced photodynamic therapy for the treatment of recurrent cutaneous metastatic breast cancer. *Cancer J. Sci. Am.* **4,** 378–378 1p (1998).

322. Dougherty, T. J. *et al.* Photoradiation in the treatment of recurrent breast carcinoma. *J. Natl. Cancer Inst.* **62,** 231–7 (1979).

323. Hayata, Y., Kato, H., Okitsu, H., Kawaguchi, M. & Konaka, C. Photodynamic therapy with hematoporphyrin derivative in cancer of the upper gastrointestinal tract. *Semin. Surg. Oncol.* **1,** 1–11 (1985).

324. Popovic, E. A., Kaye, A. H. & Hill, J. S. Photodynamic therapy of brain tumors. *Semin Surg Oncol* **11,** 335–45. (1995).

325. Barr, H., Krasner, N., Boulos, P. B., Chatlani, P. & Bown, S. G. Photodynamic therapy for colorectal cancer: a quantitative pilot study. *Br. J. Surg.* **77,** 93–6 (1990).

326. Bown, S. G. *et al.* Photodynamic therapy for cancer of the pancreas. *Gut* **50,** 549–57 (2002).

327. Schuitmaker, J. J. *et al.* Photodynamic therapy: a promising new modality for the treatment of cancer. *J. Photochem. Photobiol. B Biol.* **34,** 3–12 (1996).

328. Senge, M. O. & Brandt, J. C. Temoporfin (Foscan®, 5,10,15,20-tetra(m-hydroxyphenyl)chlorin)--a second-generation photosensitizer. *Photochem. Photobiol.* **87,**

1240–96 (2011).

329. Berlanda, J., Kiesslich, T., Engelhardt, V., Krammer, B. & Plaetzer, K. Comparative in vitro study on the characteristics of different photosensitizers employed in PDT. *J. Photochem. Photobiol. B.* **100,** 173–80 (2010).

330. Allison, R. R. & Sibata, C. H. Oncologic photodynamic therapy photosensitizers: a clinical review. *Photodiagnosis Photodyn. Ther.* **7,** 61–75 (2010).

331. Castano, A. P., Demidova, T. N. & Hamblin, M. R. Mechanisms in photodynamic therapy: part one—photosensitizers, photochemistry and cellular localization. *Photodiagnosis Photodyn. Ther.* **1,** 279–293 (2004).

332. Calzavara-Pinton, P. G., Venturini, M. & Sala, R. Photodynamic therapy: update 2006. Part 1: Photochemistry and photobiology. *J. Eur. Acad. Dermatol. Venereol.* **21,** 293–302 (2007).

333. Ochsner, M. Photophysical and photobiological processes in the photodynamic therapy of tumours. *J. Photochem. Photobiol. B.* **39,** 1–18 (1997).

334. Ding, H. *et al.* Photoactivation switch from type II to type I reactions by electron-rich micelles for improved photodynamic therapy of cancer cells under hypoxia. *J. Control. Release* **156,** 276–280 (2011).

335. Nyman, E. S. & Hynninen, P. H. Research advances in the use of tetrapyrrolic photosensitizers for photodynamic therapy. *J. Photochem. Photobiol. B Biol.* **73,** 1–28 (2004).

336. Ding, H. *et al.* Photoactivation switch from type II to type I reactions by electron-rich micelles for improved photodynamic therapy of cancer cells under hypoxia. *J. Control. Release* **156,** 276–80 (2011).

337. Denk, W. *et al.* Anatomical and functional imaging of neurons using 2-photon laser scanning microscopy. *J. Neurosci. Methods* **54,** 151–62 (1994).

338. Zhou, L. *et al.* An efficient two-photon ratiometric fluorescent probe platform for dual-channel imaging of lysosomes in living cells and tissues. *Sensors Actuators B Chem.* **238,** 274–280 (2017).

339. Kearns, D. R. Physical and chemical properties of singlet molecular oxygen. *Chem. Rev.* **71,** 395–427 (1971).

340. Frederiksen, P. K., Jørgensen, M. & Ogilby, P. R. Two-photon photosensitized production of singlet oxygen. *J. Am. Chem. Soc.* **123,** 1215–1221 (2001).

341. Fisher, W. G., Partridge, W. P., Dees, C. & Wachter, E. A. Simultaneous Two-Photon

Activation of Type-I Photodynamic Therapy Agents. *Photochem. Photobiol.* **66,** 141–155 (1997).

342. Mang, T. S. Lasers and light sources for PDT: past, present and future. *Photodiagnosis Photodyn. Ther.* **1,** 43–48 (2004).

343. Marcus, S. L. & McIntyre, W. R. Photodynamic therapy systems and applications. *Expert Opin. Emerg. Drugs* **7,** 321–34 (2002).

344. Enk, C. D. & Levi, A. Low-irradiance red LED traffic lamps as light source in PDT for actinic keratoses. *Photodermatol. Photoimmunol. Photomed.* **28,** 332–334 (2012).

345. Schmidt, M. H. *et al.* Light-emitting diodes as a light source for intraoperative photodynamic therapy. *Neurosurgery* **38,** 552-6-7 (1996).

346. Marmur, E. S., Schmults, C. D. & Goldberg, D. J. A review of laser and photodynamic therapy for the treatment of nonmelanoma skin cancer. *Dermatol. Surg.* **30,** 264–271 (2004).

347. Jeffes, E. W. *et al.* Photodynamic therapy of actinic keratoses with topical aminolevulinic acid hydrochloride and fluorescent blue light. *J. Am. Acad. Dermatol.* **45,** 96–104 (2001).

348. Perria, C. *et al.* Photodynamic therapy of malignant brain tumors: clinical results of, difficulties with, questions about, and future prospects for the neurosurgical applications. *Neurosurgery* **23,** 557–63 (1988).

349. Gossner, L. *et al.* KTP laser destruction of dysplasia and early cancer in columnar-lined Barrett's esophagus. *Gastrointest. Endosc.* **49,** 8–12 (1999).

350. Zoepf, T. *et al.* Photodynamic therapy for palliation of nonresectable bile duct cancer-preliminary results with a new diode laser system. *Am. J. Gastroenterol.* **96,** 2093–2097 (2001).

351. Wilson, B. C. Photodynamic therapy: light delivery and dosage for second-generation photosensitizers. *Ciba Found. Symp.* **146,** 60-73–7 (1989).

352. Rausch, P. C. *et al.* Pulsed versus continuous wave excitation mechanisms in photodynamic therapy of differently graded squamous cell carcinomas in tumor-implanted nude mice. *Eur. Arch. Otorhinolaryngol.* **250,** 82–7 (1993).

353. Brancaleon, L. & Moseley, H. Laser and Non-laser Light Sources for Photodynamic Therapy. *Lasers Med. Sci.* **17,** 173–186 (2002).

354. Ris, H. B. *et al.* Effect of drug-light interval on photodynamic therapy with meta-tetrahydroxyphenylchlorin in malignant mesothelioma. *Int. J. Cancer* **53,** 141–6 (1993).

355. Ris, H. B. *et al.* Photodynamic therapy with m-tetrahydroxyphenylchlorin in vivo: optimization of the therapeutic index. *Int. J. cancer* **55,** 245–9 (1993).

356. Chen, B., Roskams, T. & de Witte, P. a M. Antivascular tumor eradication by hypericin-mediated photodynamic therapy. *Photochem. Photobiol.* **76,** 509–513 (2002).

357. Ahmad, N., Gupta, S., Feyes, D. K. & Mukhtar, H. Involvement of Fas (APO-1/CD-95) during photodynamic-therapy-mediated apoptosis in human epidermoid carcinoma A431 cells. *J. Invest. Dermatol.* **115,** 1041–6 (2000).

358. Teiten, M.-H., Marchal, S., D'Hallewin, M. A., Guillemin, F. & Bezdetnaya, L. Primary photodamage sites and mitochondrial events after Foscan photosensitization of MCF-7 human breast cancer cells. *Photochem. Photobiol.* **78,** 9–14 (2003).

359. Xu, D. D. *et al.* Photodynamic therapy induced cell death of hormone insensitive prostate cancer PC-3 cells with autophagic characteristics. *Photodiagnosis Photodyn. Ther.* **10,** 278–287 (2013).

360. Martin, N. E. & Hahn, S. M. Interstitial photodynamic therapy for prostate cancer: a developing modality. *Photodiagnosis Photodyn. Ther.* **1,** 123–136 (2004).

361. Riesenberg, R., Fuchs, C. & Kriegmair, M. Photodynamic effects of 5-aminolevulinic acid-induced porphyrin on human bladder carcinoma cells in vitro. *Eur. J. Cancer* **32,** 328–334 (1996).

362. Pinthus, J. H., Bogaards, A., Weersink, R., Wilson, B. C. & Trachtenberg, J. Photodynamic Therapy for Urological Malignancies: Past to Current Approaches. *J. Urol.* **175,** 1201–1207 (2006).

363. Kawczyk-Krupka, A. *et al.* Photodynamic therapy in colorectal cancer treatment-The state of the art in preclinical research. *Photodiagnosis Photodyn. Ther.* **13,** 158–74 (2016).

364. Ahn, P. H. *et al.* Toxicities and early outcomes in a phase 1 trial of photodynamic therapy for premalignant and early stage head and neck tumors. *Oral Oncol.* **55,** 37–42 (2016).

365. Moghissi, K., Dixon, K., Stringer, M. & Thorpe, J. A. C. Photofrin PDT for early stage oesophageal cancer: Long term results in 40 patients and literature review. *Photodiagnosis Photodyn. Ther.* **6,** 159–166 (2009).

366. Yamaguchi, S. *et al.* Photodynamic therapy for cervical intraepithelial neoplasia. *Oncology* **69,** 110–6 (2005).

367. Nathan, T. R. *et al.* Photodynamic therapy for cancer of the pancreas. *Gut* **50,** 549–57 (2002).

368. Muller, P. J. & Wilson, B. C. Photodynamic therapy of malignant primary brain tumours:

clinical effects, post-operative ICP, and light penetration of the brain. *Photochem. Photobiol.* **46,** 929–35 (1987).

369. Mathur, P. N., Edell, E., Sutedja, T. & Vergnon, J.-M. Treatment of Early Stage Non-small Cell Lung Cancer. *Chest* **123,** 176S–180S (2003).

370. Khan, S. A., Dougherty, T. J. & Mang, T. S. An evaluation of photodynamic therapy in the management of cutaneous metastases of breast cancer. *Eur. J. Cancer* **29,** 1686–1690 (1993).

371. Svanberg, K. *et al.* Photodynamic therapy of non-melanoma malignant tumours of the skin using topical delta-amino levulinic acid sensitization and laser irradiation. *Br. J. Dermatol.* **130,** 743–51 (1994).

372. Sibata, C. H., Colussi, V. C., Oleinick, N. L. & Kinsella, T. J. Photodynamic therapy in oncology. *Expert Opin. Pharmacother.* **2,** 917–27 (2001).

373. Jiang, F. *et al.* Photodynamic therapy using Photofrin in combination with buthionine sulfoximine (BSO) to treat 9L gliosarcoma in rat brain. *Lasers in surgery and medicine* **23,** 161–6 (1998).

374. Murant, R. S., Gibson, S. L. & Hilf, R. Photosensitizing effects of Photofrin II on the site-selected mitochondrial enzymes adenylate kinase and monoamine oxidase. *Cancer Res.* **47,** 4323–8 (1987).

375. Kwitniewski, M. *et al.* Diamino acid derivatives of PpIX as potential photosensitizers for photodynamic therapy of squamous cell carcinoma and prostate cancer: in vitro studies. *J. Photochem. Photobiol. B.* **94,** 214–22 (2009).

376. Hopper, C. Photodynamic therapy: a clinical reality in the treatment of cancer. *Lancet Oncol.* **1,** 212–219 (2000).

377. Detty, M. R., Gibson, S. L. & Wagner, S. J. Current clinical and preclinical photosensitizers for use in photodynamic therapy. *J. Med. Chem.* **47,** 3897–915 (2004).

378. Szeimies, R. M., Calzavara-Pinton, P., Karrer, S., Ortel, B. & Landthaler, M. Topical photodynamic therapy in dermatology. *J. Photochem. Photobiol. B.* **36,** 213–9 (1996).

379. Ishizuka, M. *et al.* Novel development of 5-aminolevurinic acid (ALA) in cancer diagnoses and therapy. *Int. Immunopharmacol.* **11,** 358–65 (2011).

380. Pizova, K. *et al.* Photodynamic therapy for enhancing antitumour immunity. *Biomed. Pap. Med. Fac. Univ. Palacky. Olomouc. Czech. Repub.* **156,** 93–102 (2012).

381. Agostinis, P. *et al.* Photodynamic therapy of cancer: an update. *CA. Cancer J. Clin.* **61,** 250–81 (2011).

382. Velpula, N. *et al.* Photodynamic therapy: A new modality treatment in pre-cancer and cancer patients. *Int. J. Case Reports Images* **250,** 1–8 (2014).

383. Tanaka, M. *et al.* Antitumor effects in gastrointestinal stromal tumors using photodynamic therapy with a novel glucose-conjugated chlorin. *Mol. Cancer Ther.* **13,** 767–75 (2014).

384. Gijsens, A. *et al.* Epidermal Growth Factor-mediated Targeting of Chlorin e 6 Selectively Potentiates Its Photodynamic Activity Epidermal Growth Factor-mediated Targeting of Chlorin e 6 Selectively Potentiates Its Photodynamic Activity. *Cancer Res.* **60,** 2197–2202 (2000).

385. Hamblin, M. R. & Newman, E. L. Photosensitizer targeting in photodynamic therapy I. Conjugates of haematoporphyrin with albumin and transferrin. *J. Photochem. Photobiol. B Biol.* **26,** 45–56 (1994).

386. Yang, S. J. *et al.* Folic acid-conjugated chitosan nanoparticles enhanced protoporphyrin IX accumulation in colorectal cancer cells. *Bioconjug. Chem.* **21,** 679–689 (2010).

387. Wang, C., Tao, H., Cheng, L. & Liu, Z. Near-infrared light induced in vivo photodynamic therapy of cancer based on upconversion nanoparticles. *Biomaterials* **32,** 6145–54 (2011).

388. Nawalany, K. *et al.* Novel nanostructural photosensitizers for photodynamic therapy: in vitro studies. *Int. J. Pharm.* **430,** 129–40 (2012).

389. Plaetzer, K., Kiesslich, T., Verwanger, T. & Krammer, B. The Modes of Cell Death Induced by PDT: An Overview. *Med. Laser Appl.* **18,** 7–19 (2003).

390. Kerr, J. F. R. Shrinkage necrosis: A distinct mode of cellular death. *J. Pathol.* **105,** 13–20 (1971).

391. Zakaria, S., Gamal-Eldeen, A. M., El-Daly, S. M. & Saleh, S. Synergistic apoptotic effect of Doxil ® and aminolevulinic acid-based photodynamic therapy on human breast adenocarcinoma cells. *Photodiagnosis Photodyn. Ther.* **11,** 227–38 (2014).

392. Almeida, R. D., Manadas, B. J., Carvalho, A. P. & Duarte, C. B. Intracellular signaling mechanisms in photodynamic therapy. *Biochim. Biophys. Acta* **1704,** 59–86 (2004).

393. Fulda, S. & Debatin, K.-M. Extrinsic versus intrinsic apoptosis pathways in anticancer chemotherapy. *Oncogene* **25,** 4798–4811 (2006).

394. Olivo, M. & Ali-Seyed, M. Apoptosis signalling mechanisms in human cancer cells induced by Calphostin-PDT. *Int. J. Oncol.* **30,** 537–48 (2007).

395. Ali, S. M., Chee, S. K., Yuen, G. Y. & Olivo, M. Photodynamic therapy induced Fas-mediated apoptosis in human carcinoma cells. *Int. J. Mol. Med.* **9,** 257–70 (2002).

396. Buytaert, E., Dewaele, M. & Agostinis, P. Molecular effectors of multiple cell death pathways initiated by photodynamic therapy. *Biochim. Biophys. Acta* **1776,** 86–107 (2007).

397. Moor, A. C. . Signaling pathways in cell death and survival after photodynamic therapy. *J. Photochem. Photobiol. B Biol.* **57,** 1–13 (2000).

398. Rello-Varona, S., Stockert, J. C., Cañete, M., Acedo, P. & Villanueva, Á.´. Mitotic catastrophe induced in HeLa cells by photodynamic treatment with Zn(II)-phthalocyanine. *Int. J. Oncol.* **32,** 1189–1196 (2008).

399. Usuda, J. *et al.* Increased cytotoxic effects of photodynamic therapy in IL-6 gene transfected cells via enhanced apoptosis. *Int. J. Cancer* **93,** 475–480 (2001).

400. Usuda, J., Azizuddin, K., Chiu, S. & Oleinick, N. L. Association Between the Photodynamic Loss of Bcl-2 and the Sensitivity to Apoptosis Caused by Phthalocyanine Photodynamic Therapy¶. *Photochem. Photobiol.* **78,** 1 (2003).

401. Oleinick, N. L. & Evans, H. H. The photobiology of photodynamic therapy: cellular targets and mechanisms. *Radiat. Res.* **150,** S146-56 (1998).

402. El-Hussein, A., Harith, M. & Abrahamse, H. Assessment of DNA damage after photodynamic therapy using a metallophthalocyanine photosensitizer. *Int. J. Photoenergy* **2012,** 1–10 (2012).

403. Tada-Oikawa, S., Oikawa, S., Hirayama, J., Hirakawa, K. & Kawanishi, S. DNA Damage and Apoptosis Induced by Photosensitization of 5,10,15,20-Tetrakis (*N* -methyl-4-pyridyl)-21 *H* ,23 *H* -porphyrin *via* Singlet Oxygen Generation. *Photochem. Photobiol.* **85,** 1391–1399 (2009).

404. Chen, Q., Marsh, J., Ames, B. & Mossman, B. Detection of 8-oxo-2'-deoxyguanosine, a marker of oxidative DNA damage, in culture medium from human mesothelial cells exposed to crocidolite asbestos. *Carcinogenesis* **17,** 2525–7 (1996).

405. Rousset, N. *et al.* Use of alkaline Comet assay to assess DNA repair after m-THPC-PDT. *J. Photochem. Photobiol. B Biol.* **56,** 118–131 (2000).

406. Casas, A., Di Venosa, G., Hasan, T. & Al Batlle, A. Mechanisms of resistance to photodynamic therapy. *Curr. Med. Chem.* **18,** 2486–515 (2011).

407. Reginato, E. Immune response after photodynamic therapy increases anti-cancer and anti-bacterial effects. *World J. Immunol.* **4,** 1 (2014).

408. Castano, A. P., Demidova, T. N. & Hamblin, M. R. Mechanisms in photodynamic therapy: Part three—Photosensitizer pharmacokinetics, biodistribution, tumor localization and

modes of tumor destruction. *Photodiagnosis Photodyn. Ther.* **2,** 91–106 (2005).

409. Gollnick, S. O., Owczarczak, B. & Maier, P. Photodynamic therapy and anti-tumor immunity. *Lasers Surg. Med.* **38,** 509–515 (2006).

410. Gollnick, S. O. & Brackett, C. M. Enhancement of anti-tumor immunity by photodynamic therapy. *Immunol. Res.* **46,** 216–226 (2010).

411. Castano, A. P., Mroz, P. & Hamblin, M. R. Photodynamic therapy and anti-tumour immunity. *Nat. Rev. Cancer* **6,** 535–545 (2006).

412. Brown, S. B., Brown, E. A. & Walker, I. The present and future role of photodynamic therapy in cancer treatment. *Lancet Oncol.* **5,** 497–508 (2004).

413. Wang, K. K. & Kim, J. Y. Photodynamic therapy in Barrett's esophagus. *Gastrointest. Endosc. Clin. N. Am.* **13,** 483–9, vii (2003).

414. Gudgin Dickson, E. F., Goyan, R. L. & Pottier, R. H. New directions in photodynamic therapy. *Cell. Mol. Biol. (Noisy-le-grand).* **48,** 939–954 (2002).

415. Nordsmark, M. *et al.* Prognostic value of tumor oxygenation in 397 head and neck tumors after primary radiation therapy. An international multi-center study. *Radiother. Oncol.* **77,** 18–24 (2005).

416. Höckel, M., Schlenger, K., Mitze, M., Schäffer, U. & Vaupel, P. Hypoxia and radiation response in human tumors. *Semin. Radiat. Oncol.* **6,** 3–9 (1996).

417. Foster, T. H. *et al.* Oxygen consumption and diffusion effects in photodynamic therapy. *Radiat. Res.* **126,** 296–303 (1991).

418. Wyld, L., Tomlinson, M., Reed, M. W. R. & Brown, N. J. Aminolaevulinic acid-induced photodynamic therapy: cellular responses to glucose starvation. *Br. J. Cancer* **86,** 1343–1347 (2002).

419. Vander Heiden, M. G., Cantley, L. C. & Thompson, C. B. Understanding the Warburg Effect: The Metabolic Requirements of Cell Proliferation. *Science (80-.).* **324,** (2009).

420. Celli, J. P. *et al.* Imaging and Photodynamic Therapy: Mechanisms, Monitoring, and Optimization. *Chem. Rev.* **110,** 2795–2838 (2010).

421. Huang, P. *et al.* Light-Triggered Theranostics Based on Photosensitizer-Conjugated Carbon Dots for Simultaneous Enhanced-Fluorescence Imaging and Photodynamic Therapy. *Adv. Mater.* **24,** 5104–5110 (2012).

422. Allison, R. R., Mota, H. C., Bagnato, V. S. & Sibata, C. H. Bio-nanotechnology and photodynamic therapy--state of the art review. *Photodiagnosis Photodyn. Ther.* **5,** 19–28

(2008).

423. Vargas, A., Eid, M., Fanchaouy, M., Gurny, R. & Delie, F. In vivo photodynamic activity of photosensitizer-loaded nanoparticles: formulation properties, administration parameters and biological issues involved in PDT outcome. *Eur. J. Pharm. Biopharm. Off. J. Arbeitsgemeinschaft für Pharm. Verfahrenstechnik e.V* **69,** 43–53 (2008).

424. Chen, B., Pogue, B. W. & Hasan, T. Liposomal delivery of photosensitising agents. *Expert Opin. Drug Deliv.* **2,** 477–87 (2005).

425. Castano, A. P., Mroz, P. & Hamblin, M. R. Photodynamic therapy and anti-tumour immunity. *Nat. Rev. Cancer* **6,** 535–45 (2006).

426. Mroz, P. *et al.* Photodynamic Therapy of Tumors Can Lead to Development of Systemic Antigen-Specific Immune Response. *PLoS One* **5,** e15194 (2010).

427. Korbelik, M. PDT-associated host response and its role in the therapy outcome. *Lasers Surg. Med.* **38,** 500–508 (2006).

428. Garg, A. D., Nowis, D., Golab, J. & Agostinis, P. Photodynamic therapy: illuminating the road from cell death towards anti-tumour immunity. *Apoptosis* **15,** 1050–1071 (2010).

429. Beck, T. J. *et al.* Two-photon photodynamic therapy of C6 cells by means of 5-aminolevulinic acid induced protoporphyrin IX. *J. Photochem. Photobiol. B.* **87,** 174–82 (2007).

430. Krammer, B. & Überriegler, K. In-vitro investigation of ALA-induced protopoyphyrin IX. *J. Photochem. Photobiol. B Biol.* **36,** 121–126 (1996).

431. Muschter, R. Photodynamic therapy: a new approach to prostate cancer. *Curr. Urol. Rep.* **4,** 221–8 (2003).

432. Regula, J. *et al.* Photosensitisation and photodynamic therapy of oesophageal, duodenal, and colorectal tumours using 5 aminolaevulinic acid induced protoporphyrin IX--a pilot study. *Gut* **36,** 67–75 (1995).

433. Atif, M. *et al.* In vitro study of 5-aminolevulinic acid-based photodynamic therapy for apoptosis in human cervical HeLa cell line. *Laser Phys. Lett.* **6,** 886–891 (2009).

434. Grebenová, D. *et al.* Selective destruction of leukaemic cells by photo-activation of 5-aminolaevulinic acid-induced protoporphyrin-IX. *J. Photochem. Photobiol. B.* **47,** 74–81 (1998).

435. Tsai, T. *et al.* Effect of 5-aminolevulinic acid-mediated photodynamic therapy on MCF-7 and MCF-7/ADR cells. *Lasers Surg. Med.* **34,** 62–72 (2004).

436. Eshghi, H. *et al.* Protoporphyrin IX-gold nanoparticle conjugates as an efficient photosensitizer in cervical cancer therapy. *Photodiagnosis Photodyn. Ther.* **10,** 304–12 (2013).

437. van Den Boogert, J. *et al.* Fractionated illumination in oesophageal ALA-PDT: effect on ferrochelatase activity. *J. Photochem. Photobiol. B.* **56,** 53–60 (2000).

438. Tan, W. . *et al.* Photodynamic therapy using 5-aminolaevulinic acid for oesophageal adenocarcinoma associated with Barrett's metaplasia. *J. Photochem. Photobiol. B Biol.* **53,** 75–80 (1999).

439. Wong, T. W., Sheu, H. M., Lee, J. Y. & Fletcher, R. J. Photodynamic therapy for Bowen's disease (squamous cell carcinoma in situ) of the digit. *Dermatol. Surg.* **27,** 452–6 (2001).

440. Ormrod, D. & Jarvis, B. Topical aminolevulinic acid HCl photodynamic therapy. *Am J Clin Dermatol* **1,** 131–133 (2000).

441. Wang, I. *et al.* Photodynamic therapy vs. cryosurgery of basal cell carcinomas: results of a phase III clinical trial. *Br. J. Dermatol.* **144,** 832–40 (2001).

442. Biel, M. A. Photodynamic therapy and the treatment of head and neck neoplasia. *Laryngoscope* **108,** 1259–68 (1998).

443. Li, Q. G. *et al.* The pharmacokinetics and bioavailability of dihydroartemisinin, arteether, artemether, artesunic acid and artelinic acid in rats. *J. Pharm. Pharmacol.* **50,** 173–82 (1998).

444. Fukuhara, H. *et al.* The inhibition of ferrochelatase enhances 5-aminolevulinic acid-based photodynamic action for prostate cancer. *Photodiagnosis Photodyn. Ther.* **10,** 399–409 (2013).

445. Huang, X. fei, Yuan, D., Zhang, C. & Zhang, X. Artesunate induces prostate cancer cell line PC-3 differentiation and cell cycle arrest. *J. Chinese Integr. Med.* **6,** 591–594 (2008).

446. Morrissey, C. *et al.* Effect of artemisinin derivatives on apoptosis and cell cycle in prostate cancer cells. *Anticancer. Drugs* **21,** 423–32 (2010).

447. Nathan, T. R. *et al.* Photodynamic therapy for prostate cancer recurrence after radiotherapy: a phase I study. *J. Urol.* **168,** 1427–32 (2002).

448. Maguire, A., Lyng, F. M. & Walsh, J. E. Solar simulated radiation induced cell death depends on spectral distribution and irradiance but not output delivery. *Radiat. Prot. Dosimetry* **140,** 147–57 (2010).

449. Zanchetta, L. M., Garcia, A., Lyng, F., Walsh, J. & Murphy, J. E. J. Mitophagy and mitochondrial morphology in human melanoma-derived cells post exposure to simulated

sunlight. *Int. J. Radiat. Biol.* **87,** 506–17 (2011).

450. Valentine, R. M., Brown, C. T. A., Moseley, H., Ibbotson, S. & Wood, K. Monte Carlo modeling of in vivo protoporphyrin IX fluorescence and singlet oxygen production during photodynamic therapy for patients presenting with superficial basal cell carcinomas. *J. Biomed. Opt.* **16,** 48002 (2011).

451. Kammerer, R. *et al.* The molecular basis of prostate cancer cell escape from protoporphyrin IX-based photodynamic therapy. *Med. Laser Appl.* **24,** 237–246 (2009).

452. Dirschka, T. *et al.* Photodynamic therapy with BF-200 ALA for the treatment of actinic keratosis: results of a multicentre, randomized, observer-blind phase III study in comparison with a registered methyl-5-aminolaevulinate cream and placebo. *Br. J. Dermatol.* **166,** 137–46 (2012).

453. O'Connor, A. E., Gallagher, W. M. & Byrne, A. T. Porphyrin and nonporphyrin photosensitizers in oncology: preclinical and clinical advances in photodynamic therapy. *Photochem. Photobiol.* **85,** 1053–74

454. Schneider, R. *et al.* Design, synthesis, and biological evaluation of folic acid targeted tetraphenylporphyrin as novel photosensitizers for selective photodynamic therapy. *Bioorg. Med. Chem.* **13,** 2799–808 (2005).

455. Matsumura, Y. & Ananthaswamy, H. N. Toxic effects of ultraviolet radiation on the skin. *Toxicol. Appl. Pharmacol.* **195,** 298–308 (2004).

456. Benachour, H. *et al.* Real-Time Monitoring of Photocytotoxicity in Nanoparticles-Based Photodynamic Therapy: A Model-Based Approach. *PLoS One* **7,** e48617 (2012).

457. Temizel, E., Sagir, T., Ayan, E., Isik, S. & Ozturk, R. Delivery of lipophilic porphyrin by liposome vehicles: Preparation and photodynamic therapy activity against cancer cell lines. *Photodiagnosis Photodyn. Ther.* **11,** 537–545 (2014).

458. Duncan, R. Polymer conjugates as anticancer nanomedicines. *Nat. Rev. Cancer* **6,** 688–701 (2006).

459. Dondorp, A. M. *et al.* Artemisinin resistance: current status and scenarios for containment. *Nat. Rev. Microbiol.* **8,** 272–80 (2010).

460. Sadava, D., Phillips, T., Lin, C. & Kane, S. E. Transferrin overcomes drug resistance to artemisinin in human small-cell lung carcinoma cells. *Cancer Lett.* **179,** 151–156 (2002).

461. DeClerck, K. & Elble, R. C. The role of hypoxia and acidosis in promoting metastasis and resistance to chemotherapy. *Front. Biosci. (Landmark Ed.* **15,** 213–25 (2010).

462. Cosse, J.-P. & Michiels, C. Tumour Hypoxia Affects the Responsiveness of Cancer Cells

to Chemotherapy and Promotes Cancer Progression. *Anticancer. Agents Med. Chem.* **8,** 790–797 (2008).

463. Birner, P., Schindl, M., Obermair, A., Breitenecker, G. & Oberhuber, G. Expression of Hypoxia-inducible Factor 1α in Epithelial Ovarian Tumors. *Clin. Cancer Res.* **7,** (2001).

464. Wu, A., Xu, Y., Qian, X., Wang, J. & Liu, J. Novel naphthalimide derivatives as potential apoptosis-inducing agents: design, synthesis and biological evaluation. *Eur. J. Med. Chem.* **44,** 4674–80 (2009).

465. Kennedy, M. Design, synthesis and biological evaluation of novel endoperoxide-containing hybrid chemotherapies. (Dublin Institute of Technology, Ireland, 2012).

466. Vennerstrom, J. L. *et al.* Dispiro-1,2,4,5-tetraoxanes: a new class of antimalarial peroxides. *J. Med. Chem.* **35,** 3023–7 (1992).

467. Dong, Y. *et al.* Synthesis and antimalarial activity of 11 dispiro-1, 2, 4, 5-tetraoxane analogues of WR 148999. 7, 8, 15, 16-Tetraoxadispiro hexadecanes substituted at the 1. *J. Med. Chem.* **42,** 1477–1480 (1999).

468. Sebaugh, J. L. Guidelines for accurate EC50/IC50 estimation. *Pharm. Stat.* **10,** 128–134 (2011).

469. Borkowska, A., Knap, N. & Antosiewicz, J. Diallyl trisulfide is more cytotoxic to prostate cancer cells PC-3 than to noncancerous epithelial cell line PNT1A: a possible role of p66Shc signaling axis. *Nutr. Cancer* **65,** 711–7 (2013).

470. Abdel-Aziz, M., Park, S.-E., Abuo-Rahma, G. E.-D. a a, Sayed, M. a & Kwon, Y. Novel N-4-piperazinyl-ciprofloxacin-chalcone hybrids: synthesis, physicochemical properties, anticancer and topoisomerase I and II inhibitory activity. *Eur. J. Med. Chem.* **69,** 427–38 (2013).

471. Liang, X., Xu, K., Xu, Y., Liu, J. & Qian, X. B1-induced caspase-independent apoptosis in MCF-7 cells is mediated by down-regulation of Bcl-2 via p53 binding to P2 promoter TATA box. *Toxicol. Appl. Pharmacol.* **256,** 52–61 (2011).

472. Liang, X., Xu, Y., Xu, K., Liu, J. & Qian, X. B1, a novel amonafide analogue, overcomes the resistance conferred by Bcl-2 in human promyelocytic leukemia HL60 cells. *Mol. Cancer Res.* **8,** 1619–1632 (2010).

473. Zhou, H. J., Wang, Z. & Li, A. Dihydroartemisinin induces apoptosis in human leukemia cells HL60 via downregulation of transferrin receptor expression. *Anticancer Drugs* **19,** 247–255 (2008).

474. Efferth, T. & Volm, M. Glutathione-related enzymes contribute to resistance of tumor cells

and low toxicity in normal organs to artesunate. *In Vivo* **19,** 225–32 (2005).

475. Braña, M. *et al.* Bis-naphthalimides. 2. Synthesis and biological activity of 5,6-acenaphthalimidoalkyl-1,8-naphthalimidoalkyl amines. *Eur. J. Med. Chem.* **30,** 235–239 (1995).

476. Banerjee, S. *et al.* Recent advances in the development of 1,8-naphthalimide based DNA targeting binders, anticancer and fluorescent cellular imaging agents. *Chem. Soc. Rev.* **42,** 1601 (2013).

477. Doyle, L. A. *et al.* A multidrug resistance transporter from human MCF-7 breast cancer cells. *Proc. Natl. Acad. Sci. U. S. A.* **95,** 15665–70 (1998).

478. A., C. *et al.* Phase II study of mitonafide in non-small cell lung cancer (NSCLC). *Investigational New Drugs* **14,** 415–417 (1996).

479. Gediya, L. K. & Njar, V. C. Promise and challenges in drug discovery and development of hybrid anticancer drugs. *Expert Opin. Drug Discov.* **4,** 1099–111 (2009).

480. Elledge, S. J. & Zhou, B.-B. S. The DNA damage response: putting checkpoints in perspective. *Nature* **408,** 433–439 (2000).

481. Lomax, M. E., Folkes, L. K. & O'Neill, P. Biological Consequences of Radiation-induced DNA Damage: Relevance to Radiotherapy. *Clin. Oncol.* **25,** 578–585 (2013).

482. de Gruijl, F. R., van Kranen, H. J. & Mullenders, L. H. . UV-induced DNA damage, repair, mutations and oncogenic pathways in skin cancer. *J. Photochem. Photobiol. B Biol.* **63,** 19–27 (2001).

483. Harper, J. W. & Elledge, S. J. The DNA damage response: ten years after. *Mol. Cell* **28,** 739–45 (2007).

484. Banin, S. *et al.* Enhanced phosphorylation of p53 by ATM in response to DNA damage. *Science* **281,** 1674–7 (1998).

485. Kannouche, P. L., Wing, J. & Lehmann, A. R. Interaction of Human DNA Polymerase η with Monoubiquitinated PCNA: A Possible Mechanism for the Polymerase Switch in Response to DNA Damage. *Mol. Cell* **14,** 491–500 (2004).

486. Kastan, M. B., Onyekwere, O., Sidransky, D., Vogelstein, B. & Craig, R. W. Participation of p53 Protein in the Cellular Response to DNA Damage1. *CANCER Res.* **5,** 6304–6311 (1991).

487. Roos, W. P. & Kaina, B. DNA damage-induced cell death by apoptosis. *Trends Mol. Med.* **12,** 440–450 (2006).

488. Maréchal, A. & Zou, L. DNA damage sensing by the ATM and ATR kinases. *Cold Spring Harb. Perspect. Biol.* **5,** 1–17 (2013).

489. Hirao, A. *et al.* DNA Damage-Induced Activation of p53 by the Checkpoint Kinase Chk2. *Science (80-.).* **287,** (2000).

490. Bartek, J. & Lukas, J. Chk1 and Chk2 kinases in checkpoint control and cancer. *Cancer Cell* **3,** 421–429 (2003).

491. Helleday, T., Petermann, E., Lundin, C., Hodgson, B. & Sharma, R. A. DNA repair pathways as targets for cancer therapy. *Nat. Rev. Cancer* **8,** 193–204 (2008).

492. Srivastava, D. K. *et al.* Mammalian Abasic Site Base Excision Repair: IDENTIFICATION OF THE REACTION SEQUENCE AND RATE-DETERMINING STEPS. *J. Biol. Chem.* **273,** 21203–21209 (1998).

493. Frosina, G. *et al.* Two pathways for base excision repair in mammalian cells. *J. Biol. Chem.* **271,** 9573–9578 (1996).

494. Selvakumaran, M., Pisarcik, D. a & Bao, R. Enhanced Cisplatin Cytotoxicity by Disturbing the Nucleotide Excision Repair Pathway in Ovarian Cancer Cell Lines. *Cancer Res.* **63,** 1311–1316 (2003).

495. Reardon, J. T. & Sancar, A. Nucleotide Excision Repair. *Prog. Nucleic Acid Res. Mol. Biol.* **79,** 183–235 (2005).

496. Sallmyr, A., Fan, J. & Rassool, F. V. Genomic instability in myeloid malignancies: Increased reactive oxygen species (ROS), DNA double strand breaks (DSBs) and error-prone repair. *Cancer Lett.* **270,** 1–9 (2008).

497. D'Amours, D., Desnoyers, S., D'Silva, I. & Poirier, G. G. Poly(ADP-ribosyl)ation reactions in the regulation of nuclear functions. *Biochem. J.* **342,** 249–268 (1999).

498. Lindahl, T., Satoh, M. S., Poirier, G. G. & Klungland, A. Post-translational modification of poly(ADP-ribose) polymerase induced by DNA strand breaks. *Trends Biochem. Sci.* **20,** 405–411 (1995).

499. Chalmers, A., Johnston, P., Woodcock, M., Joiner, M. & Marples, B. PARP-1, PARP-2, and the cellular response to low doses of ionizing radiation. *Int. J. Radiat. Oncol.* **58,** 410–419 (2004).

500. Huber, A., Bai, P., Murcia, J. M. de & Murcia, G. de. PARP-1, PARP-2 and ATM in the DNA damage response: functional synergy in mouse development. *DNA Repair (Amst).* **3,** 1103–1108 (2004).

501. Schreiber, V. *et al.* Poly(ADP-ribose) polymerase-2 (PARP-2) is required for efficient base

excision DNA repair in association with PARP-1 and XRCC1. *J. Biol. Chem.* **277,** 23028–36 (2002).

502. Skidmore, C. J. *et al.* The involvement of poly(ADP-ribose) polymerase in the degradation of NAD caused by γ-radiation and N-methyl-N-nitrosourea. *Eur. J. Biochem.* **101,** 135–142 (1979).

503. Juarez-Salinas, H., Sims, J. L. & Jacobson, M. K. Poly(ADP-ribose) levels in carcinogen-treated cells. *Nature* **282,** 740–741 (1979).

504. Moser, J. *et al.* Sealing of Chromosomal DNA Nicks during Nucleotide Excision Repair Requires XRCC1 and DNA Ligase IIIα in a Cell-Cycle-Specific Manner. *Mol. Cell* **27,** 311–323 (2007).

505. Lehmann, A. R. Nucleotide excision repair and the link with transcription. *Trends Biochem. Sci.* **20,** 402–405 (1995).

506. Audebert, M., Salles, B. & Calsou, P. *Effect of double-strand break DNA sequence on the PARP-1 NHEJ pathway*. *Biochemical and Biophysical Research Communications* **369,** (2008).

507. Satoh, M. S. & Lindahl, T. Role of poly(ADP-ribose) formation in DNA repair. *Nature* **356,** 356–358 (1992).

508. Amours, D. D., Desnoyers, S., Silva, I. D. & Poirier, G. G. Poly (ADP-ribosyl) ation reactions in the regulation of nuclear functions. *Biochem. J.* **268,** 249–268 (1999).

509. Schreiber, V. *et al.* Poly(ADP-ribose) Polymerase-2 (PARP-2) Is Required for Efficient Base Excision DNA Repair in Association with PARP-1 and XRCC1. *J. Biol. Chem.* **277,** 23028–23036 (2002).

510. Flohr, C., Bürkle, A., Radicella, J. P. & Epe, B. Poly(ADP-ribosyl)ation accelerates DNA repair in a pathway dependent on Cockayne syndrome B protein. *Nucleic Acids Res.* **31,** 5332–7 (2003).

511. de Murcia, J. M. *et al.* Requirement of poly(ADP-ribose) polymerase in recovery from DNA damage in mice and in cells. *Proc. Natl. Acad. Sci. U. S. A.* **94,** 7303–7 (1997).

512. Parker, R. J., Eastman, A., Bostick-Bruton, F. & Reed, E. Acquired cisplatin resistance in human ovarian cancer cells is associated with enhanced repair of cisplatin-DNA lesions and reduced drug accumulation. *J. Clin. Invest.* **87,** 772–7 (1991).

513. Yu, S.-W. *et al.* Apoptosis-inducing factor mediates poly(ADP-ribose) (PAR) polymer-induced cell death. *Proc. Natl. Acad. Sci. U. S. A.* **103,** 18314–9 (2006).

514. Curtin, N. J. in *Poly (ADP-Ribosyl) ation* 218–233 (Springer US, 2006).

515. Tentori, L. Chemopotentiation by PARP inhibitors in cancer therapy. *Pharmacol. Res.* **52,** 25–33 (2005).

516. Xie, S. Q. *et al.* 3-Nitro-naphthalimide and nitrogen mustard conjugate NNM-25 induces hepatocellular carcinoma apoptosis via PARP-1/p53 pathway. *Apoptosis* **17,** 725–734 (2012).

517. Fr??hlich, T. *et al.* Synthesis of Novel Hybrids of Thymoquinone and Artemisinin with High Activity and Selectivity Against Colon Cancer. *ChemMedChem* **12,** 226–234 (2017).

518. van Gent, D. C., Hoeijmakers, J. H. & Kanaar, R. Chromosomal stability and the DNA double-stranded break connection. *Nat. Rev. Genet.* **2,** 196–206 (2001).

519. Khanna, K. K. & Jackson, S. P. DNA double-strand breaks: signaling, repair and the cancer connection. *Nat. Genet.* **27,** 247–54 (2001).

520. Kasparek, T. R. & Humphrey, T. C. DNA double-strand break repair pathways, chromosomal rearrangements and cancer. *Semin. Cell Dev. Biol.* **22,** 886–897 (2011).

521. Lieber, M. R. NHEJ and its backup pathways in chromosomal translocations. *Nat. Struct. Mol. Biol.* **17,** 393–395 (2010).

522. Mari, P.-O. *et al.* Dynamic assembly of end-joining complexes requires interaction between Ku70/80 and XRCC4. *Proc. Natl. Acad. Sci. U. S. A.* **103,** 18597–602 (2006).

523. Uematsu, N. *et al.* Autophosphorylation of DNA-PK $_{CS}$ regulates its dynamics at DNA double-strand breaks. *J. Cell Biol.* **177,** 219–229 (2007).

524. Walker, J. R., Corpina, R. A. & Goldberg, J. Structure of the Ku heterodimer bound to DNA and its implications for double-strand break repair. *Nature* **412,** 607–614 (2001).

525. Doherty, A. J. & Jackson, S. P. DNA repair: How Ku makes ends meet. *Curr. Biol.* **11,** R920–R924 (2001).

526. Zhang, Z. *et al.* The three-dimensional structure of the C-terminal DNA-binding domain of human Ku70. *J. Biol. Chem.* **276,** 38231–6 (2001).

527. Downs, J. A. & Jackson, S. P. A means to a DNA end: the many roles of Ku. *Nat. Rev. Mol. Cell Biol.* **5,** 367–378 (2004).

528. Zhang, Z. *et al.* Solution Structure of the C-Terminal Domain of Ku80 Suggests Important Sites for Protein-Protein Interactions. *Structure* **12,** 495–502 (2004).

529. Downs, J. A. & Jackson, S. P. A means to a DNA end: the many roles of Ku. *Nat. Rev. Mol. Cell Biol.* **5,** 367–378 (2004).

530. Blier, P. R., Griffith, A. J., Craft, J. & Hardin, J. A. Binding of Ku protein to DNA.

Measurement of affinity for ends and demonstration of binding to nicks. *J. Biol. Chem.* **268,** 7594–601 (1993).

531. Carr, A. M. & Hoekstra, M. F. The cellular responses to DNA damage. *Trends Cell Biol.* **5,** 32–40 (1995).

532. Junop, M. S. *et al.* Crystal structure of the Xrcc4 DNA repair protein and implications for end joining. *EMBO J.* **19,** 5962–70 (2000).

533. Costantini, S., Woodbine, L., Andreoli, L., Jeggo, P. A. & Vindigni, A. Interaction of the Ku heterodimer with the DNA ligase IV/Xrcc4 complex and its regulation by DNA-PK. *DNA Repair (Amst).* **6,** 712–722 (2007).

534. Nick McElhinny, S. A., Snowden, C. M., McCarville, J. & Ramsden, D. A. Ku recruits the XRCC4-ligase IV complex to DNA ends. *Mol. Cell. Biol.* **20,** 2996–3003 (2000).

535. Yano, K. *et al.* Ku recruits XLF to DNA double-strand breaks. *EMBO Rep.* **9,** 91–6 (2008).

536. Gu, J. *et al.* XRCC4:DNA ligase IV can ligate incompatible DNA ends and can ligate across gaps. *EMBO J.* **26,** 1010–23 (2007).

537. Fell, V. L. & Schild-Poulter, C. Ku regulates signaling to DNA damage response pathways through the Ku70 von Willebrand A domain. *Mol. Cell. Biol.* **32,** 76–87 (2012).

538. Ellenberger, T. & Tomkinson, A. E. Eukaryotic DNA ligases: structural and functional insights. *Annu. Rev. Biochem.* **77,** 313–38 (2008).

539. Ma, Y. *et al.* A Biochemically Defined System for Mammalian Nonhomologous DNA End Joining. *Mol. Cell* **16,** 701–713 (2004).

540. Callebaut, I. *et al.* Cernunnos Interacts with the XRCC4{middle dot}DNA-ligase IV Complex and Is Homologous to the Yeast Nonhomologous End-joining Factor Nej1. *J. Biol. Chem.* **281,** 13857–13860 (2006).

541. Ropars, V. *et al.* Structural characterization of filaments formed by human Xrcc4-Cernunnos/XLF complex involved in nonhomologous DNA end-joining. *Proc. Natl. Acad. Sci. U. S. A.* **108,** 12663–8 (2011).

542. Andres, S. N., Modesti, M., Tsai, C. J., Chu, G. & Junop, M. S. Crystal Structure of Human XLF: A Twist in Nonhomologous DNA End-Joining. *Mol. Cell* **28,** 1093–1101 (2007).

543. Riballo, E. *et al.* XLF-Cernunnos promotes DNA ligase IV-XRCC4 re-adenylation following ligation. *Nucleic Acids Res.* **37,** 482–92 (2009).

544. Tsai, C. J., Kim, S. A. & Chu, G. Cernunnos/XLF promotes the ligation of mismatched and noncohesive DNA ends. *Proc. Natl. Acad. Sci. U. S. A.* **104,** 7851–6 (2007).

545. Gu, J., Lu, H., Tsai, A. G., Schwarz, K. & Lieber, M. R. Single-stranded DNA ligation and XLF-stimulated incompatible DNA end ligation by the XRCC4-DNA ligase IV complex: influence of terminal DNA sequence. *Nucleic Acids Res.* **35,** 5755–62 (2007).

546. Kroemer, G. *et al.* Classification of cell death: recommendations of the Nomenclature Committee on Cell Death. *Cell Death Differ.* **12,** 1463–1467 (2005).

547. Galluzzi, L. *et al.* Molecular definitions of cell death subroutines: recommendations of the Nomenclature Committee on Cell Death 2012. *Cell Death Differ.* **19,** 107–20 (2012).

548. Galluzzi, L. *et al.* Molecular definitions of cell death subroutines: recommendations of the Nomenclature Committee on Cell Death 2012. *Cell Death Differ.* **19,** 107–120 (2012).

549. Kroemer, G. *et al.* Classification of cell death: recommendations of the Nomenclature Committee on Cell Death. *Cell Death Differ.* **12,** 1463–1467 (2005).

550. Golstein, P. & Kroemer, G. Cell death by necrosis: towards a molecular definition. *Trends in Biochemical Sciences* **32,** 37–43 (2007).

551. Festjens, N., Vanden Berghe, T. & Vandenabeele, P. Necrosis, a well-orchestrated form of cell demise: Signalling cascades, important mediators and concomitant immune response. *Biochim. Biophys. Acta - Bioenerg.* **1757,** 1371–1387 (2006).

552. Kerr, J. F., Wyllie, A. H. & Currie, A. R. Apoptosis: a basic biological phenomenon with wide-ranging implications in tissue kinetics. *Br. J. Cancer* **26,** 239–57 (1972).

553. Taylor, R. C., Cullen, S. P. & Martin, S. J. Apoptosis: controlled demolition at the cellular level. *Nat. Rev. Mol. Cell Biol.* **9,** 231–241 (2008).

554. Wang, C. & Youle, R. J. The role of mitochondria in apoptosis*. *Annu. Rev. Genet.* **43,** 95–118 (2009).

555. Clarke, P. G. H. in *Cell Death and Diseases of the Nervous System* 3–28 (Humana Press, 1999).

556. Elmore, S. Apoptosis: A Review of Programmed Cell Death. *Toxicol. Pathol.* **35,** 495–516 (2007).

557. Riedl, S. J. & Shi, Y. Molecular mechanisms of caspase regulation during apoptosis. *Nat. Rev. Mol. Cell Biol.* **5,** 897–907 (2004).

558. McIlwain, D. R., Berger, T. & Mak, T. W. Caspase functions in cell death and disease. *Cold Spring Harb. Perspect. Biol.* **5,** a008656 (2013).

559. Wang, S. & El-Deiry, W. S. TRAIL and apoptosis induction by TNF-family death receptors. *Oncogene* **22,** 8628–8633 (2003).

560. Bachmeier, B. E. *et al.* Analysis of tissue distribution of TNF-??, TNF-??-receptors, and the activating TNF-??-converting enzyme suggests activation of the TNF-?? system in the aging intervertebral disc. *Ann. N. Y. Acad. Sci.* **1096,** 44–54 (2007).

561. Amewu, R. K. *et al.* Synthesis and evaluation of the antimalarial, anticancer, and caspase 3 activities of tetraoxane dimers. *Bioorganic Med. Chem.* **21,** 7392–7397 (2013).

562. van Horssen, R., Ten Hagen, T. L. M. & Eggermont, A. M. M. TNF-alpha in cancer treatment: molecular insights, antitumor effects, and clinical utility. *Oncologist* **11,** 397–408 (2006).

563. Holler, N. *et al.* Fas triggers an alternative, caspase-8|[ndash]|independent cell death pathway using the kinase RIP as effector molecule. *Nat. Immunol.* **1,** 489–495 (2000).

564. Guicciardi, M. E. & Gores, G. J. Life and death by death receptors. *FASEB J.* **23,** 1625–37 (2009).

565. Bergeron, A., Geanta, P. & Bergeron, D. The Death Factors: A Combinatorial Analysis. *In Silico Biol.* **1,** 147–158 (1999).

566. Hsu, H., Shu, H.-B., Pan, M.-G. & Goeddel, D. V. TRADD–TRAF2 and TRADD–FADD Interactions Define Two Distinct TNF Receptor 1 Signal Transduction Pathways. *Cell* **84,** 299–308 (1996).

567. Scheel-Toellner, D. *et al.* The death-inducing signalling complex is recruited to lipid rafts in Fas-induced apoptosis. *Biochem. Biophys. Res. Commun.* **297,** 876–879 (2002).

568. Kataoka, T. *et al.* FLIP prevents apoptosis induced by death receptors but not by perforin/granzyme B, chemotherapeutic drugs, and gamma irradiation. *J. Immunol.* **161,** 3936–42 (1998).

569. Scaffidi, G. *et al.* Differential modulation of apoptosis sensitivity in CD95 type I and type II cells. *J. Biol. Chem.* **274,** 22532–22538 (1999).

570. Dharmadhikari, G. *et al.* TOSO promotes β-cell proliferation and protects from apoptosis. *Mol. Metab.* **1,** 70–8 (2012).

571. Safa, A. R. c-FLIP, a master anti-apoptotic regulator. *Exp. Oncol.* **34,** 176–84 (2012).

572. Li, H., Zhu, H., Xu, C. & Yuan, J. Cleavage of BID by Caspase 8 Mediates the Mitochondrial Damage in the Fas Pathway of Apoptosis. *Cell* **94,** 491–501 (1998).

573. Jänicke, R. U., Sprengart, M. L., Wati, M. R. & Porter, A. G. Caspase-3 is required for DNA fragmentation and morphological changes associated with apoptosis. *J. Biol. Chem.* **273,** 9357–60 (1998).

574. Porter, A. G. & Jänicke, R. U. Emerging roles of caspase-3 in apoptosis. *Cell Death Differ.* **6,** 99–104 (1999).

575. Elmore, S. Apoptosis: a review of programmed cell death. *Toxicol. Pathol.* **35,** 495–516 (2007).

576. Green, D. R. & Reed, J. C. Mitochondria and apoptosis. *Science* **281,** 1309–12 (1998).

577. Srinivasula, S. M. *et al.* A conserved XIAP-interaction motif in caspase-9 and Smac/DIABLO regulates caspase activity and apoptosis. *Nature* **410,** 112–116 (2001).

578. Zou, H., Li, Y., Liu, X. & Wang, X. An APAF-1.cytochrome c multimeric complex is a functional apoptosome that activates procaspase-9. *J. Biol. Chem.* **274,** 11549–56 (1999).

579. Daugas, E. *et al.* Apoptosis-inducing factor (AIF): a ubiquitous mitochondrial oxidoreductase involved in apoptosis. *FEBS Lett.* **476,** 118–123 (2000).

580. Susin, S. A. *et al.* Two Distinct Pathways Leading to Nuclear Apoptosis. *J. Exp. Med.* **192,** (2000).

581. Li, L. Y., Luo, X. & Wang, X. Endonuclease G is an apoptotic DNase when released from mitochondria. *Nature* **412,** 95–99 (2001).

582. Walensky, L. D. BCL-2 in the crosshairs: tipping the balance of life and death. *Cell Death Differ.* **13,** 1339–50 (2006).

583. Westphal, D., Dewson, G., Czabotar, P. E. & Kluck, R. M. Molecular biology of Bax and Bak activation and action. *Biochim. Biophys. Acta - Mol. Cell Res.* **1813,** 521–531 (2011).

584. Hardwick, J. M. & Soane, L. Multiple functions of BCL-2 family proteins. *Cold Spring Harb. Perspect. Biol.* **5,** (2013).

585. Yang, E. *et al.* Bad, a heterodimeric partner for Bcl-xL and Bcl-2, displaces bax and promotes cell death. *Cell* **80,** 285–291 (1995).

586. Adams, J. M. The Bcl-2 Protein Family: Arbiters of Cell Survival. *Science (80-.).* **281,** 1322–1326 (1998).

587. Arnoult, D. *et al.* Mitochondrial release of apoptosis-inducing factor occurs downstream of cytochrome c release in response to several proapoptotic stimuli. *J. Cell Biol.* **159,** 923–9 (2002).

588. Lin, B. *et al.* 7-b, a novel amonafide analogue, cause growth inhibition and apoptosis in Raji cells via a ROS-mediated mitochondrial pathway. *Leuk. Res.* **35,** 646–56 (2011).

589. Favaloro, B., Allocati, N., Graziano, V., Di Ilio, C. & De Laurenzi, V. Role of apoptosis in disease. *Aging (Albany. NY).* **4,** 330–49 (2012).

590. Brunner, T. *et al.* Fas (CD95/Apo-1) ligand regulation in T cell homeostasis, cell-mediated cytotoxicity and immune pathology. *Semin. Immunol.* **15,** 167–176 (2003).

591. Kam, C. M., Hudig, D. & Powers, J. C. Granzymes (lymphocyte serine proteases): Characterization with natural and synthetic substrates and inhibitors. *Biochim. Biophys. Acta - Protein Struct. Mol. Enzymol.* **1477,** 307–323 (2000).

592. Trapani, J. A. & Smyth, M. J. Functional significance of the perforin/granzyme cell death pathway. *Nat. Rev. Immunol.* **2,** 735–747 (2002).

593. Nagata, S. *et al.* A caspase-activated DNase that degrades DNA during apoptosis, and itsinhibitor ICAD. *Nature* **391,** 43–50 (1998).

594. Barry, M. & Bleackley, R. C. Cytotoxic T lymphocytes: all roads lead to death. *Nat. Rev. Immunol.* **2,** 401–9 (2002).

595. Liou, G.-Y. & Storz, P. Reactive oxygen species in cancer. *Free Radic. Res.* **44,** 479–96 (2010).

596. Murphy, M. P. How mitochondria produce reactive oxygen species. *Biochem. J.* **417,** 1–13 (2009).

597. Sarsour, E. H., Venkataraman, S., Kalen, A. L., Oberley, L. W. & Goswami, P. C. Manganese superoxide dismutase activity regulates transitions between quiescent and proliferative growth. *Aging Cell* **7,** 405–17 (2008).

598. Trachootham, D., Lu, W., Ogasawara, M. A., Nilsa, R.-D. V. & Huang, P. Redox regulation of cell survival. *Antioxid. Redox Signal.* **10,** 1343–74 (2008).

599. Wu, W.-S. The signaling mechanism of ROS in tumor progression. *Cancer Metastasis Rev.* **25,** 695–705 (2006).

600. Wang, M. *et al.* Manganese superoxide dismutase suppresses hypoxic induction of hypoxia-inducible factor-1alpha and vascular endothelial growth factor. *Oncogene* **24,** 8154–66 (2005).

601. Fulda, S. & Debatin, K.-M. Extrinsic versus intrinsic apoptosis pathways in anticancer chemotherapy. *Oncogene* **25,** 4798–811 (2006).

602. Chung, Y. M., Bae, Y. S. & Lee, S. Y. Molecular ordering of ROS production, mitochondrial changes, and caspase activation during sodium salicylate-induced apoptosis. *Free Radic. Biol. Med.* **34,** 434–442 (2003).

603. Cadenas, E. Mitochondrial free radical production and cell signaling. *Mol. Aspects Med.* **25,** 17–26 (2004).

604. Papadakis, E. S. *et al.* The regulation of Bax by c-Jun N-terminal protein kinase (JNK) is a prerequisite to the mitochondrial-induced apoptotic pathway. *FEBS Lett.* **580,** 1320–6 (2006).

605. Pan, J. *et al.* Reactive oxygen species-activated Akt/ASK1/p38 signaling pathway in nickel compound-induced apoptosis in BEAS 2B cells. *Chem. Res. Toxicol.* **23,** 568–77 (2010).

606. Weitzman, S., Weitberg, A., Clark, E. & Stossel, T. Phagocytes as carcinogens: malignant transformation produced by human neutrophils. *Science (80-.).* **227,** 1231–1233 (1985).

607. Zimmerman, R. & Cerutti, P. Active oxygen acts as a promoter of transformation in mouse embryo C3H/10T1/2/C18 fibroblasts. *Proc. Natl. Acad. Sci.* **81,** 2085–2087 (1984).

608. Nishikawa, M. Reactive oxygen species in tumor metastasis. *Cancer Lett.* **266,** 53–59 (2008).

609. Szatrowski, T. P. & Nathan, C. F. Production of Large Amounts of Hydrogen Peroxide by Human Tumor Cells. *Cancer Res.* **51,** 794–798 (1991).

610. Kawanishi, S., Hiraku, Y., Pinlaor, S. & Ma, N. Oxidative and nitrative DNA damage in animals and patients with inflammatory diseases in relation to inflammation-related carcinogenesis. *Biol. Chem.* **387,** 365–72 (2006).

611. Toyokuni, S., Okamoto, K., Yodoi, J. & Hiai, H. Persistent oxidative stress in cancer. *FEBS Lett.* **358,** 1–3 (1995).

612. Storz, P. Reactive oxygen species-mediated mitochondria-to-nucleus signaling: a key to aging and radical-caused diseases. *Sci. STKE* **2006,** re3 (2006).

613. Wu, L. L., Chiou, C.-C., Chang, P.-Y. & Wu, J. T. Urinary 8-OHdG: a marker of oxidative stress to DNA and a risk factor for cancer, atherosclerosis and diabetics. *Clin. Chim. Acta* **339,** 1–9 (2004).

614. Compton, S. *et al.* Mitochondrial dysfunction impairs tumor suppressor p53 expression/function. *J. Biol. Chem.* **286,** 20297–312 (2011).

615. Pelicano, H., Carney, D. & Huang, P. ROS stress in cancer cells and therapeutic implications. *Drug Resist. Updat.* **7,** 97–110 (2004).

616. Brandes, N., Schmitt, S. & Jakob, U. Thiol-based redox switches in eukaryotic proteins. *Antioxid. Redox Signal.* **11,** 997–1014 (2009).

617. Liu, B., Chen, Y. & St Clair, D. K. ROS and p53: a versatile partnership. *Free Radic. Biol. Med.* **44,** 1529–35 (2008).

618. Morgan, M. J. & Liu, Z. Crosstalk of reactive oxygen species and NF-κB signaling. *Cell*

Res. **21,** 103–15 (2011).

619. Okoh, V. O., Felty, Q., Parkash, J., Poppiti, R. & Roy, D. Reactive oxygen species via redox signaling to PI3K/AKT pathway contribute to the malignant growth of 4-hydroxy estradiol-transformed mammary epithelial cells. *PLoS One* **8,** e54206 (2013).

620. Trachootham, D., Alexandre, J. & Huang, P. Targeting cancer cells by ROS-mediated mechanisms: a radical therapeutic approach? *Nat. Rev. Drug Discov.* **8,** 579–591 (2009).

621. Gao, N., Rahmani, M., Dent, P. & Grant, S. 2-Methoxyestradiol-induced apoptosis in human leukemia cells proceeds through a reactive oxygen species and Akt-dependent process. *Oncogene* **24,** 3797–809 (2005).

622. Trachootham, D. *et al.* Selective killing of oncogenically transformed cells through a ROS-mediated mechanism by β-phenylethyl isothiocyanate. *Cancer Cell* **10,** 241–252 (2006).

623. Matsumura, Y. & Maeda, H. A new concept for macromolecular therapeutics in cancer chemotherapy: mechanism of tumoritropic accumulation of proteins and the antitumor agent smancs. *Cancer Res.* **46,** 6387–92 (1986).

624. Fang, J., Seki, T. & Maeda, H. Therapeutic strategies by modulating oxygen stress in cancer and inflammation. *Adv. Drug Deliv. Rev.* **61,** 290–302 (2009).

625. Dickinson, D. a. & Forman, H. J. Cellular glutathione and thiols metabolism. *Biochem. Pharmacol.* **64,** 1019–1026 (2002).

626. Lu, S. C. Regulation of glutathione synthesis. *Mol. Aspects Med.* **30,** 42–59 (2011).

627. Pompella, A., Visvikis, A., Paolicchi, A., Tata, V. De & Casini, A. F. The changing faces of glutathione, a cellular protagonist. *Biochem. Pharmacol.* **66,** 1499–1503 (2003).

628. Townsend, D. M., Tew, K. D. & Tapiero, H. The importance of glutathione in human disease. *Biomed. Pharmacother.* **57,** 145–155 (2003).

629. Stipanuk, M. H., Dominy, J. E. . J., Lee, J.-I. & Coloso, R. M. Mammalian Cysteine Metabolism: New Insights into Regulation of Cysteine Metabolism. *J. Nutr.* **136,** 1652S–1659 (2006).

630. Mihm, S., Galter, D. & Droge, W. Modulation of transcription factor NF kappa B activity by intracellular glutathione levels and by variations of the extracellular cysteine supply. *FASEB J* **9,** 246–252 (1995).

631. Akamatsu, Y. Redox Regulation of the DNA Binding Activity in Transcription Factor PEBP2. THE ROLES OF TWO CONSERVED CYSTEINE RESIDUES. *J. Biol. Chem.* **272,** 14497–14500 (1997).

632. Griffith, O. W. Biologic and pharmacologic regulation of mammalian glutathione synthesis. *Free Radic. Biol. Med.* **27,** 922–935 (1999).

633. Griffith, O. W. & Meister, A. Origin and turnover of mitochondrial glutathione. *Proc. Natl. Acad. Sci. U. S. A.* **82,** 4668–72 (1985).

634. Kryston, T. B., Georgiev, A. B., Pissis, P. & Georgakilas, A. G. Role of oxidative stress and DNA damage in human carcinogenesis. *Mutat. Res.* **711,** 193–201 (2011).

635. Guilford, F. T. & Hope, J. Deficient glutathione in the pathophysiology of mycotoxin-related illness. *Toxins (Basel).* **6,** 608–23 (2014).

636. Chai, Y. C., Ashraf, S. S., Rokutan, K., Johnston, R. B. & Thomas, J. A. S-thiolation of individual human neutrophil proteins including actin by stimulation of the respiratory burst: evidence against a role for glutathione disulfide. *Arch. Biochem. Biophys.* **310,** 273–81 (1994).

637. Saydam, N. *et al.* Determination of glutathione, glutathione reductase, glutathione peroxidase and glutathione S-transferase levels in human lung cancer tissues. *Cancer Lett.* **119,** 13–19 (1997).

638. Harvey, C. J. *et al.* Nrf2-regulated glutathione recycling independent of biosynthesis is critical for cell survival during oxidative stress. *Free Radic. Biol. Med.* **46,** 443–53 (2009).

639. Yang, M. S., Chan, H. W. & Yu, L. C. Glutathione peroxidase and glutathione reductase activities are partially responsible for determining the susceptibility of cells to oxidative stress. *Toxicology* **226,** 126–30 (2006).

640. Utomo, A. *et al.* Identification of a Novel Putative Non-selenocysteine Containing Phospholipid Hydroperoxide Glutathione Peroxidase (NPGPx) Essential for Alleviating Oxidative Stress Generated from Polyunsaturated Fatty Acids in Breast Cancer Cells. *J. Biol. Chem.* **279,** 43522–43529 (2004).

641. Cheng, W.-H. *et al.* Cellular Glutathione Peroxidase Is the Mediator of Body Selenium To Protect against Paraquat Lethality in Transgenic Mice. *J. Nutr.* **128,** 1070–1076 (1998).

642. Weisbrot-Lefkowitz, M. *et al.* Overexpression of human glutathione peroxidase protects transgenic mice against focal cerebral ischemia/reperfusion damage. *Mol. Brain Res.* **53,** 333–338 (1998).

643. Fu, Y., Cheng, W.-H., Porres, J. M., Ross, D. A. & Lei, X. G. Knockout of cellular glutathione peroxidase gene renders mice susceptible to diquat-induced oxidative stress. *Free Radic. Biol. Med.* **27,** 605–611 (1999).

644. Sengupta, R. & Holmgren, A. Thioredoxin and glutaredoxin-mediated redox regulation of

ribonucleotide reductase. *World J. Biol. Chem.* **5,** 68–74 (2014).

645. Elledge, S. J., Zhou, Z. & Allen, J. B. Ribonucleotide reductase: regulation, regulation, regulation. *Trends Biochem. Sci.* **17,** 119–123 (1992).

646. Carretero, J. *et al.* Growth-associated changes in glutathione content correlate with liver metastatic activity of B16 melanoma cells. *Clin. Exp. Metastasis* **17,** 567–74 (1999).

647. Carretero, J. *et al.* Growth-associated changes in glutathione content correlate with liver metastatic activity of B16 melanoma cells. *Clin. Exp. Metastasis* **17,** 567–574

648. Hanigan, M. H. & Pitot, H. C. Gamma-glutamyl transpeptidase--its role in hepatocarcinogenesis. *Carcinogenesis* **6,** 165–72 (1985).

649. Kalengayi, M. M. R., Ronchi, G. & Desmet, V. J. Histochemistry of Gamma-Glutamyl Transpeptidase in Rat Liver During Aflatoxin B1-Induced Carcinogenesis. *J Natl Cancer Inst* **55,** 579–588 (1975).

650. Hanigan, M. H., Frierson, H. F. . J., Brown, J. E., Lovell, M. A. & Taylor, P. T. Human Ovarian Tumors Express {gamma}-Glutamyl Transpeptidase. *Cancer Res.* **54,** 286–290 (1994).

651. Fiala, S., Fiala, A. E., Keller, R. W. & Fiala, E. S. Gamma glutamyl transpeptidase in colon cancer induced by 1,2-dimethylhydrazine. *Arch. für Geschwulstforsch.* **47,** 117–22 (1977).

652. Prezioso, J. A., Wang, N., Duty, L., Bloomer, W. D. & Gorelik, E. Enhancement of pulmonary metastasis formation and ?-glutamyltranspeptidase activity in B16 melanoma induced by differentiation in vitro. *Clin. Exp. Metastasis* **11,** 263–274 (1993).

653. Bard, S., Noël, P., Chauvin, F. & Quash, G. gamma-Glutamyltranspeptidase activity in human breast lesions: an unfavourable prognostic sign. *Br. J. Cancer* **53,** 637–42 (1986).

654. Meister, A. Glutathione deficiency produced by inhibition of its synthesis, and its reversal; applications in research and therapy. *Pharmacol. Ther.* **51,** 155–94 (1991).

655. Bailey, H. H. l-S,R-buthionine sulfoximine: historical development and clinical issues. *Chem. Biol. Interact.* **111–112,** 239–254 (1998).

656. Maeda, H. *et al.* Effective treatment of advanced solid tumors by the combination of arsenic trioxide and L-buthionine-sulfoximine. *Cell Death Differ.* **11,** 737–46 (2004).

657. Anderson, C. P. & Reynolds, C. P. Synergistic cytotoxicity of buthionine sulfoximine (BSO) and intensive melphalan (L-PAM) for neuroblastoma cell lines established at relapse after myeloablative therapy. *Bone Marrow Transplant.* **30,** 135–40 (2002).

658. Bailey, H. H. *et al.* Phase I study of continuous-infusion L-S,R-buthionine sulfoximine with

intravenous melphalan. *J. Natl. Cancer Inst.* **89,** 1789–1796 (1997).

659. O'Dwyer, P. J. *et al.* Phase I trial of buthionine sulfoximine in combination with melphalan in patients with cancer. *J. Clin. Oncol.* **14,** 249–256 (1996).

660. Anderson, C. P. *et al.* Pilot study of intravenous melphalan combined with continuous infusion L-S,R-buthionine sulfoximine for children with recurrent neuroblastoma. *Pediatr. Blood Cancer* **62,** 1739–46 (2015).

661. Ongaro, A. *et al.* Enhancement of melphalan activity by buthionine sulfoximine and electroporation in melanoma cells. *Anticancer. Drugs* **26,** 284–92 (2015).

662. Lewis-Wambi, J. S. *et al.* Buthionine sulfoximine sensitizes antihormone-resistant human breast cancer cells to estrogen-induced apoptosis. *Breast cancer research : BCR* **10,** R104 (2008).

663. Reliene, R. & Schiestl, R. H. Glutathione depletion by buthionine sulfoximine induces DNA deletions in mice. *Carcinogenesis* **27,** 240–4 (2006).

664. Wu, X. X., Ogawa, O. & Kakehi, Y. Enhancement of arsenic trioxide-induced apoptosis in renal cell carcinoma cells by L-buthionine sulfoximine. *Int. J. Oncol.* **24,** 1489–1497 (2004).

665. Chen, D., Chan, R., Waxman, S. & Jing, Y. Buthionine sulfoximine enhancement of arsenic trioxide-induced apoptosis in leukemia and lymphoma cells is mediated via activation of c-Jun NH2-terminal kinase and up-regulation of death receptors. *Cancer Res.* **66,** 11416–23 (2006).

666. Hernández-Breijo, B. *et al.* Preclinical evaluation of azathioprine plus buthionine sulfoximine in the treatment of human hepatocarcinoma and colon carcinoma. *World J. Gastroenterol.* **17,** 3899–911 (2011).

667. Chowdhury, A. A. *et al.* Synergistic apoptosis of CML cells by buthionine sulfoximine and hydroxychavicol correlates with activation of AIF and GSH-ROS-JNK-ERK-iNOS pathway. *PLoS One* **8,** e73672 (2013).

668. Hamilton, D., Wu, J. H. & Batist, G. Structure-based identification of novel human gamma-glutamylcysteine synthetase inhibitors. *Mol. Pharmacol.* **71,** 1140–7 (2007).

669. Bailey, H. *et al.* Phase I clinical trial of intravenous L-buthionine sulfoximine and melphalan: an attempt at modulation of glutathione. *J. Clin. Oncol.* **12,** 194–205 (1994).

670. Kunze, T. & Heps, S. Phosphono analogs of glutathione: inhibition of glutathione transferases, metabolic stability, and uptake by cancer cells. *Biochem. Pharmacol.* **59,** 973–981 (2000).

671. Tew, K. D. TLK-286: a novel glutathione S-transferase-activated prodrug. *Expert Opin.*

Investig. Drugs (2005).

672. Dourado, D. F. A. R., Fernandes, P. A., Ramos, M. J. & Mannervik, B. Mechanism of Glutathione Transferase P1-1-Catalyzed Activation of the Prodrug Canfosfamide (TLK286, TELCYTA). *Biochemistry* **52,** 8069–8078 (2013).

673. Yao, K.-S. *et al.* Evidence for Altered Regulation of {gamma}-Glutamylcysteine Synthetase Gene Expression among Cisplatin-sensitive and Cisplatin-resistant Human Ovarian Cancer Cell Lines. *Cancer Res.* **55,** 4367–4374 (1995).

674. Godwin, A. K. *et al.* High resistance to cisplatin in human ovarian cancer cell lines is associated with marked increase of glutathione synthesis. *Proc. Natl. Acad. Sci. U. S. A.* **89,** 3070–4 (1992).

675. Oguri, T. *et al.* Expression of gamma-glutamylcysteine synthetase (gamma-GCS) and multidrug resistance-associated protein (MRP), but not human canalicular multispecific organic anion transporter (cMOAT), genes correlates with exposure of human lung cancers to platinum drug. *Br. J. Cancer* **77,** 1089–96 (1998).

676. Jefferies, H. *et al.* Glutathione. *ANZ J. Surg.* **73,** 517–22 (2003).

677. Allen, T. C. *et al.* Expression of glutathione S-transferase pi and glutathione synthase correlates with survival in early stage non-small cell carcinomas of the lung. *Hum. Pathol.* **38,** 220–227 (2007).

678. Hanigan, M. H. gamma-glutamyl transpeptidase accelerates tumor growth and increases the resistance of tumors to cisplatin in vivo. *Carcinogenesis* **20,** 553–559 (1999).

679. Ishikawa, T. *et al.* Coordinated induction of MRP/GS-X pump and gamma-glutamylcysteine synthetase by heavy metals in human leukemia cells. *J. Biol. Chem.* **271,** 14981–8 (1996).

680. Gomi, A., Shinoda, S., Masuzawa, T., Ishikawa, T. & Kuo, M. T. Transient induction of the MRP/GS-X pump and gamma-glutamylcysteine synthetase by 1-(4-amino-2-methyl-5-pyrimidinyl)methyl-3-(2-chloroethyl)-3- nitrosourea in human glioma cells. *Cancer Res.* **57,** 5292–9 (1997).

681. Kuo, M. T. *et al.* Frequent coexpression of MRP/GS-X pump and gamma-glutamylcysteine synthetase mRNA in drug-resistant cells, untreated tumor cells, and normal mouse tissues. *Biochem. Pharmacol.* **55,** 605–15 (1998).

682. Benlloch, M. *et al.* Acceleration of glutathione efflux and inhibition of gamma-glutamyltranspeptidase sensitize metastatic B16 melanoma cells to endothelium-induced cytotoxicity. *J. Biol. Chem.* **280,** 6950–9 (2005).

683. Schmittgen, T. D. & Livak, K. J. Analyzing real-time PCR data by the comparative CT method. *Nat. Protoc.* **3,** 1101–1108 (2008).

684. Pfaffl, M. W. A new mathematical model for relative quantification in real-time RT-PCR. *Nucleic Acids Res.* **29,** e45 (2001).

685. Dowling, C. M., Walsh, D., Coffey, J. C. & Kiely, P. A. The importance of selecting the appropriate reference genes for quantitative real time PCR as illustrated using colon cancer cells and tissue. *F1000Research* **5,** 99 (2016).

686. Sashidhara, K. V, Avula, S. R., Sharma, K., Palnati, G. R. & Bathula, S. R. Discovery of coumarin-monastrol hybrid as potential antibreast tumor-specific agent. *Eur. J. Med. Chem.* **60,** 120–7 (2013).

687. Vazquez-Rodriguez, S. *et al.* Design, synthesis and antibacterial study of new potent and selective coumarin-chalcone derivatives for the treatment of tenacibaculosis. *Bioorg. Med. Chem.* **23,** 7045–7052 (2015).

688. Ogunrinu, T. A. & Sontheimer, H. Hypoxia increases the dependence of glioma cells on glutathione. *J. Biol. Chem.* **285,** 37716–24 (2010).

689. Guzy, R. D. *et al.* Mitochondrial complex III is required for hypoxia-induced ROS production and cellular oxygen sensing. *Cell Metab.* **1,** 401–408 (2005).

690. Shen, K. *et al.* A ROS-mediated lysosomal-mitochondrial pathway is induced by a novel Amonafide analogue, 7c, in human Hela cervix carcinoma cells. *Cancer Lett.* **333,** 229–38 (2013).

691. Tsujimoto, Y., Gorham, J., Cossman, J., Jaffe, E. & Croce, C. M. The t(14;18) chromosome translocations involved in B-cell neoplasms result from mistakes in VDJ joining. *Science* **229,** 1390–3 (1985).

692. Bakhshi, A. *et al.* Cloning the chromosomal breakpoint of t(14;18) human lymphomas: clustering around JH on chromosome 14 and near a transcriptional unit on 18. *Cell* **41,** 899–906 (1985).

693. Ren, G., Zhao, Y., Yang, L. & Fu, C.-X. Anti-proliferative effect of clitocine from the mushroom Leucopaxillus giganteus on human cervical cancer HeLa cells by inducing apoptosis. *Cancer Lett.* **262,** 190–200 (2008).

694. Mukherjee, A. *et al.* 6-Nitro-2-(3-hydroxypropyl)-1H-benz[de]isoquinoline-1,3-dione, a potent antitumor agent, induces cell cycle arrest and apoptosis. *J. Exp. Clin. Cancer Res.* **29,** 175 (2010).

695. Reichert, S. *et al.* A radiosensitizing effect of artesunate in glioblastoma cells is associated

with a diminished expression of the inhibitor of apoptosis protein survivin. *Radiother. Oncol.* **103,** 394–401 (2012).

696. Efferth, T. Willmar Schwabe Award 2006: antiplasmodial and antitumor activity of artemisinin--from bench to bedside. *Planta Med.* **73,** 299–309 (2007).

697. Berdelle, N., Nikolova, T., Quiros, S., Efferth, T. & Kaina, B. Artesunate induces oxidative DNA damage, sustained DNA double-strand breaks, and the ATM/ATR damage response in cancer cells. *Mol. Cancer Ther.* **10,** 2224–33 (2011).

698. Ahnesorg, P., Smith, P. & Jackson, S. P. XLF interacts with the XRCC4-DNA ligase IV complex to promote DNA nonhomologous end-joining. *Cell* **124,** 301–13 (2006).

699. Cereser, C., Boget, S., Parvaz, P. & Revol, A. Thiram-induced cytotoxicity is accompanied by a rapid and drastic oxidation of reduced glutathione with consecutive lipid peroxidation and cell death. *Toxicology* **163,** 153–162 (2001).

700. Belotte, J. *et al.* The role of oxidative stress in the development of cisplatin resistance in epithelial ovarian cancer. *Reprod. Sci.* **21,** 503–8 (2014).

701. Storz, P. Reactive oxygen species in tumor progression. *Front. Biosci.* **10,** 1881–96 (2005).

702. Jayakumar, S., Kunwar, A., Sandur, S. K., Pandey, B. N. & Chaubey, R. C. Differential response of DU145 and PC3 prostate cancer cells to ionizing radiation: role of reactive oxygen species, GSH and Nrf2 in radiosensitivity. *Biochim. Biophys. Acta* **1840,** 485–94 (2014).

703. Crompton, M. The mitochondrial permeability transition pore and its role in cell death. *Biochem. J.* **341 (Pt 2,** 233–49 (1999).

704. Rahman, I., Kode, A. & Biswas, S. K. Assay for quantitative determination of glutathione and glutathione disulfide levels using enzymatic recycling method. *Nat. Protoc.* **1,** 3159–65 (2006).

705. Lluis, J. M. *et al.* Critical role of mitochondrial glutathione in the survival of hepatocytes during hypoxia. *J. Biol. Chem.* **280,** 3224–32 (2005).

706. Lu, J. J. *et al.* Dihydroartemisinin induces apoptosis in HL-60 leukemia cells dependent of iron and p38 mitogen-activated protein kinase activation but independent of reactive oxygen species. *Cancer Biol.Ther* **7,** 1017–1023 (2008).

707. Huang, X.-J., Ma, Z.-Q., Zhang, W.-P., Lu, Y.-B. & Wei, E.-Q. Dihydroartemisinin exerts cytotoxic effects and inhibits hypoxia inducible factor-1α activation in C6 glioma cells. *J. Pharm. Pharmacol.* **59,** 849–856 (2007).

708. Singh, N. P. & Lai, H. Selective toxicity of dihydroartemisinin and holotransferrin toward human breast cancer cells. *Life Sci.* **70,** 49–56 (2001).

709. Gu, Y., Li, Q., Melendez, V. & Weina, P. Comparison of HPLC with electrochemical detection and LC-MS/MS for the separation and validation of artesunate and dihydroartemisinin in animal and human plasma. *J. Chromatogr. B Anal. Technol. Biomed. Life Sci.* **867,** 213–218 (2008).

710. Ji, Y. *et al.* Anti-tumor effects of dihydroartemisinin on human osteosarcoma. *Mol. Cell. Biochem.* **351,** 99–108 (2011).